UNIVERSITY OF BIRMINGHAM

Development of new techniques and assessment of existing methodologies for investigating how particle size influences the behaviour of bentonite colloids under conditions relevant to those likely to be found in Geological Disposal Facilities

Lauren Jennifer Dackombe

A thesis submitted to the University of Birmingham

for the degree of Doctor of Philosophy

School of Chemistry

College of Engineering and Physical Sciences

University of Birmingham

September 2019

Abstract

An increase in the global demand for low-carbon energy generation has resulted in renewed interest in nuclear power over recent years, making it more important that a safe means by which to dispose of long-lived radioactive waste be implemented. Two geological disposal facilities (GDFs) are currently in either the planning or construction stages in Scandinavia, but more will be needed globally in order to deal with the stockpiles held by many nations around the world.

Bentonite clay is very likely to be used as a backfill in these GDFs because its properties make it particularly well-suited for nuclear waste disposal: it swells on contact with water, thereby inhibiting the migration of dissolved contaminants, and sorbs many radionuclides strongly. However, colloids produced in this backfill may enhance the movement of some contaminants in the environment, as colloids that are eroded from the buffer and carried towards the surface by groundwater can transport radionuclides adsorbed onto them. The role of colloids in radionuclide migration therefore has potential implications for the performance of a GDF. It is crucial that these implications are understood thoroughly in order to best inform performance assessments for the facility, and the aim of this project was to develop, use, and assess experimental techniques which would lead to greater understanding of how particle size affects the behaviour and transport of bentonite colloids, so as to expand the existing knowledge that is available to inform performance assessments for GDFs.

In order to do this, suspensions of bentonite colloids were fractionated to produce samples with distinct size distributions, and then characterised. A flow system was constructed, and

the colloid fractions were used in flow experiments. New methodologies were developed, and existing ones critiqued when the fractionation and characterisation techniques used during these steps presented unexpected challenges. Finally, the adsorption and desorption of Eu, Cs and Ni, onto and off the colloids was investigated.

The outcome of these experiments was that against expectations after reviewing the literature, the size of the colloids did not appear to influence their behaviour in the flow experiments. Additionally, this project highlighted that producing and characterising suspensions of clay colloids with narrow, distinct size distributions is very difficult, and that approaches described in the literature may not be suitable for bentonite. If further investigation into the influence size has on the behaviour of bentonite colloids is necessary in order to satisfy waste management organisations that it is unlikely to present problems in a GDF, more advanced laboratory and modelling approaches need to be developed.

Word count: 49400

Acknowledgements

Firstly, and most importantly, I want to thank Dr Joe Hriljac for agreeing to take me on instead of leaving me at the mercy of university bureaucracy, for welcoming me into the School of Chemistry, and for the understanding and kindness you have shown me over the last three years.

Thanks are also due to my second supervisor, Dr Mark Read.

Thank you to DREAM CDT and to RWM for funding this project, and additional thanks to Dr Rosie Hibberd of RWM for her guidance.

Thank you to FENAC for the instrument access, to Dr Xianjin Cui for his input and sample imaging, and to Dr Loren Picco of the University of Bristol for the AFM images.

The MX80 used throughout this project was kindly provided by Dr Christopher Reid of the University of Strathclyde.

Dr Richard Greswell, your guidance when building the nephelometer was invaluable, but I owe you a greater debt of gratitude than that: you have succeeded at keeping another PhD student a close approximation of sane, and I would not have got to this point without your reassurance, excellent diagrams, and terrible jokes. Love to yourself and to Carol.

Thanks also to the fifth-floor crew, in particular Dr George Day for his help in building the flow system, and Abbey and Dan for the moral support, the constant talk of food, and the excessive amounts of coffee. Good luck to those of you still going with your PhDs. You'll get there, I promise.

Dr Kathryn George, you've been my inspiration and academic oracle for the last decade, and I wouldn't be here without you and without the many, many kilos of satsumas and jars of peanut butter you've given me! Dr Lucy Morris, it has been an honour and a privilege to share this somewhat bumpy journey with you. I am so proud of both of us, and I can't wait to celebrate with you.

To the Moseley rugby girls, thank you for always being there, and for letting me tackle you after a bad day! I promise I won't make any of you read my thesis.

Mum, thank you for always making my education a priority, and for your constant and unwavering belief in me, especially when I didn't believe in myself.

Finally, to Nel. You've been there for me through all of this, through the stress and the tears, and I can't thank you enough, but I'll try. Thank you for everything you've done for me. Here's to some happier times together in the future.

Table of Contents

List of figures

List of tables

List of equations

Table of abbreviations

ADC	Analog-to-digital converter
AFM	Atomic Force Microscopy
AGR	Advanced Gas-Cooled Reactor
AsFlFFF	Asymmetric Flow Field-Flow Fractionation
BELBaR project	Bentonite Erosion: effects on the Long-term performance of the engineered Barrier and Radionuclide transport
CIEMAT	Centro de Investigaciones Energéticas, Medioambientales y Tecnológicasn (Centre for Energy, Environment and Technology)
CRR	Colloid and Radionuclide Retardation
DLS	Dynamic Light Scattering
DLVO Theory	Derjaguin, Landau, Verwey and Overbeek Theory
EBS	Engineered Barrier System
EDS	Energy-dispersive X-ray spectroscopy
EDTA	Ethylenediaminetetraacetic acid
ESEM	Environmental Scanning Electron Microscopy
EXAFS	Extended X-Ray Absorption Fine Structure
FEBEX	Full-scale Engineered Barriers Experiment
FFM	Fracture-filling material
GDF	Geological Disposal Facility
GPIO	General Purpose Input Output
GTS	Grimsel Test Site
HLW	High Level Waste
ICP-AES	Inductively Coupled Plasma Atomic Emission Spectroscopy
ICP-MS	Inductively Coupled Plasma Mass Spectrometry
ICP-OES	Inductively Coupled Plasma - Optical Emission Spectrometry

ILW	Intermediate Level Waste
KIT	Karlsruhe Institute of Technology
LED	Light Emitting Diode
LLW	Low Level Waste
NDA	Nuclear Decommissioning Authority
PCS_v	Photon Correlation Spectroscopy
PEG	Polyethylene glycol
PTFE	Polytetrafluoroethylene
PVP	Polyvinylpyrrolidone
PWR	Pressurized water reactor
RWM	Radioactive Waste Management
SEM	Scanning Electron Microscopy
SF	Spent Fuel
SKB	Svensk Kärnbränslehantering Aktiebolag, (Swedish Nuclear Fuel and Waste Management Company)
TEM	Transmission Electron Microscopy
XRD	X-Ray Diffraction
XRF	X-Ray Fluorescence
µPIXE	Micro-Particle Induced X-Ray Emission

Chapter 1

Introduction

Chapter 1: Introduction

1.1 Introduction

Small volumes of extremely radioactive high-level waste arise from the reprocessing of spent nuclear fuel. At present, no suitable facilities exist for its disposal anywhere in the world, although one is currently under construction in Finland, and thus over fifty years' worth of this high level waste (HLW) and spent fuel is currently stockpiled in various storage facilities (Chapman & Hooper 2012; SKB 2018). Concerns about energy security and a demand for low-carbon electricity have led to a renewed interest in nuclear power in recent years, meaning that these waste volumes will continue to expand. It is therefore of vital importance that a safe method of waste disposal is identified and implemented. Several different strategies have been considered for this disposal, but internment in a Geological Disposal Facility (GDF) using an engineered barrier system (EBS) is the only approach that has been implemented; construction of the Onkalo facility in Finland is currently underway.

Current policy in the UK is to dispose of HLW and intermediate level waste (ILW) together (DECC 2014). The KBS-3 concept, a Swedish repository design, was identified as an "example reference HLW/ spent fuel concept" by Radioactive Waste Management (RWM), the organisation responsible for delivering a GDF in the UK, but the repository design that is implemented will be site-specific (Beard & Roberts 2012). The use of different types of EBS is referenced in multiple RWM reports (RWM 2016a; RWM 2016b), but the KBS-3 was the reference waste disposal concept used in this project.

As the name suggests, an EBS provides a number of layers of protection that complement each other and their environment in order to contain the waste over very long timescales, potentially >100000 years (Chapman & Hooper 2012; Johansson *et al.* 2007). Figure 1.1 shows a schematic of an EBS.

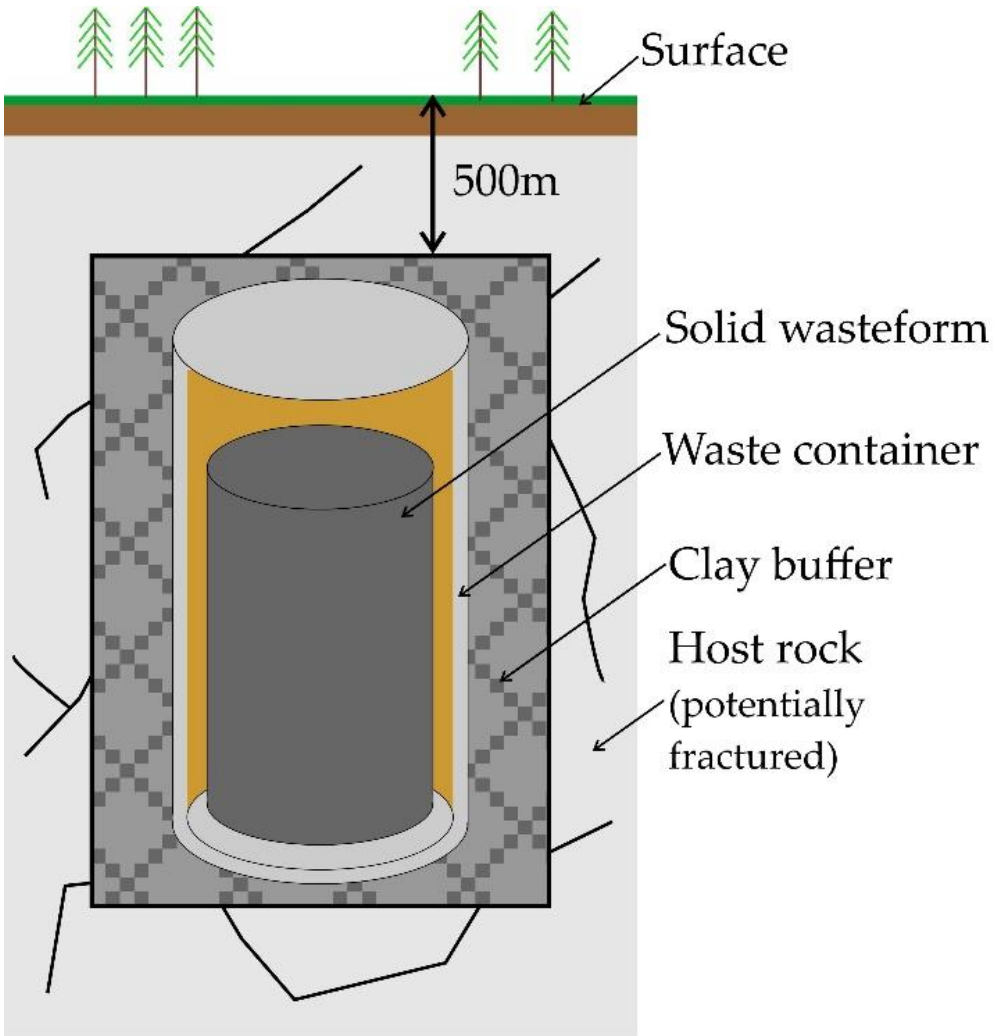

Figure 1.1. The design of an EBS. The facility consists of a solid wasteform inside a metal or concrete canister. This is then placed around 500 m underground, and the facility backfilled with a buffer such as bentonite clay.

The first layer of protection is the wasteform itself. The waste must be solid because liquids have the potential to leak and diffuse through small gaps or porous media. If the waste is

already in a solid form, such as unprocessed spent nuclear fuel, then it requires little pre-treatment, but if it is not, then it requires conversion into a solid before it may be disposed of. Vitrification is currently favoured for HLW, although encasement in ceramic materials and Synroc, a mixture of different mineral phases, is also feasible, albeit not widely implemented at present due to insufficient research into its properties (RWM 2016a). During vitrification, liquid waste is mixed with borosilicate glass frit and heated to over 1000 °C. When it cools, the waste is contained in the glass matrix. Vitrification provides good radiation resistance, but some components of HLW, notably actinides, are poorly soluble in glass and may therefore separate out, making the wasteform unstable (Stefanovsky *et al.* 2004).

The next layer is the waste canister. ILW is housed in concrete, stainless steel or iron containers (DECC 2014). HLW is likely to be encased in canisters consisting of a copper inner layer and an iron or steel outer layer. The former provides corrosion resistance, and the latter provides mechanical stability to protect against stress induced by, for example, seismic activity (Beard & Roberts 2012).

This project will focus on the next layer: the buffer. It will consist of a compacted bentonite clay and will perform several roles: to protect the container from movement of the bedrock, and to inhibit the movement of groundwater and any corrodents it may carry towards the canister. The buffer suppresses microbial activity, permits the diffusion of any gases away from the waste, and hinders the movement of water away from the canister, which would form a pathway for radionuclides to enter the far-field (Chapman & Hooper 2012).

The final barrier is provided by burying the waste deep underground. This may be in higher-strength, crystalline rocks with low porosity and permeability, such as the migmatic gneiss

found at Onkalo, lower-strength sedimentary rocks, or evaporites (Fransson *et al*. 2019; Johansson *et al*. 2007; RWM 2016c). This project is focused on the first type in order to continue the work of the original supervisory team.

The properties of bentonite clay make it particularly well-suited for nuclear waste disposal: it swells on contact with water and exhibits a high degree of plasticity, which combine to make it self-sealing, and it buffers for Eh and pH extremely well (Missana *et al*. 2003). It also sorbs many radionuclides strongly, protects the wasteform, inhibits groundwater flow towards and away from it, which aids in suppressing microbial activity and corrosion, and it permits the diffusion of gases away from the waste (Chapman & Hooper 2012; Norrfors et al. 2016). However, colloids produced in this backfill and in the natural environment may enhance the movement of contaminants in the environment, as colloids that are eroded from the buffer and carried towards the surface by groundwater may also transport radionuclides adsorbed onto them (Missana *et al*. 2003; Norrfors *et al*. 2016). The role of colloids in radionuclide migration therefore has potential implications for the performance of a GDF (Missana *et al*. 2003). It is crucial that these implications are understood thoroughly in order to best inform performance assessments for the facility (NDA 2010).

Research into natural analogues can be applied to the different barriers in an EBS in order to understand how they are likely to perform under different conditions over timescales of thousands of years. One such example is the Littleham Mudstone Formation in Devon, England. It contains sheets of copper and has been used to understand the long-term behaviour of a copper-coated canister in a clay-based geology. It is not a perfect analogue;

the porosity, permeability and chemical composition of the porewaters are different from what would be expected of a bentonite clay; but the copper has resisted corrosion well despite not being specifically engineered for the purpose (Alexander *et al*. 2015). This bodes well for the behaviour of these two materials in a repository environment.

1.2 Project structure and aims

This project had three aims:

1. To assess the suitability and effectiveness of methods described in the literature for producing and characterising bentonite colloids;
2. To develop alternative approaches for producing and characterising these colloids;
3. To use the new experimental techniques and methodologies in conjunction with pre-existing ones to develop a greater understanding of how particle size affects the behaviour and transport of bentonite colloids, so as to expand the existing knowledge that is available to inform performance assessments for GDFs. In order to meet this aim, the following objectives were defined:
    a. To produce and characterise three or more suspensions of bentonite particles with distinct, narrow size distributions, suitable for use in flow experiments;
    b. To conduct flow experiments by passing these fractions of bentonite clay colloids across or through samples of granite, to investigate how differently sized colloids eroded from the buffer of a GDF would move under conditions relevant to the far-field environment;
    c. To undertake an investigation into how cations relevant to nuclear waste disposal bind to the bentonite colloids by conducting batch sorption experiments.

How successfully these aims have been met, any consequences their findings may have for the safety case of a GDF, and any potential for future work that was identified whilst completing them are discussed in Chapter 8.

Chapters 1 and 2 contain relevant background information, details about the project, and a review of the existing literature, and Chapter 3 details the instruments used to characterise bentonite colloids.

The aim of Chapter 4 was to produce and characterise narrow colloidal size fractions. Techniques including milling, sieving, filtration and centrifugation were used to try and isolate stable, colloidal-sized particles from bulk bentonite and separate them into different size ranges. Analytical techniques including light scattering and electron microscopy were then used to characterise them.

The colloids produced in Chapter 4 were then used in laboratory-scale flow experiments to assess their transport behaviour under controlled conditions. A custom-built nephelometer and flow system were constructed in order to do this. Chapter 5 details the design of the flow system, and the methodology and results of the flow experiments are described in Chapter 6.

Chapter 7 describes the investigation of the sorption and desorption behaviour of various stable analogues for radionuclides onto and off bentonite colloids, Chapter 8 draws conclusions about the findings of the project and suggestions for further work, and Chapter 9 contains the appendices.

1.3 References

Alexander, W.R., Reijonen, H.M. & McKinley, I.G., 2015. Natural analogues: studies of geological processes relevant to radioactive waste disposal in deep geological repositories. Swiss Journal of Geosciences, 108(1), pp.75–100.

Beard, R. & Roberts, D., 2012. State-of-the-art report on the treatment of colloids and related issues in the long-term safety case, UK: NDA RWMD.

Chapman, N. & Hooper, A., 2012. The disposal of radioactive wastes underground. Proceedings of the Geologists' Association, 123(1), pp.46–63.

DECC, 2014. Implementing Geological Disposal: A Framework for the long-term management of higher activity radioactive waste, UK: DECC.

Fransson, Å., Lönnqvist, M. & Viola, G., 2019. Rock mechanical modelling of the Bentonite Rock Interaction Experiment, Aspo Hard Rock Laboratory, Sweden. International Journal of Rock Mechanics and Mining Sciences, 113(April 2018), pp.255–267.

Hunter, R.J., 2001. Foundations of colloid science, Oxford: Oxford University Press.

Johansson, E., Siren, T. & Kemppainen, K., 2007. Nuclear Waste Management in Finland, Finland: Finnish Energy Industries.

Missana, T., Alonso, U. & Turrero, M.J., 2003. Generation and stability of bentonite colloids at the bentonite/granite interface of a deep geological radioactive waste repository. Journal of Contaminant Hydrology, 61(1–4), pp.17–31.

NDA, 2010. Geological Disposal: An overview of the generic Disposal System Safety Case, UK: NDA.

Norrfors, K.K. *et al.*, 2016. Montmorillonite colloids: II. Colloidal size dependency on radionuclide adsorption. Applied Clay Science, 123, pp.292–303.

RWM, 2016a. Geological Disposal: Behaviour of Radionuclides and Non-radiological Species in Groundwater Status Report, UK: RWM.

RWM, 2016b. Geological Disposal: Generic Post-closure Safety Assessment, UK: RWM.

RWM, 2016c. Generic Environmental Safety Case - Main Report, UK: RWM.

SKB, 2018. Two statements on the Spent Fuel Repository. Available at: http://www.skb.com/news/two-statements-on-the-spent-fuel-repository/. Last accessed December 2018.

Stefanovsky, S.V. *et al.*, 2004. Nuclear waste forms. Energy, Waste, and the Environment: a Geochemical Perspective, 236, pp.37–63

Chapter 2

Background

Chapter 2: Background

2.1 Bentonite

Several terms are frequently used in academic literature to describe and classify bentonite, often with little explanation of their meanings and their relationships to each other. MX80 bentonite is a montmorillonite-rich smectite clay. In geology and pedology, the term 'clay' is often used to refer to materials of particle size <2 μm, regardless of their composition (Hunter 2001). That is not the case here; the use of the term 'clay' in this report refers to clay minerals, rather than this broader definition. Clay minerals are highly heterogeneous, but Bergaya & Lagaly (2013) describe their properties thusly:

- Composed of hydrated phyllosilicates,
- A structure composed of tetrahedral silicon-oxygen and octahedral aluminium-oxygen layers as shown in Figure 2.1.,

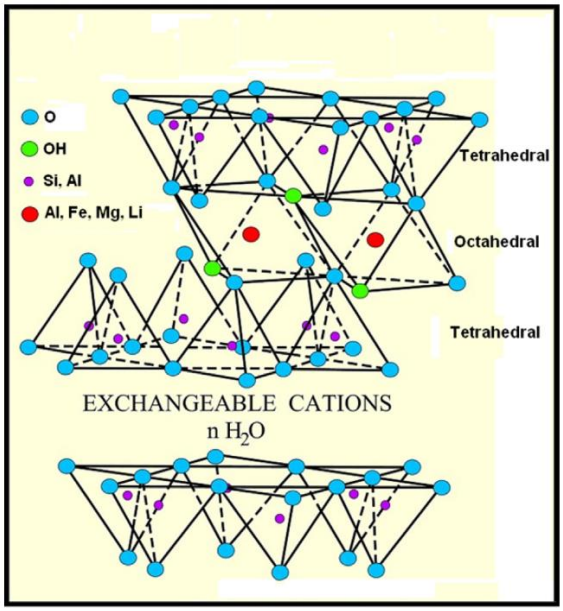

Figure 2.1. The structure of smectites. These materials contain octahedral aluminium-oxygen layers sandwiched between tetrahedral silicon-oxygen layers. Image courtesy of Kotal *et al.* 2015. Copyright Elsevier.

- They contain several surface types: planar, edge and interlayer,
- Plastic, easily modified, and often harden when dried or heated.

Smectites are a diverse group of clays. In addition to the above properties, they are highly disordered and are characterised by colloidal-size particles, high specific surface areas and cation exchange capacities, low, pH-dependent anion exchange capacities, considerable interlayer swelling in water, and moderate layer charge (Bergaya & Lagaly 2013). The silicon-oxygen and aluminium-oxygen layers have a 2:1 ratio and a maximum thickness of about 1 nm (Karnland 2010).

Montmorillonite is a commonly occurring dioctahedral smectite. There tend to be few cationic substitutions in the tetrahedral layer, but approximately one-sixth of the aluminium ions are substituted for a divalent ion such as magnesium in the octahedral layer. The silicon and aluminium layers are joined by hydrogen bonds, and the 2:1 silicon-aluminium-silicon groups are bonded to each other by van der Waals forces and by ionic bonds between the interlayer cations and oxygen atoms in the outer layers (Hunter 2001). They tend to have a low iron content, and >90 % of the mineral's charge occurs in the octahedral layers (Emmerich 2013; Hunter 2001).

Bentonites are rich in montmorillonite and are either authigenic (where granite rocks are eroded and the material deposited, forming sedimentary rock), or formed by anoxic surface weathering of volcanic tuff (Bergaya & Lagaly 2013; Hazen *et al*. 2013). They also contain some beidellite, a mineral similar to montmorillonite but with some of the silicon ions substituted by aluminium (Hunter 2001), and are likely to contain accessory minerals such as nontronite (Karnland 2010; Schatz *et al*. 2015). Bentonites come from numerous sources and all have slightly different compositions. These varieties include Asha 505, which is mined

in India, IBECO from Greece, Bentonite 75 from the Czech Republic, FEBEX from Spain, and MX80 from the USA (Missana *et al*. 2016).

MX80 and FEBEX have been researched more thoroughly for use in nuclear waste disposal than any of the other varieties. MX80 is a sodium bentonite that originates in Wyoming, and FEBEX, a calcium bentonite, is mined in the Cortijo de Archidona deposit in Almeria, Spain (Garcia-Gutierrez *et al*. 2001; N. Sherriff *et al*. 2015). However, sodium bentonites have higher swelling capacities than calcium bentonites, which is what gives the clay its desirable self-sealing properties (Missana & Geckeis 2006; Tripathy *et al*. 2004). Thus, sodium bentonites such as MX80 are the material that is currently most favoured for repository buffers (Cui 2017), hence why it was used in this project. The body of knowledge that is required in order to produce and support the environmental safety case for a GDF is vast and detailed, and this project aims to advance the understanding of one small aspect in order to contribute to it: how particle size affects the behaviour and transport of bentonite colloids.

2.2 Nomenclature

From here on in, 'clay' will refer to clay minerals, rather than the broader geological definition of clay as being any material of particle size <2 μm (Hunter 2001).

The terms 'bentonite', 'clay' and 'MX80' will, unless stated otherwise, be used interchangeably to refer to the same material, a bentonite mined in Wyoming, USA, that is commonly given the name MX80.

'Buffer', 'backfill' and 'overpack' will all refer to the layer of clay placed around waste canisters and used to fill the void in a GDF.

Although there may be colloids derived from other sources present in the repository environment, the term 'colloids' will refer to those consisting of bentonite layers unless otherwise specified. The colloids will also be referred to as 'particles' or 'aggregates' or 'agglomerates', where these terms are relevant.

2.3 Colloids

Colloids are particles with a minimum of one dimension of between 1 nm and 1 µm in size, dispersed within another substance. Most, including those of interest here, are solid particles in a liquid, but colloidal systems may be found in all combinations of phases, *i.e.* solid in solid, gas in liquid, apart from gas in gas (Hunter 2001). The colloidal system being researched for this project is composed of bentonite particles suspended in groundwater. They are formed by the erosion of bulk bentonite either by tectonic activity or water movement, and this erosion is affected by both the physics and chemistry of the environment (Alonso *et al*. 2006; BELBaR 2016; Möri *et al*. 2003). This will be discussed further below. There are likely to be colloids derived from other sources present in the repository environment, but only those eroded from the bentonite buffer are of relevance to this project.

These colloids from the bentonite backfill present a potential downside because they have the potential to enhance the movement of contaminants in the natural environment (Missana *et al*., 2003). Ryan and Elimelech (1996) describe how plutonium in the vicinity of Los Alamos National Laboratory was transported far more rapidly than expected due to its association with colloidal phases, and Matsunaga *et al*. (2004) reported on the tendency of natural colloids to alter the chemical form, and therefore the solubility, of actinides in the

vicinity of Chernobyl. The production of these colloids by erosion also weakens and degrades the clay buffer (Beard & Roberts 2012).

Therefore, if a waste canister should be breached, allowing the radioactive waste within it to come into contact with the clay backfill, the role colloids play in radionuclide migration could have implications for the performance of a GDF (Missana *et al*., 2003), and it is crucial that these are understood thoroughly so as to best inform the facility's safety assessment (NDA 2010).

In light of this, considerable research has already been conducted into the potential behaviour of bentonite colloids in a repository environment. The Grimsel Test Site (GTS) in Switzerland is dedicated to the research and development of geological disposal techniques, and several of the projects based there are focused on the impacts colloids may have on such a facility. The BELBaR (Bentonite Erosion: effects on the Long term performance of the engineered Barrier and Radionuclide transport) project was a collaboration between fourteen waste management organisations and research institutions, funded by Euratom, that aimed to use experimental and modelling techniques to expand the existing knowledge about clay colloids in an EBS designed to hold spent fuel and HLW, and is intended to help to inform the safety assessments for such systems. The partners included the NDA, CIEMAT, SKB, Posiva, KIT and the University of Manchester, and the project concluded in 2016. BELBaR publications were used extensively to inform this project both because of their direct relevance and because they provided up-to-date research on the subject of clay colloids in the repository environment (Shelton *et al*. 2016). The findings of the BELBaR project indicated that the effect colloids have on contaminant transport is often minimal and can be disregarded, and indicate that the way in which colloids are currently treated in relation to

the safety case for the use of bentonite in GDFs is reasonable, and if anything slightly pessimistic (BELBaR 2016).

However, the safety assessments performed by the three waste management organisations involved in the BELBaR project; Posiva of Finland, SKB of Sweden and RWM of the UK; indicate that different countries judge the risk colloids present to a GDF very differently. Posiva and SKB consider them to present few issues and to have little effect on the integrity of a repository. Colloids are treated with greater caution in the UK because plans for a GDF there are still at the siting stage. The risk presented by colloids is very site-specific and therefore further research into the interactions between radionuclides and colloids will be needed when a site has been identified and characterised (Beard & Roberts 2012). Finland and Sweden have both adopted the KBS-3 design for a repository. The UK has selected it as an example disposal method for HLW and spent fuel, but has not finalised its use because a final site has not yet been identified (Beard & Roberts 2012; RWM 2018).

2.3.1 The Colloid Ladder

For colloid-facilitated radionuclide transport to have an impact on the long-term integrity of a GDF, five criteria must be met:

- Colloids must be present.
- The colloids must be mobile.
- They must be stable.
- There must be radionuclide uptake onto the colloids.
- This uptake must be irreversible (or at least slow).

(BELBaR 2016)

These criteria constitute the ‘Colloid Ladder’ and are shown schematically in Figure 2.2.

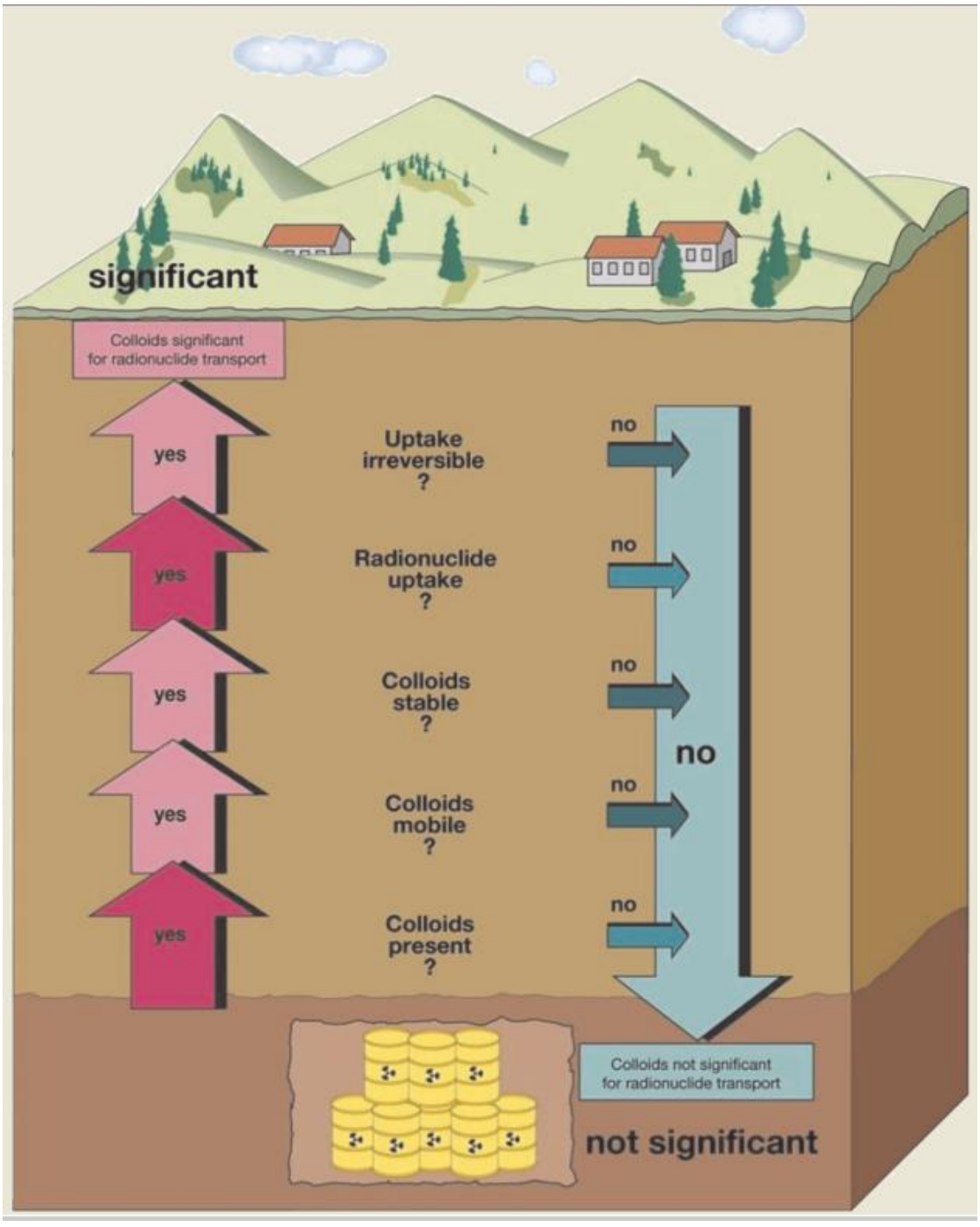

Figure 2.2. The 'Colloid Ladder'. This demonstrates schematically the five conditions which must be met in order for bentonite colloids to influence radionuclide transport: colloids must be present, mobile, and stable, they must sorb radionuclides, and must not desorb them too rapidly. Image courtesy of BELBaR 2016.

2.3.1.1 Presence of colloids

There are four possible sources of colloids in a repository environment:

a) Radionuclides may be released from the waste in a colloidal form (‘*eigencolloids’*),
b) They may pre-exist naturally in groundwaters. However, the concentrations of these are low in the crystalline rock types of interest to this project (Beard & Roberts 2012),
c) They can arise from corrosion of the waste container and its overpack,
d) They may be generated in the clay buffer by the chemical and/or mechanical processes described below.

(Alonso *et al*. 2006; Missana & Geckeis 2006)

This project will focus on those that originate in the clay backfill.

2.3.1.1.1 Chemical processes

Geochemical conditions including ionic strength of the groundwater, pH, the composition of porewater, the presence of organic material (such as humic substances and fulvic acid found in natural groundwater), and the type of clay can all impact the production, equilibrium concentration and size distribution of colloids (Norrfors et al. 2015; Norrfors 2015; Schatz et al. 2015; Sherriff et al. 2016). Norrfors *et al*. (2016) noted that low-ionic strength groundwaters such as those found in the granitic environment of the GTS were effective at releasing stable colloids from the clay overpack.

When bentonite expands into fractures, it forms a gel containing very low concentrations of solid clay (as little as 1 % by volume), which may transform into a sol (a weakly-interacting suspension of particles of low concentration) if the density falls sufficiently. These types of materials have very low shear viscosity, which can increase their transport in the GDF environment (Schatz *et al*. 2015). Despite this, at a velocity typical of groundwater, there is

unlikely to be enough mechanical shear to detach colloids from the surface of the gel. However, when Missana *et al.* (2003) simulated the quasi-static flow conditions likely to be found in a repository environment, colloid production still occurred. Schatz *et al*. (2015) determined that it was due to chemical effects rather than mechanical processes, and postulated that it occurs through an osmotic process, whereby the water uptake by the clay forces the colloids further apart, until their attractive forces are weak enough that they may be eroded from the gel surface.

2.3.1.1.2 Mechanical processes

Mechanical processes may also impact colloid generation. Increased flow velocity and greater amounts of erosion are well correlated for a sodium montmorillonite and deionised water (Schatz *et al*. 2015). In fractured rock, the width of the fracture affects the degree of colloid production because it controls the surface area available for erosion. Schatz *et al*. (2015) identified that the rate of mass loss of bulk bentonite was an order of magnitude lower for montmorillonite in a fracture with a 0.1 mm aperture, compared to a fracture 1 mm wide.

Schatz *et al*. (2015) determined that the degree of clay erosion that occurs, and therefore the number of colloids that are produced, is most dependent on the properties of the clay and the water chemistry, but that the movement of water may augment the detachment of colloids from the gel surface, and therefore the least-optimal conditions for a GDF in crystalline geology is where groundwater is moving through fractures near to the surface of the clay buffer because it can enhance their production and then transport them more easily than other conditions. Additionally, the BELBaR project concluded that chemical processes exert greater control over bentonite erosion than mechanical processes do (BELBaR 2016).

This is contradicted by Alonso *et al.* (2006), who determined that the detachment of colloids from the backfill appears to depend far more heavily on the mechanical processes in the environment than on its geochemistry. However, the authors conceded that the subject merited further investigation, and the final conclusions of the BELBaR project stated that chemical forces exert far greater influence over bentonite erosion, and by default colloid production, than mechanical processes (BELBaR 2016).

2.3.1.2 Colloid mobility

Both the Colloid and Radionuclide Retardation (CRR) project at the GTS and the BELBaR project provided strong evidence that radionuclide transport can be influenced by the movement of bentonite colloids (Alonso *et al*. 2006; Sherriff *et al*. 2016). A significant amount of research has been carried out into the production and movement of colloids at the bentonite/host rock boundary because it is a vulnerable point in the repository design (Alonso *et al*. 2006; Missana *et al*. 2003; Möri *et al*. 2003; Nagra 2004).

Areas of crystalline geology are good host rocks for GDFs because they have low porosity and permeability and high mechanical strength (Delage *et al*. 2010). These rock types are often fractured, and advection through these fractures is the primary groundwater pathway in this kind of geological setting (Alonso *et al*. 2006). The permeability of bentonite clay is also extremely low due to its self-sealing nature, so erosion of colloids within the bulk of the clay is improbable (Delage *et al*. 2010; Madsen 1998). Colloid-associated transport of radionuclides is therefore unlikely within the bulk of both the buffer and of the host rock. At the boundary, however, not only can the colloids be generated, they may then enter the fractures and be transported rapidly though the environment.

Colloidal transport may be influenced by particle morphology, concentration, and size, hydrodynamics, and chemical factors such as pH and ionic strength that in turn affect colloidal stability and adsorption to rock surfaces (Norrfors *et al*. 2015; Sherriff *et al*. 2016). Sedimentation, flocculation, filtration and retardation in fractures in the host rock all mitigate their transport, and therefore reduce the speed and distance the radionuclides associated with the colloids can move (Beard & Roberts 2012). These processes are shown in Figure 2.3.

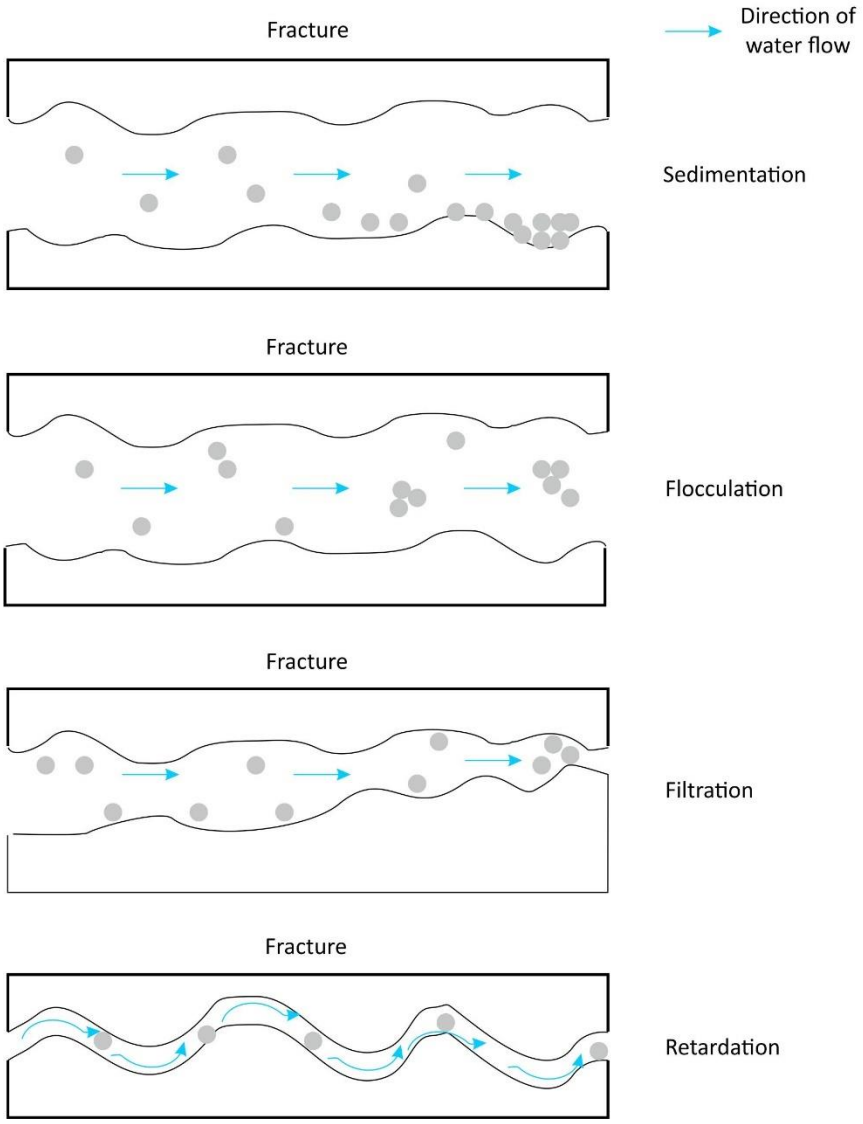

Figure 2.3. Schematic representation of the processes of sedimentation, flocculation, filtration, and retardation. All of these can slow the transport of colloids through fractures.

If complex, the fracture geometry can significantly slow colloid movement and cause tailing of the breakthrough curve (Sherriff *et al*. 2016). A breakthrough curve is a chart showing the change of concentration in the colloids over time. The shape of the curve can be used to infer patterns in their behaviour, for example if their concentration does not increase immediately after their introduction, it is implied that there is a mechanism slowing down their movement, perhaps retardation, as shown in Figure 2.3. The cations present in the groundwater may also have an effect; flow experiments conducted by ÚJV Řež and described by Sherriff *et al.* in one of the BELBaR Deliverables Reports found that colloid migration through a fracture in deionised water was similar to that of tritium, a conservative tracer. However, when other radionuclides were present, the colloids moved more slowly. This is probably due to the radionuclides causing the colloids to interact more with the granite (see Figure 4.7d) (Sherriff *et al*. 2016). Surface complexation reactions such as these are discussed further below in section 2.3.1.4.

2.3.1.3 Colloid stability

The more stable a colloidal system is, the longer the particles take to agglomerate. This stability depends on the chemical and physical properties of the clay, and the temperature, pH, and ionic strength of its environment. The conditions that make colloids stable also enhance their transport and make them more likely to detach and be eroded from the bulk bentonite (Missana *et al*. 2016).

Many texts on the subject (Alonso et al. 2006; Suttiponparnit et al. 2011; Tombácz & Szekeres 2004) state that the stability of colloids depends on the balance between electrostatic repulsion and attractive van der Waals' forces. When attractive forces dominate, aggregation of colloids occurs. This is known as the DLVO theory (named for its

pioneers, Derjaguin, Landau, Verwey and Overbeek) (Hunter 2001; Ryan & Elimelech 1996). However, Missana and Adell (2000) determined that it is not completely applicable to clay colloids because of their plate-like structure: the bonds at the edges of each colloid are broken, and therefore the charge there is pH dependent. The faces of the colloids are permanently negatively charged due to the substitution of around 1/6th of the aluminium ions for other divalent ions, such as magnesium. However, the hydroxyl groups on the broken edge sites develop different charges depending on the pH of the solution. At pH<6.5, Al-OH sites become protonated, but as the pH increases, the Si-OH and then the Al-OH sites undergo deprotonation, giving them a negative charge (Hunter 2001; Tombácz & Szekeres 2004; Ozsoy & Bekbolet 2018). This is shown in Figure 2.4.

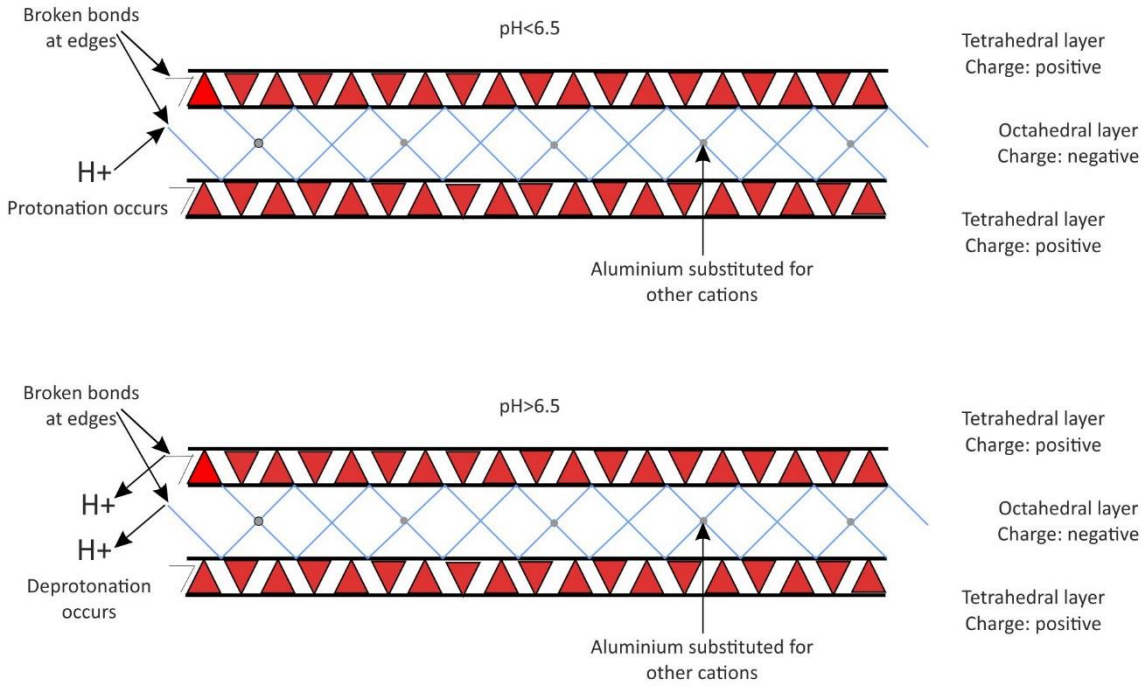

Figure 2.4. The structure of bentonite. The substitution of aluminium for other cations may be observed in the middle layers, and the different protonation and deprotonation behaviour of the edge sites at different pH levels is also shown.

DLVO theory cannot take this pH-dependent edge charge into account, meaning that experimental findings differ from predictions, compromising the validity of using DLVO theory in GDF performance assessments (Missana & Adell, 2000). The colloids in both the sols ('sol' is the term used by Hunter (2001) to describe a colloidal suspension of small, solid particles in a liquid) and attractive gels discussed below are likely to agglomerate due to Coulombic interactions between the negatively-charged faces and, depending on the pH levels, the positively-charged edge sites (Missana *et al*. 2016; Pusch 1999). This can be investigated by measuring the zeta potential of colloidal suspensions and is discussed further in Chapters 3 and 4.

Some factors that are known to affect clay stability will be discussed here. The geochemistry of the environment may influence clay stability because given the extensive time periods over which repositories will need to maintain their integrity, ice ages and subsequent deglaciations are likely to occur. The meltwater that arises from these deglaciations will have low salinity levels and will dilute the salt concentrations of the groundwater. As shown by the phase diagram in Figure 2.5, low NaCl concentrations can promote the formation of 'sols' (Hansen & Hedstrom 2013).

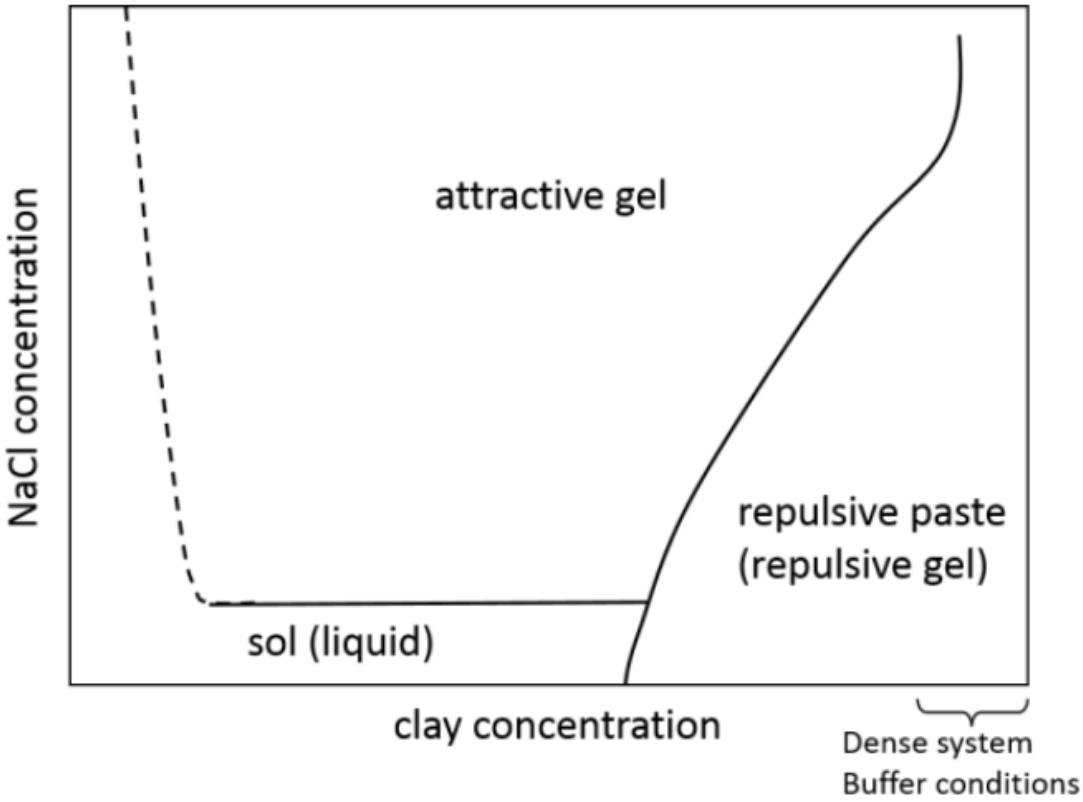

Figure 2.5. This phase diagram for sodium montmorillonite in NaCl shows how the mixture may change phase depending on salt and clay concentrations. Image courtesy of Missana et al. 2016.

Sols are weakly-interacting suspensions of solid particles in a liquid medium. They do aggregate, probably due to interactions between the edge of one particle and the face of another, but these have little yield strength (Missana *et al*. 2016). As a result, they can be eroded easily, which damages the clay overpack and introduces colloids into the system.

It may also exist as a gel. The colloids in these gels may attract or repel each other depending on the concentration of the clay in suspension, and whether the attractive Coulombic forces or attractive van der Waals' forces are dominant, as was discussed on page 41.

The presence of Na^+ ions may increase or decrease agglomeration depending on their concentration in solution and forms the basis of the dispersion experiments described below

in Chapter 4 and the appendices. If their concentration is >10 mM, it promotes aggregation; at lower concentration, it encourages the particles to disperse (Missana *et al*. 2016). This in turn is explained by zeta potential, (zeta potential is a measure of the size and nature of the charges on particles and the media in which they are suspended. This charge arises, in the case of bentonite colloids, from the non-equivalent substitutions of magnesium and other divalent cations for aluminium in the clay structure. Zeta potential is discussed in detail in Chapter 3), but is highly pH-dependent, and is affected by but is highly pH dependent, as shown in Figure 2.6, a chart relating the zeta potential of kaolinite clay in the presence of different concentrations of LiCl, NaCl, $CaCl_2$ and $MgCl_2$ across a range of pH values.

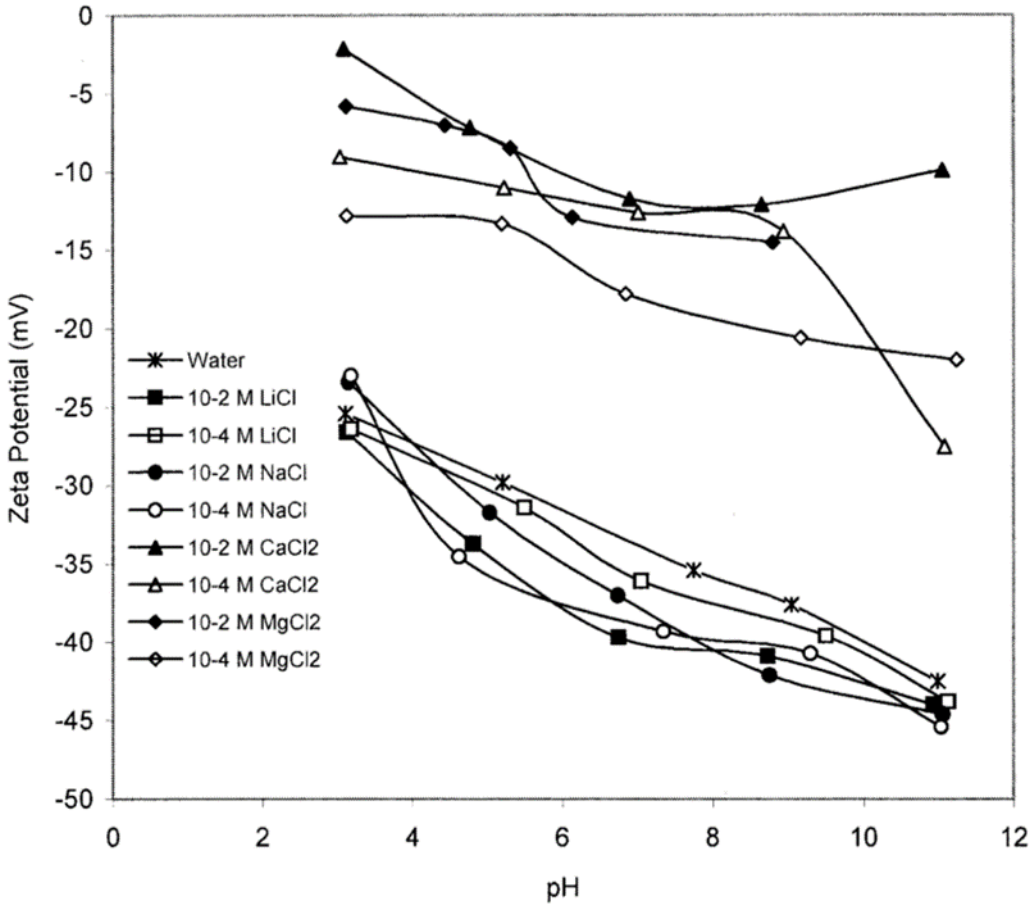

Figure 2.6. The relationship between pH and the zeta potential of bentonite colloids in the presence of different ions. This can be used to try and predict whether particles will agglomerate or not under certain conditions. Image courtesy of Yukselen & Kaya 2003. Copyright Springer Nature.

At low pH, the presence of NaCl makes the zeta potential of kaolinite, another clay mineral, less negative than it is in water, which makes the clay more likely to agglomerate. At higher pH the zeta potential is more negative, encouraging dispersion (Yukselen & Kaya 2003). This occurs due to deprotonation (Sherriff *et al*. 2016). If the concentration of cations is favourable for causing agglomeration, *i.e.* it is above the critical coagulation concentration for that particular clay dispersion, then the colloids agglomerate rapidly. If the concentration is close to that boundary, coagulation happens far more slowly (Missana *et al*. 2016).

If divalent cations such as Ca^{2+} are present even in low concentrations, they should be taken into account when preparing safety assessments because they make the zeta potential less negative, causing greater agglomeration of the colloids than monovalent ions, which in turn can influence their transportation (BELBaR 2016).

Bentonite colloids are more stable in alkaline (pH≥8), low-salinity (~$1x10^{-3}$ M) conditions (Missana *et al*., 2003). The pH of pore water in a GDF is likely to be 9-10 due to the buffering properties of the bentonite (*i.e.* the potential for the -OH groups at the edge sites to undergo both protonation and deprotonation) (Nessa *et al*. 2007), and the ionic strength of a typical granitic groundwater, such as those found at the GTS, will also be low (around $1.2x10^{-3}$M) (Bouby *et al*. 2011 [Appendix 1]). Typical repository conditions are therefore favourable to stability and unfortunately to promoting colloidal transport.

2.3.1.4 Adsorption of radionuclides onto colloids

Logically, colloids can only augment contaminant transport if radionuclides actually bind to them (Sherriff *et al*. 2015). Their small size and correspondingly large surface area mean

colloids adsorb low-solubility contaminants effectively through the mechanisms of ion exchange and surface complexation reactions (Ryan & Elimelech 1996).

At low pH values, ion exchange is the dominant mechanism for radionuclide sorption to colloids. At pH 7-14, surface complexation of radionuclides with edge sites on the colloids is the significant sorption mechanism (Norrfors *et al*. 2016; Sherriff *et al*. 2015). This may be explained by Figure 2.4: at high pH levels, the edge sites on the colloids are negative due to deprotonation, so cations in solution can just bind to them. At pH<6.5, however, this is not the case: the edges are positive due to protonation, so the cations have to exchange with them rather than just attaching to them.

Sorption is usually linear due to ion exchange (with caesium being the only exception to that rule), which is logical: a greater concentration of cations in solution may be expected to lead to a greater degree of sorption. However, it may be reduced if the sorption sites are already saturated, or by competition with other cationic species (Beard & Roberts 2012; Missana & Geckeis 2006; Sherriff *et al*. 2016), although cations of different oxidation states sorb to different sites on the colloids, and do not compete with each other (Bradbury & Baeyens 2005; Norrfors *et al*. 2016). The diagrams below in Figures 2.4a-d demonstrate four possible surface complexation mechanisms by which radionuclides may sorb to colloids. The O-species in these diagrams demonstrate the possible presence of oxide species such as UO_2, which may be found in reactor fuel rods, and subsequently nuclear waste.

In Figure 2.7a, the radionuclides bind to a site on the colloid surface. The dissociation rate is slow and is affected only by the chemistry of the radionuclide. Figure 2.7b shows how the radionuclides may initially form a surface complex, which then expands to form a precipitate on the colloid surface. Figure 2.7c demonstrates how the cations may diffuse in and out of

the interlayer regions of colloids rather than onto edge sites, and Figure 2.7d shows how radionuclides may attach to multiple colloids and cause them to aggregate, as was discussed in section 2.3.1.2. This may prevent them from being available for further reactions and dissociation from the colloids may be slow (Sherriff *et al*. 2016). Reversibility is discussed further in 2.3.1.5.

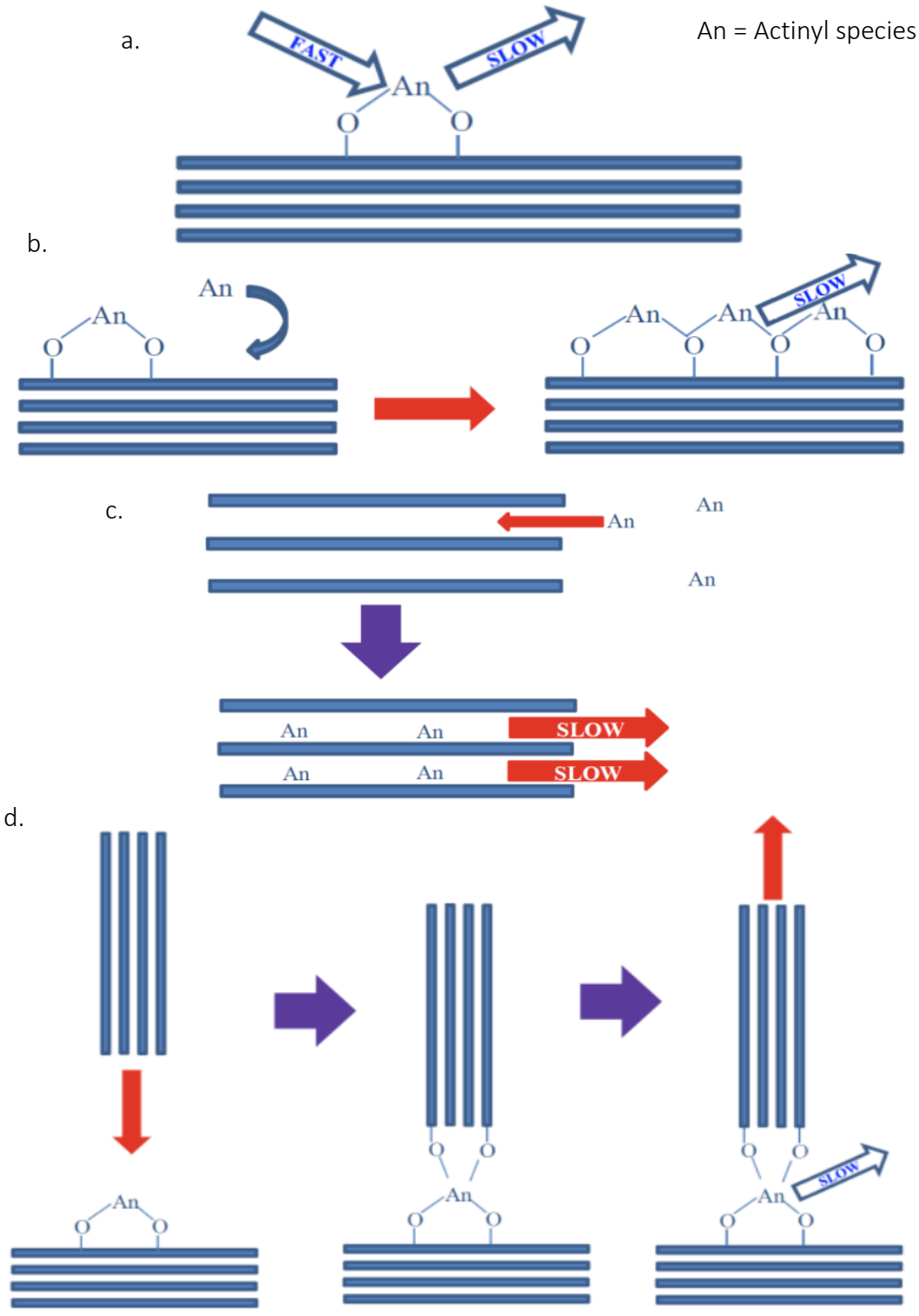

Figure 2.7. There are four possible surface complexation mechanisms by which radionuclides may sorb to colloids: a) radionuclides can bind to a site on the colloid surface, b) radionuclides may initially form a surface complex, which then expands to form a precipitate on the colloid surface, c) the cations may diffuse in and out of the interlayer regions of colloids rather than onto edge sites, and d) shows how radionuclides may attach to multiple colloids and cause them to aggregate. Images courtesy of Sherriff et al. 2016.

Particle size may impact the sorption capacity of the colloids. There are two main mechanisms by which size may have an effect. Firstly, when standardised for different colloid sizes, the density of edge sites can vary by up to a factor of six between the biggest and smallest fractions. This may affect how well different-sized colloids can sorb cations in solution (Norrfors *et al*. 2016). Secondly, the density of surface charges can change with particle size for nano-scale colloids. Abbas *et al*. (2008) report that this is due to better screening efficiency; as the particles become smaller their surfaces become more curved, so ions in solution are attracted to the surface sites from more directions than they would have been on a planar surface. This may alter the adsorption capacity and therefore their interaction with radionuclides (Norrfors *et al*. 2016). However, bentonite colloids are flat due to their lamellar structure, so this effect may not be as pronounced as would be expected for more spherical particles.

2.3.1.5 Reversibility of sorption

Radionuclides that are irreversibly bound onto colloids are transported until the colloid they are attached to ceases to move. The surface of the GDF host rock has the potential to sorb radionuclides as well as colloids. If the colloid-radionuclide bond is reversible, the released contaminants may desorb from the colloid and attach to binding sites available on the rock instead, as these are available in excess, thereby reducing the influence the colloids have on their transport. They may also just return to solution. This reversibility may be tested by measuring the dissociation constants of the association and dissociation reactions; if they are similar, the sorption is reversible (Möri *et al*. 2003; Sherriff *et al*. 2015).

Past research stated that the radionuclide-colloid bonding must be completely irreversible in order to fulfil the final requirement on the colloid ladder (Möri *et al*. 2003), but more

recent findings suggest that the association of a radionuclide and a colloid does not need to be strictly irreversible in order to enhance pollutant transport: providing the dissociation rate is slow in comparison to the transport time through the far field of the repository, the presence of colloids can still have an effect (Sherriff *et al*. 2016).

The BELBaR project determined that for the majority of radionuclides, it can be assumed that their association with colloids is reversible, reducing their potential for transportation in the environment, which is positive from a waste disposal perspective (BELBaR 2016). However, if the dissociation rate is comparable to, or longer than, the transport residence time, then the presence of clay colloids will still increase the speed of radionuclide transport. Total irreversibility will have a greater effect than slow reversibility, but even the latter will still have an impact (Sherriff *et al*. 2016). However, it should be noted that the reversibility behaviour of clay colloids is not yet fully known, because the nature of their edge sites is not yet understood: Okumura et al. (2018) describe how difficult both crystallographic and computational investigations of edge sites are, which impact reversibility behaviour, and how incomplete the knowledge in the literature is as a result. Without fully understanding the colloid structure, it is not possible to completely understand their behaviour.

2.4 Potential implications for a GDF

As stated in Chapter 1, the use of bentonite clay as a buffer in an EBS has both benefits and potential consequences for the integrity of a GDF. Its swelling capacity and self-sealing properties would help to prevent the movement of groundwater towards and away from the waste canisters, which could potentially transport any leaked radionuclides into the far-field environment, but the erosion of colloids from the buffer may compromise its integrity

and can enhance radionuclide migration (Chapman & Hooper 2012; Missana *et al*. 2003; Missana *et al*. 2018).

The types of materials that the UK government anticipates may be disposed of in a GDF when one is constructed include:

- HLW from reprocessing activities,
- ILW
- Some Low Level Waste (LLW) that is unsuitable to go to the existing Low Level Waste Repository facility at Drigg, Cumbria,
- Spent fuel (although this is not currently regarded as a waste material),
- Plutonium and uranium stocks (these are also not currently regarded as waste materials),
- Some fuel and other materials from the UK defence programme (again, this is currently not regarded as waste).

(DECC 2014; RWM 2016b)

These materials can be hazardous to both humans and to the environment and may remain so for thousands of years whilst undergoing radioactive decay. To account for this, waste management organisations have to consider the potential health effects over timescales of 10000-1000000 years (Swift 2017). After around 100000 years, the waste has a radiotoxicity level similar to that of natural uranium ore, and the hazard it presents has reduced substantially (Chapman & Hooper 2012). However, nothing humans have built to date is older than 5000-10000 years, and having to construct a facility that retains its integrity for ten times that long is a challenge the human race has not encountered before. It is therefore necessary to research and understand every aspect of the repository design; from the

wasteform itself, the materials used to build it, to the geology of the host rock, and even the potential consequences of future human interference; in order to inform the 'environmental safety case', a document that identifies risks, defines how they are managed, and provides evidence that a GDF will provide a safe means by which to dispose of radioactive waste (RWM 2016b; Swift 2017). The body of knowledge that is required in order to produce and support this document is vast and detailed, and this project aims to advance the understanding of one small aspect of it: how particle size affects the behaviour and transport of bentonite colloids.

The suitability of bentonite for use as buffers in engineered barrier systems, particularly those in crystalline rock, has been investigated since the 1970s (Birgersson *et al*. 2017). As was discussed above, clay colloids produced from the erosion of this backfill may enhance the movement of radionuclides in the far-field environment if their binding is irreversible or the desorption rate is slow (Sherriff *et al*. 2016). The aim of this project is to develop a greater understanding of how particle size affects the behaviour and transport of bentonite colloids. This is important because size can influence the transport, diffusion, surface structure, sorption capacity, stability, reactivity and sedimentation properties of colloids, and influence their interactions with radionuclides (Birgersson *et al*. 2017; Missana *et al*. 2018; Norrfors *et al*. 2015). The colloids produced by the erosion of a bentonite buffer are unlikely to be uniform in size, but fractionation can occur naturally in the environment, for example by filtration through crushed material in a fracture, so conditions in the far-field of a GDF may cause differently-sized colloids to be transported differently depending on their size (Norrfors *et al*. 2016).

In order to achieve the aim of investigating how particle size affects colloid transport and behaviour, three or more suspensions of bentonite particles with distinct, narrow size distributions will be produced, used in flow experiments where the conditions are relevant to the far-field environment, and then batch experiments will be used to examine how radionuclides sorb onto and desorb from the colloids. Existing methodologies will be critiqued, and new ones developed if necessary when the fractionation and characterisation techniques present unexpected challenges. As was discussed above, a significant amount of research already exists that investigates bentonite colloids in relation to nuclear waste disposal, and relevant examples are listed here:

- Norrfors *et al*. (2016) produced seven different-sized clay dispersions, spiked them with radionuclides and used them for batch adsorption experiments and geochemical speciation modelling, but their size distributions were broad, and no flow experiments were conducted.
- Missana *et al*. (2008) produced and characterised FEBEX colloids, mixed them with Eu and Pu, and passed them through a fracture, but this study did not use different size fractions.
- Vilks & Bachinski (1996) passed natural and synthetic colloids through a piece of fractured granite. The natural colloids contained some clay, but not specifically montmorillonite, and although the size distributions were characterised, the impact size had on colloid behaviour was not investigated in depth.

This project aims to improve upon the work of Norrfors *et al*. (2016) by conducting flow experiments, the work of Missana *et al*. (2008) by producing different size fractions and by using MX80 instead of FEBEX bentonite (as discussed in section 2.1, MX80 bentonite is

currently favoured over FEBEX for use in EBS barriers (Cui 2017)), and the work of Vilks & Bachinski (1996) by using bentonite colloids.

This review of the literature indicates that if the aims of this project can be achieved, they will help to develop the currently rather limited understanding about how the size of bentonite colloids affects their transport and sorption behaviours under conditions relevant to those of the far-field environment of a GDF.

2.5 Conclusions

The construction of a GDF represents a time, resource and cost-intensive undertaking, with potential consequences for the health of future generations and their environment if its integrity is not maintained. It is therefore vital that every aspect of its design is understood as thoroughly as possible. This project aims to contribute to this by investigating the effect particle size has on the behaviour and transportation properties of bentonite colloids by using different-sized fractions of clay colloids in flow experiments, and through investigating their interactions with radionuclides by means of a range of experimental techniques.

2.6 References

Abbas, Z. *et al.*, 2008. Size-dependent surface charging of nanoparticles. Journal of Physical Chemistry C, 112(15), pp.5715–5723.

Alexander, W.R., Reijonen, H.M. & McKinley, I.G., 2015. Natural analogues: studies of geological processes relevant to radioactive waste disposal in deep geological repositories. Swiss Journal of Geosciences, 108(1), pp.75–100.

Alonso, U. *et al*., 2006. Role of inorganic colloids generated in a high-level deep geological repository in the migration of radionuclides: Open questions. Journal of Iberian Geology, 32(1), pp.79–94.

Beard, R. & Roberts, D., 2012. State-of-the-art report on the treatment of colloids and related issues in the long-term safety case, UK: NDA RWMD.

BELBaR, 2016. Summary of the BELBaR project, The BELBaR Project. EU: BELBaR.

Bergaya, F. & Lagaly, G., 2013. General introduction: Clays, clay minerals, and clay science 1st ed., Elsevier Inc.

Birgersson, M. *et al*., 2017. Chapter 12- Function and requirements on bentonite in repository components. In Geological Repository Systems for Safe Disposal of Spent Nuclear Fuels and Radioactive Waste. pp. 319–364.

Bouby, M. *et al*., 2011. Interaction of bentonite colloids with Cs, Eu, Th and U in presence of humic acid: A flow field-flow fractionation study. Geochimica et Cosmochimica Acta, 75(13), pp.3866–3880.

Bradbury, M.H. & Baeyens, B., 2005. Modelling the sorption of Mn(II), Co(II), Ni(II), Zn(II), Cd(II), Eu(III), Am(III), Sn(IV), Th(IV), Np(V) and U(VI) on montmorillonite: Linear free energy relationships and estimates of surface binding constants for some selected heavy metals and actinide. Geochimica et Cosmochimica Acta, 69(4), pp.875–892.

Chapman, N. & Hooper, A., 2012. The disposal of radioactive wastes underground. Proceedings of the Geologists' Association, 123(1), pp.46–63.

Cui, Y.J., 2017. On the hydro-mechanical behaviour of MX80 bentonite-based materials. Journal of Rock Mechanics and Geotechnical Engineering, 9(3), pp.565–574.

DECC, 2014. Implementing Geological Disposal: A Framework for the long-term management of higher activity radioactive waste, UK: DECC.

Delage, P., Cui, Y.J. & Tang, A. M., 2010. Clays in radioactive waste disposal. Journal of Rock Mechanics and Geotechnical Engineering, 2(2), pp.111–123.

Emmerich, K., 2013. Chapter 2.13 – Full Characterization of Smectites 2nd ed., Elsevier Ltd.

Garcia-Gutierrez, M. *et al*., 2001. Solute transport properties of compacted Ca-bentonite used in FEBEX project. Journal of Contaminant Hydrology, 47, pp.127–137.

Hansen, E. & Hedstrom, M., 2013. Behaviour of montmorillonite at low ionic strength. In BELBaR first workshop, Helsinki 2013-03-07. Clay Technology AB.

Hazen, R.M. *et al*., 2013. Clay mineral evolution. American Mineralogist, 98(11–12), pp.2007–2029.

Hunter, R.J., 2001. Foundations of colloid science, Oxford: Oxford University Press.

Karnland, O., 2010. Chemical and mineralogical characterization of the bentonite buffer for the acceptance control procedure in a KBS-3 repository, Sweden: SKB.

Kotal, M. & Bhowmick, A.K., 2015. Polymer nanocomposites from modified clays: Recent advances and challenges. Progress in Polymer Science, 51 (December 2015), p.p. 127-187.

Madsen, F.T., 1998. Clay Mineralogical Investigations Related to Nuclear Waste Disposal. Clay Minerals, 33(1), pp.109–129.

Missana, T. *et al*., 2018. Analysis of the stability behaviour of colloids obtained from different smectite clays. Applied Geochemistry, 92(December 2017), pp.180–187.

Missana, T. *et al*., 2008. Role of bentonite colloids on europium and plutonium migration in a granite fracture. Applied Geochemistry, 23(6), pp.1484–1497.

Missana, T. *et al*., 2016. WP4 Partners Final report on experimental results on clay colloid stability, EU: BELBaR.

Missana, T. & Adell, A., 2000. On the Applicability of DLVO Theory to the Prediction of Clay Colloids Stability. Journal of colloid and interface science, 230, pp.150–156.

Missana, T., Alonso, U. & Turrero, M.J., 2003. Generation and stability of bentonite colloids at the bentonite/granite interface of a deep geological radioactive waste repository. Journal of Contaminant Hydrology, 61(1–4), pp.17–31.

Missana, T. & Geckeis, H., 2006. The CRR Final Project Report Series II: Supporting Laboratory Experiments with Radionuclides and Bentonite Colloids, Switzerland: Nagra.

Möri, A. *et al*., 2003. The colloid and radionuclide retardation experiment at the Grimsel Test Site: Influence of bentonite colloids on radionuclide migration in a fractured rock. Colloids and Surfaces A: Physicochemical and Engineering Aspects, 217(1–3), pp.33– 47.

Nagra, 2004. The CRR final project report series 1: Description of the Field Phase-Methodologies and Raw Data, Switzerland: Nagra.

Nessa, S.A. *et al*., 2007. Measurement of pH of the Compacted Bentonite under the Reducing Condition. Memoirs of the Faculty of Engineering, Kyushu University, 67(1), pp.25–31.

Norrfors, K.K., 2015. Stability and sorption capacity of montmorillonite colloids. Doctor of Philosophy (PhD) in the School of Chemical Science and Engineering. KTH Royal Institute of Technology, Sweden.

Norrfors, K.K. *et al*., 2015. Montmorillonite colloids: I. Characterization and stability of dispersions with different size fractions. Applied Clay Science, 114, pp.179–189.

Norrfors, K.K. *et al*., 2016. Montmorillonite colloids: II. Colloidal size dependency on radionuclide adsorption. Applied Clay Science, 123, pp.292–303.

Okumura, M. et al., 2018. Radiocesium interaction with clay minerals: Theory and simulation advances Post – Fukushima. Journal of Environmental Radioactivity, 189 (November 2017), pp.135–145.

Ozsoy, O. & Bekbolet, M., 2018. Surface interactions of Cs+ and Co2+ with bentonite. Environmental Science and Pollution Research, 25(4), pp.3020–3029.

Pusch, R., 1999. Clay colloid formation and release from MX-80 buffer. SKB Technical Report TR 99-31.

RWM, 2016. Geological Disposal: Generic Post-closure Safety Assessment, UK: RWM.

RWM, 2018. Government launches new policy to deal with radioactive waste. Available at: https://www.gov.uk/government/news/government-launches-new-policy-to-deal-with-radioactive-waste. Last accessed January 2019.

Ryan, J.N. & Elimelech, M., 1996. Colloid mobilization and transport in groundwater. Colloids and Surfaces A: Physicochemical and Engineering Aspects, 107(95), pp.1–56.

Schatz, T. *et al.*, 2015. WP2 partners final report on bentonite erosion, EU: BELBaR.

Shelton, A. *et al.*, 2016. WP1 Synthesis Report: Colloids and related issues in the long term safety case, EU: BELBaR.

Sherriff, N. *et al.*, 2015. BELBaR Deliverable: Understanding of Radionuclide Colloid Interaction, EU: BELBaR.

Sherriff, N. *et al.*, 2016. WP3 partners final report on experimental results on micro- to macroscale colloid rock interaction and colloid radionuclide interaction, EU: BELBaR.

Suttiponparnit, K. et al., 2011. Role of Surface Area, Primary Particle Size, and Crystal Phase on Titanium Dioxide Nanoparticle Dispersion Properties. Nanoscale Research Letters, 6(27), pp.1–8.

Swift, P.N., 2017. Chapter 15- Safety assessment for deep geological disposal of high-level radioactive waste. In Geological Repository Systems for Safe Disposal of Spent Nuclear Fuels and Radioactive Waste. Elsevier Ltd, pp. 451–473.

Tombácz, E. & Szekeres, M., 2004. Colloidal behaviour of aqueous montmorillonite suspensions: The specific role of pH in the presence of indifferent electrolytes. Applied Clay Science, 27(1–2), pp.75–94.

Tripathy, S., Sridharan, A. & Schanz, T., 2004. Swelling pressures of compacted bentonites from diffuse double layer theory. Canadian Geotechnical Journal, 450, pp.437–450.

Vilks, P. & Bachinski, D.B., 1996. Colloid and suspended particle migration experiments in granite fracture. Journal of Contaminant Hydrology, 21, pp.269–279.

Yukselen, Y. & Kaya, A., 2003. Zeta Potential of Kaolinite in the Presence of Alkali, Alkaline Earth and Hydrolyzable Metal Ions. Water, Air and Soil Pollution, 145, pp.155–1

Chapter 3

Instrumentation

Chapter 3: Instrumentation

3.1 Dynamic Light Scattering (DLS)

Dynamic Light Scattering (DLS) is a rapid and inexpensive means by which to measure the size distribution of particles <10 µm suspended in a liquid medium (Malvern Instruments 2004). It is sometimes referred to as Quasi-Electric Light Scattering or Photon Correlation Spectroscopy (PCS), and where it was listed under one of these names in literature referenced in this project, it is referred to by the name used in the original document. Along with zeta potential, a means by which to determine the surface charge of suspended particles, it is an important tool for the characterisation of nanoparticles, and a Malvern Zetasizer Nano ZS was used to measure both (Bhattacharjee 2016; Malvern Instruments 2004).

According to the theory of Brownian motion, particles suspended in a liquid move randomly when they collide with the molecules of the liquid itself, and the speed of this movement is dependent on the size of the particle: smaller particles undergo more rapid Brownian motion. The speed of the Brownian motion is measured by the instrument and is defined by the translational diffusion coefficient, which, when entered into the Stokes-Einstein equation along with the viscosity of the solvent, the temperature of the sample, and Boltzmann's constant, can be used to calculate the hydrodynamic diameter of the particles in the sample.

The Stokes-Einstein equation is shown in Equation 1:

$$d(H) = \frac{kT}{3\pi\eta D}$$

Equation 3.1

Where *d(H)* is the hydrodynamic diameter, *D* is the translational diffusion coefficient, *k* is Boltzmann's constant, *T* is the temperature, and *η* is the viscosity.

(Malvern Instruments 2000).

DLS has been used in this project to obtain a fast and inexpensive estimate of particle size distribution, which is advantageous when testing large numbers of samples. However, as was mentioned above, the hydrodynamic diameter of particles in suspension is determined, which is defined by the manufacturer, Malvern Instruments (2000), as "the diameter of a sphere that has the same translational diffusion coefficient as the particle". Given the flat, plate-like nature of clay particles, their size cannot be reliably described by one number alone. Additionally, it is not possible to determine from DLS whether particles or agglomerates of smaller particles are being measured: for this, an imaging technique such as electron microscopy is necessary (see section 3.3). However, as discussed in Chapter 4, obtaining accurate size measurements of nanoparticles is difficult; it is necessary to use a combination of different, imperfect techniques to try to characterise them as well as can possibly be achieved; so DLS was used despite these shortfalls.

The DLS data used and discussed in this project has been averaged from at least three measurements. The settings used were a value of 0.01 for the absorption, and a refractive index of 1.5. These values account for the different optical properties of different materials.

Absorption needs to be estimated to within an order of magnitude, and information provided by the manufacturer was used to inform the value chosen. Malvern Instruments do not recommend a specific refractive index for bentonite, but suggest somewhere in the range of 1.48-1.64 for montmorillonite, and 1.469-1.544 for different silica minerals, so 1.5 was selected as it fell within both of these ranges (Malvern Instruments 2007).

DLS sizing data can be presented in three different ways: as intensity, number, or volume distributions. Each of these divide the particles in the sample into different size 'bins' or groups, but they then characterise them in different ways: the intensity distribution indicates how much light is scattered by the particles in the different bins, the number distribution indicates how many particles are in the different groups, and the volume distribution shows the total volume of each of the bins. The intensity distribution is what is measured by the instrument, and is therefore the default distribution and the one from which the number and volume distributions are calculated, but that does not make it inherently better than any of the others: provided that only like measurements are compared (*i.e.* only number to number and not the number of one sample to the volume of another, for example) they are all valid measurements. The intensity distribution emphasises the contribution of large or reflective particles in the sample, and the number distribution the smaller ones (Malvern Instruments 2017). However, in order for the volume and number distributions to be calculated reliably, it is important to have accurate values for the absorption and refractive indices. As was mentioned above, it was not possible to get a single value for the refractive index of the MX80, but rather two separate ranges. This is probably because it is a natural, heterogeneous material consisting of many different minerals, and so its surface properties cannot be summarised by a single number. Therefore, the majority

of the DLS data used in this project is displayed using the intensity distribution, as it does not require a value for the refractive index or absorption indices. Some number distributions are presented in Chapter 4, but they are shown with the caveat that they are for representative purposes only, in order to highlight the presence of significant numbers of small particles in the samples, and that they are not quantitative, and the data contained within them is unlikely to be accurate.

3.2 Zeta potential

Zeta potential is a measurement of the surface charge of nanoparticles (Bhattacharjee 2016) and in this project was determined using a Malvern Zetasizer ZS, the same instrument that was used for DLS.

The Coulombic forces between the particles in suspension can be determined by measuring the zeta potential. If the surface of a particle holds a charge, then a layer of strongly bound counter ions will accumulate close to its surface. This is the 'Stern layer'. Outside of this, the counterions also bond, but more weakly, and the layer is more diffuse. Together, these form what is termed the 'electrical double layer'. Within the more weakly-bound outer layer is a plane called the 'surface of hydrodynamic shear'. Inside of this plane, the particle and the counter ions behave as one unit, so if the particle moves, the counter ions do too. Outside of the plane, they move independently. The potential across this plane is the 'zeta potential'. The structure of this double layer is shown in Figure 3.1. The more positive or more negative the zeta potential of a sample, the more likely it is to remain discrete in solution, because more strongly opposing charges on the particles results in greater repulsion and a reduced

chance of them agglomerating. If a suspension has a zeta potential below -30 mv or above +30 mv, it can generally be regarded as stable (Malvern Instruments 2004).

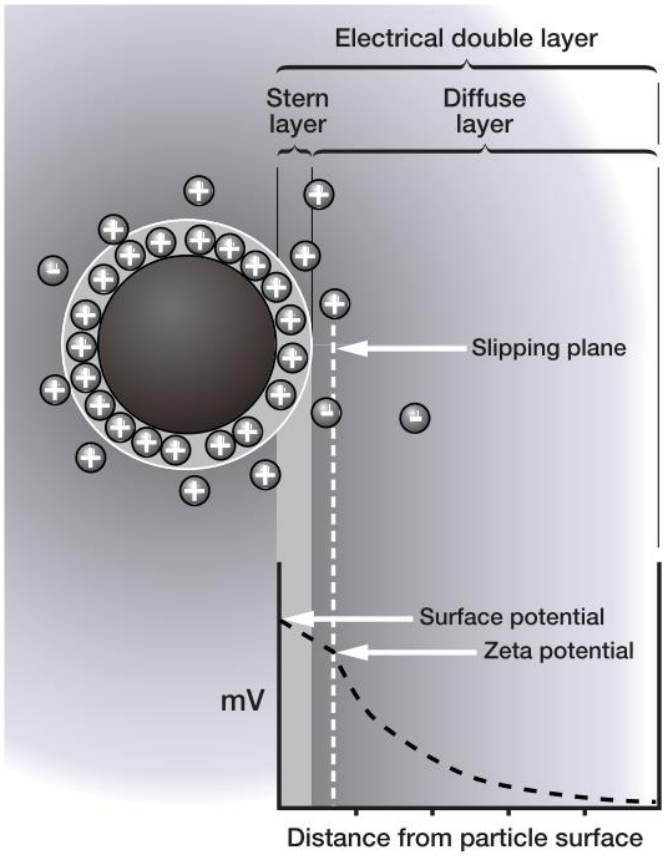

Figure 3.1. A diagram showing the tightly-bound Stern layer and more weakly bound outer layer, which together form the electrical double layer. The potential difference between the Stern layer and the surrounding medium is the 'zeta potential', and measuring it can provide information about the likely stability of the colloidal suspension. Malvern Instruments 2004. Copyright Malvern Panalytical.

The nature of the charge on clay colloids is pH-dependent; the faces hold a permanent negative charge, but the edges have a positive charge at low pH levels, and more negative charge at pH>6.5 (Tombácz & Szekeres 2004). Therefore, it may be expected that bentonite colloids are more stable at a higher pH, because Coulombic repulsion occurs between the negative faces and edges, reducing the likelihood of them sticking together. It is therefore expected that a higher pH would lead to a more negative zeta potential, greater repulsion

between the colloids, and therefore greater stability. An investigation into this is described in Chapter 4.

Zeta potential of a suspension is calculated by measuring the electrophoresis of the colloids, which is how, upon application of an electric field, a charged particle moves relative to the liquid in which it is suspended. The sample of interest is placed into a cell with two electrodes, and when a potential is applied across it, the particles move towards the electrode that holds the opposite charge. This movement is resisted by the viscosity of the liquid suspending the particles. When the attractive force equals the resisting viscosity, the velocity of the particle is constant, and is called the 'electrophoretic mobility'. By measuring this, it is then possible to calculate the zeta potential for the particles in the sample.

Three measurements were taken for each of the samples that underwent zeta potential measurements, and the material parameters that were used were the same as were used for the sizing measurements that are discussed above in section 3.1.

3.3 Environmental Scanning Electron Microscopy (ESEM)

Scanning Electron Microscopy (SEM) allows particles a few hundred nanometres in size to be viewed and imaged. These images provide information about the morphology of the particles and can be used in conjunction with image analysis software to determine the size distribution of the sample. Environmental Scanning Electron Microscopy (ESEM) differs from SEM in that it can be used to observe specimens in their natural state, *i.e.* wet, or uncoated, but the operating principle remains the same. However, ESEM was used in this project not

because of the nature of the samples, but because the instrument, a Philips XL30 ESEM-FEG, had the best resolution of any of the SEMs available.

A source of electrons, such as a tungsten filament, produces and accelerates a narrow (~10 nm wide) beam of electrons and directs them through a series of lenses and onto the sample of interest. They scatter off its surface and into a detector, and a signal is produced which then forms a raster image of the specimen on a monitor. This can be observed and photographed, if a suitable camera is incorporated into the system (Egerton 2005).

Being able to observe the nature of the samples, visually investigating whether they are actually agglomerates of smaller particles, for example, can provide valuable insights which measuring them via a method such as DLS cannot. However, the size analysis is conducted on at most hundreds of particles, rather than the thousands that a technique such as DLS would measure, and so size estimation may not be reliable if the sample is heterogeneous (CPS Instruments Europe N.D.). In this project, ESEM was used to observe the morphology of the bentonite colloids and to investigate their non-spherical nature and to produce images of the samples. No size analysis was carried out due to concerns that even at the maximum magnification, significant amounts of nanoparticles could not be focused upon and imaged, which risked discounting an important fraction of the particles.

The samples were prepared by taking the fractions that resulted from the filtration of clay suspensions in Chapter 4, and then placing a drop of each filtrate onto a platinum-backed glass disk, before coating the sample in either gold or more platinum. This makes the sample conductive and prevents an accumulation of charge, which would affect the image quality.

3.4 Transmission Electron Microscopy (TEM)

Like SEM, Transmission Electron Microscopes (TEMs) work by directing a beam of electrons at a sample and focusing it using a series of lenses. However, where SEMs measure the electrons that scatter off the surface of the sample, TEMs detect the electrons that pass through it. TEM can therefore be used to probe the atomic structure of materials, and have better resolution than SEMs (Kogure 2013).

The TEM images presented in Chapter 4 were provided by a colleague from the university. In addition to visual examination, size analysis was done on the images using the ImageJ software package in order to highlight the difference in size distribution between samples, and this was used in conjunction with DLS and ESEM data to characterise colloidal size distributions.

The samples were prepared by taking the fractions that resulted from the filtration of clay suspensions in Chapter 4, placing a drop onto a TEM grid, and leaving it to dry. They were then coated in a carbon film before being placed into the chamber of the instrument and imaged.

3.5 X-ray Fluorescence (XRF)

X-Ray Fluorescence spectroscopy (XRF) provides rapid qualitative and quantitative analysis of materials. The sample is irradiated by an X-Ray source, exciting the electrons within it. During the relaxation process these electrons drop back down energy levels, releasing photons characteristic of that element. Their energy and intensity are measured by the detector and used to determine the concentration by weight of the elements. It is a non-destructive technique, so the sample may be retained for further experimentation.

XRF was used during the characterisation of the MX80 in Chapter 4 to determine its elemental composition. The results indicated that the bentonite contained around 4 % iron, which was indicative of the presence of nontronite, an iron-rich smectite (Karnland 2010).This was used to inform the choice of XRD spectrometer that was also used for characterisation (see below).

3.6 X-ray Diffraction (XRD)

X-Ray Diffraction is used to investigate the structure of crystalline materials. X-Rays are produced by firing accelerated electrons at a target, causing it to emit X-rays. These are directed at a sample and are then diffracted by its crystal lattice. By measuring the intensity and angles of this scatter, it is possible to gain a better understanding of the crystal structure, specifically the dimensions of their unit cells and the position and atomic number of the atoms within them.

XRD was utilised during the work described in Chapter 4, when it was used to characterise the structure of the bentonite. The high iron content identified by the XRF meant that it was necessary to use a Bruker D2 diffractometer with a cobalt tube, rather than the more standard copper, because the X-Rays produced by a copper tube make the iron in the sample fluoresce. This would have resulted in a very high background, which would have made the peaks harder to distinguish, but the use of a cobalt tube eliminates this issue.

3.7 Atomic Force Microscopy (AFM)

Atomic Force Microscopy (AFM) is used to image the topography of materials of interest at sub-nanometer resolutions, and when used in conjunction with image analysis software, it can be used to investigate particle size distribution (Doucet *et al*. 2005). A sharp tip, attached to a cantilever, is passed over the sample, and the topography of the surface of the sample moves the cantilever up and down. This vertical movement is measured by a detector, and as the probe moves back-and-forth across the sample in a grid, this movement is used to form a raster image of the differing heights of the material (Brown *et al*. 2013).

However, the nature of the measurement technique leads to an overestimation of the horizontal dimensions of the particles (Doucet *et al*. 2005). Figure 3.2 demonstrates that in order for the wider part of the tip to clear the particle, the point follows an arc across it (West & Starostina 2002). This results in the tip recording elevation at the edges of the particles that may not be correct.

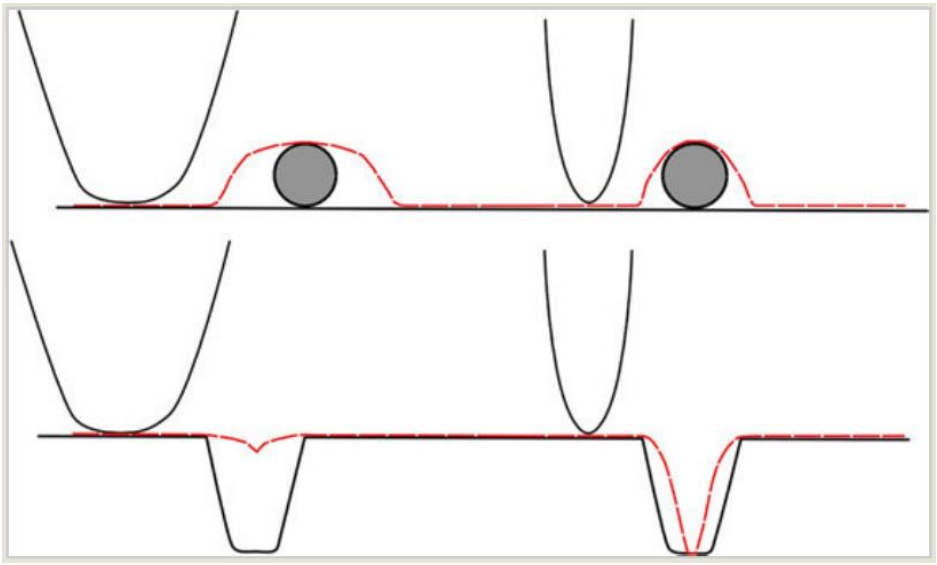

Figure 3.2. Visualisation of how the shape of an AFM probe induces errors in the measurement of the lateral dimensions of particles by producing wider profiles of extruding features and narrower profiles of dips in the surface (Eaton & West 2010). Copyright Oxford Publishing Limited.

This is not an issue for spherical particles because measuring their height gives a reliable estimate of their dimensions in the lateral plane. However, the 'plate-like' nature of clay colloids is far removed from the spherical ideal. AFM therefore gives a reliable estimate of their height, but not of their other dimensions in the lateral plane. However, as is discussed in both section 3.1 and Chapter 4, obtaining size distributions of nanoparticles is difficult; there is no single optimal method for doing so; and it is therefore necessary to characterise the suspensions in as many ways as possible and to take all of the results into account.

The AFM images in Figures 4.33a and b were obtained through collaboration with researchers at the University at Bristol who have pioneered the use of 'high-speed' AFM, a technique that uses small cantilevers and high-frequency detection systems to measure rapid tip movement and provides faster imaging of samples than conventional AFM without compromising on resolution or damaging the samples.

The samples were prepared by taking the filtered clay fractions that were produced in Chapter 4, diluting them by a factor of 2 million, and depositing them onto freshly cleaved mica sheets that were glued onto microscope slides. After drying, they were transported in new, clean petri dishes. Figures 4.33a and b are included to highlight how non-spherical the clay platelets are: a property that has made characterising their size distribution more complex.

3.8 Nephelometry

In a nephelometer, light scattering is used to measure the concentration of particles suspended in a liquid medium. A light beam (such as a laser) is directed at a sample, and a

photodetector measures the amount of light that scatters off the particles at 90 ° to the incident beam. The higher the concentration, the greater the scatter, although some particle characteristics such as reflectivity, shape and size may also influence the scattering measurement (Omar & MatJafri 2009). However, if the concentration of particles in the sample reaches too high a level, the output may begin to drop as the light may be blocked completely by the sample, rather than scattering and passing through it.

Small, portable nephelometers exist which measure the concentration of a single sample, but a flow-through instrument capable of recording changes in concentration over time was required and constructed for this application. This is discussed in detail in Chapter 5. This custom-built nephelometer was incorporated into a flow system, which was used to pass bentonite colloids across and through samples of rock relevant to those likely to form the host rock for a GDF, measure their change in concentration over time, and produce breakthrough curves. It was also used to measure the concentration of colloid suspensions after filtration by producing a standard curve using samples of known concentration and using this to calculate the colloid content of the filtered samples.

3.9 Inductively Coupled Plasma Mass Spectrometry (ICP-MS)

Inductively Coupled Plasma Mass Spectrometry (ICP-MS) is used to determine the chemical composition of solutions. It is rapid, works over a wide range of concentrations, and may be used to identify different isotopes in addition to elemental species. The sample is first pumped into a nebuliser where it is mixed with argon gas and converted into an aerosol. This mixture then enters a spray chamber, before being injected into a plasma torch. This

generates a beam of cations, which are then directed into a mass spectrometer, where they are separated according to their mass before reaching an ion detector. This generates a corresponding electrical signal, which is compared to known calibration standards by the data analyser in order to determine the amount of each elemental species present (Thomas 2013).

ICP-MS was used in Chapter 7 to determine the cation content of samples that were used in sorption and desorption experiments. Norrfors *et al*. (2015) used ICP-OES to determine the concentration of colloids remaining after centrifugation by measuring key cations in the sample and calculating how much bentonite remained by relating the cation concentration to the theoretical structural formula of the clay. A similar method was trialled in the project, where ICP-MS was used to try and estimate the colloid concentration remaining in suspension after the samples were filtered through differently-sized membranes, but it was unsuccessful because it was not possible to use a digestion method with the instrument available, and nephelometry was used instead (see Chapters 4 and 5).

The samples were acidified with ultrapure 2 % HNO_3 and then passed through 0.22 µm disk filters, in order to prevent any clay agglomerates from blocking the nebuliser.

3.10 References

Bhattacharjee, S., 2016. DLS and zeta potential - What they are and what they are not? Journal of Controlled Release, 235, pp.337–351.

Brown, B.P. *et al*., 2013. Opportunities in High-Speed Atomic Force Microscopy. Small, 9(19), pp.3201–3211.

CPS Instruments Europe, Comparison of Particle Sizing Methods. Available at: http://www.cpsinstruments.eu/pdf/Compare Sizing Methods.pdf. Last accessed January 2019.

Doucet, F.J., Maguire, L. & Lead, J.R., 2005. Assessment of cross-flow filtration for the size fractionation of freshwater colloids and particles. Talanta, 67(1), pp.144–154.

Eaton, P. & West, P., 2010. Chapter 6: AFM image artefacts. In Atomic Force Microscopy. Oxford: Oxford Scholarship Online, pp. 1–23.

Egerton, R.F., 2005. Chapter 5: The Scanning Electron Microscope. In Physical Principles of Electron Microscopy. New York: Springer Science and Business Media Inc., pp. 125–126.

Karnland, O., 2010. Chemical and mineralogical characterization of the bentonite buffer for the acceptance control procedure in a KBS-3 repository, Sweden: SKB.

Kogure, T., 2013. Chapter 2.9- Electron Microscopy. In Developments in Clay Science. Elsevier Ltd., pp. 275–317.

Malvern Instruments, 2000. Dynamic Light Scattering: An Introduction in 30 Minutes. Malvern Instruments Ltd.

Malvern Instruments, 2017. Intensity - Volume - Number. Malvern Instruments Ltd.

Malvern Instruments, 2007. Sample Dispersion and Refractive Index Guide. Malvern Instruments Ltd.

Malvern Instruments, 2004. Zetasizer Nano Series User Manual. Malvern Instruments Ltd.

Norrfors, K.K. *et al.*, 2015. Montmorillonite colloids: I. Characterization and stability of

dispersions with different size fractions. Applied Clay Science, 114, pp.179–189.

Omar, A.F. Bin & MatJafri, M.Z. Bin, 2009. Turbidimeter design and analysis: A review on optical fibre sensors for the measurement of water turbidity. Sensors, 9(10), pp.8311–8335.

Thomas, R., 2013. Practical Guide to ICP-MS 3rd Edition., Boca Raton, Florida: Taylor & Francis Group.

Tombácz, E. & Szekeres, M., 2004. Colloidal behaviour of aqueous montmorillonite suspensions: The specific role of pH in the presence of indifferent electrolytes. Applied Clay Science, 27(1–2), pp.75–94.

West, P. & Starostina, N., 2002. A Guide to AFM Image Artefacts. New Zealand: Pacific Nanotechnology, pp.1–12.

Chapter 4

Production of the bentonite colloids

Disclaimer: TEM images were provided by Dr Xianjin Cui of the FENAC Laboratory, University of Birmingham.

AFM images were supplied by Dr Loren Picco of the University of Bristol.

Chapter 4: Production of bentonite colloids

4.1 Introduction

The main aim of this chapter was to produce and characterise three or more suspensions of bentonite particles with distinct, narrow size distributions, suitable for use in the flow experiments in Chapter 6. For this aim to have been met, the suspensions had to have the following characteristics:

- The size distribution of the colloids in suspension should be as narrow as possible, distinct from each other, and their production repeatable.
- They should remain stable for a minimum of 48 hours to allow them to be used in the flow experiments without the size distribution changing significantly.

In line with Aims 2 and 3, new methodologies were developed, and existing ones critiqued when the fractionation and characterisation techniques used during the work described in this chapter presented unexpected challenges.

Differently-sized colloids may have different surface structures, which can affect properties such as stability and sorption capacity (Norrfors *et al*. 2015). Although colloids produced in an EBS are unlikely to have a narrow size range, it is important to investigate the influence colloid size has on their behaviour because filtration effects in the environment can cause fractionation naturally. Granite fracture systems may contain fracture-filling material (FFM), such as crushed bedrock. Small colloids may become trapped in small holes or narrow fissures in the FFM and are therefore more likely to interact with it, reducing their movement. If no FFM is present and the fracture is clean, the groundwater flows faster and laminar flow may occur, where larger colloids move more rapidly than smaller colloids of the

same density, separating them out. Therefore, the conditions in the far-field of an EBS can cause size fractions to be transported differently depending on their size. The better-defined the colloidal size fractions are, the easier the influence of this effect will be to isolate and investigate (Norrfors *et al*. 2016).

Relevant examples of colloid production and characterisation were identified in the literature and are compiled below in Table 4.1. Some are natural colloids present in the environment rather than bentonite ones, but they were included because the methodology was relevant.

Table 4.1. A tabulated summary of the colloid fractionation methods described in the literature, along with the size distribution of the colloids produced (if given), and any relevant notes on their relevance to this application.

Author	Fractionation method	Size distribution characterisation method	Size range and error (if given)	Comments
Bouby *et al*. 2008	AsFlFFF (Asymmetric Flow Field-Flow Fractionation)	AsFlFFF	30-200 nm	-
Degueldre *et al*. 1989	Cross-flow diaultrafiltration	TEM	40-1000 nm	Errors induced by nucleation, aggregation, disaggregation, decomposition and artefact production.
Degueldre *et al*. 1996	Membrane filtration	Single particle analysis (a counting unit on an SEM)	Colloids occurring in the natural groundwaters are 10-1000 nm, does not give values for individual fractions	Resolution limited by sample preparation for SEM, and quality of microscope and counting unit. Gel forms on membranes, changing cut-off points.
Doucet *et al*. 2005	Cross-flow filtration	SEM and AFM	Size classes were >0.45, 0.1–0.45 and <0.1 µm, but every fraction contained particles <50 nm, even the retentates.	All fractions contained particles <50 nm, even those that should only have retained much larger ones

Michot *et al*. 2004	Centrifugation	TEM (The sizing software is not given, but measured particles according to their longest dimension because of their irregular shapes)	Average sizes of 400, 290 and 75 nm	Only measured 500 particles for each sample.
Missana *et al*. 2003	Sieving, settling, centrifugation	PCS and SEM (intensity size distribution)	Average size of 300 nm, but aggregates composed of ~50 nm particles were observed	Inexpensive, can centrifuge relatively large volumes due to low g-force needed. Only one size fraction.
Missana & Geckeis 2006	Washing and centrifugation	PCS (intensity size distribution)	235 ± 90 nm in the intensity size distribution, and a peak of ~70 nm in the number size distribution	Inexpensive, can centrifuge relatively large volumes due to low g force needed. Only one size fraction.
Missana *et al*. 2008	Washing and centrifugation	PCS (does not state which distribution was used)	250±50 nm	States that the method produces very reproducible colloid sizes. Remains within the starting size distribution for several days.

Missana *et al*. 2016	Centrifugation	PCS (intensity size distribution)	300-400 nm	-
Möri *et al*. 2003	Washing and centrifugation	PCS (does not state which distribution was used)	200-300 nm	-
Norrfors *et al*. 2015	Centrifugation	AsFlFFF, PCS (both intensity and volume distribution)	1452±632 nm 513±60 nm 404±95 nm 248±28 nm 181±28 nm 180±39 nm	Produced six distinct fractions (N.B. The paper states that seven were produced, but the seventh, which was not listed here, was made using fulvic acid and was not relevant to this project)
Sherriff 2015	Sieving, stirring, centrifugation, then ultrafiltration through 450, 200 and 100 nm filters	Ultrafiltration, visual examination with SEM but there does not seem to have been any empirical image analysis	>450, >200 and >100 nm	Relatively narrow size fractions produced. Stirring was used to aid abrasion. This may affect the number of edge sites on the colloids by making them smaller and increasing their surface area, which may affect their reactivity. SEM has been used for rough visual confirmation of colloid size distribution, rather than size analysis.
Vilks *et al*. 1991	Tangential-flow ultrafiltration	Visual evaluation using SEM	<5000, 400, 100, 50 and 10 nm	-

Most of the studies used centrifugation or variations on filtration to produce colloids, with the exception of Bouby *et al*. (2008), where Asymmetric Flow Field-Flow Fractionation (AsFlFFF) was used, in which a laminar and a cross flow separate particles out by their differing degrees of Brownian motion, which in turn is related to their size (this technique can also be used for characterisation of size distributions). A much wider range of methods have been used to characterise colloids: from PCS (another term for DLS, see section 3.1) which measures the hydrodynamic diameters of thousands of particles in suspension, through to particle counting and image analysis of only a few hundred particles on images taken using SEM or TEM, to visual confirmation that particles had been separated according to the nominal pore sizes of filters using microscopy.

Four of the investigations summarised in the table aimed to produce multiple fractions of clay colloids with narrow size distributions. Sherriff (2015) used a combination of sieving, stirring, centrifugation, ultrafiltration, and presents a chart detailing the size distribution of the different fractions, but it is not clear how this data was arrived at. Some SEM was also done, but the main focus was on imaging the colloids, and so this was more a visual confirmation of size fractionation rather than an empirical assessment. Vilks *et al*. (1991) used tangential-flow ultrafiltration, followed by SEM, to visually confirm that the particles separated by filtration matched the nominal pore sizes of the filters, but, once again, did not do any empirical size analysis. Doucet *et al*. (2005) used cross-flow filtration to fractionate the particles, and then used SEM to measure the lateral dimensions of colloids taken from a river, and AFM their height. They determined that all fractions contained particles <50 nm, even those that should only have retained much larger ones because smaller particles should have passed through the filters. This led the authors to conclude that cross-flow

filtration is not fully quantitative and may be affected by molecular weight, but also noted that it could have been due to aggregation after filtration. Finally, Norrfors *et al*. (2015) used sequential centrifugation, followed by AsFlFFF and PCS, to produce different size fractions. The mean diameter of two of the fractions listed in Table 4.1 are almost identical, but in a follow-up paper which investigated the sorption behaviour of differently-sized clay colloids, the authors explained that although the mean particle sizes differed little, the distributions were different, and the fraction that was made only in an ultracentrifuge (see Figure 4.4 for the centrifugation sequence) contained more small fractions than the one that was centrifuged at slower speeds first (Norrfors *et al*. 2016).

Of these four investigations, the one by Norrfors *et al*. (2015) was the most relevant: it provided details of the fractionation method, characterised the size distributions using multiple sizing techniques, and provided average sizes and error values. This was therefore used as a starting point (see Section 4.3.1). A slightly different filtration method from the one used by Doucet *et al*. (2005) was also tested, and this, when combined with a surfactant, was the most successful fractionation method. The characterisation that was carried out was very different, however, and is discussed in Section 4.3.3.4. This chapter details the methods that were used to produce and characterise the clay fractions and evaluates how successful they were.

4.2 Characterisation of the natural bentonite

A sample of the MX80 was prepared and characterised in order to provide a reference against which the fractionated clay samples could be compared. It was sieved to <25 µm to remove the largest of the particles, then mixed to 1 g/l with deionised water and shaken

vigorously by hand to disperse, before placing it on a shaker overnight. It was then left to stand overnight so that the largest remaining particles dropped out of suspension. A sample was removed from the top of the vial and characterised, leaving approximately 20 % of the clay-and-water mix at the bottom so that the sediment was not disturbed.

The size distribution and zeta potential of this sample were measured a short time afterwards using a Zetasizer Nano ZS, and a microscopy sample was prepared and retained for imaging. XRD can only be carried out on dry powders, so the sample was dried overnight, ground up by hand, and scanned. XRF was then used to determine the elemental composition of this powder.

When the Malvern Zetasizer Nano ZS is used for DLS (see section 3.1), the instrument can be programmed to take as many measurements as required, which it then displays individually. These may be averaged, and the result displayed in order to gain a broader overview of the size distribution trends, or viewed individually, which allows variations in the data to be observed. The majority of DLS data presented in this thesis are the averages of the measurements taken for each sample, but the results below in Figures 4.1a, b, and c show both in order to give the reader an understanding of the innate variability of the clay samples; something that is discussed throughout the project. Figure 4.1a shows the result of each of the ten individual size distribution measurements that were taken, and the data in Figures 4.1b and c is the average of those runs, shown at different magnifications.

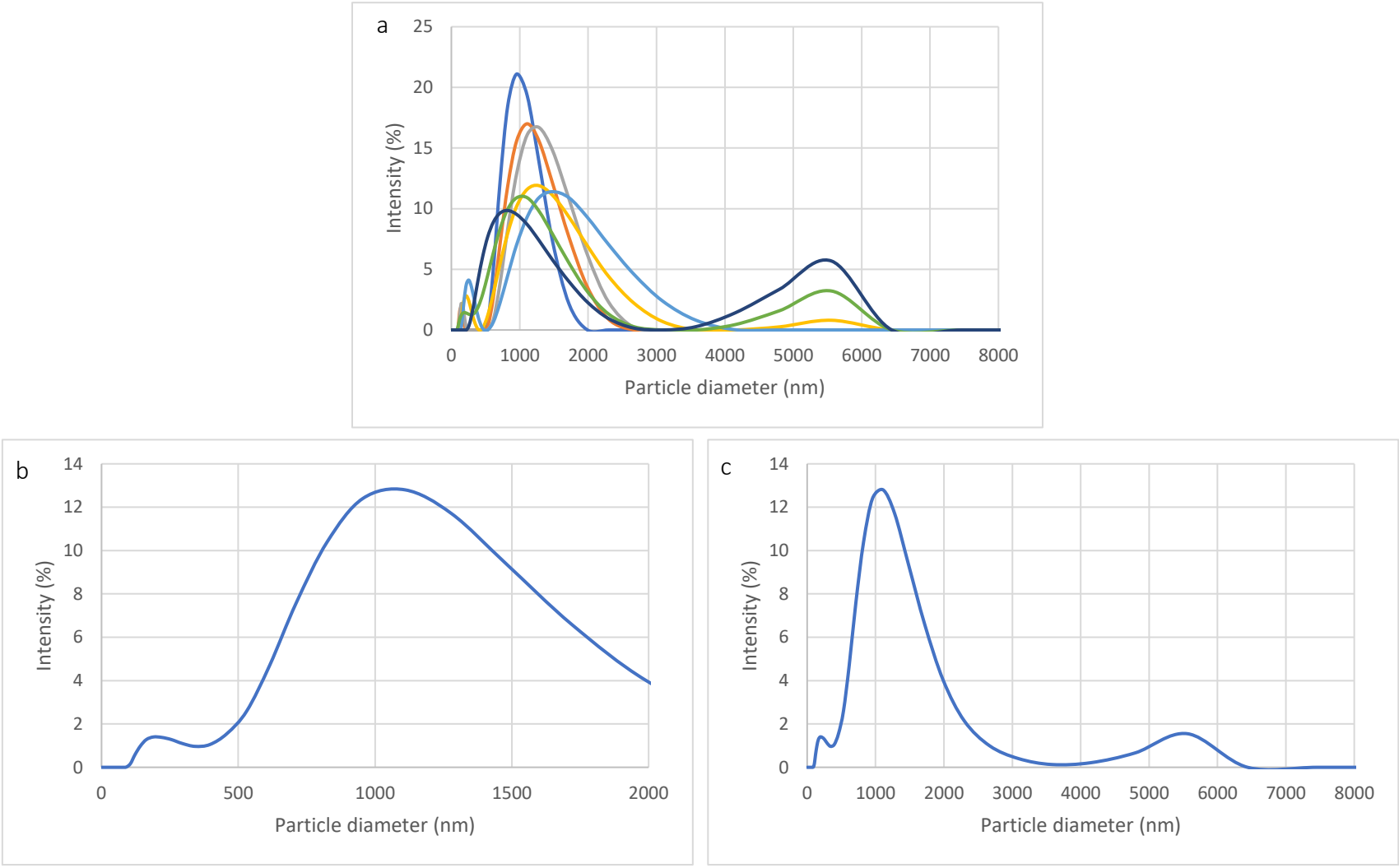

Figures 4.1a-c. The size distribution of the reference sample shown as a) the individual runs that were measured by the Malvern Zetasizer, b) the average of all of the measurements shown across the entire size range and c) focused on the colloidal size range in the average of the measurements. Average DLS measurements were used far more frequently than individual ones, but they were included here in order to give the reader an understanding of the innate variability of the clay samples; something that is discussed throughout the project.

The size distribution of the reference sample was very broad: the largest peak was at 1110 nm, but there were smaller secondary and tertiary peaks at 5500 nm and 220 nm. The majority of the particles were between 100-3500 nm in size, but Figure 4.1a shows that the distribution of particles within that range varied considerably, as the broader peaks had maxima at 10 % of the sample total, and the narrower ones up to 21 %.

The largest particles that were measured had diameters of around 6500 nm. It is possible that there was material present that was larger than 10 µm across, which is the maximum size that the Malvern Zetasizer ZS can measure, but as there were no particles detected at all above 6500 nm, they probably dropped out of suspension during the settling period (Malvern Instruments 2004). Despite the large range of particle sizes, the data met the quality criteria embedded in the Malvern software. This means that the settling process removed particles that were likely to sediment whilst the measurement was taken, thereby producing better quality datasets.

The zeta potential was measured at -23 mV. This was less negative than the -30 mV that the instrument manufacturer recommends as the dividing line between a suspension being stable or unstable, but as discussed in Chapter 3, the stability of bentonite depends on many factors besides its zeta potential. It was presented here to allow a comparison between the starting material and the fractions produced later in the chapter.

Figures 4.2a-d are images of the reference sample taken using an ESEM.

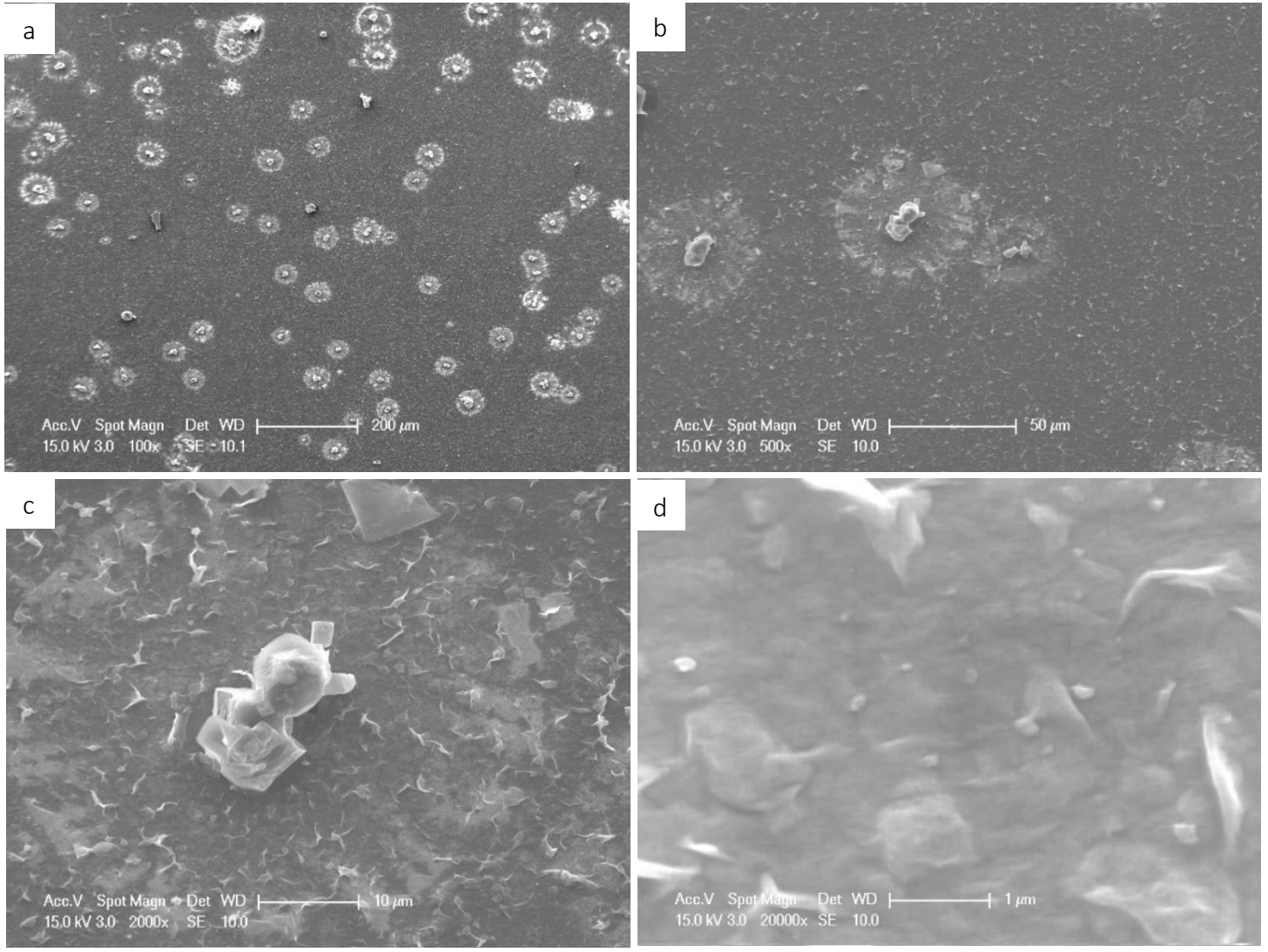

Figures 4.2a-d. Images of the reference sample, taken at a range of magnifications on an electron microscope. It Is possible to see the individual colloids in each of the images, surrounded by dried bentonite gel.

The SEM sample was prepared by taking a drop from the top of the vial containing the reference sample, which had been allowed to settle overnight, and then placing it onto a platinum-backed glass disk, before then coating the sample in gold. This made the sample conductive and prevents an accumulation of charge, which would affect the image quality.

Figures 4.2a-d are all images of the same area, but at different magnifications. The roughly circular features in Figure 4.2a consist of a clay agglomerate approximately 10 µm across, surrounded by a disk of material that appears to be the same texture as the background, but a lighter colour. This may be bentonite gel that dried after it was deposited, forming a thicker, more clearly identifiable layer.

Figure 4.2d shows an image of an area slightly to the right of the large colloid in Figure 4.2c, taken at x20000 magnification. It is possible to make out a number of colloids amongst the patterned background material, all around 100-200 nm across, but the resolution is too poor to be able to observe them in detail. Figures 4.1a-c and Figures 4.2a-d all emphasize the heterogeneity of the sample, and the images support the conclusion of the DLS results: that it contained a very wide range of particle sizes. The fact that the size distribution produced by the DLS measurements does not correspond well to what may be observed in the SEM images has a number of possible explanations. Firstly, DLS measures the hydrodynamic diameter of the particles, whereas SEM images will show their physical size. It is not that one is more correct than the other, but that they are different ways of measuring the sample, and both should be used to try and form a clearer picture of the properties of the sample. Secondly, the clay particles may behave differently depending on whether they are in suspension or not: as the solution they are in dries on the slide the inter-particle distance

reduces, potentially promoting agglomeration, which would account for larger particles being observed in the dry sample rather than the solution that underwent DLS, despite it measuring the hydrodynamic diameter, which should theoretically be larger than the physical one. The non-spherical nature of the particles is also likely to have an effect. This is discussed in more detail in Chapter 3.

Table 4.2 contains the elemental composition as measured by XRF.

Table 4.2. The elemental composition of the reference sample. It has, as would be expected of an aluminosilicate, larger amounts of silicon and aluminium in its structure, but it also contains 4 % iron, which indicates that the MX80 may contain some nontronite, an iron-rich smectite

Formula	Concentration (%)
Si	22.80
Al	8.28
Fe	4.01
Ca	1.82
Na	1.42
Mg	1.15
S	0.46
Sr	0.30
Cl	0.27
K	0.26
P	0.13

The XRF sample was prepared by leaving the settled reference sample to dry, and then breaking it up gently with a mortar and pestle in order to avoid altering its crystal structure. As would be expected of an aluminosilicate, the reference sample contains a large percentage of silicon and aluminium. It also contains around 4 % iron, which suggests that the MX80 may contain some nontronite, an iron-rich smectite (Karnland 2010). As is

discussed in Chapter 3, this influenced the decision to use an XRD instrument with a cobalt tube instead of the more standard copper. The calcium, sodium and magnesium ions present may result from the substitution of aluminium ions in the octahedral layer, or they may be components in accessory minerals.

An XRD scan is shown in Figure 4.3.

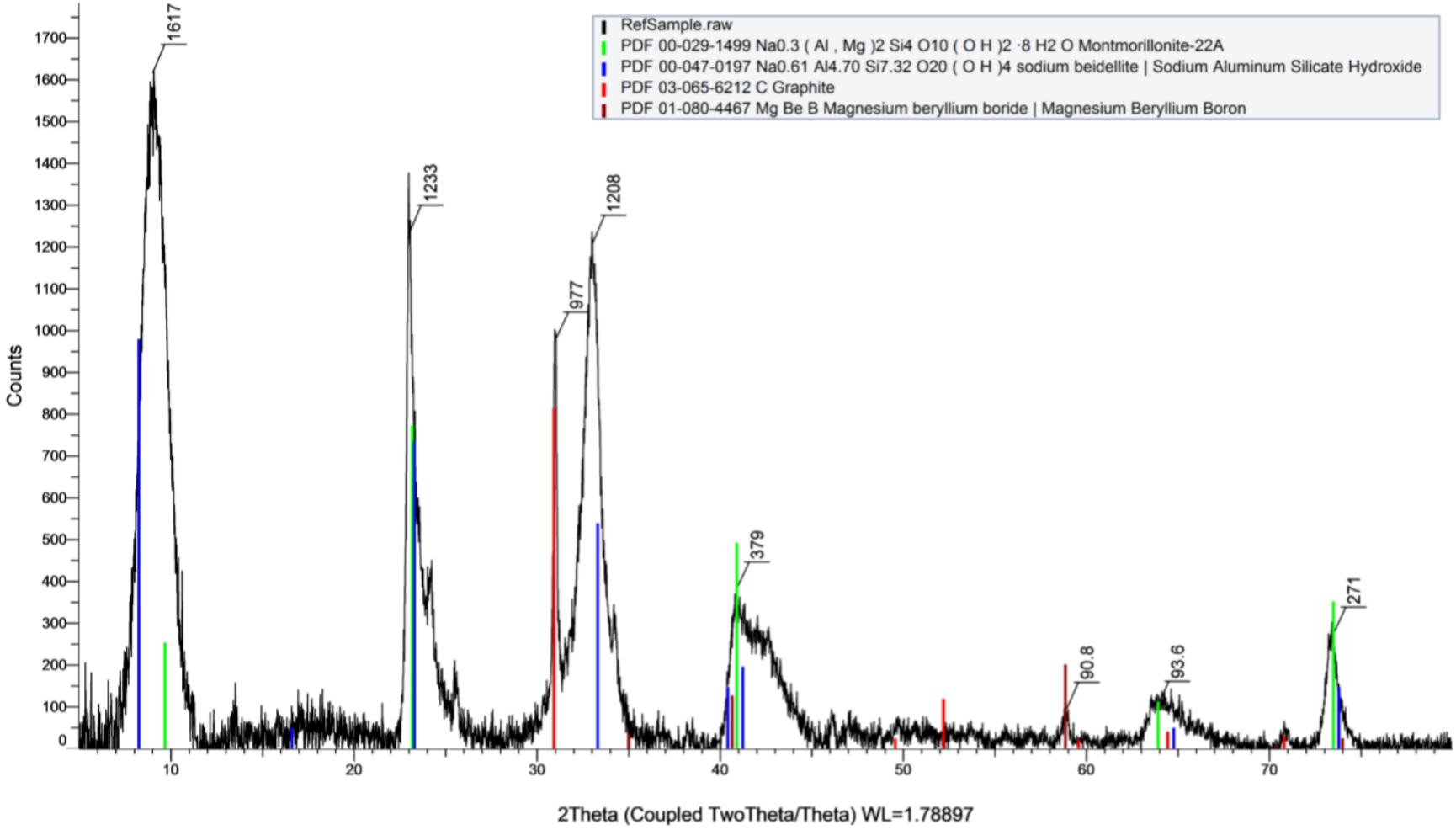

Figure 4.3. An XRD scan of the reference sample. It contains montmorillonite, the most prevalent material in bentonite, and beidellite, a common accessory mineral, but the provenance of the other two phases, graphite and magnesium beryllium boron, is unclear.

The XRD sample was prepared by leaving the settled reference sample to dry, and then breaking it up gently with a mortar and pestle in order to avoid altering its crystal structure.

The sample contained both sharp and narrow peaks and some broader ones, which suggests that multiple phases were present, as would be expected of a heterogenous natural material. Several of the peaks matched those of montmorillonite, the most prevalent material in bentonite, and others matched a beidellite, which is a common accessory mineral in this type of clay (Hunter 2001). The provenance of the other two phases, graphite and magnesium beryllium boron, is unclear.

To summarise the findings of the characterisation of the reference sample:

- Despite being left to sediment, it had a large size distribution, with the majority of particles of 100-3500 nm in diameter, and some larger material (~6500 nm) was also present.
- The zeta potential of the reference sample was -23 mV. Due to the complexity of the surface charge on the colloids it is not possible to determine what effect that is likely to have on their stability, but the measurement was compared to surface-modified clays later on.
- The ESEM images did not directly support the DLS measurements in terms of the size of the clay particles, but they did emphasize that a wide range of different sizes were present. Additionally, the images showed their non-spherical morphology very clearly, highlighting why the DLS sizing data may not be reliable.

- The XRF results identified the presence of iron in addition to the silicon and aluminium that make up the structure of MX80, which influenced the choice of XRD instrument.
- The XRD results indicated that a range of phases were present, as would be expected of a heterogenous natural material.

4.3 Fractionation methods

Three different approaches were used to produce the clay fractions: centrifugation; milling with sedimentation; and filtration and dispersion. The resulting samples were then investigated using DLS, and where the results of that technique indicated that the size distribution of the sample may be suitable for use in the flow experiments, further size characterisations were carried out.

A range of methods were tried within each of these approaches. The different combinations of methods are listed below:

- Centrifugation
- Milling and sedimentation
    - Ring milling and settling
    - Ball milling and settling
    - Cryogenic milling
- Dispersion and filtration
    - pH adjustment

- pH adjustment, with Sodium Chloride and Sodium Pyrophosphate
- Polyvinylpyrrolidone (PVP)

The background, methodology and results of each of these approaches is described below.

4.3.1 Centrifugation

4.3.1.1 Introduction

There are numerous examples in the literature of centrifugation being used to produce bentonite colloids (Michot *et al*. 2004; Missana *et al*. 2018; Möri *et al*. 2003), but Norrfors *et al*. (2015), as discussed above in section 4.1, used centrifugation to produce seven different size fractions, and so this methodology was used and the resulting fractions were characterised using DLS. More details on centrifugation may be found in Appendix 1.

4.3.1.2 Method

The method used was the same as that of Norrfors *et al*. (2015), but the suspension containing fulvic acid was excluded because it was not within the scope of this investigation. MX80 was mixed with deionised water at a concentration of 10 g/L, stirred occasionally throughout the first day, and then left to stand for three days. After this, approximately 80 % of the mixture was removed from the top, leaving the larger particles behind that had dropped out of suspension. This upper fraction constitutes the dispersion S0. S0 provided the starting point for the centrifugation sequence shown below in Figure 4.4. Fractions S1, S2 and S3 were produced by placing them into 50 ml polypropylene tubes in an Eppendorf 5804 centrifuge and spinning them at the g-forces indicated in Figure 4.4. S3.5 and $S3.5^{UC}$

required greater g-force than this instrument provided, so a high-speed Avanti JXN-26 centrifuge was used to make those suspensions. The size distribution of each fraction was then characterised using DLS on a Malvern Zetasizer Nano ZS. Unless otherwise specified, the DL t three measu for the refract

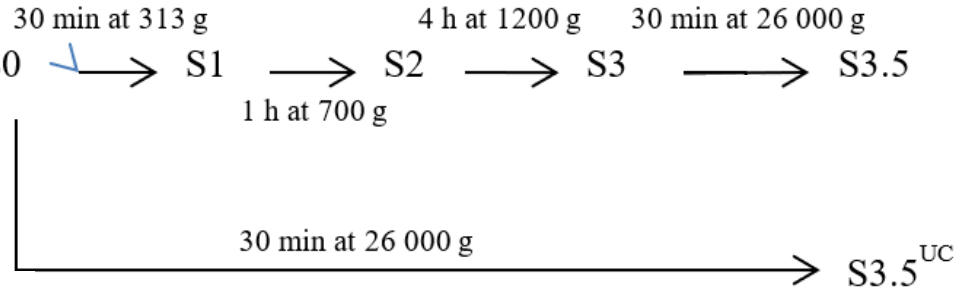

Figure 4.4. The centrifugation sequence that was used by Norrfors *et al.*, and that was replicated in this project. Image courtesy of the supplementary material document from Norrfors *et al.* (2015). Copyright Elsevier.

4.3.1.3 Results and discussion

Figures 4.5a and b show the size distribution of the centrifuged fractions.

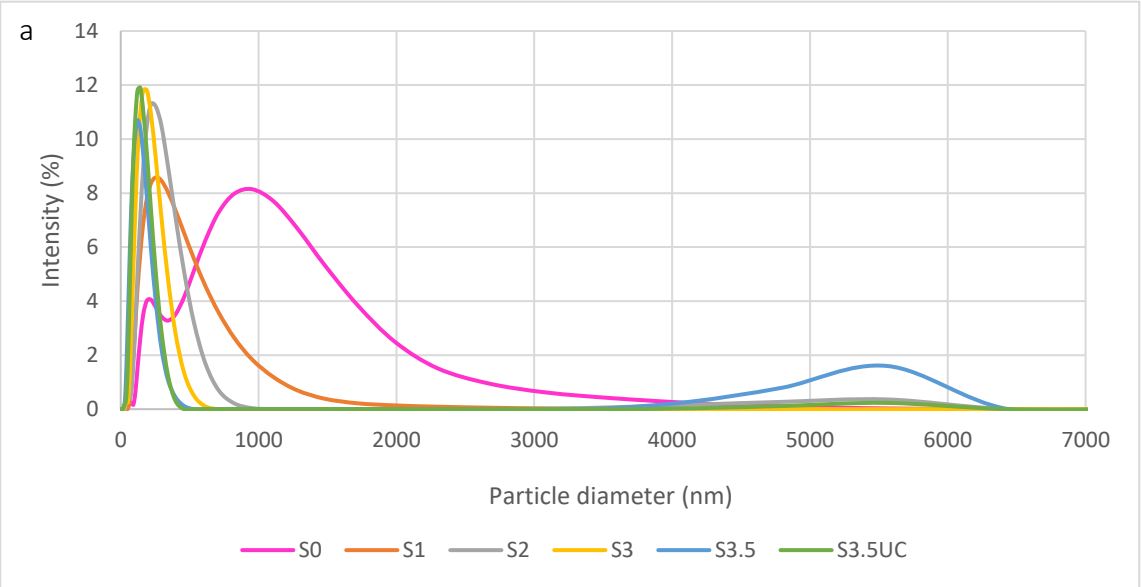

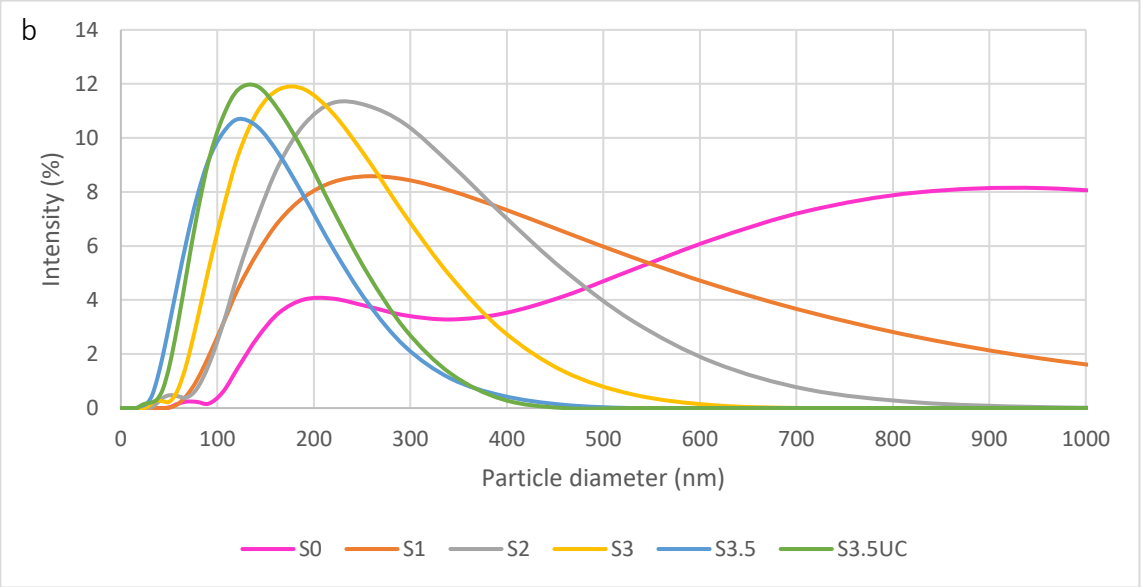

Figures 4.5a&b. The intensity-weighted size distributions of the different centrifuged fractions, shown at two different magnifications. There is a notable reduction in particle size and the distribution of sizes in sample S1 compared to S0, indicating that even a single, short centrifugation sequence removes a lot of the larger material from suspension.

Table 4.3 Contains the intensity-weighted DLS measurements of the mean diameter of the fractions produced by Norrfors *et al*. (2015) using the same centrifugation protocol, alongside the z-averages produced here, for comparison.

Table 4.3. The mean size of the centrifuged fractions produced by Norrfors *et al*. (2015), and in this experiment. The sometimes-considerable differences between them are discussed below.

Sample	Mean diameter from Norrfors *et al*. 2015 (nm)	Mean diameter from centrifuged fractions (nm)
S0	1452±632	459.0
S1	513±60	251.1
S2	404±95	217.1
S3	248±28	159.5
S3.5	181±28	120.7
$S3.5^{UC}$	180±39	119.3

The mean diameters of all of the fractions produced were smaller than those made by Norrfors *et al*. Given that the characterisation and the method used to produce them were the same, there is no clearly identifiable reason for this difference. However, it is probably due to the natural heterogeneity of clay used in the experiments. Apart from S0, all of the fractions produced here had undergone considerable size reduction in comparison to the reference sample: none of them had peaks at 5000-6000 nm or ~1000 nm, and instead were

closer in diameter to its 220 nm peak, indicating that there had been a considerable reduction in the average size.

However, although the average sizes have been reduced considerably, even the smallest and narrowest of the clay fractions made here contain a wide range of particle sizes; S3.5 and S3.5^{UC} have distributions from around 50 nm up to 400 nm in diameter. The fractions produced by Norrfors *et al*. (2016) were multimodal and the authors describe all but S3 and S3.5 as containing "both larger and smaller colloids", suggesting that their fractions were very broad as well. These are too polydisperse to be of use in the flow experiments, and therefore centrifugation will not be used again in this project. This is unfortunate, because centrifugation could be used to produce large volumes of solution rapidly.

4.3.2 Milling and sedimentation

Three different milling processes were used in this project. The first two, ring milling, and ball milling, were used in conjunction with settling, where the milled clay was mixed with water and left to stand. This allowed the largest particles to drop out of solution, with the aim of making the overall size distribution smaller and more uniform. The third milling method, cryomilling, was not combined with settling. The fractionation methods and results are discussed below, and more information on the techniques may be found in Appendix 1.

4.3.2.1 Ring mill and settling

4.3.2.1.1 Introduction

There are numerous examples in the literature of bentonite clay undergoing ring milling for various reasons (Jönsson *et al*. 2009; Missana *et al*. 2016; Segad *et al*. 2012), but it was not

possible to find any examples of it being used for the sole purpose of producing colloids. Thus, to the best of the author's knowledge, this application was a novel one.

Each of the ring milled samples was mixed with deionised water, sampled immediately, and then allowed to settle. Further samples were taken from the top of the mixtures at various time intervals, allowing the largest particles to drop out of suspension, with the intention of producing more uniform samples. The size distribution of each of these was characterised using DLS.

4.3.2.1.2 Method

4 g of bentonite clay was ring milled under wet and dry conditions for between 1 and 10 minutes using a TEMA Laboratory Mill, with a ring approximately 10 cm in diameter. The wet conditions were produced by adding 3 ml of ethanol to the clay before milling. In line with best practice for handling nanomaterials, the dry samples were opened in a Waysafe cabinet after milling and 3 ml of ethanol was added. This prevents particles from becoming airborne and allows the clay to be handled safely without the need for special containment. As this was added after the milling was complete, it would not have had any effect on the milling process and the size of the particles produced. After the 1-10 minute milling times had little effect on the particle size distribution, a wet sample was prepared and milled for 1 hour. Due to a long-running technical malfunction, it was not possible to prepare a corresponding dry sample for comparison.

0.01 g of each milled clay was mixed with 5 ml of deionised water (producing a concentration of 2 g/l), sonicated for approximately 10 minutes to disperse it, sampled immediately from the top of the vials, and then left to stand for 24, 48 and 72 hours, and two weeks. This

allowed for settling and sedimentation to take place, theoretically removing the largest of the remaining particles, and producing the samples below in Table 4.4.

Table 4.4. The conditions under which the ring milled clay samples were produced, and the sample numbers assigned to each. Only one 1 hour sample was done owing to technical difficulties.

Time (mins)	Conditions under which it was milled									
	Wet					Dry				
	Settled for: 0 h	Settled for: 24 h	Settled for: 48 h	Settled for: 72 h	Settled for: 2 weeks	Settled for: 0 h	Settled for: 24 h	Settled for: 48 h	Settled for: 72 h	Settled for: 2 weeks
1	RMa_0	RMa_{24}	RMa_{48}	RMa_{72}	RMa_{2w}	RMd_0	RMd_{24}	RMd_{48}	RMd_{72}	RMd_{2w}
5	RMb_0	RMb_{24}	RMb_{48}	RMb_{72}	RMb_{2w}	RMe_0	RMe_{24}	RMe_{48}	RMe_{72}	RMe_{2w}
10	RMc_0	RMc_{24}	RMc_{48}	RMc_{72}	RMc_{2w}	RMf_0	RMf_{24}	RMf_{48}	RMf_{72}	RMf_{2w}
1 hour	$RM.1h_0$	-	-	-	-	-	-	-	-	-

4.3.2.1.3 Results and discussion

Figures 4.6a-f show the size distributions of the 1-10-minute wet milled samples after settling for 0, 24, 48, 72 hours and two weeks, at two different magnifications.

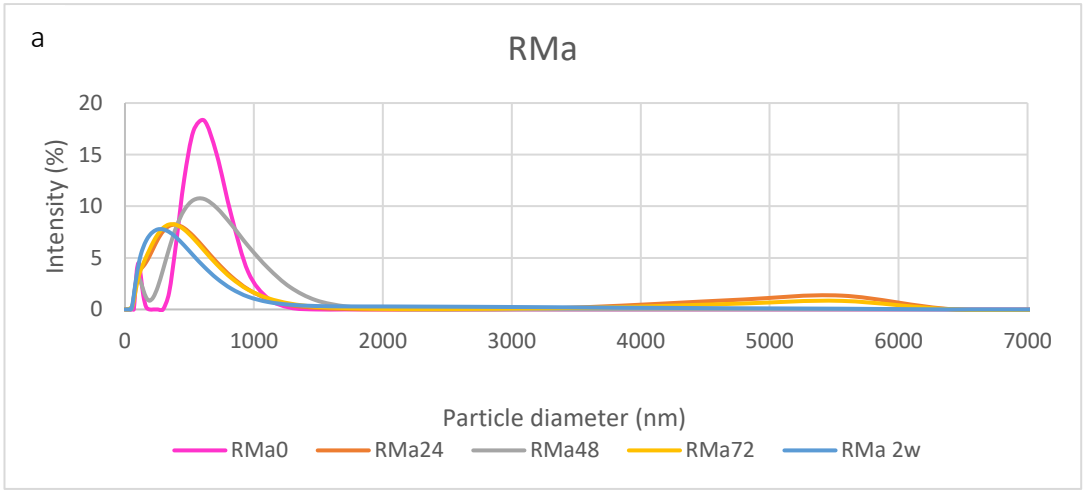

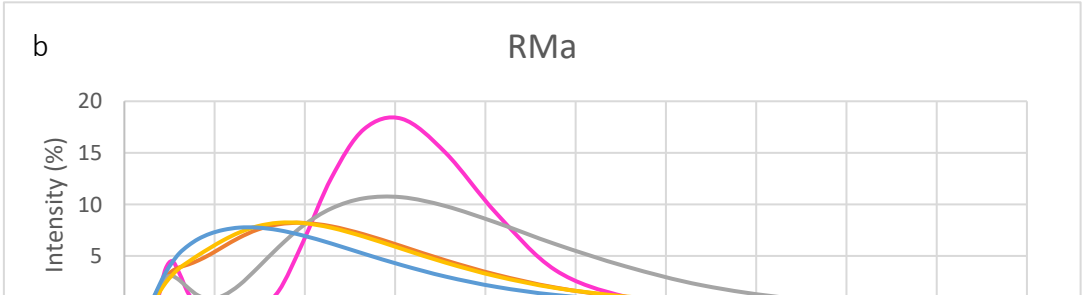

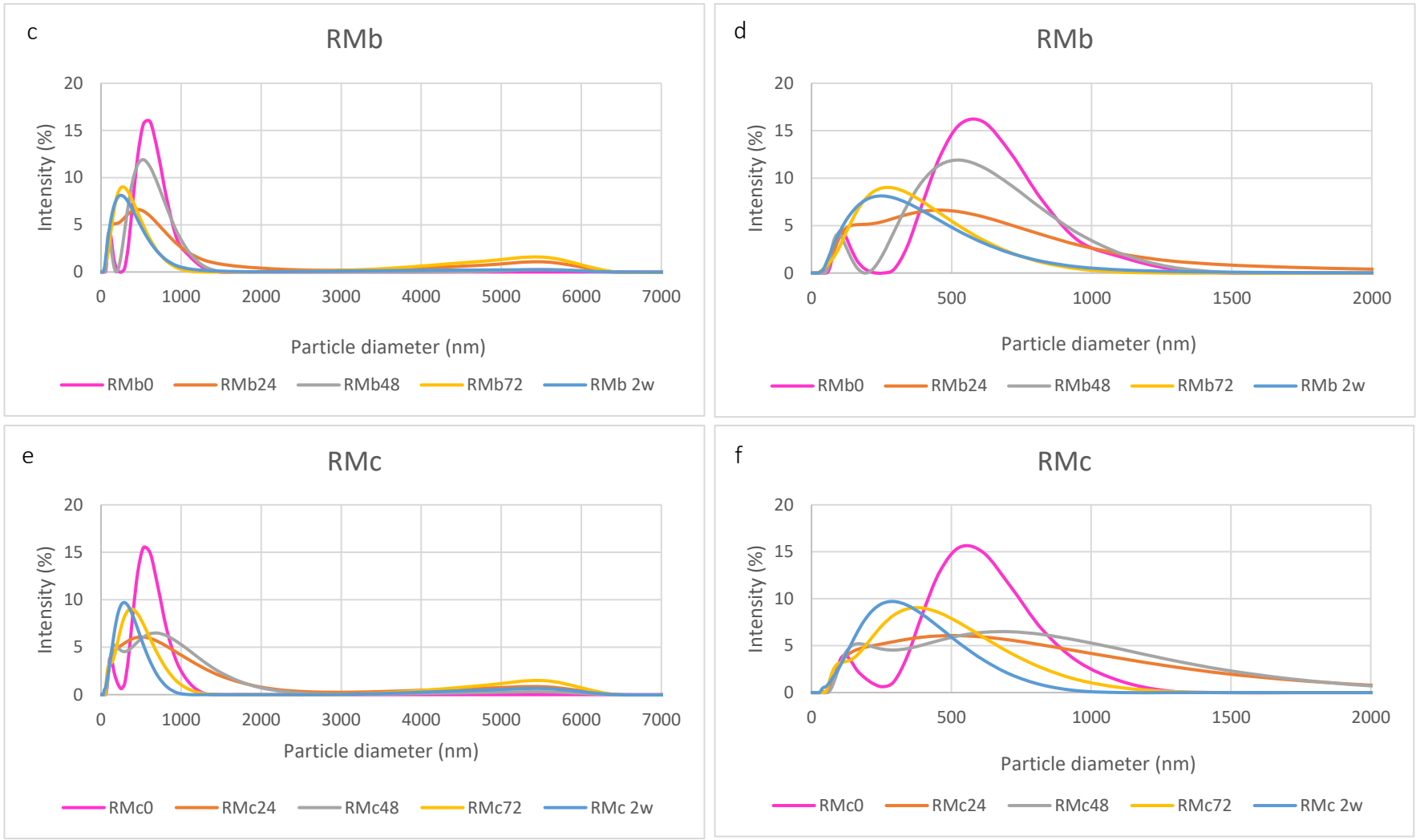

Figures 4.6a-f. DLS data showing the size distributions of the fractions that were milled wet for 1 (RMa), 5 (RMb) and 10 (RMc) minutes, and the results of the settling experiments. All of the samples retained a broad size distribution unsuitable for use in flow experiments.

Figures 4.7a and b show the size distribution of the sample that was wet milled for an hour.

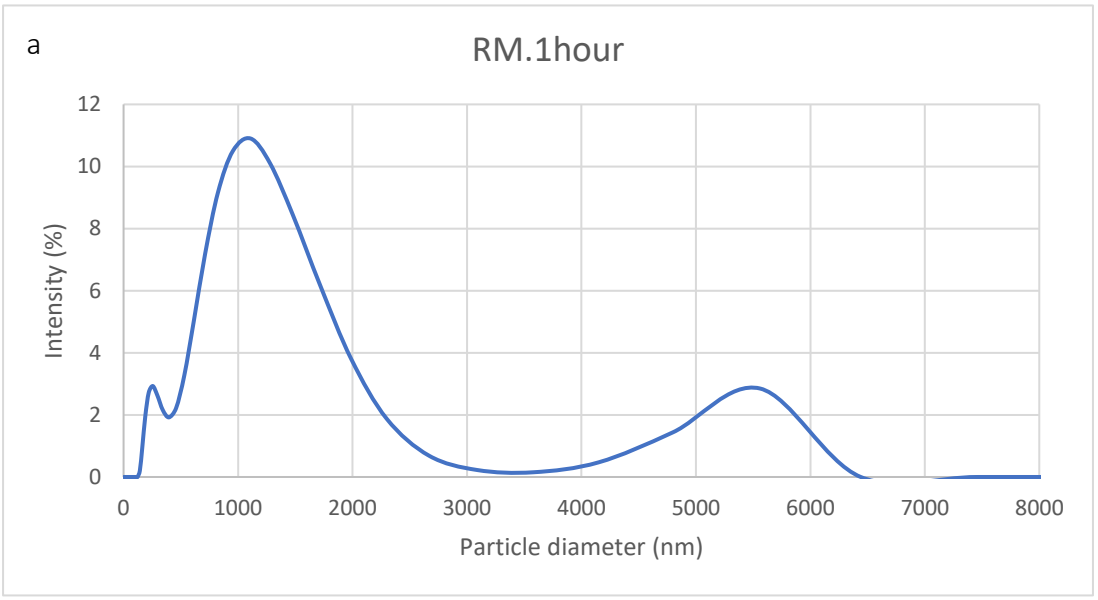

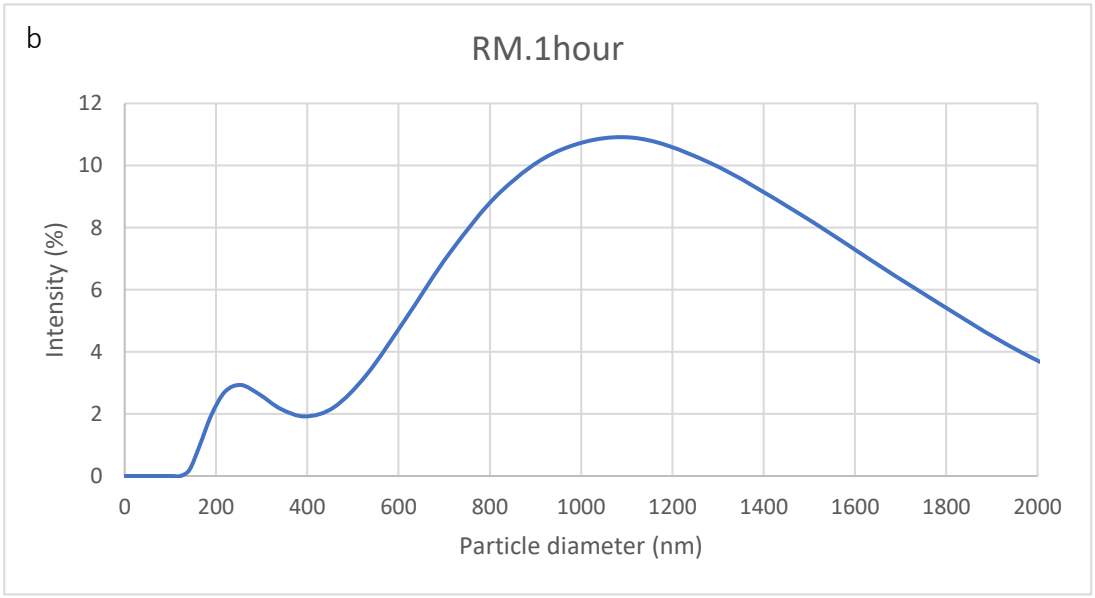

Figures 4.7a&b. The size distribution of the fraction that was milled for 1 hour. It was only possible to produce one 1 hour sample owing to technical difficulties.

This was produced after the other ring milled samples, and it did not undergo settling because that had already proved unsuccessful on the others, and as its size distribution was similar to the other wet milled samples, it was unlikely that it contained significant amounts of smaller colloids which would have been isolated by settling.

Figures 4.8a-e show the wet-milled samples from above, but with the different milling times on each graph, arranged by how long they were left to settle for.

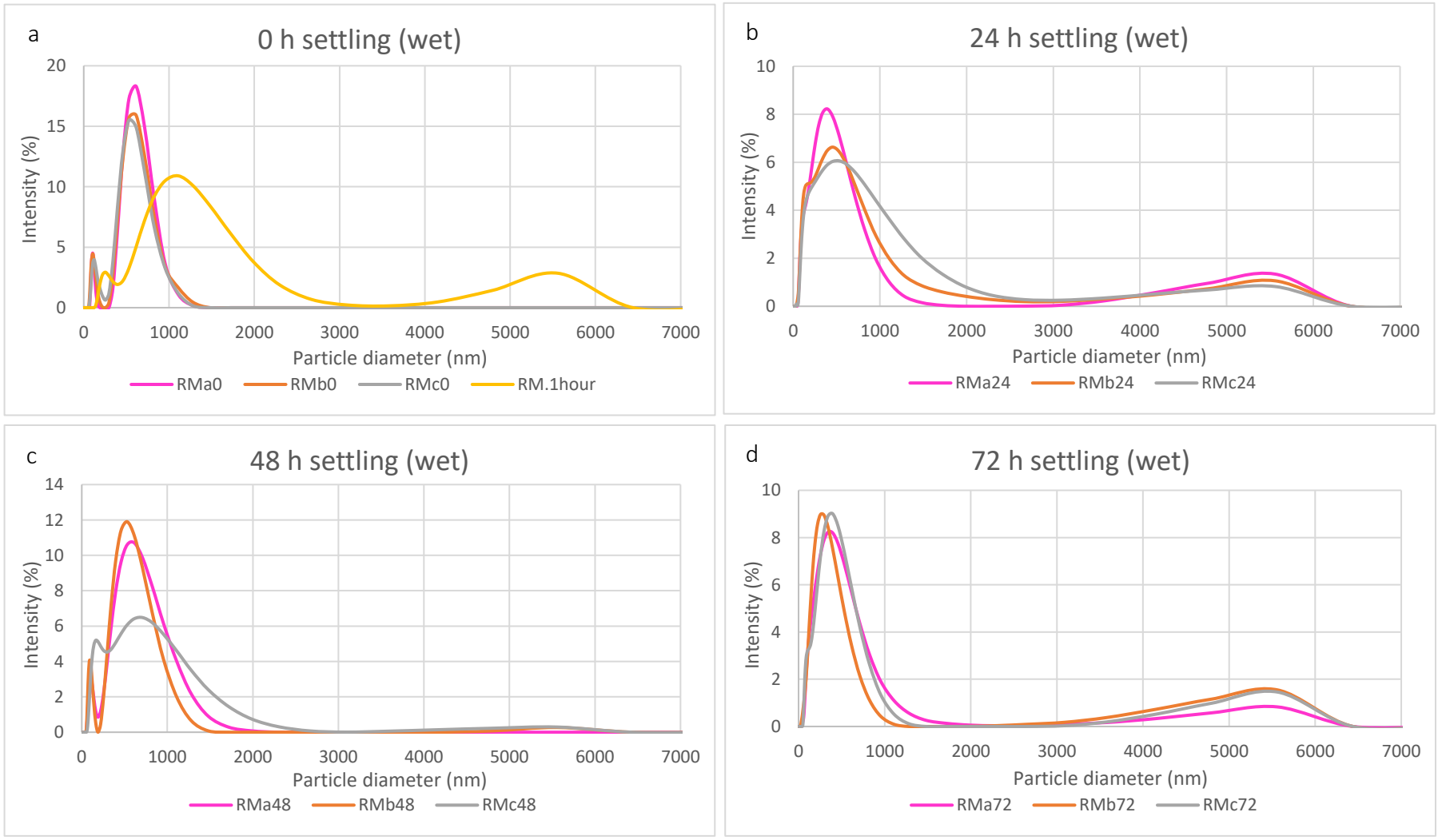

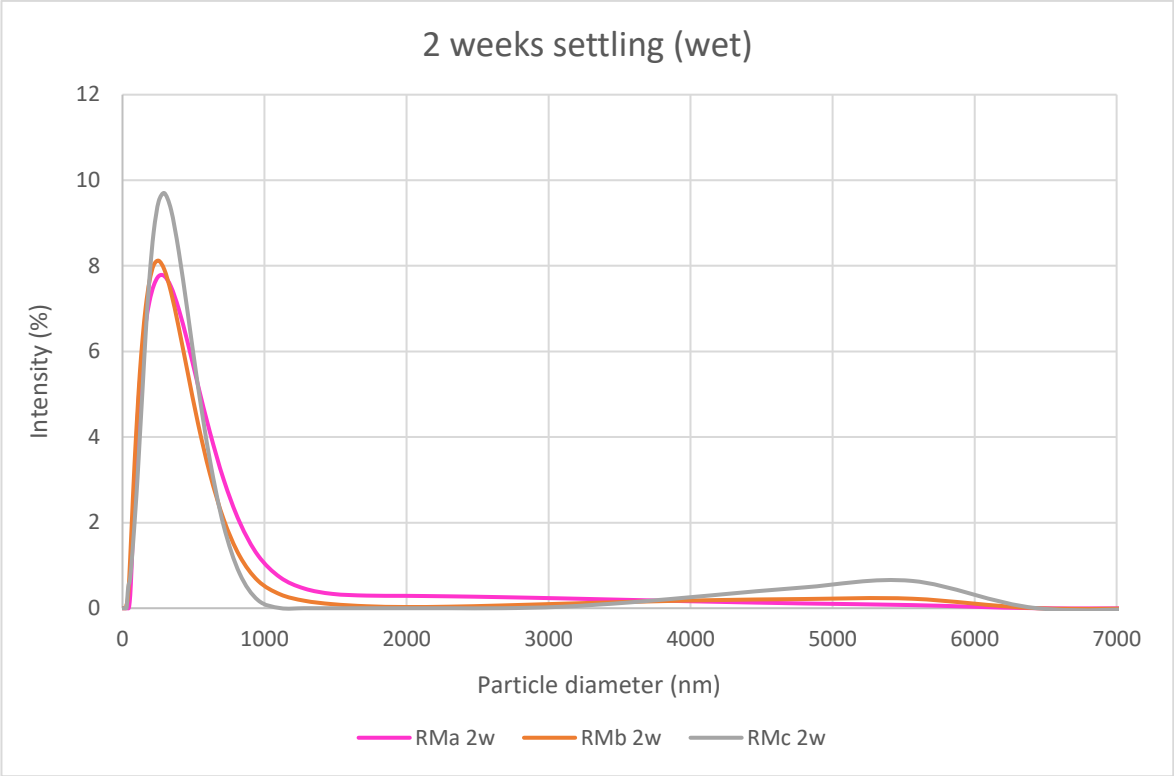

Figures 4.8a-e The wet-milled samples from above, but with the different milling times on each graph, arranged by how long they were left to settle for.

Figures 4.9a-f show the size distributions of the 1-10-minute dry milled samples after 0, 24, 48, 72 hours and two weeks, at different magnifications.

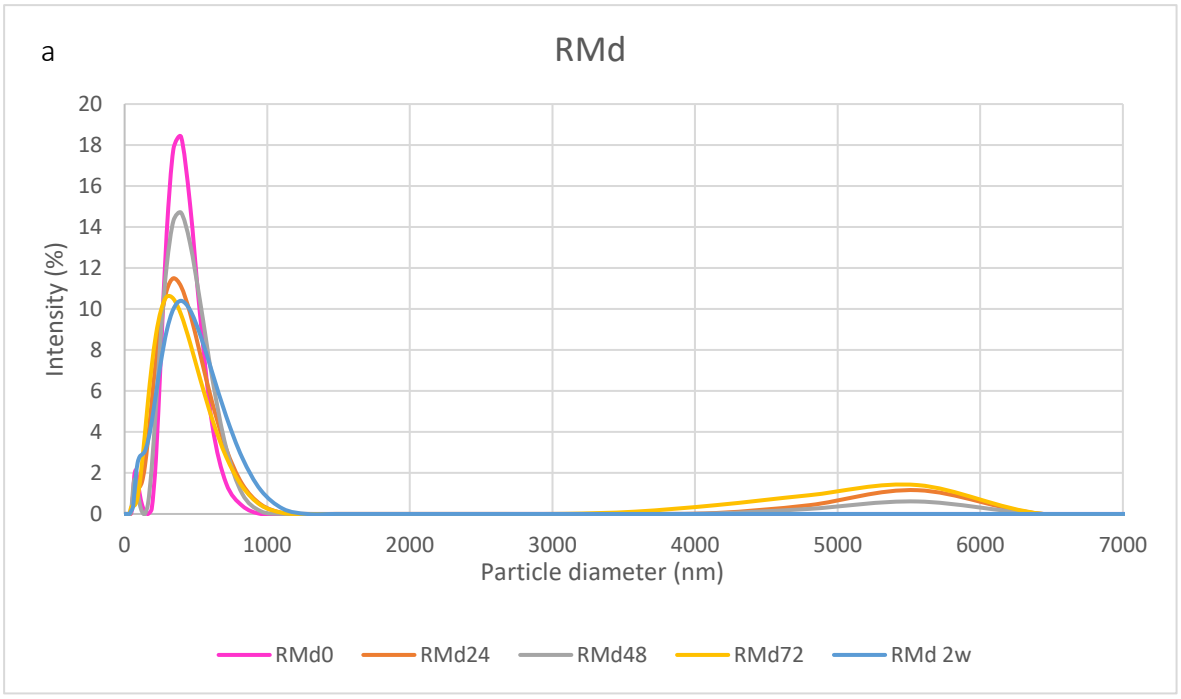

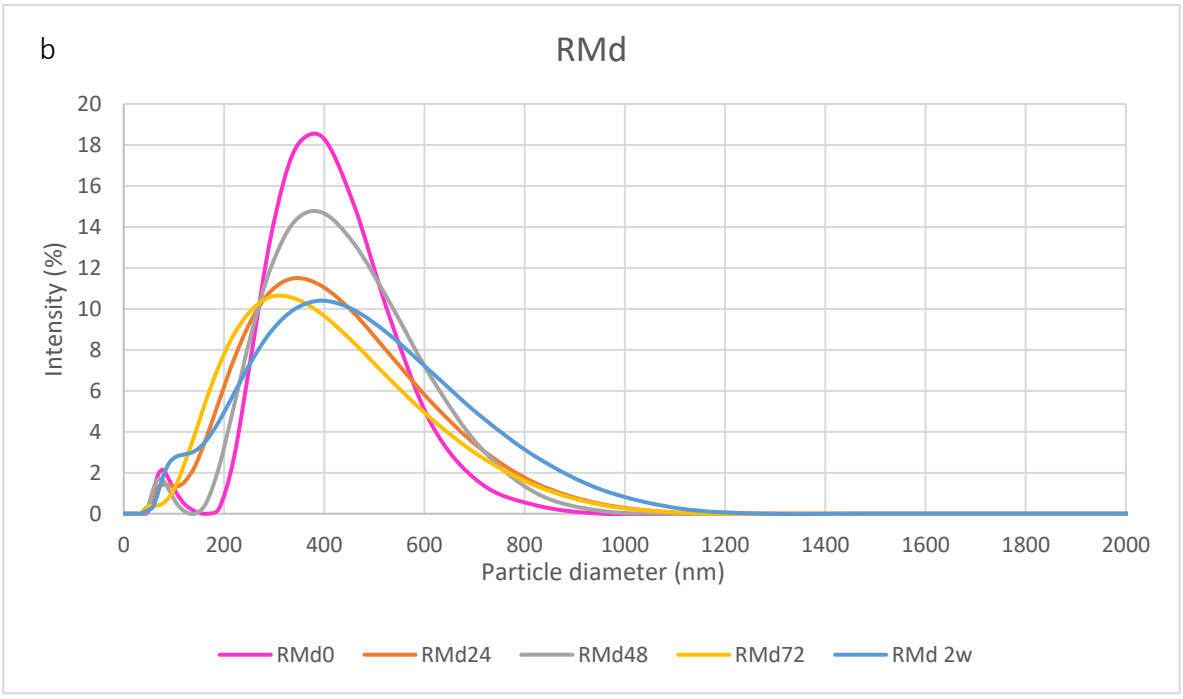

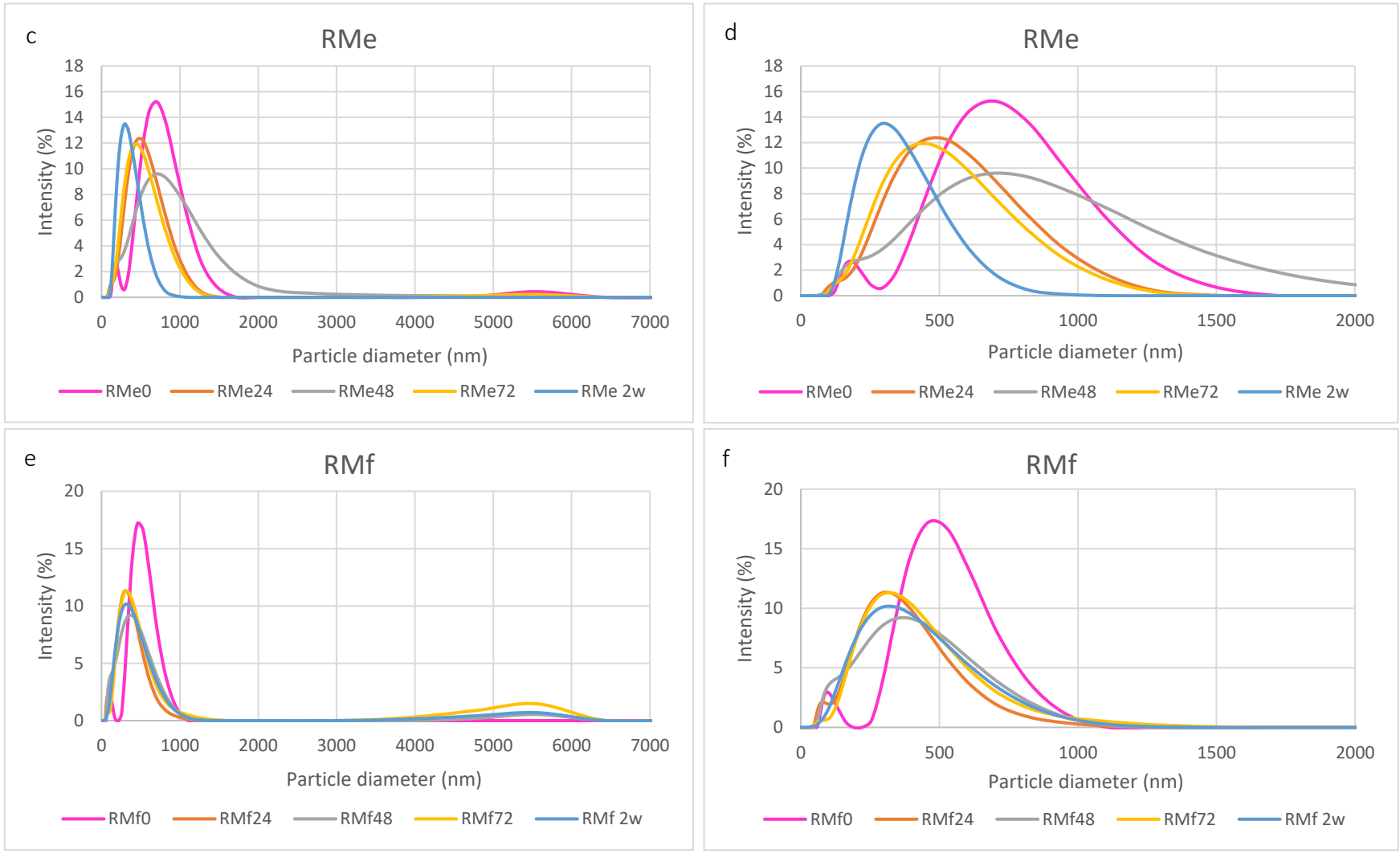

Figures 4.9a-f. DLS data showing the size distributions of the fractions that were milled dry for 1 (RMa), 5 (RMb) and 10 (RMc) minutes, and the results of the settling experiments. All of the samples retained a broad size distribution unsuitable for use in flow experiments.

Figures 4.10a-e show the dry-milled samples from above, but with the different milling times on each graph, arranged by how long they were left to settle for.

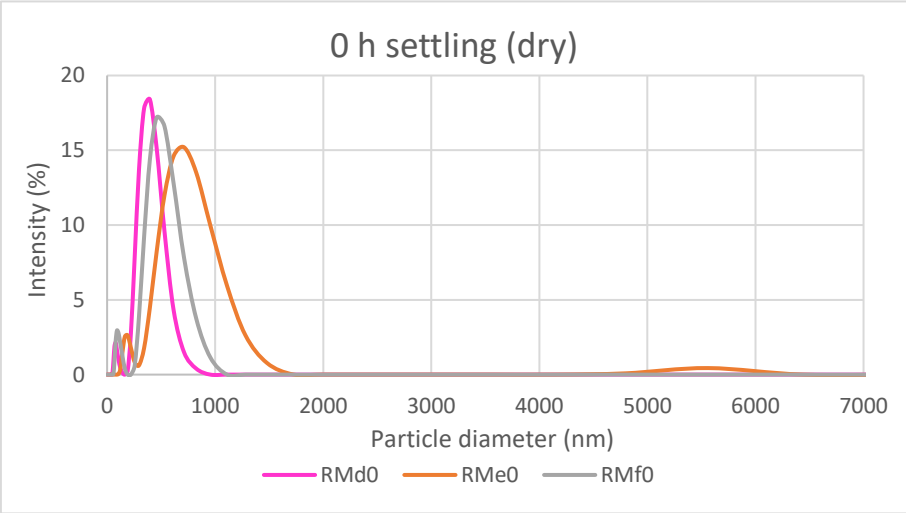

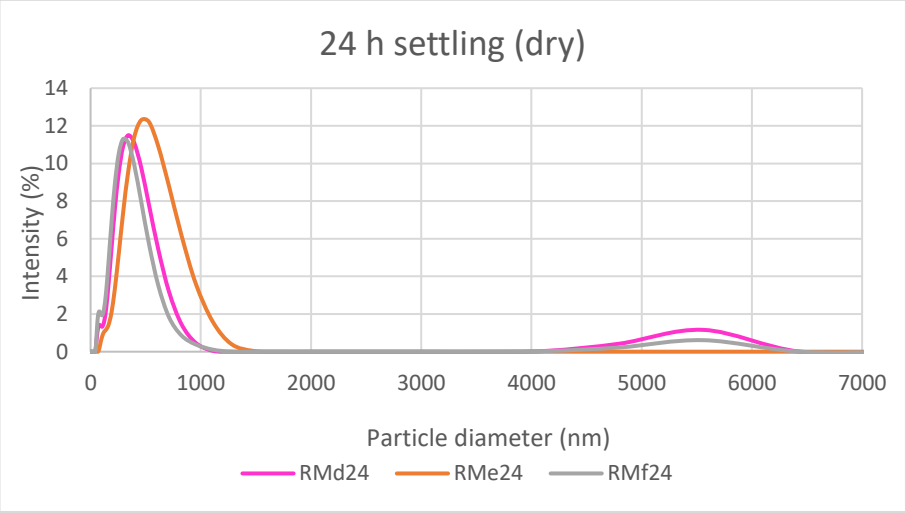

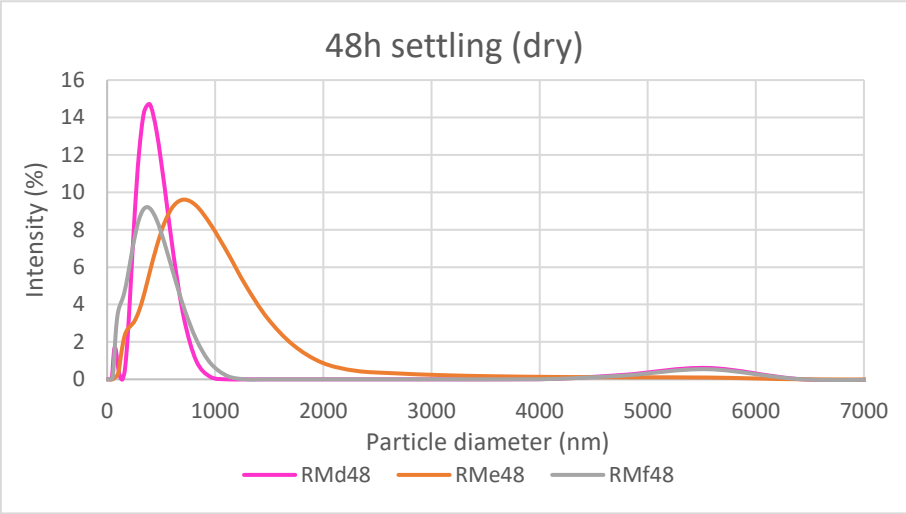

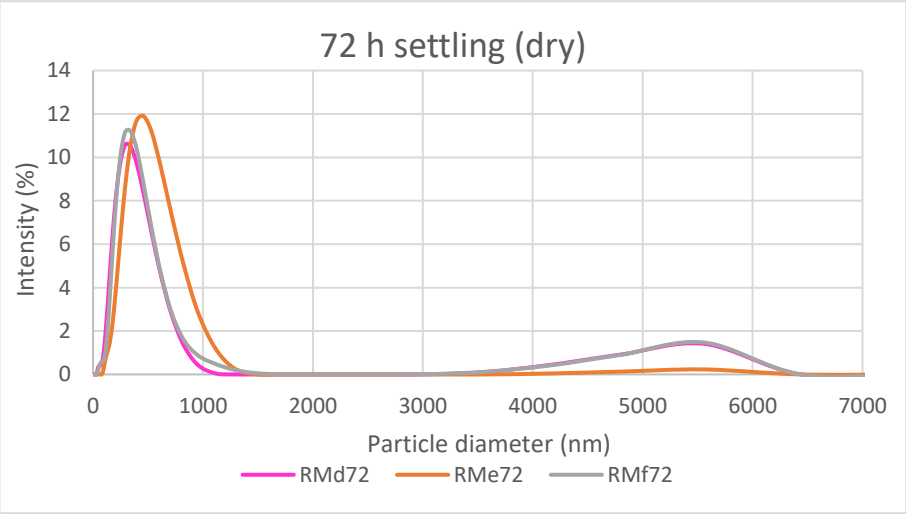

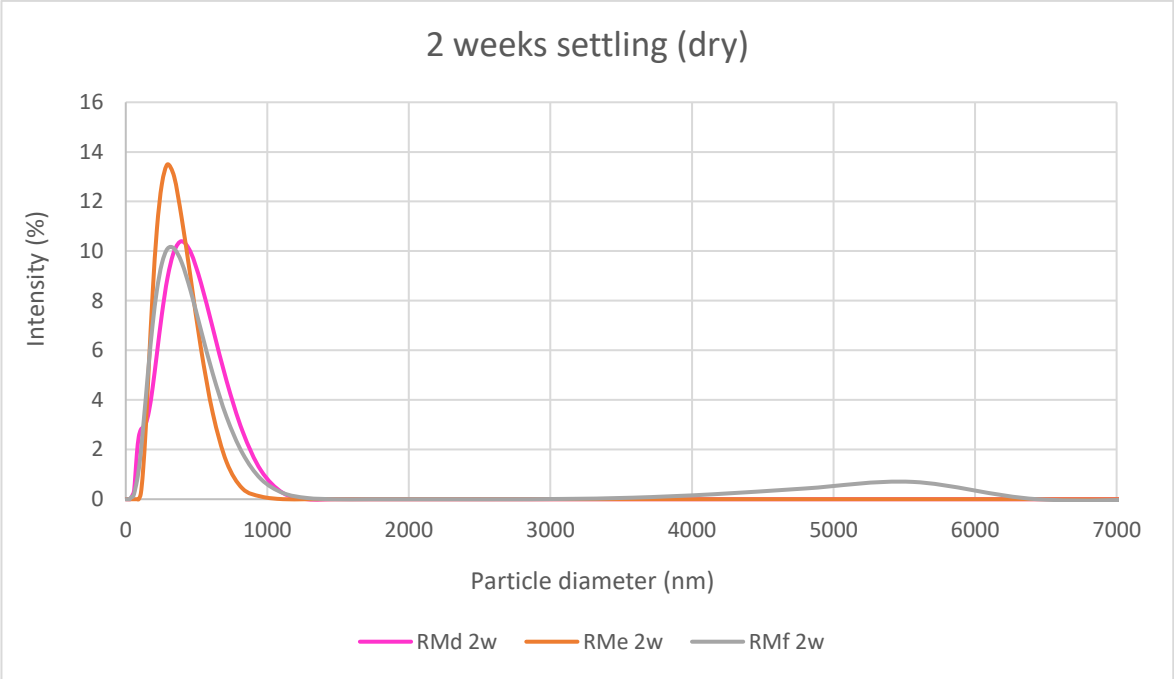

Figures 4.10a-e. The dry-milled samples from above, but with the different milling times on each graph, arranged by how long they were left to settle for.

As may be seen in Figures 4.6-4.10, ring milling did not produce clay fractions with a narrow size distribution, even when combined with settling. As shown in Figures 4.6a-f, wet milling for 1-10 minutes caused the largest peak to shift from the 1110 nm observed in the reference sample to 500-600 nm, and the smaller peak to shift to approximately 100 nm, but all of the samples retained a very broad size distribution. The sample that was milled for 1 hour (see Figures 4.7a and b) changed little in comparison to the reference sample, suggesting that although milling may break the particles down initially, it then causes them to join together again. Kumar & Biswas (2017) reported on how milling can increase or decrease average particle size depending on the time for which the material was milled, which may have happened here. The authors state that the pressure applied to the particles during the milling process increases the area of contact between them, which increases the chances of them sticking together (Kumar & Biswas 2017).

The graphs in Figures 4.8a-e show that the samples become highly uniform when left to settle for 72 hours or more, regardless of milling time. This suggests that milling breaks down the larger particles in the samples, but has little effect on the smaller ones, and the resulting samples are all very similar. It also indicates that leaving the samples to settle for longer than 72 hours is unnecessary, as there was little change between 72 hours and two weeks. The difference between the sample that was milled for 1 hour and the ones that were milled for less is very pronounced in Figure 4.8e; Kumar & Biswas (2017) reported on how milling can actually increase average particle size, and as two of its peaks are shifted to the right compared to the other samples, indicating large particle diameters, that may have happened here.

The samples that were dry milled also exhibit very little change in size distribution compared to the reference sample. RMd_0, which was milled for just 1 minute, actually had a narrower size distribution before it was settled, which could be anomalous, or could be the result of the particles in suspension agglomerating faster than the larger particles were settling out. When comparing the data in Figures 4.9a-f, it is possible to observe that the peaks in RMe and RMf (5 and 10 minutes respectively) shifted from 700nm to 295nm and 460nm to 295nm respectively over the course of the settling process, indicating that their average particle size did reduce, but the distribution remained wide.

When comparing the different milling times in Figures 4.10a-e, it is clear that sample RMe, which was milled for 5 minutes, has a larger peak than the others, which only changes after it has been settled for two weeks, by which time the size distribution in the samples are all very similar. The reason for this is not clear, it was not observed in the wet samples, so it may be due to the sample clumping and not being ground properly in the milling vessel.

After the two-week settling period all of the samples were relatively uniform in size. This was slower than the samples that were milled dry, suggesting that the wet-milled sample had more larger-sized particles which dropped out of suspension rapidly, whereas those in the dry milled sample were not quite so large, and so the settling process was more gradual. Settling the samples for two weeks shifted the peaks slightly towards smaller particle diameters, particularly in the case of the wet milled samples, indicating that a reduction of size had occurred relative to the samples taken at 0 hours, but it was not significant enough to produce samples suitable for use in the flow experiments. The effect was less pronounced on the samples that were settled for less time, which could simply mean that they were not left to stand for long enough, but it may have been because they were agglomerating as well as settling, which could not be identified from the DLS results. This would have increased the diameter of the particles remaining in suspension, effectively nullifying the effect of the pre-existing large particles dropping to the bottom of the vessel.

In summary, ring milling did not produce fractions that were narrow or uniform enough to be used in the flow experiments. Had milling proven successful, it may have raised some issues with the reactivity of the clay particles later on during the sorption experiments in Chapter 7. Breaking the colloids down artificially reduces their diameter, increases their relative surface area, and potentially exposes more edge sites in comparison to a comparative sample produced by isolating pre-existing small colloids by a method such as centrifugation. The edge sites exert a strong influence over the cation-binding ability of the colloids, and this could have induced errors into the experiments (Newton *et al*. 2017). If the scope of the experiment allowed, it may have been possible to compare the reactivity of milled clay colloids compared to those produced through less energetic methods, but there

was not time to do that here. Additionally, when these broken colloid edges are exposed by milling it makes the clays more likely to aggregate, which could affect their size distribution and therefore suitability for use in the flow experiments in Chapter 6 (Mingelgrin *et al*. 1978).

4.3.2.2. Ball mill and some settling

4.3.2.2.1 Introduction

Mingelgrin *et al*. (1978) reported the formation of colloidal-sized material when ball milling bentonite, which was one of the aims of this project. Therefore, samples of wet and dry MX80 were milled for up to 24 hours to try and produce small, uniform particles suitable for use in the flow experiments.

4.3.2.2.2 Method

4g of bentonite clay was ball milled under wet and dry conditions with either ten 5 mm or two 10 mm diameter zirconium balls for increasing lengths of time, using a Fritsch Pulverisette 7 ball mill. The runs were conducted at 500 RPM and paused at 15-minute intervals both to prevent the material from reaching high temperatures and to allow the clay to fall from the sides as the Coriolis forces were reduced, thereby helping to ensure more even grinding of the material. 3 ml of ethanol was added into the milling vessel and stirred through the clay before milling in order to achieve the wet conditions, and as with the ring milled samples, ethanol was added to the dry samples after milling to reduce the risk of inhalation.

The clays were initially only milled for a maximum of 15 hours, but after few changes were observed it was determined necessary to investigate longer milling times. Only one sample was tested in order to see if longer milling times were likely to be more successful for ball

milling than they had been for ring milling, and so a sample was milled dry, with 10 mm balls, for 24 hours. The samples were prepared for DLS in the same way as was described above for the ring milled samples. All of them were sampled at zero hours, but only the dry samples made using the 10 mm balls were left to undergo settling, again, to see if the method showed any potential. These were settled at the same time intervals as the ring milled samples. The samples and their assigned codes may be found below in Table 4.5.

Table 4.5. The samples that were produced using a ball mill. This table lists whether they were produced under wet or dry conditions, how long they were milled for, what size balls were used for grinding, and the code that was assigned to each sample.

Time (hours)	Conditions				
	Wet samples		Dry samples		
	5 mm	10 mm	5 mm	10 mm	10 mm settled 24, 48, 72 h, and 2 weeks
1	BMa	BMd	BMg	BMj_0	BMj_{24}, BMj_{48}, BMj_{72}, BMj_{2w}
4	BMb	BMe	BMh	BMk_0	BMk_{24}, BMk_{48}, BMk_{72}, BMk_{2w}
15	BMc	BMf	BMi	BMl_0	BMl_{24}, BMl_{48}, BMl_{72}, BMl_{2w}
24	-	-	-	BMm_0	BMm_{24}, BMm_{48}, BMm_{72}, BMm_{2w}

4.3.2.2.3 Results and discussion

Figures 4.11a-h show the size distribution of the ball milled samples that were made with a wet mixture of clay and ethanol, displayed according to milling time.

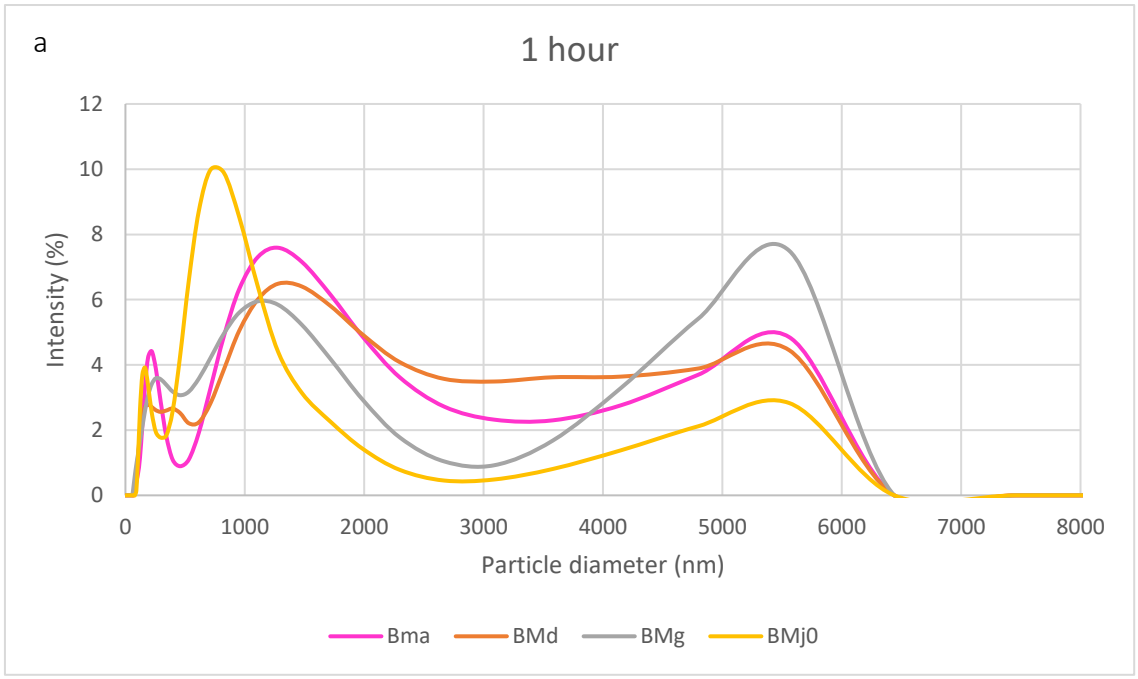

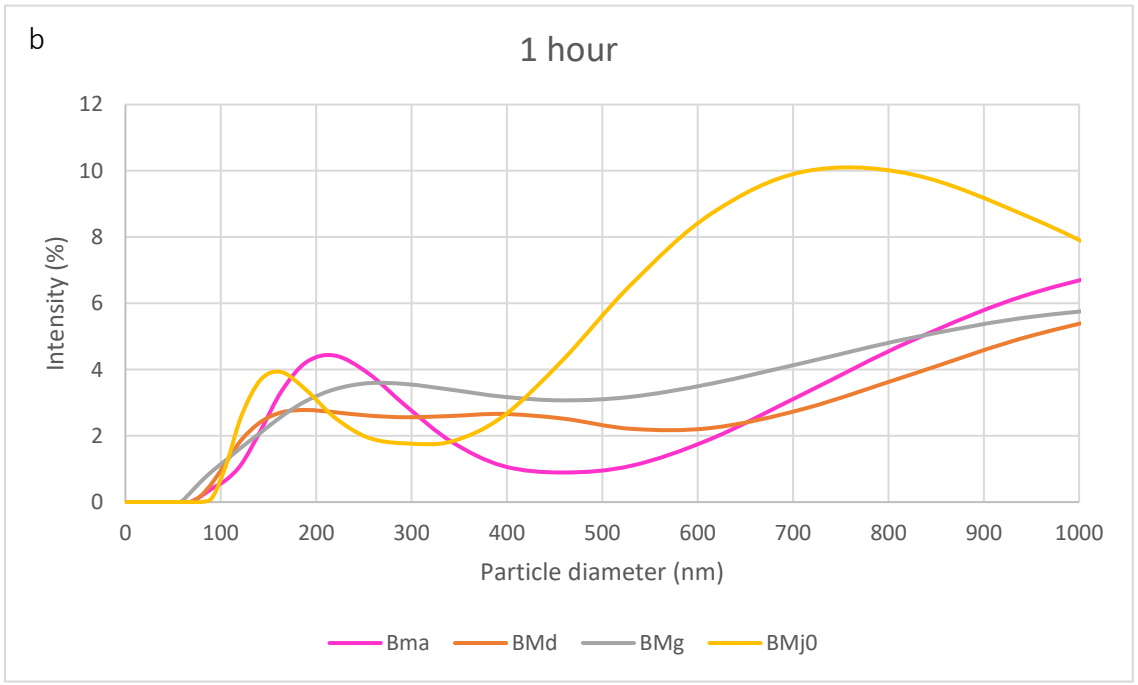

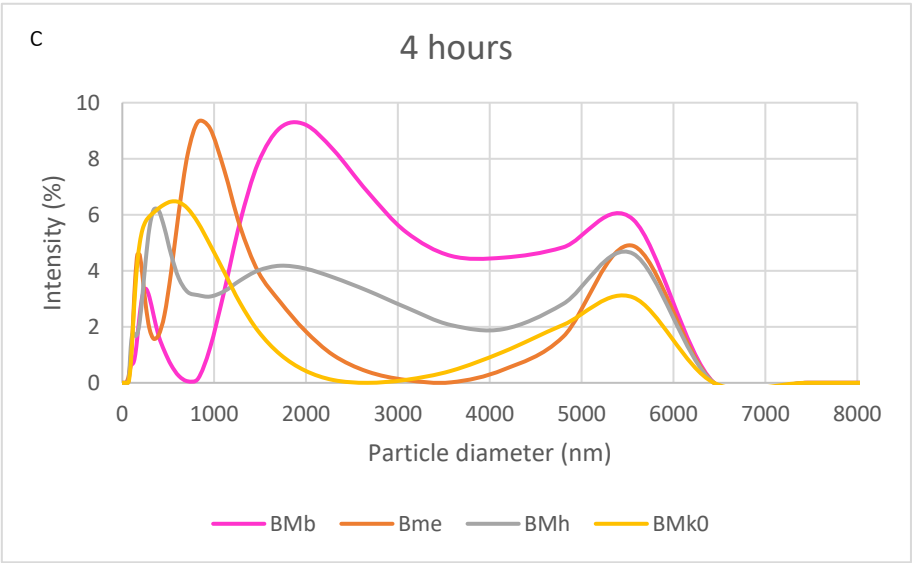
c
4 hours
Intensity (%)
Particle diameter (nm)
BMb
Bme
BMh
BMk0

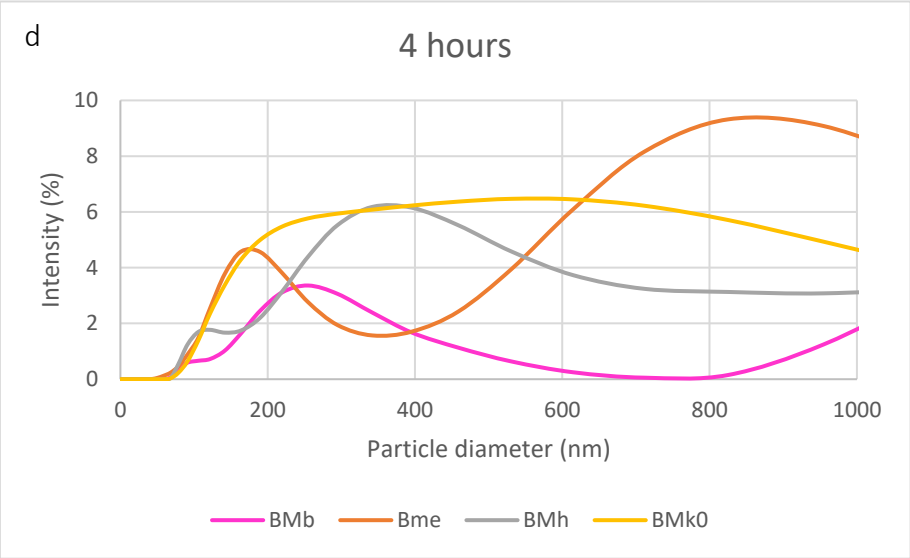
d
4 hours
Intensity (%)
Particle diameter (nm)
BMb
Bme
BMh
BMk0

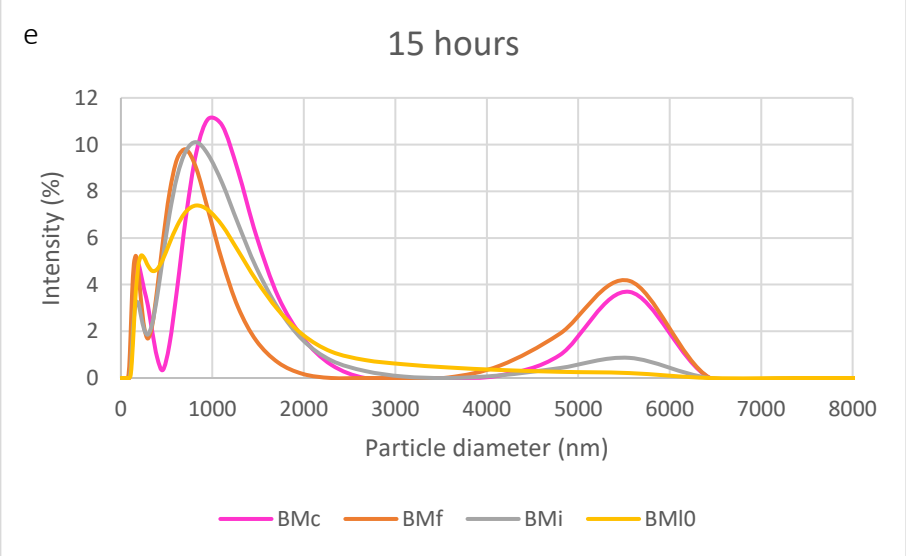
e
15 hours
Intensity (%)
Particle diameter (nm)
BMc
BMf
BMi
BMl0

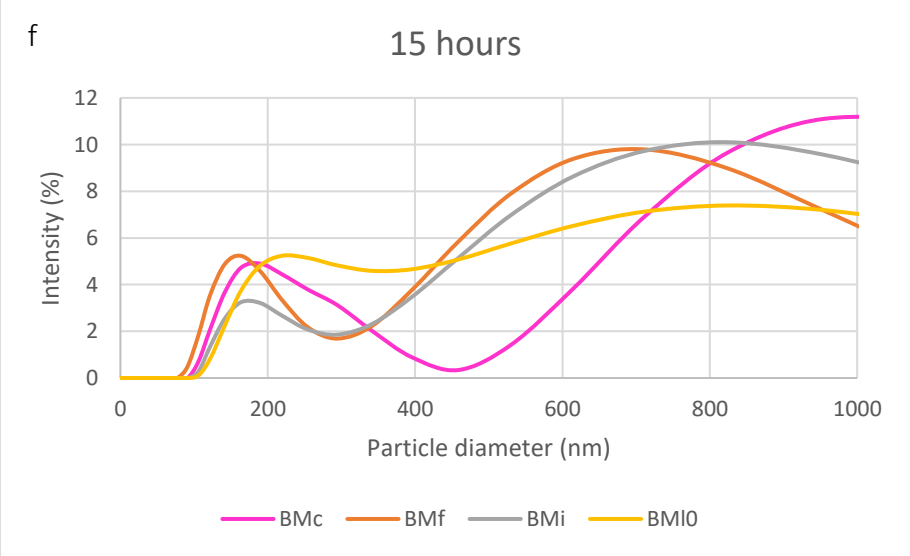
f
15 hours
Intensity (%)
Particle diameter (nm)
BMc
BMf
BMi
BMl0

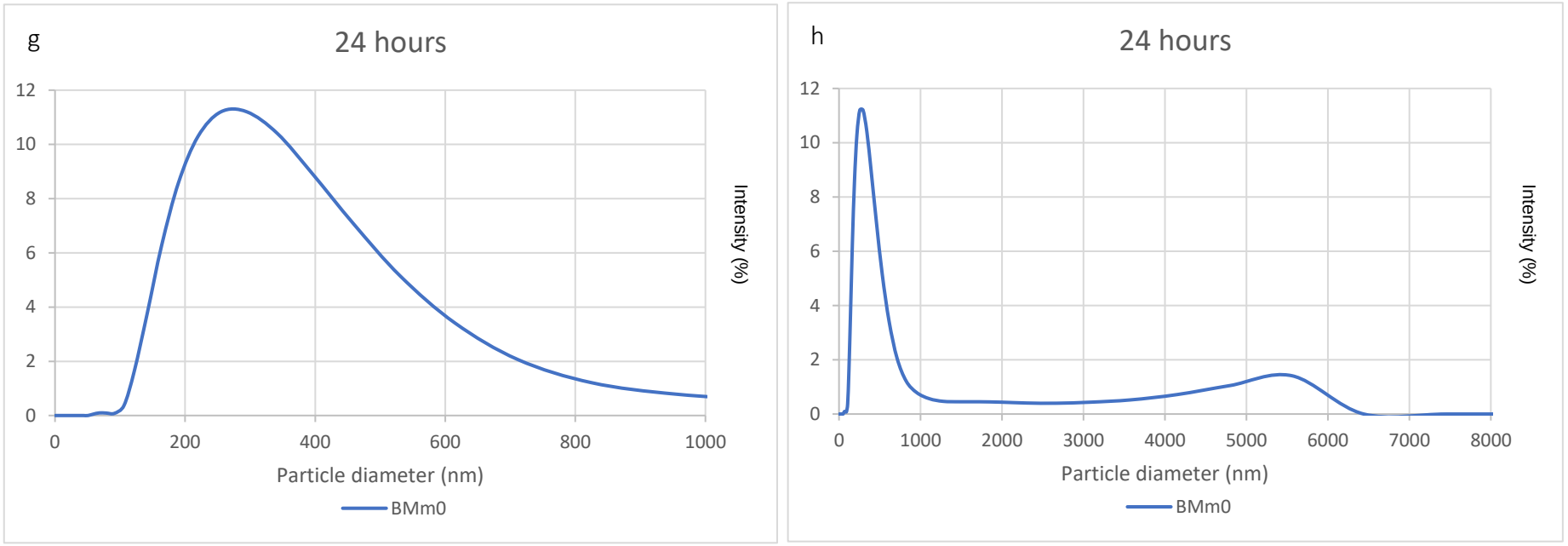

Figures 4.11a-h. These charts show the size distributions of the ball milled fractions that were made with a wet clay and ethanol mixture, and are displayed according to milling time. They were milled for 1, 4, 15 or 24 hours, and are shown at different magnifications.

Figures 4.12a and b show the size distribution of the wet ball milled samples, displayed according to which ball size was used in their preparation, to allow for comparison of the effect of milling time on each sample set.

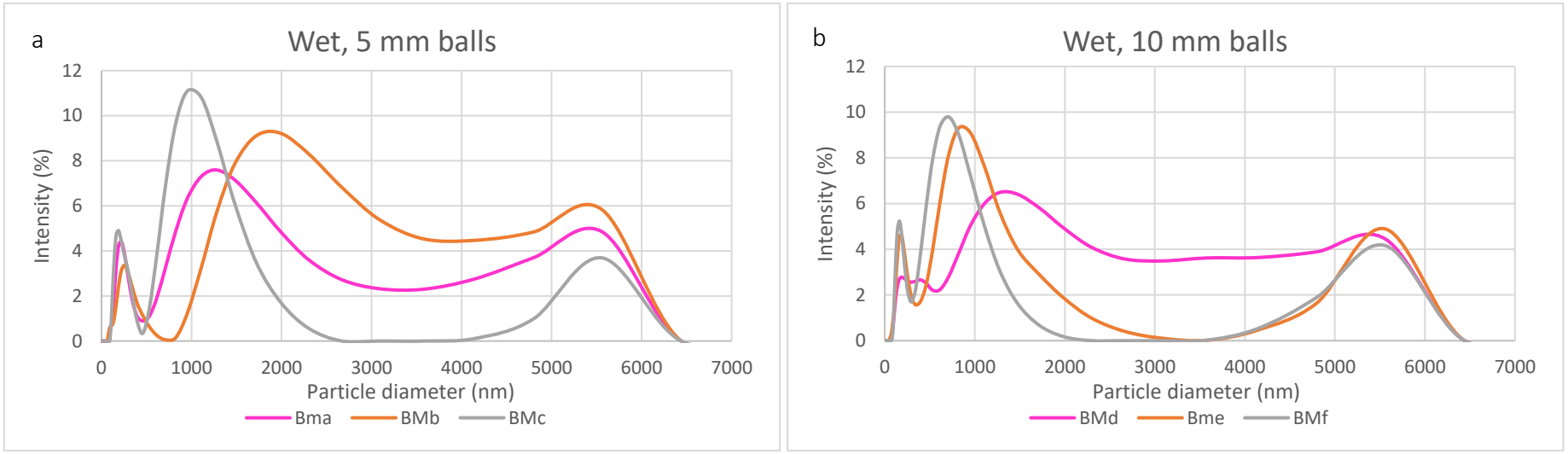

Figure 4.12. The size distribution of the wet ball milled samples, displayed according to which ball size was used in their preparation, to allow for comparison of the effect of milling time on each sample set.

Figures 4.13a-h show the 10 mm dry samples, displayed according to how long they were milled for before being left to settle.

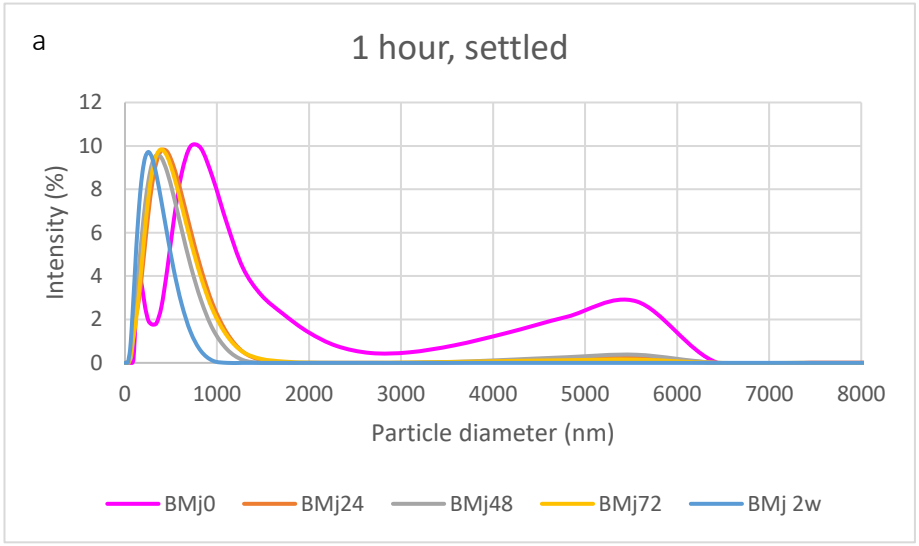

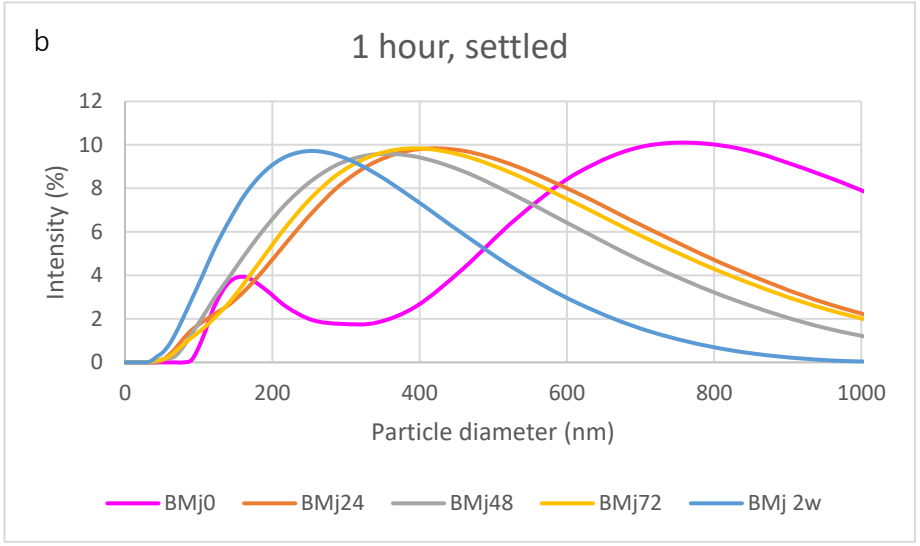

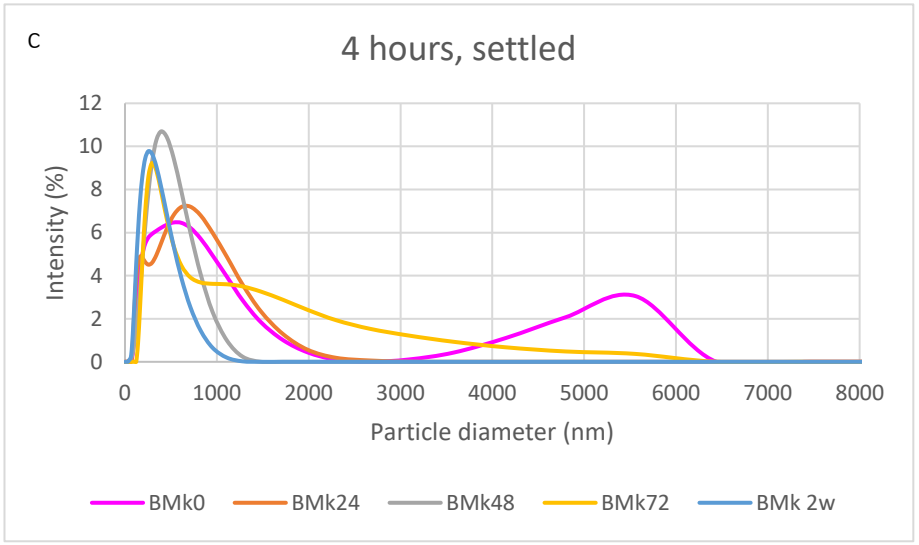

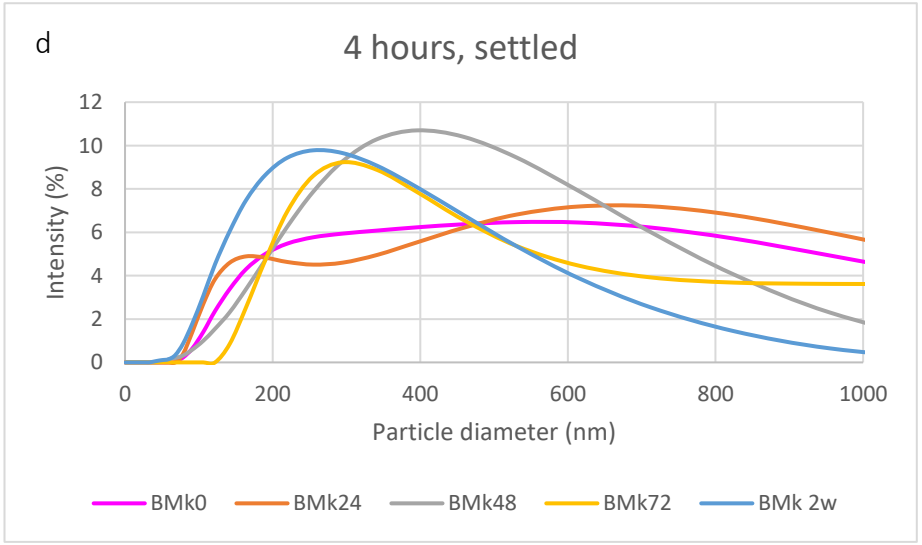

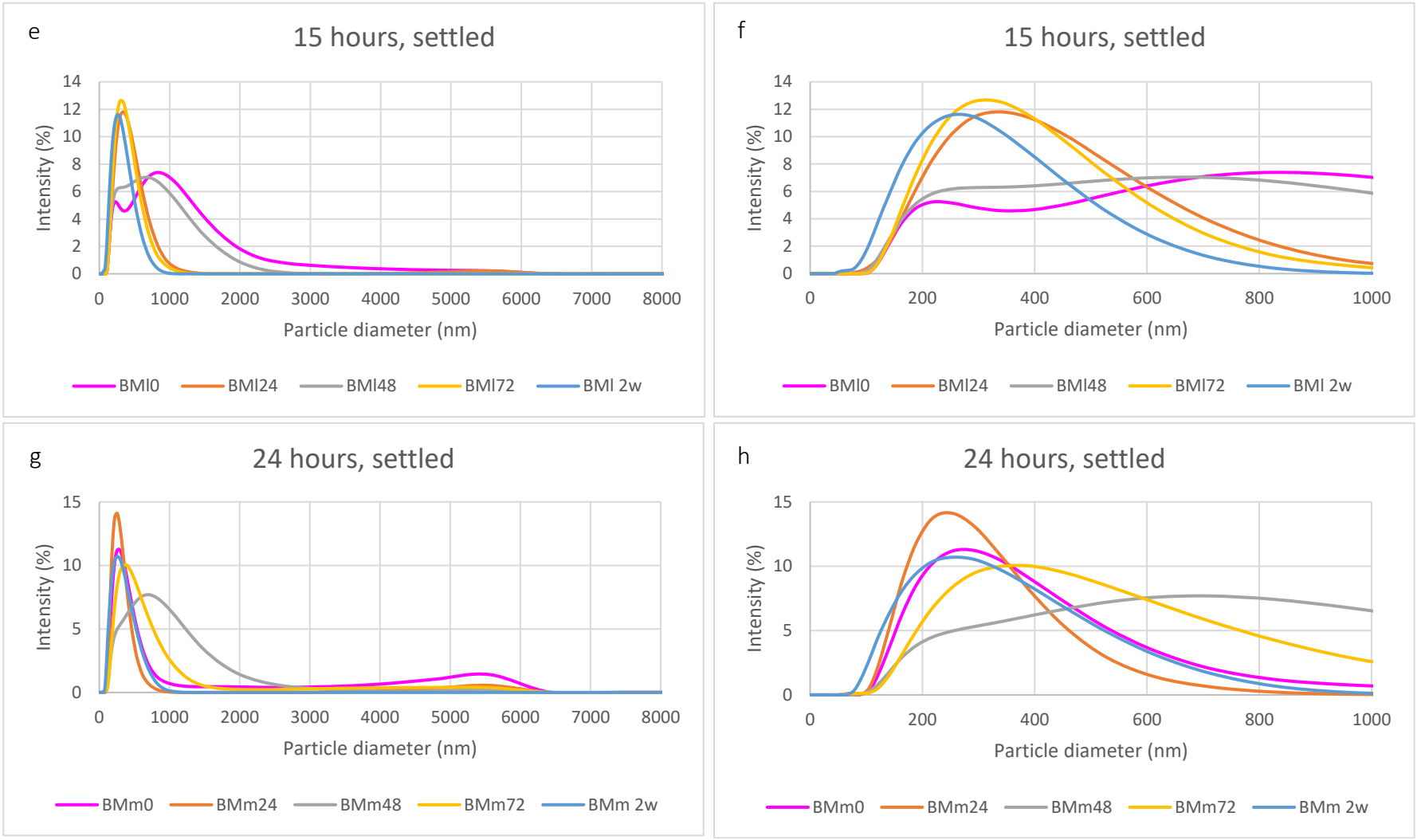

Figures 4.13a-h. The size distributions of the samples that were milled using 10mm balls, under dry conditions, for 1, 4, 15, and 24 hours, and then allowed to settle for up to two weeks. They are displayed according to how long they were milled for before settling.

Figures 4.14a and b show the size distribution of the dry ball milled samples, displayed according to which ball size was used in their preparation, to allow for comparison of the effect of milling time on each sample set.

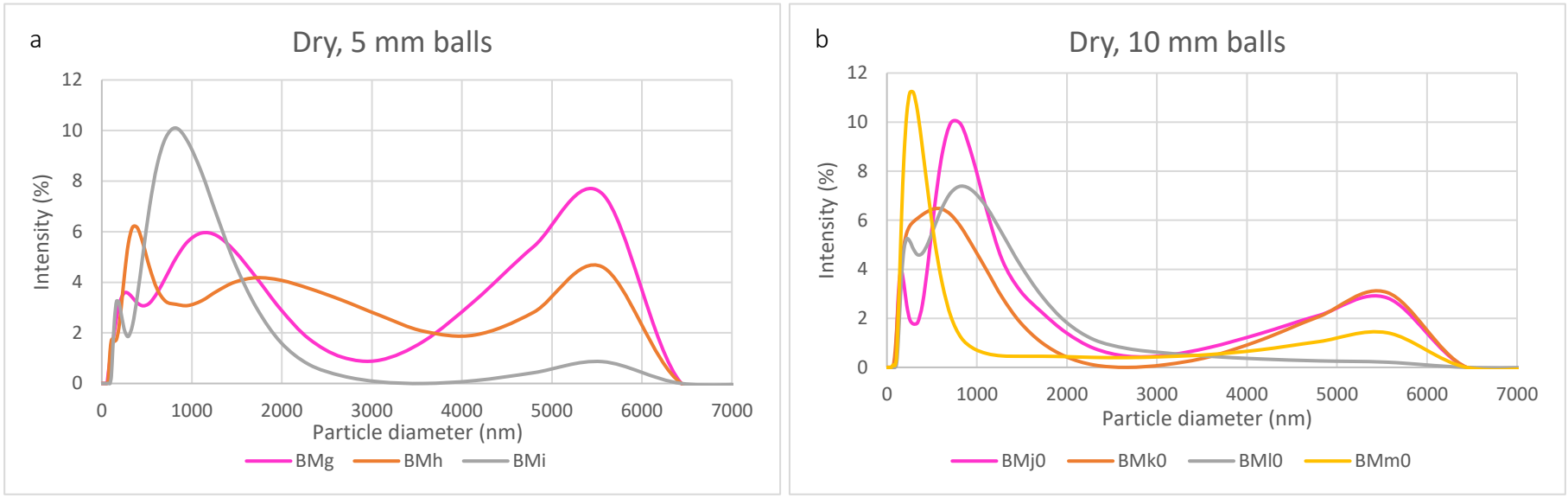

Figures 4.14. The size distribution of the dry ball milled samples, displayed according to which ball size was used in their preparation, to allow for comparison of the effect of milling time on each sample set.

Figures 4.15a-d contain the DLS measurements for the samples that were milled dry, using 10mm balls, and they are separated according to how long they were left to settle for, in order to highlight any effects that the milling time had on their size distribution as different stages of the settling process.

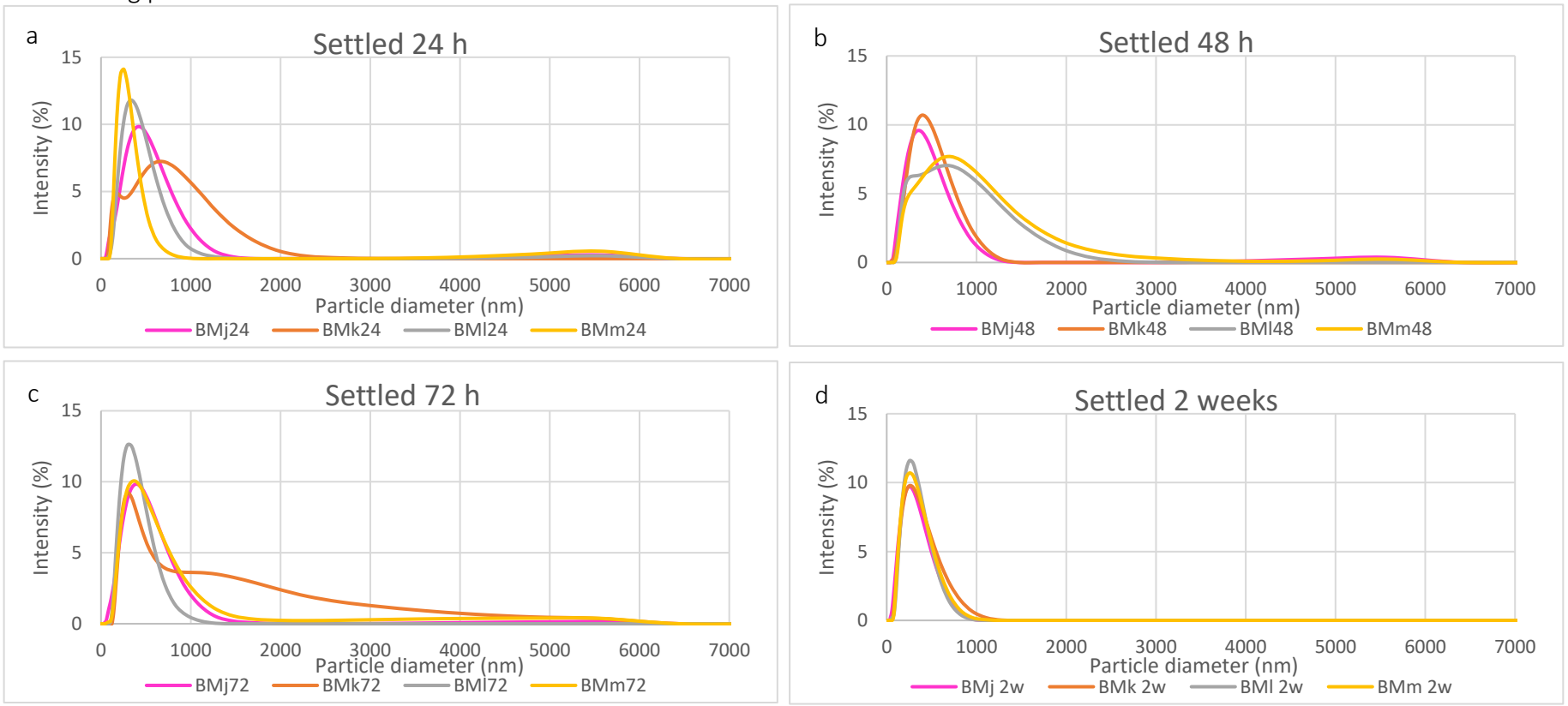

Figures 4.15a-d. DLS measurements for the samples that were milled dry, using 10mm balls, and they are separated according to how long they were left to settle for, in order to highlight any effects that the milling time had on their size distribution as different stages of the settling process.

As with ring milling, ball milling, with and without settling, could not produce a suspension of clay colloids with an average size small enough, and a size distribution narrow enough, to be suitable for use in the flow experiments.

Figures 4.11a-h show the size distribution of the ball milled samples that were made with a wet mixture of clay and ethanol, displayed according to milling time, *e.g.* all of the samples that were milled for one hour are displayed on the same graph, followed by all of the four hour samples. This enables any trends that arose as a result of sample preparation method to be observed. All of the samples that were milled for 1, 4 and 15 hours, both wet and dry, had an increased intensity distribution of large particles 5000-6000 nm in diameter, as shown by the peak heights being higher than that of the reference sample, and in the 1 and 4 hour milled samples (Figures 4.11a-d), the two clear peaks had been almost completely replaced by a very broad spread of particle sizes. BMm_0, the sample milled for 24 hours (shown in Figures 4.11g and h), retained the peak seen in the reference sample at 5000-6000 nm, but the largest peak shifted from 1110 nm to 295 nm. This indicates that milling it for 24 hours resulted in greater uniformity and a smaller particle size than in the reference sample.

Figures 4.12a and b show the size distribution of the wet ball milled samples, displayed according to which ball size was used in their preparation, to allow for comparison of the effect of milling time on each sample set. All of the samples retained the peak at ~5500 nm that was observed in the reference sample, and the smallest peak (~200-300 nm), appears to be shifted more to the left with increased milling time for both sets of conditions, but the change is negligible. When the largest peaks in both Figures 4.12a and b are compared, the samples which have been milled for 15 hours (BMc and BMf), have moved furthest to the

left, indicating that they have undergone the most significant reduction in particle size: they were measured at 955 nm and 712 nm respectively, compared to 1110 nm for the reference sample. The amount of shift the same peaks in the other samples have undergone does not appear to follow the same trend, suggesting that the samples need to be milled for more than four hours in order for there to be any observable difference. There is no significant difference between the samples produced using the 5 mm balls, and those using the 10 mm. Figures 4.13a-h show the results of the only settling tests that were run on the ball milled samples. These are dry samples made with 10 mm balls, and they are displayed according to how long they were milled for before being left to settle, *e.g.* Figures 4.13a and b show sample BMj_0, which was milled for 1 hour, and the results of it being left to settle for 24, 48 and 72 hours, and two weeks.

BMj_0 appears to have benefitted the most from being left to settle of any of the samples. It is the only one to show a clearly defined reduction in particle size across all of the settled samples, and the peak at 164 nm is no longer present. However, all of the samples are still too heterogeneous in size to be suitable for use in flow experiments. As BMJ_0 was milled for just one hour, the milling process would have broken the larger particles down less than in the longer milled samples, resulting in a greater proportion of large particles than in the other samples which are more likely to drop out of suspension than smaller ones, thereby resulting in a greater benefit from settling than would be observed in the other samples that were milled for longer. The opposite effect is shown by sample BMm_0: the 24-hour milling period has broken the clay down to the extent that settling it, even for as long as two weeks, produces very little change in particle size. It is also possible that, like in the ring milled samples, the colloids agglomerated in suspension as rapidly as they were sedimenting, which

could have masked any size reduction that occurred, and could not be identified by the DLS results. There are no clear trends in BMk_0 (4 hours), but sample (15 hours) is uniform after being left to settle for 48 hours or more. This is logical, as the clay particles will have been broken down more than in BMJ_0, but less than BMm_0, so the impact of settling would be expected to be greater than the former, but less than the latter.

Figures 4.14a and b. show the size distribution of the dry ball milled samples, displayed according to which ball size was used in their preparation, to allow for comparison of the effect of milling time on each sample set. BMg (1 hour) and BMh (4 hours) both have very broad particle size distributions, and it is only when the milling time reached 15 hours (BMi), that the three defined peaks common to most of the milled samples became pronounced. In Figure 4.12b, where the samples were prepared using the 10 mm balls, the three characteristic peaks become defined after 4 hours of milling. It is possible that the 10 mm balls ground the clay more effectively, but as the same trend was not observed in Figures 4.12a and b, where the effect of 5 mm balls compared to 10 mm balls was investigated for wet samples, it is not possible to be certain.

The most significant feature of the datasets in Figures 4.15a-d is that after 2 weeks of settling, the peak at 5000-6000 nm that was found in the reference sample and in many of the milled ones was no longer present, which suggests that all of the large material had finally dropped out of suspension (see Figure 4.15d). The 2 week settled samples are the most uniform, as would be expected, and the 24 hours the least.

As with ring milling, ball milling, with and without settling, could not produce a suspension of clay colloids with an average size small enough, and a size distribution narrow enough, to be suitable for use in the flow experiments. However, as was discussed in Section 4.3.2.1.3,

milling may introduce an artificially high number of edge sites, which could affect the reactivity and aggregation of the clay, so discounting this method may eliminate some complications later on in Chapters 6 and 7.

4.3.2.3 Cryomilling

4.3.2.3.1 Introduction

It was not possible to find an example in the literature of cryomilling being used to produce bentonite colloids, and as ring and ball- milling had already been used without success, just one sample was produced and tested, and it did not undergo settling.

4.3.2.3.2 Method

The cryomill used in this application was a SPEX 6750 freezer mill. 1 g of clay was placed into the cryomill vessel before lowering it into a bath of liquid nitrogen, which was at a temperature of approximately -195 °C. The impactor moved back and forth inside the tube roughly twice per second and ran for five cycles of approximately one minute. The liquid nitrogen levels were checked in between these cycles. A diagram showing the design and operation of the freezer mill is shown in Figure 4.16.

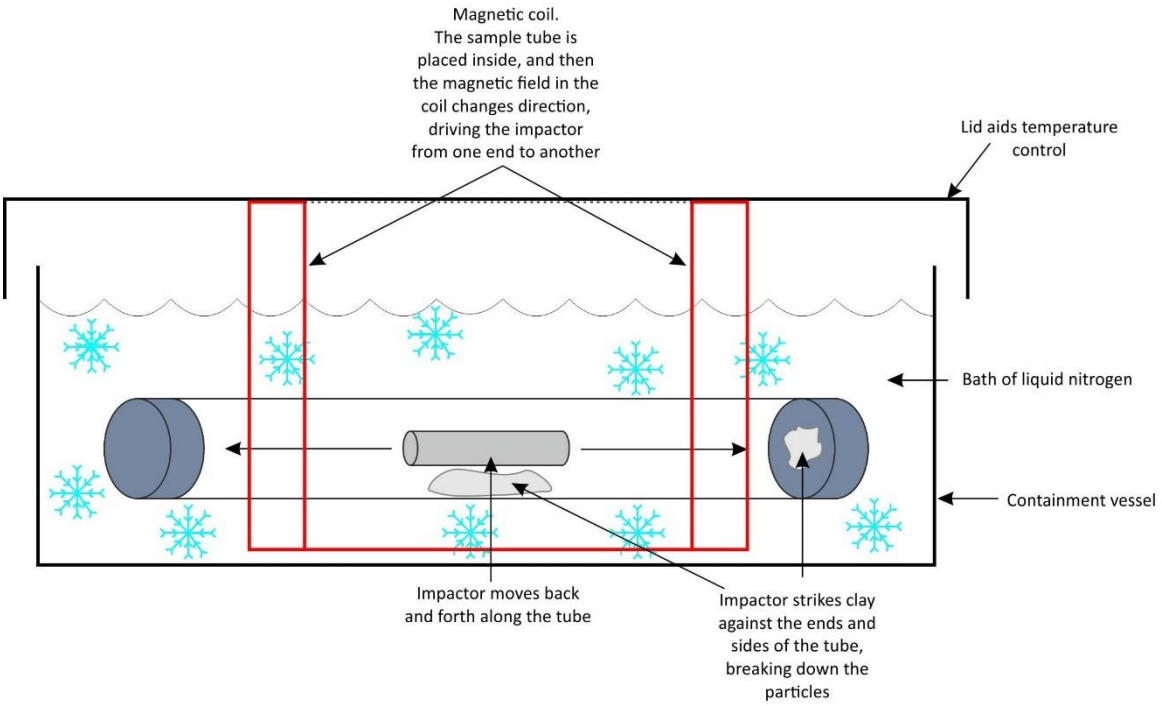

Figure 4.16. A diagram showing the design of the freezer mill, and how it works. An impactor is moved from one end of the sample tube to the other by an alternating magnetic field, breaking the clay down as it compacts it against the ends and sides of the tube.

0.01 g clay was mixed with 5 ml of deionised water, dispersed, and then the size distribution measured using DLS. Settling experiments were not conducted on the cryomilled sample because the results from the ring and ball milled samples had not been very successful, so the DLS results presented below were measured the same day as the suspension was made.

4.3.2.3.3 Results and discussion

Figures 4.17a and b show the size distribution of the particles in the cryomilled sample.

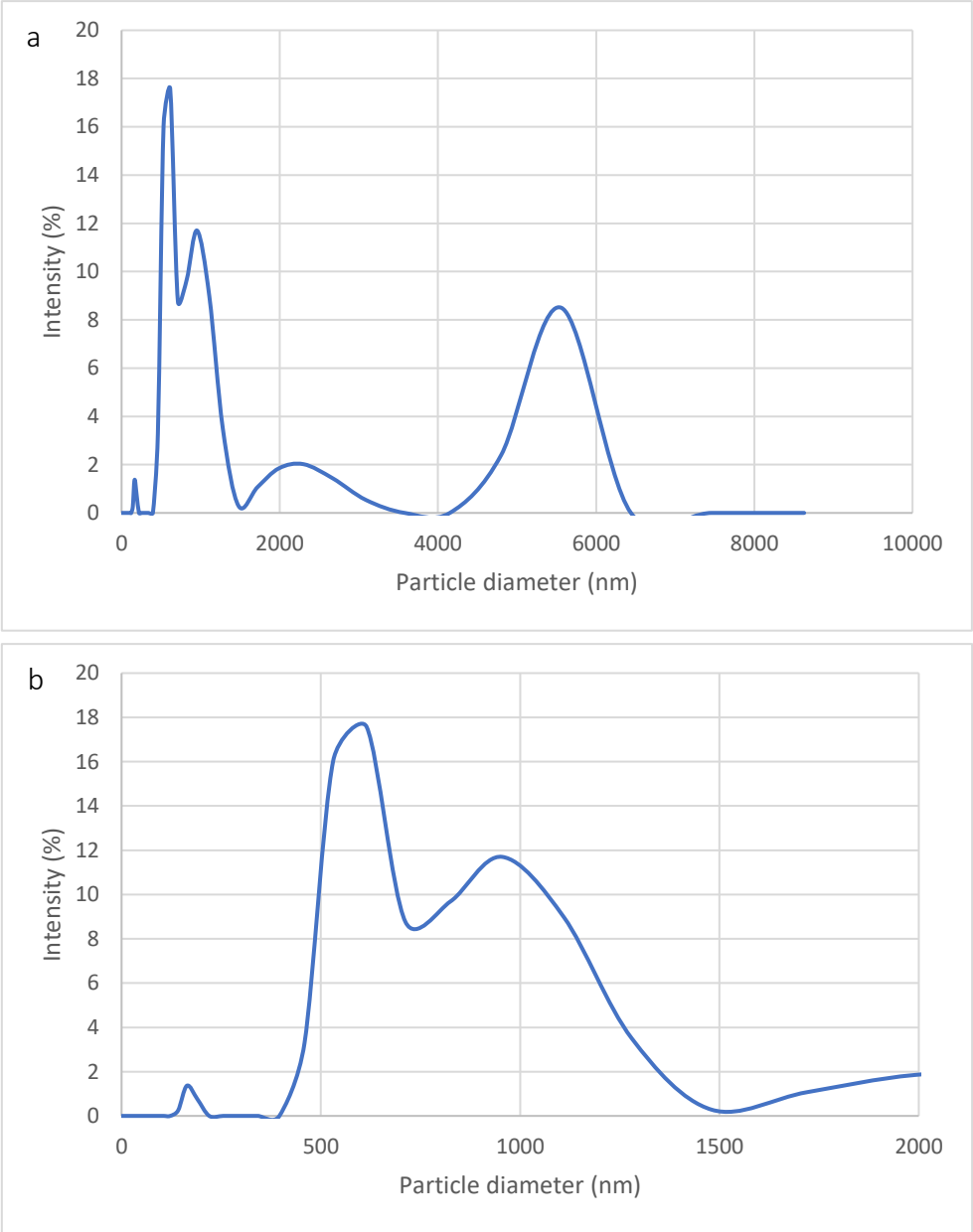

Figures 4.17a&b. The size distributions of the cryomilled fraction. It has five peaks, two more than the reference sample, and a greater percentage of large particles, which indicates that agglomeration occurred during the milling process.

The size distribution is very heterogeneous and has five peaks, compared to the three seen in the reference sample. The highest peak is at 615 nm, but there are significant numbers of

particles in the ranges 450-1500 nm, and the percentage of large (~4000-6500 nm) particles has actually increased in comparison to the reference sample, suggesting that, as was suggested in section 4.3.2.1.3 and by Kumar & Biswas (2017), some particles may have aggregated while others were broken down.

Cryomilling did not produce clay samples with the narrow size distribution required for use in the flow experiments in Chapter 6, and as sedimentation had already proven to make little difference to ring and ball milled samples, it was unlikely to do so for this sample. Like the other milling techniques however, there was a risk of the artificially exposed edge sites affecting the reactivity and aggregation behaviour of the clay colloids later in the project, so again, it may actually help to avoid future complications.

4.3.3 Filtration and dispersion

The introduction of a filtration method was an improvement upon the previous attempts to fractionate the MX80. The methodology still required considerable refinement, and the resulting particle size distributions did not always correspond with the nominal sizes of the filters, but it was possible to produce clay fractions with sizes within set boundaries for the first time. Dispersion of the bentonite was also key. Different combinations of pH adjustment and surfactants were used in addition to filtration to try and separate the clay aggregates before filtering them, and to prevent re-agglomeration afterwards. This helped to maintain the fractions as true to their filtered sizes as possible: if the colloids passed through a filter of specific pore size and then agglomerated, then their size distribution would bear little resemblance to the size of that filter. Those that did not produce suitable clay fractions are

discussed in sections 4.3.3.2 and 4.3.3.3 and Appendix 1. and the most successful method, dispersion using PVP, is detailed in section 4.3.3.4.

All of the methods in this section involve filtration, so the equipment is described first in section 4.3.3.1, and then how it was used specifically to assist with each individual method is described throughout the rest of section 4.3.3.

4.3.3.1 The filter system

The filter system used was a vacuum filtration device manufactured by GE Healthcare UK Ltd. A clay suspension was placed in the funnel at the top, and then drawn downwards by a vacuum pump through a filter and a glass frit into a large flask at the bottom. The vacuum pump that was used was a KNF N920G, and the filters were a mixture of glass microfiber filters and track-etched membranes with sizes that ranged from 50-1000 nm. A SciQuip

Figure 4.18. The filtration system setup. A vacuum pump draws the suspension through a filter, and the overhead stirrer helps to prevent it blocking the pores.

overhead stirrer was often used when filtering out the larger clay particles to help reduce caking on the filter paper, which blocks the pores. The setup is shown below in Figure 4.12

4.3.3.2 pH adjustment

4.3.3.2.1 Introduction

Chapter 2 discussed the pH-dependent nature of the charge on clay colloids; the faces hold a permanent negative charge, but the edges have a positive charge at low pH levels, and a more negative charge at pH>6.5 (Tombácz & Szekeres 2004). Therefore, it may be expected that bentonite colloids are more stable at a higher pH, because Coulombic repulsion occurs between the negative faces and edges, reducing the likelihood of them aggregating. Increased stability was desirable because it meant that the colloids could be fractionated more accurately (*i.e.* they would not agglomerate during fractionation, or shortly afterwards), and retained that same size distribution for longer, so that if they needed to be stored for a short period of time before they could be used in flow experiments, their size distribution would not have changed substantially.

The Coulombic forces between the particles in suspension can be determined by measuring the zeta potential. This was explained in Chapter 3. It is expected that a higher pH would lead to a more negative zeta potential, greater repulsion between the particles, and therefore greater stability. This experiment was designed to investigate whether this is indeed the case. Acid and base were added to a suspension of bentonite colloids in order to adjust the pH, and then the zeta potential and size were measured.

4.3.3.2.2 Method

Nitrogen was bubbled through ultrapure water (Millipore, 18.2MΩ, 2 ppb TOC) for two minutes to remove as much CO_2 as possible in an attempt to mirror the experimental

protocol of Maher *et al*. (2016), where stable brucite colloids were produced by preparing a starting solution of magnesium hydroxide and deionised water under nitrogen, and then filtering them to different sizes.. This is discussed in more detail in Appendix 1. MX80 was sieved to <25 μm to remove the larger particles, and then mixed with the ultrapure water at a concentration of 400 mg/l and sonicated until it dispersed, which took approximately five minutes. The suspension was then put through a 200 nm filter.

Next, the pH of the mixture was adjusted using 0.1 M HCl and NaOH, as per Yukselen & Kaya (2003). It was not possible to obtain a pH reading for the starting dispersion using an electronic pH probe because the ion levels in ultrapure water are so low that an accurate reading cannot be obtained with an electrode, so a few drops of HCl were added to it before taking the first pH measurement, and that was used as a starting point. From there, a few drops of HCl or NaOH were added to each sample in order to adjust their pH. Eleven readings were taken within the pH range 1.5- 12.3 using a Hanna Instruments Microprocessor pH meter. Measurements of the size distribution and zeta potential of each sample were then taken using a Zetasizer Nano ZS.

4.3.3.2.3 Results and discussion

Table 4.6 and Figure 4.13 show the zeta potential for each of the adjusted pH values, and Figures 4.14a and b show the corresponding size distributions for each, over different scales.

Table 4.6. The zeta potential at different pH values. It ranged from -22 mV under very acidic conditions, to -37.5 mV at highly basic ones.

pH	Zeta Potential (mV)
1.50	-22
2.33	-19.6
3.23	-19.1
4.15	-28.1
5.83	-26.9
6.94	-29.3
7.98	-33.9
9.29	-30.1
10.06	-32.7
11.06	-34.3
12.31	-37.5

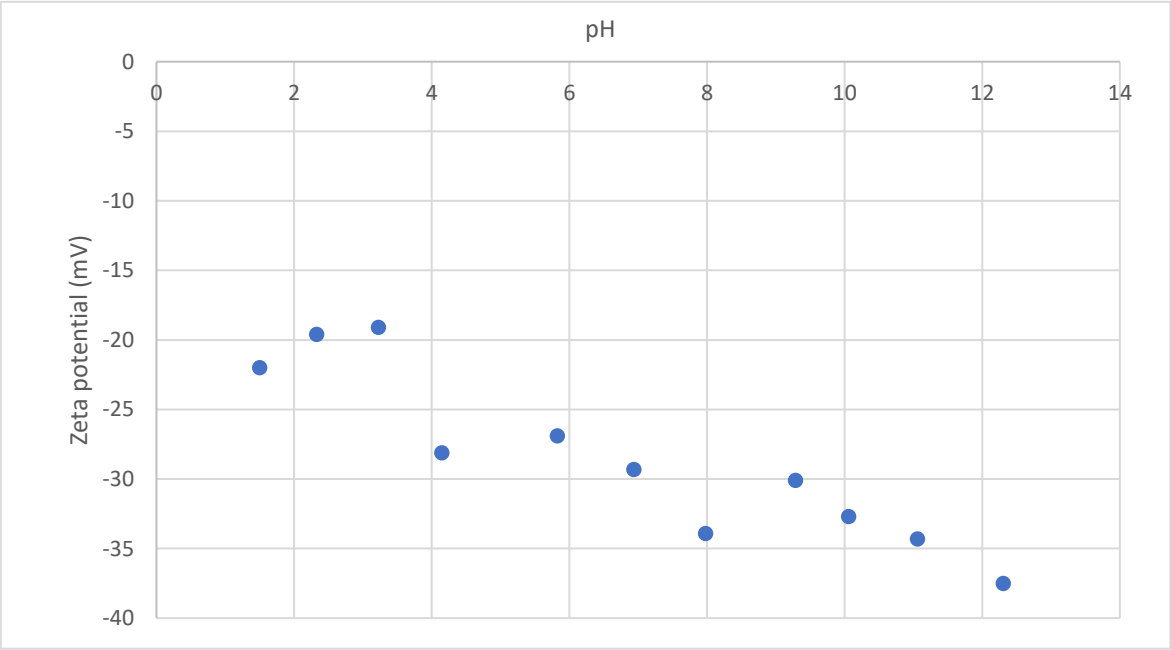

Figure 4.19. The same dataset as is shown in Table 4.6, the zeta potential at different pH values, but displayed on a graph to allow for visual comparison.

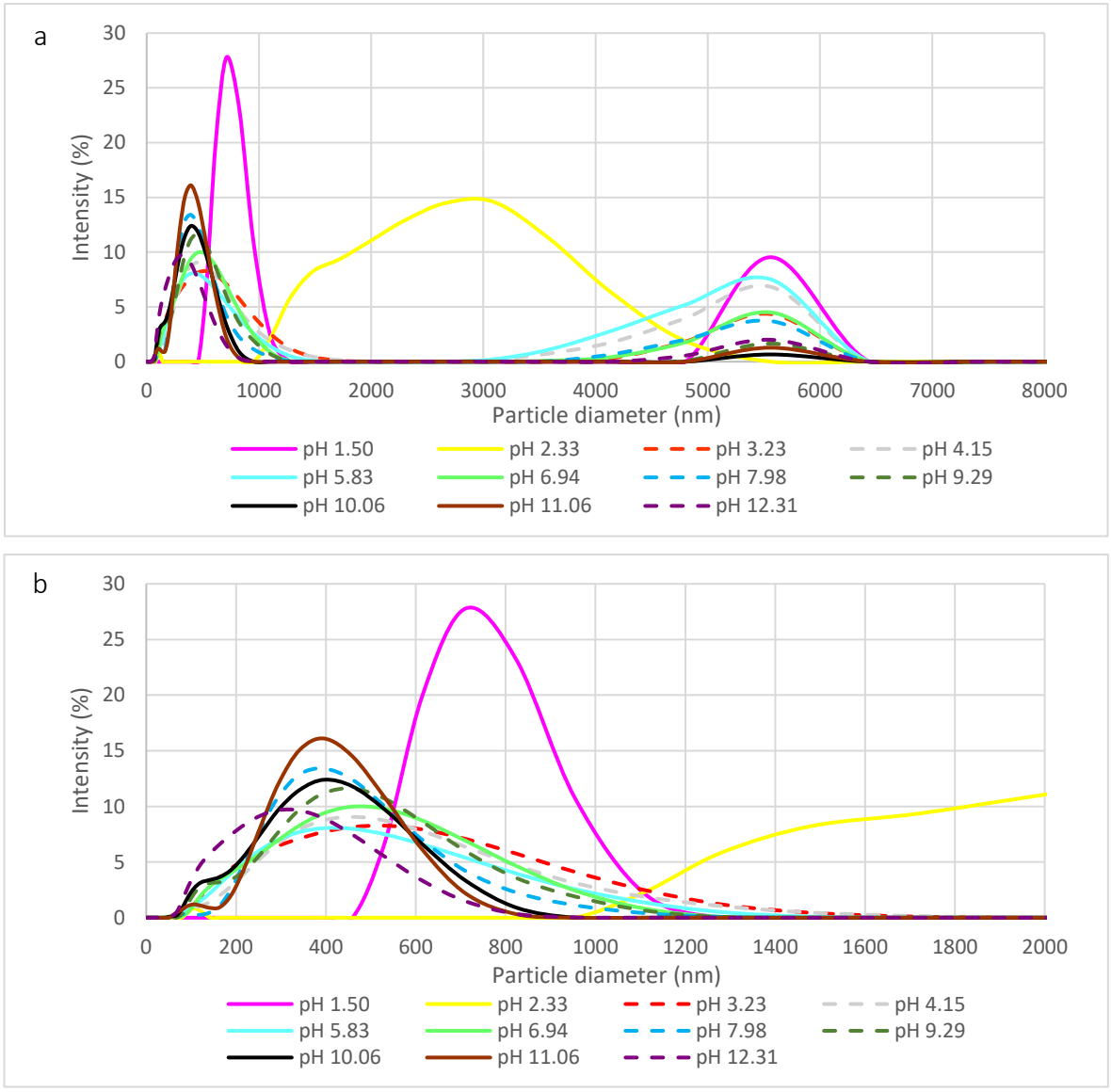

Figures 4.20a&b. The size distributions at different pH values, shown at two different magnifications. Particles substantially bigger than would have passed through the <200 nm filter are present in all of the fractions, which suggests that agglomeration occurred in all of the suspensions after filtration, indicating that they are unstable.

Table 4.6 and Figure 4.13 show that as the pH increases, zeta potential becomes more negative, which corresponds with what was expected from reviewing the literature (Tombácz & Szekeres 2004). This should theoretically promote repulsion between the particles, making them more stable and less likely to agglomerate. However, the size distribution shows particles substantially bigger than would have passed through the <200

nm filter in all of the fractions, which suggests that agglomeration occurred in all of the fractions after filtration, and therefore that the colloids were not stable. Apart from the sample measured at pH 2.33, all of the suspensions broadly retain a similar distribution to that of the reference sample: one peak at 5000-6000 nm, and a narrower peak of higher intensity, albeit shifted to a maximum of around 400 nm, around half the size of the 1110 nm peak in the reference sample. These peaks still tend to be somewhat broad, with particles ranging from 200-800 nm. The sample made at pH 2.33 has a single, very broad peak, containing particles from 1000-5500 nm in diameter. It is unclear why it has a distribution so different from the others, so it is likely to be an anomalous sample.

Anomalies aside, all of the samples had size distributions far too broad to be of use in the flow experiments. Missana & Adell (2000) acknowledged that the stability of montmorillonite colloids differs significantly from what was predicted through the use of DLVO theory because of the pH-dependent nature of the edge charges, and therefore adjusting the pH alone is unlikely to produce stable clay colloids, so it is unclear how long they would retain their size distributions for when in solution, which could affect their suitability for use in the flow experiments. Despite these shortcomings, a follow-up experiment was carried out, where surfactants were used in addition to pH adjustment and filtration to try and stabilise the colloids more effectively. This is discussed below in Section 4.3.3.3.

4.3.3.3 pH adjustment, with sodium chloride and sodium pyrophosphate

4.3.3.3.1 Introduction

Dispersants are a type of surfactant that reduce the interfacial tension between adjacent phases, causing them to separate and reducing the likelihood of them agglomerating or

settling (Fiocco & Lewis 1999). They are commonly used to clean up oil spills, where their ability to break up slicks then allows the oil to be distributed by the movement of the ocean, but in this application, they were used to try and disperse the clay agglomerates so that they could then be separated by size, and to prevent the formation of flocculants during or after this fractionation. Two different materials were used to try and encourage the clay aggregates to disperse in deionised water: sodium chloride and sodium pyrophosphate.

Yukselen & Kaya (2003) made the zeta potential of a clay suspension more negative by introducing different mono- and divalent cations and adjusting the pH, theoretically reducing its tendency to agglomerate. As per their method, 10^{-4} M NaCl was used to make a clay suspension, the pH adjusted to three different levels, and then the zeta measurements taken. Kaolinite was used in this study, which is a type of clay similar to bentonite, but its tetrahedral silica and octahedral alumina sheets have a 1:1 ratio instead of 2:1. The monovalent cations reduced the zeta potential successfully because exchange between those and H^+ ions expanded the more diffuse outer section of the electrical double layer, making it more negative. Higher pH levels also resulted in more negative zeta potentials (Yukselen & Kaya 2003). pH adjustment alone had already been unsuccessful (see section 4.3.3.2), but the results had been promising for kaolinite, so this combination of pH modification and dispersion was worth investigating for bentonite.

Pusch (2002) discussed the use of sodium pyrophosphate for disintegrating soil samples before carrying out grain size analysis, and Goh *et al*. (2011) investigated the effect of the pyrophosphate ion on bentonite slurries, which are used to assist drilling operations in the petroleum industry. The pyrophosphate anions reduce yield stress of mixtures by forming a barrier at particle edges, reducing the edge-to-face interaction (Goh *et al*. 2011). Sodium

pyrophosphate was mixed with bentonite colloids with the intention of weakening this interaction enough to disperse them and prevent re-agglomeration.

Clay suspensions made with these two dispersants (and with deionised water, to provide a baseline) were filtered to a colloidal size and tested at three different pH levels; acidic (pH=4), basic (pH=11) and pH=8.8, which was the level at which Sherriff (2015) reported that the MX80 colloids used in their research were stable.

4.3.3.3.2 Method

Deionised water, 10^{-4} M NaCl and 0.1 M $Na_4P_3O_7$ were each mixed with MX80 (sieved to <25 µm) at a concentration of 10 mg/l and sonicated until the clay was fully dispersed. Each sample was divided into three and the pH of these adjusted to 4, 8.8 and 11 using 0.1 M NaOH or HCl. Each of these were then filtered to produce fractions of <200 nm, <100 nm and <50 nm. The result was twenty-seven samples in total: three different size fractions of three different dispersants at three different pH levels. Their size distributions were measured using DLS.

4.3.3.3.3 Results and discussion

The size distributions of the different samples are shown below in Figures 4.21a-f, separated by the reagent used.

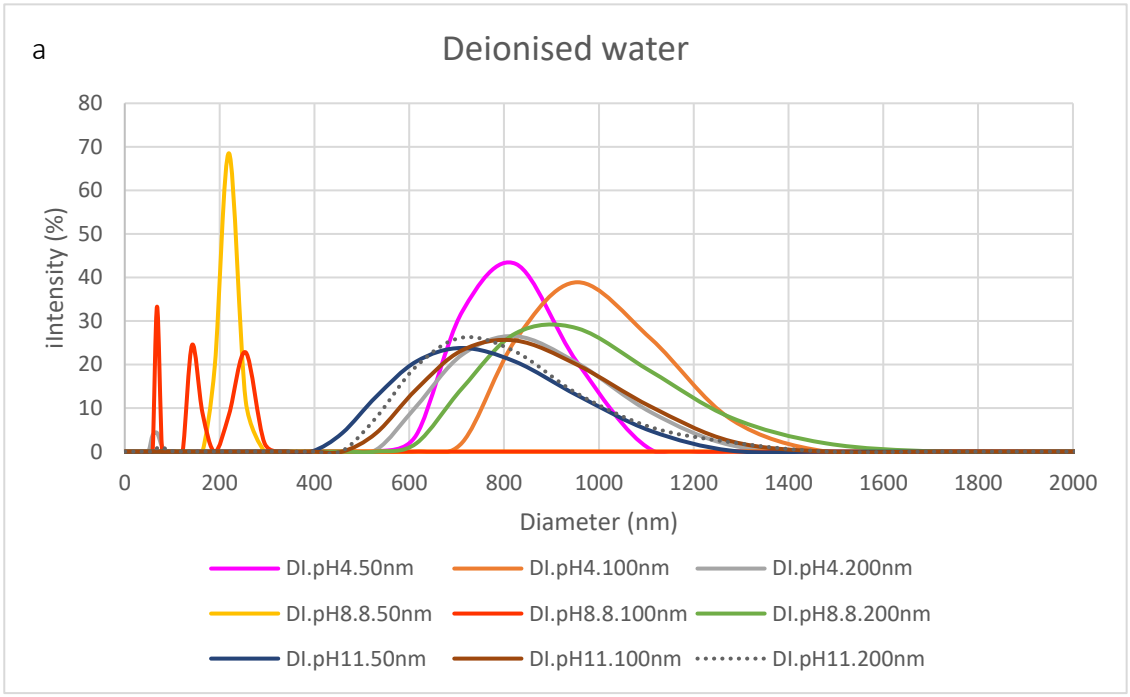

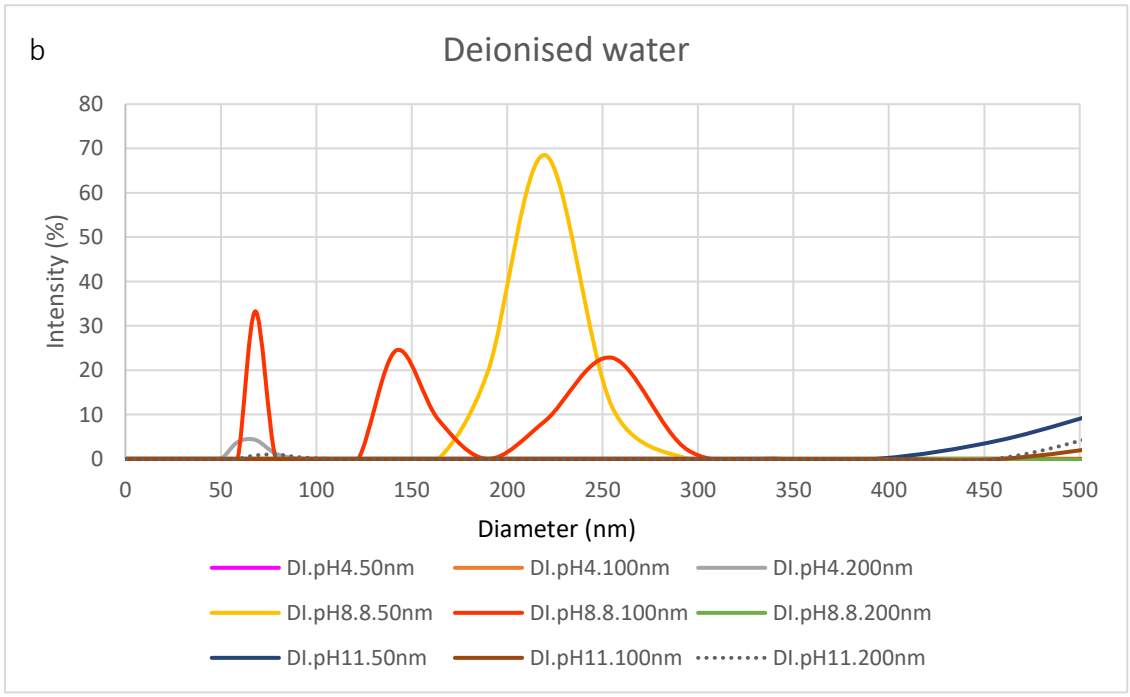

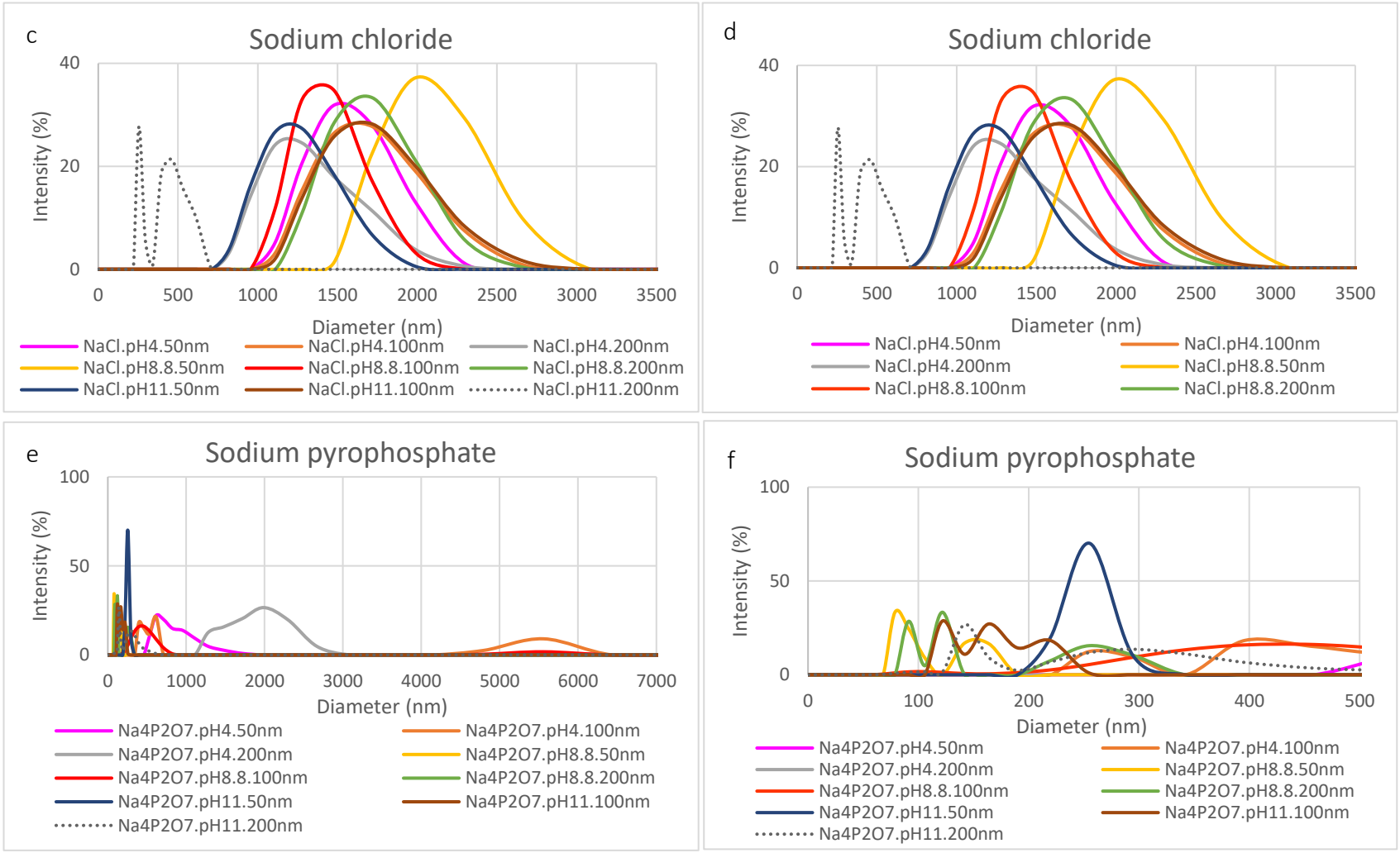

Figures 4.21a-f. DLS measurements showing the size distributions of samples that were produced by filtering colloidal suspensions that had been coated with a dispersant, and their pH adjusted to three different levels. The filter sizes used were 200, 100 and 50 nm, the dispersants were sodium chloride and sodium pyrophosphate, and the pH levels were adjusted to 4, 8.8, and 11.

The samples made with deionised water were included as a baseline, so that the effects of filtration without any additional dispersing agents can be seen. The most notable factor is that all but two of the samples have large, broad peaks between 500-1500 nm. The largest membrane filter used in this experiment had a pore size of 200 nm, so these particles should not be present. Doucet *et al*. (2005) observed similar results, where particles found in the permeate were larger than the pore sizes of the membranes used in cross-flow filtration, and therefore should not have passed through them. The authors offer two explanations that could be relevant here: firstly, that molecules with a high molecular weight may be able to pass through smaller pores, or alternatively that the clay particles may change shape and size during or after fractionation, *e.g.* due to agglomeration. Contamination, either from the air or due to fibres being detached from the filters, could also be at fault. The other two samples, which were produced using 50 nm and 100 nm pore size filters at pH 8.8, are closer to the expected pore size. If bentonite colloids are stable at pH 8.8 as Sherriff (2015) suggested, then this supports the theory that agglomeration is occurring after filtration: it is reduced at the pH where the colloids are reportedly more stable, so less agglomeration occurred.

The samples made with sodium chloride have an even broader size distribution; wide peaks, ranging from 1000-2000 nm, and only the sample produced using a 200 nm filter at pH 11 was near the expected size, albeit still too large. It appears that the work of Yukselen & Kaya (2003) on kaolinite cannot be applied to bentonite.

With one exception (pH 4, 100 nm filter, which may be the result of contamination by airborne dust, or a bubble), the samples made using sodium pyrophosphate tend to have smaller particle sizes and narrower size distributions than those made using deionised water

and NaCl. There is no clear trend; pH does not have a discernible impact, and larger particles than expected are found in every sample, but the particle size distributions are smaller and more uniform than any produced previously.

Apart from the anomalous sodium pyrophosphate sample that was discussed above, all three methods have eliminated the very large particles observed in the reference sample (*i.e.* those 4000-6000 nm in diameter), and those made using sodium pyrophosphate have reduced the sizes and size distribution of the colloids considerably. However, preliminary tests carried out on those samples indicated that the sodium pyrophosphate interfered significantly with some of the analytical techniques that were going to be used to carry out further characterisation, most notably ICP-MS, which made it very difficult to take measurements. Its use was discontinued for this reason.

4.3.3.4 Polyvinylpyrrolidone (PVP)

4.3.3.4.1 Introduction.

Dispersants, discussed earlier in section 4.3.3.3, are materials that can reduce the interfacial tension between adjacent phases, aiding separation and reducing re-agglomeration. Surfactants can be used, often blended with solvents, to form dispersants suitable for use in applications such as the clean-up of oil spills (Fiocco & Lewis 1999). PVP is a soluble, non-ionic surfactant which can be used to improve dispersion and reduce the size of suspensions by coating the particles and reducing surface tension, and its structure is shown in Figure 4.22 (Fainerman *et al*. 2001; Van Den Mooter *et al.* 1998; Malekzadeh *et al.* 2012).

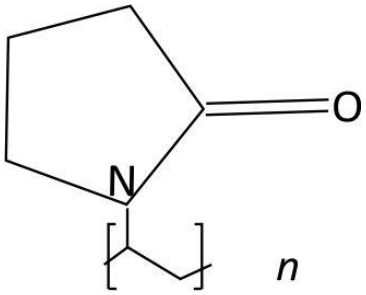

Figure 4.22. The structure of PVP. The information provided by Malekzadeh *et al.* 2012, but the image is of the author's own design.

In addition to PVP, polyethylene glycol (PEG) and gelatine were tested at the suggestion of one of the collaborators on this project to examine how well they dispersed and stabilised the clay particles before filtration, and to reduce aggregation afterwards, but their use was discontinued for a number of reasons, including issues with the supply of PEG, and the propensity of gelatine to decompose rapidly. More detail about this may be found in Appendix 1.

It has not been possible to identify any research in which it was PVP was used in the process of producing small, stable clay particles, so this application was a novel one.

4.3.3.4.2 Preliminary experiments

This method, the filtration of clay particles that had been stabilised by PVP, was the method that was taken forward to be used in the flow experiments, but it went through many iterations before a method was settled upon. There is insufficient space to describe them all, but some key steps and results are presented below.

The quantity of PVP that was used was based on the findings of Séquaris *et al*. (2000). Their research determined that adsorption of PVP onto sodium montmorillonite levelled off at around 0.6 g/g; or 0.6 g/l PVP for 1 g/l of clay, so this was used as a starting point initially. That investigation used 44000 g/mol PVP, but only 40000 g/mol was available, so the quantity used had to be modified by 10 % to account for the difference in materials. Due to

human error, the starting point for PVP adsorption was scaled down rather than up, to 0.545 g PVP in a 1 g/l clay suspension. However, despite this mistake, preliminary experiments in which the clay and PVP mixture was sonicated, filtered and characterised showed some promise, such as those in Figures 4.23a-d.

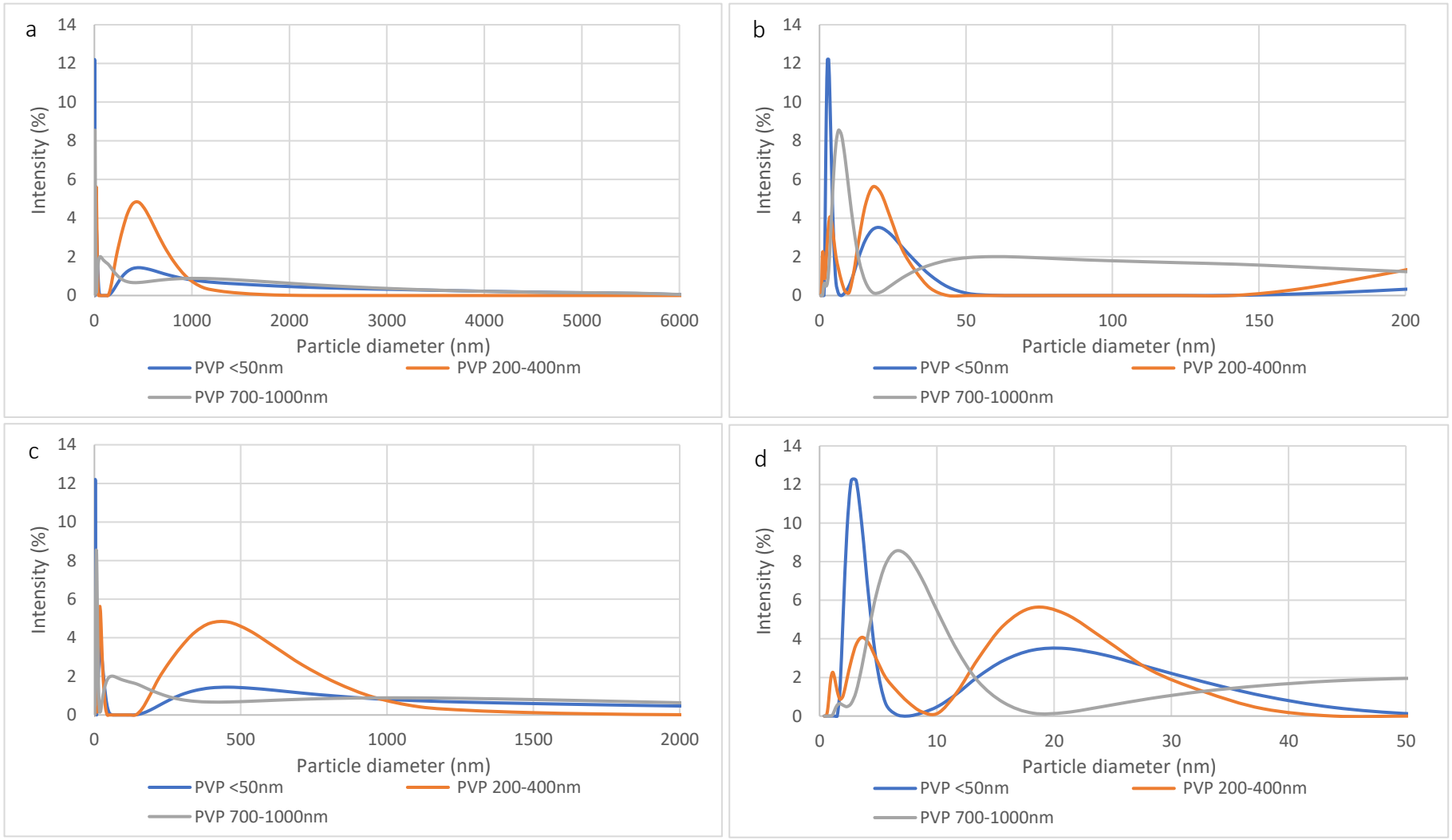

Figures 4.23a-d. The results of preliminary experiments where clay and PVP were filtered and characterised. Graphs a-d all show the same dataset but at a range of magnifications, so that the features at the different size ranges may be observed.

The aim was to produce small clay particles. These would have a larger surface area than a sample with similar concentration but larger particles, so after the preliminary results looked positive, the amount of PVP used in the experiments was quadrupled to ensure that there was enough surfactant to coat the clay surfaces, to 2.18 g in a 1 g/l clay suspension. The results shown below in Figures 4.24a and b are the results of an experiment where this was tested.

Three fractions were made: <50 nm, 100-200 nm, made via resuspension, and <1000 nm. Resuspension allowed fractions with size distributions between selected filter sizes to be produced, as opposed to just isolating all of the particles that were small enough to pass through a certain pore size. To make a 100-200 nm fraction, a clay suspension was filtered first through a 200 nm filter, and then through a 100 nm filter. The 100 nm filter was retained, placed into deionised water, and then either shaken or sonicated in order to release the particles that had collected on it back into suspension. These particles had passed through the 200 nm pores, but not through the 100 nm, so they were nominally of 100-200 nm in size.

Figures 4.23a-d show the size distribution of a 700-1000 nm fraction, but the experiment shown in Figures 4.24a and b and 4.25a and b produced a <1000 nm fraction. The <1000 nm fraction was made in place of the earlier 700-1000 nm fraction because of the concerns about contamination; resuspending the colloids from the surface of the soft glass microfiber filters caused them to visibly disintegrate and release fibres into the suspension, regardless of whether it was done by shaking, or the more energetic sonication process. The <1000 nm fraction was expected to have a very broad size distribution but was included to provide a comparison to the other fractions.

The 100-200 nm fraction was made in place of the 200-400 nm fraction to try and make one with a narrower size distribution. The <50 nm and <1000 nm fractions were both made from a clay suspension that was made by shaking it by hand until it dispersed before filtering it, and the 100-200 nm was made from a suspension that had been dispersed by sonicating it for 1 hour, with the PVP added half way through (trial-and-error tests had been used to determine whether sonication or shaking were more successful at producing the desired size fraction). Preliminary experiments suggested that shaking by hand and sonicating resulted in fractions, and this combination (shaking the <50 nm and <1000 nm and sonicating the 100-200 nm) appeared to be the most successful when measured by DLS. This was probably because the more energetic sonication can result in either dispersion or aggregation of particles depending on factors such as the material and sonication time. The 100-200 nm fraction was passed through a 200 nm membrane again to remove any particles that had aggregated during resuspension. The resulting fractions are shown in Figures 4.24a and b.

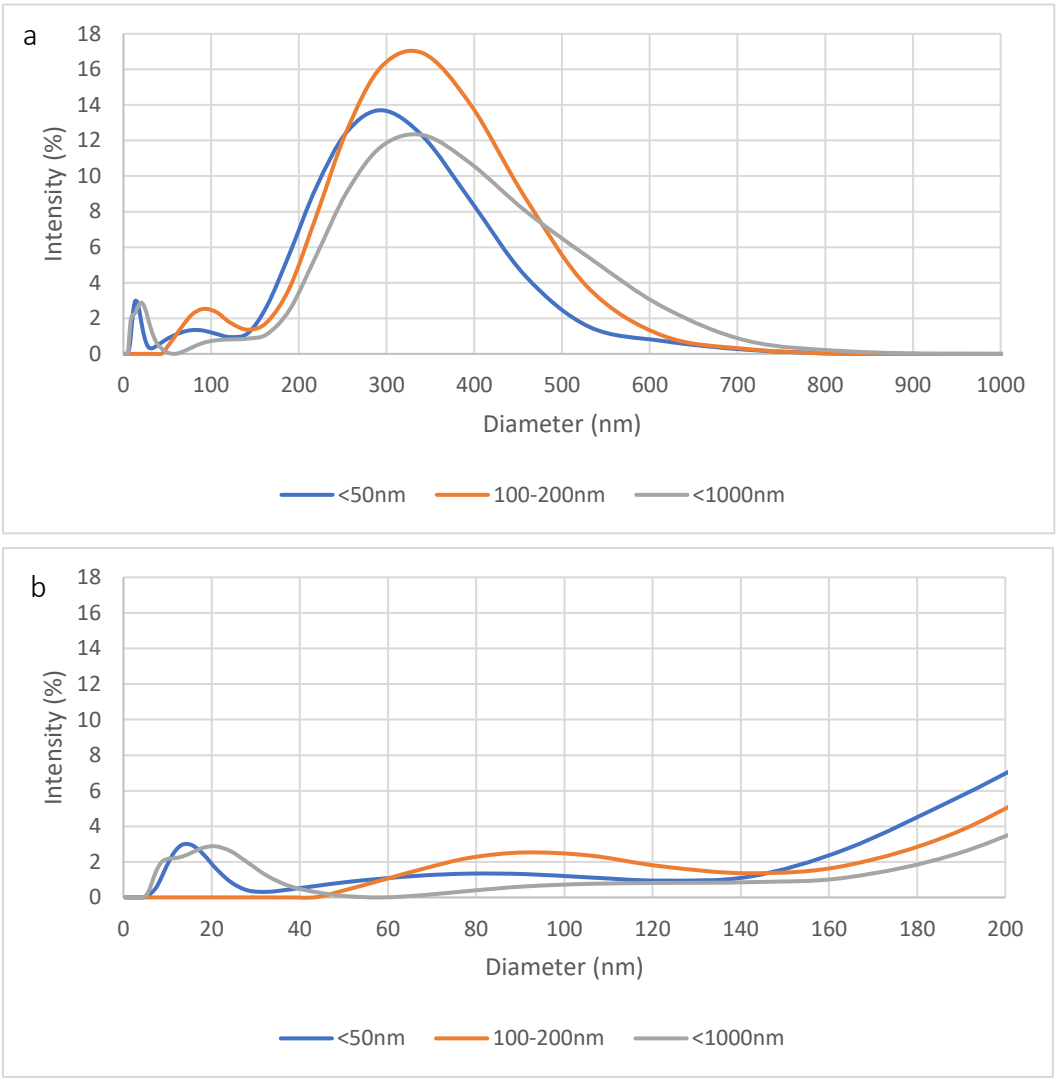

Figures 4.24a&b. The size distribution of fractions that were produced by filtration of clays stabilised with 2.18 g/l of PVP. The <50 nm and <1000 nm fractions were produced by filtration, and the 100-200 nm fraction by filtration and resuspension off the 100nm filter.

These fractions have similar average sizes despite being produced by filtration though different membranes. However, the number distribution in Figures 4.25a and b indicated that there were a large number of very small particles present in the <50 nm and <1000 nm samples:

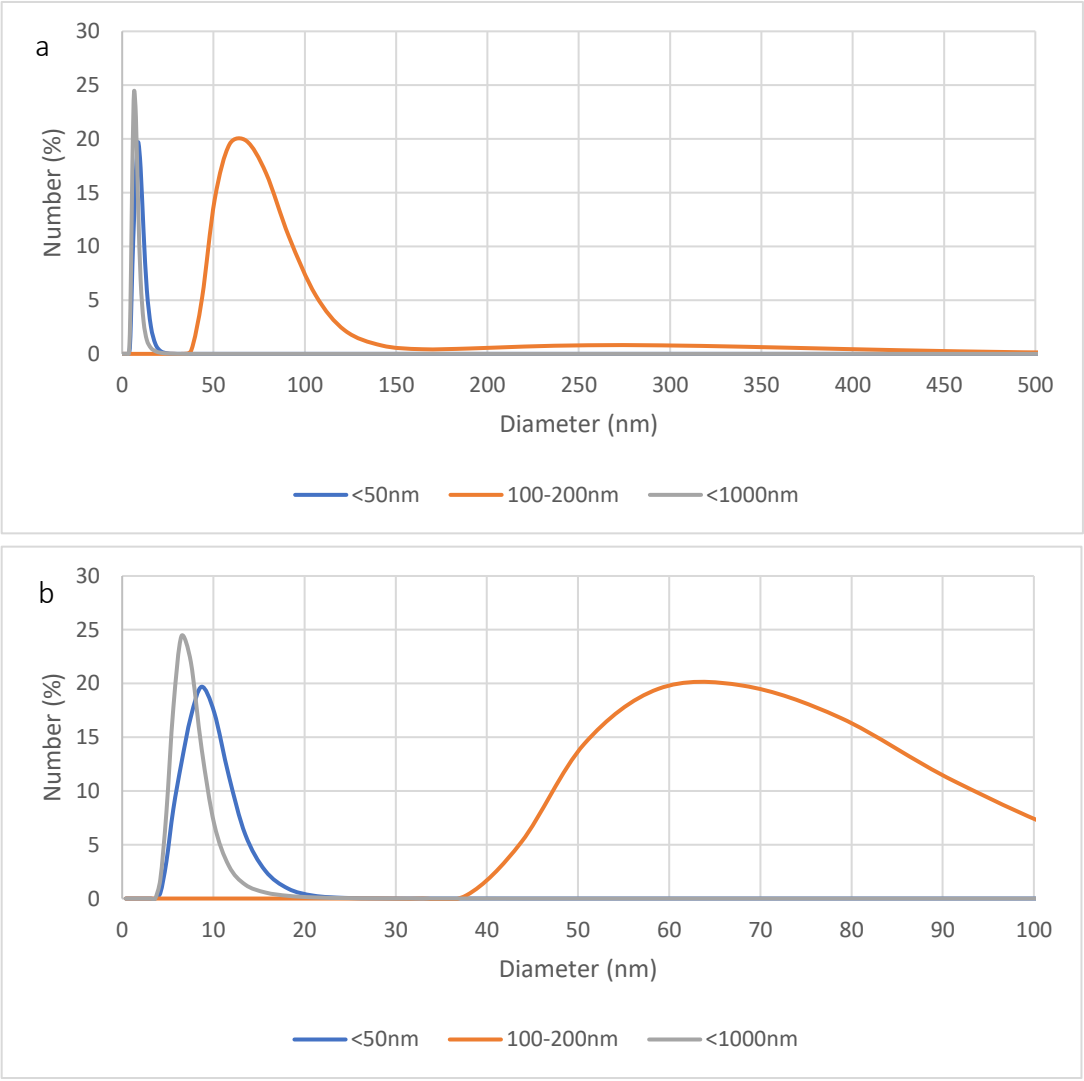

Figures 4.25a&b. The number distributions of the fractions shown in Figures 4.17a and b. The shortcomings of the number distributions of DLS data were discussed in Chapter 3, and this data is shown only to demonstrate that there were large numbers of small particles in the sample.

The shortcomings of the number distributions of DLS data were discussed in Chapter 3, and Figures 4.25a and b are shown only to demonstrate that there were large numbers of small particles in the sample; the heterogeneity of the particle size and mineral composition of MX80 made it impossible to get accurate absorption and refractive index numbers, which are very important for number distributions, and so the data was unlikely to be reliable. It is presented only for reference. It should be noted that the number distributions of all of the solutions discussed in this chapter and Appendix 1 were examined, but none of them indicated that they were worth investigating further.

DLS measurements of other samples containing PVP indicated that the <20 nm peaks shown on the graphs of number distribution may actually have been from PVP that was not adsorbed onto the clay particles. However, the presence of peaks indicating small average particle size and a narrow size distribution meant that this method was compelling enough to warrant further investigation.

TEM images of the <50 nm and <1000 nm fractions were provided by a colleague at the university and are shown in Figures 4.26a and b respectively, and are discussed and analysed in detail below. It was not possible to get images of the 100-200 nm fraction because the concentration of the resuspended particles was so low that no particles could be found on the TEM grid. For this reason, this fraction was not made again, because if the resulting suspension was of such low concentration that it could not be imaged, it was likely to be below the limits of detection for the nephelometer, and therefore unsuitable for use in the flow experiments, which was the key motivation behind making the suspensions. This was proven correct when the flow experiments were started, because even the <50 nm fractions,

which were relatively easy to image, were only just of a high enough concentration to be detected above the background.

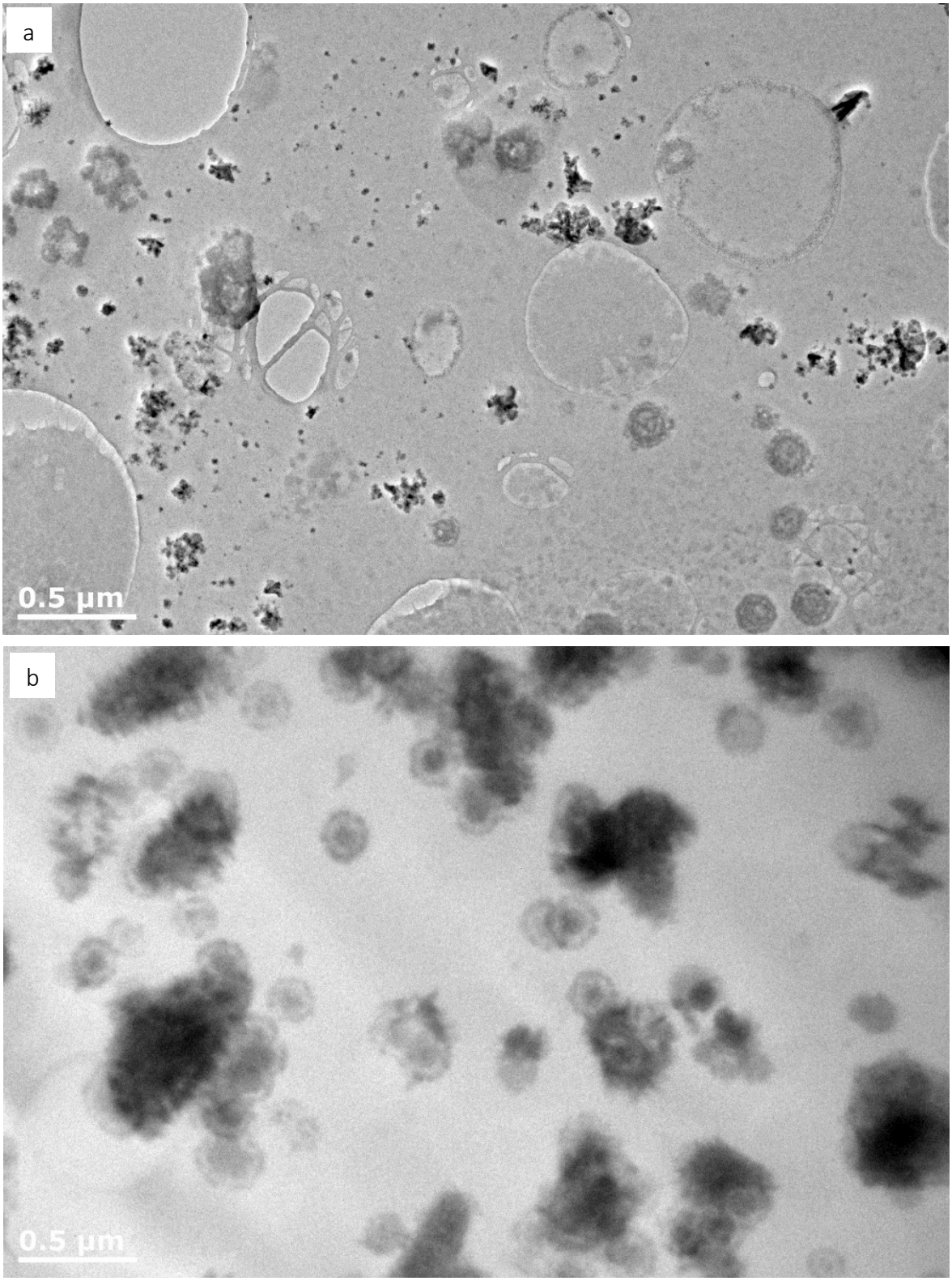

Figures 4.26a&b TEM images of a) the <50 nm and b) the <1000 nm fractions, both taken at 6000x magnification.

Both of these images were taken at 6000x magnification. The large, pale circles in Figure 4.26a are holes in the carbon film that was used to coat the samples. Over thirty TEM images of the two samples were analysed using the image processing program ImageJ, and the data was grouped and used to produce histograms, which are shown below in Figures 4.27a-c. ImageJ analyses the area of particles by counting the number of pixels that they cover. These may be defined either by automatic thresholding, or by the user drawing around them manually, and the software then relates this to the scale on the image. The irregular shapes of the particles meant that giving lateral dimensions for them would have been inaccurate, so the graphs below show the frequency by which particles in different size bins occur, but do not attempt to assign diameters to them; rather, the histograms are simply representative of the two fractions having different size distribution profiles, rather than attempting to define those distributions.

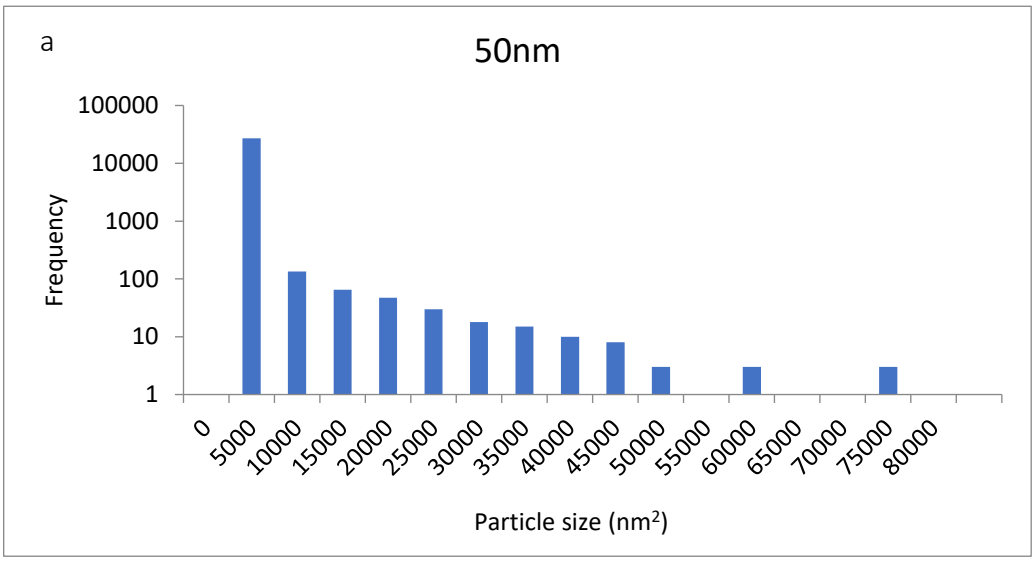

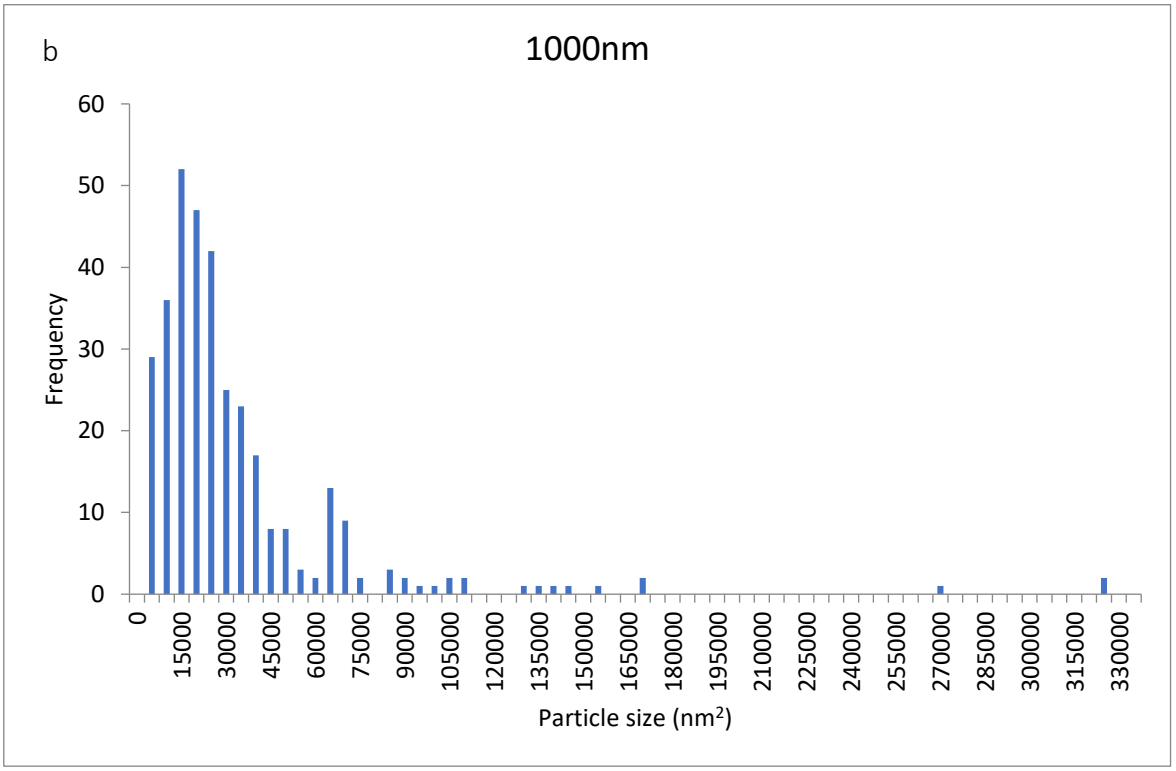

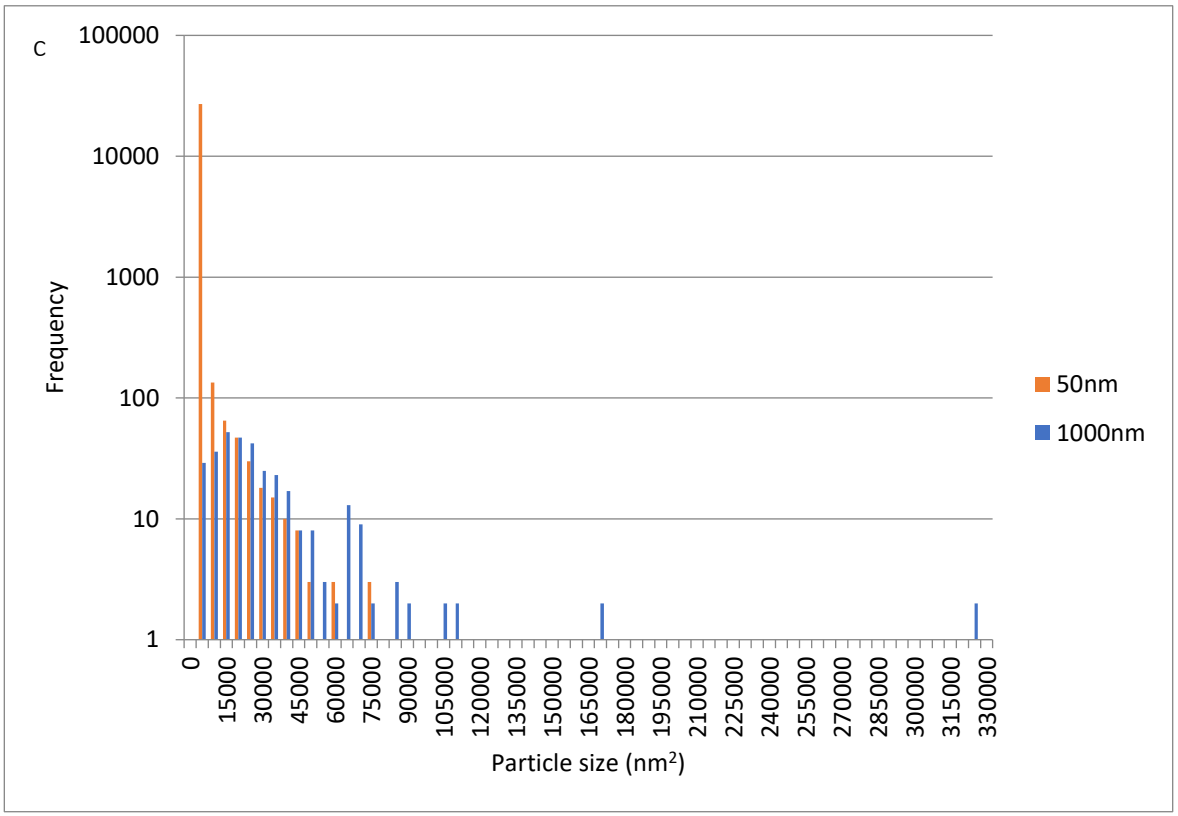

Figures 4.27a-c. The histograms in Figures 27a and b show the frequency of particles across a range of sizes, and Figure 27c shows the two distributions on the same chart, but this time with a logarithmic scale.

Figure 4.27a contains large numbers of small clay particles <100 nm across, and some larger aggregates of up to 500 nm which must have aggregated after filtration, suggesting that the PVP could only reduce it agglomeration, not prevent it entirely. This is supported by the data in Figures 4.27b and c, which suggest low numbers (<10) of large particles, and large numbers of small ones (>10000).

As would be expected, the <1000 nm fraction contains the particles found in the <50 nm fraction as they were filtered sequentially from the same sample, but they are found in far greater numbers in the <50 nm sample. The <1000 nm fraction would have contained a higher concentration of particles because the pore size of the membrane was larger and therefore fewer particles would have been removed from the sample, so it is possible that the smaller interparticle distances resulted in more agglomeration because the colloids were in closer proximity to each other and the opposite charges on the edges and the faces were therefore more likely to undergo electrostatic attraction, leaving fewer of the <50 nm particles and making them harder to identify.

The outcome of the preliminary experiments, supported by DLS and TEM data, was two different fractions, approximately <50 nm and <1000 nm in diameter, which could be produced by the filtration of clay suspensions that had been stabilised with 2.18 g PVP in a 1 g/l clay suspension, provided that it had been dispersed by hand and not by sonication. Whilst this did not align perfectly with the aims of this chapter that were set out in Section 4.1, being able to produce two consistent fractions of distinct particle size allowed the effect that colloidal size distribution had on flow behaviour to be investigated. This is the focus of Chapter 6.

4.3.3.4.3 Method for making clay samples for the flow experiments

0.05 g of bentonite clay (sieved to <25 µm) and 0.1092 g of PVP were weighed out and stirred together whilst dry. 50 ml of deionised water was added to the powders and they were shaken by hand until dispersed, and then shaken overnight at 140 RPM. This resulted in a suspension containing 2.18 g of PVP and 1 g of clay per litre of deionised water. They were then filtered in order to produce <1000 nm and <50 nm fractions. An intermediate filtering step was needed to prevent the 50 nm membrane from blocking, so the suspensions were passed through a 700 nm beforehand. Their size distributions were then determined using DLS.

4.3.3.4.4 Results and discussion

4.3.3.4.4.1 Characterisation

Figures 4.28a and b show the intensity distributions, and Figures 4.28c and d the number distributions of the <50 nm and <1000 nm fractions made with PVP, alongside fractions that were prepared without PVP, but that were otherwise identical, to allow easy comparison.

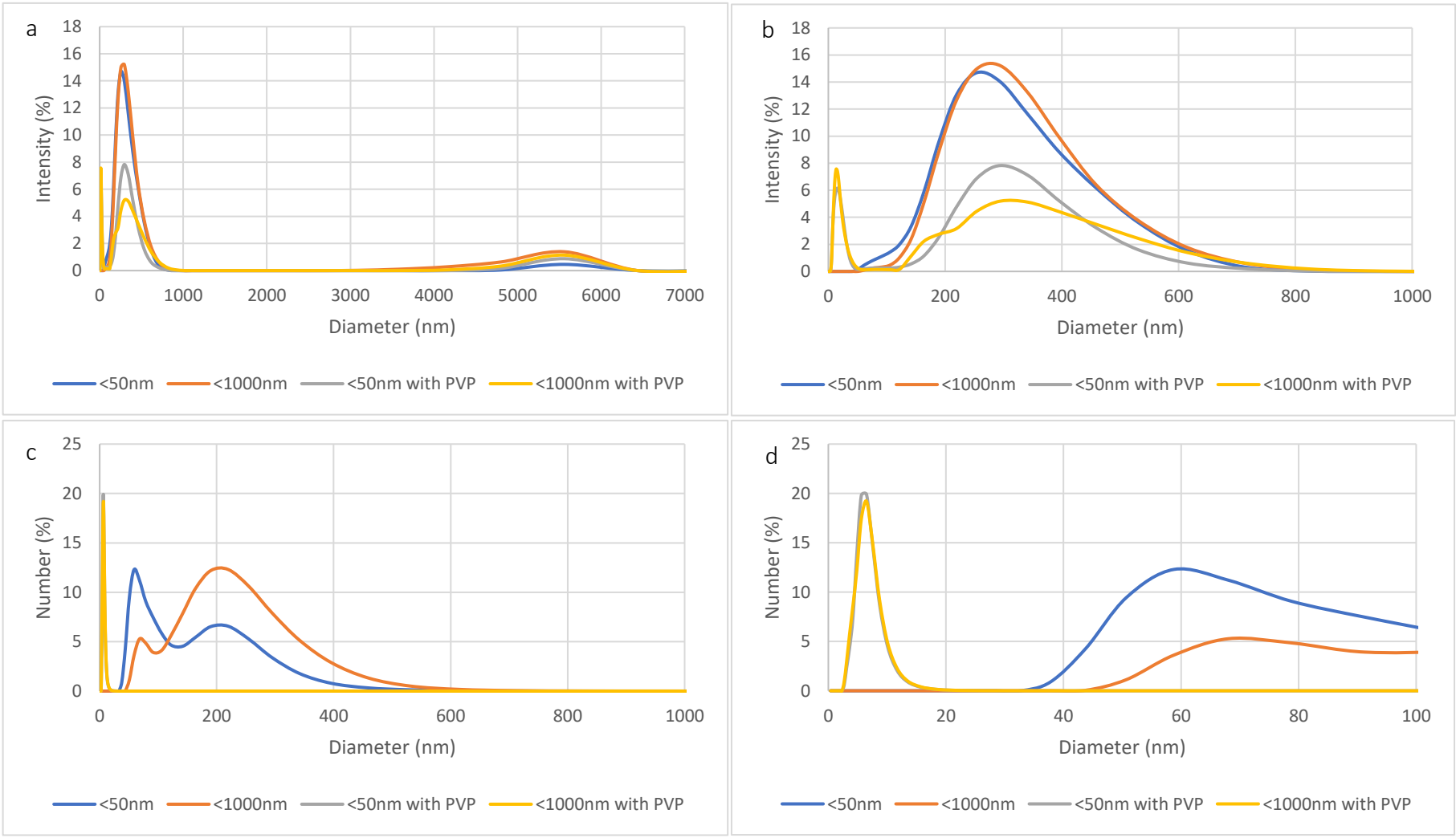

Figures 4.28a-d. Intensity distributions (a and b) and number distributions (c and d) of the <50 nm and <1000 nm samples, made with and without PVP. They are alongside fractions that were prepared without PVP, but that were otherwise identical, to allow easy comparison.

The intensity distributions all have large, broad peaks at 250-300 nm, but the samples that were made using PVP also have narrow, secondary peaks at <50 nm, suggesting that they contain significant numbers of small particles. The number distribution supports this but should be treated with the same caution as Figures 4.25a and b in Section 4.3.3.4.2.

Zeta potentials of these samples are shown in Table 4.7.

Table 4.7. Zeta potentials of the samples made with and without PVP. The samples coated in PVP have less negative zeta values than those without, indicating that the surfactant has successfully formed a steric barrier on the surface of the clay colloids.

Sample	Zeta potential (mV)
<50 nm	-28.6
<1000 nm	-26.5
<50 nm with PVP	-4.67
<1000 nm with PVP	-5.59

The addition of PVP made the zeta potentials less negative. This may seem counterintuitive, as when trying to produce a more stable suspension, it would be expected that a sample that is more negative would contain particles that repel more strongly, making them less likely to aggregate. However, Tunç & Duman (2008) noted a similar effect with PEG molecules on bentonite, and stated that it was an indication that the surfactant had sorbed successfully onto the clay particles. This suggests therefore that the coating was successful, and that although it resulted in the system being less negative overall, the negative faces of the clay colloids were being shielded from positive charges on the edge sites by the PVP molecules.

Images of each of the fractions were taken using an ESEM and are included below in Figures 4.29-4.32. All of the fractions were imaged at 100x, 500x and 2000x magnification, and at 10000x where the quality was high enough.

a

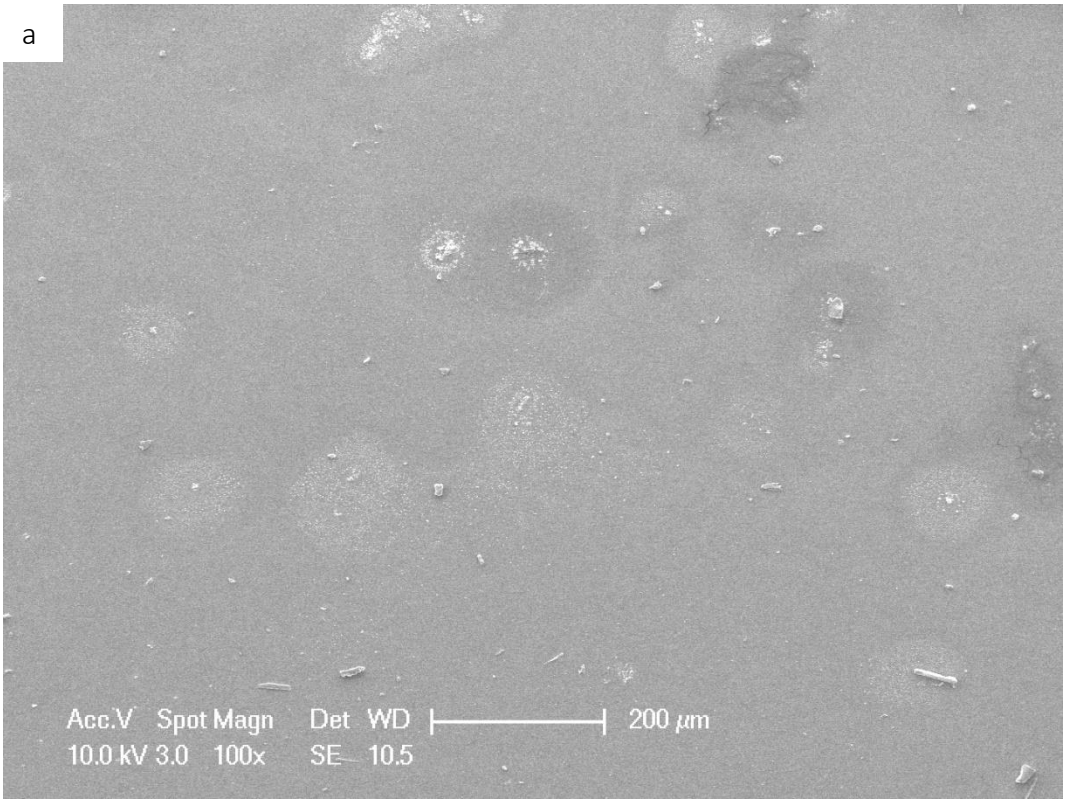
Acc.V Spot Magn Det WD 200 µm
10.0 kV 3.0 100x SE 10.5

b

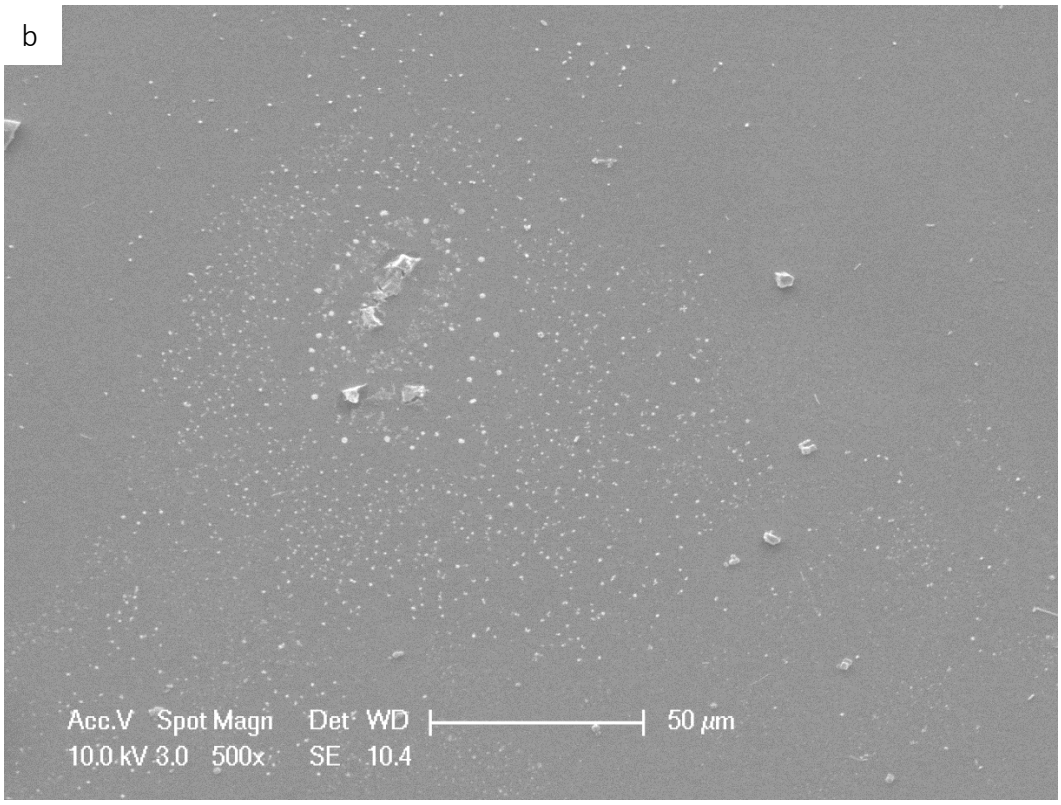
Acc.V Spot Magn Det WD 50 µm
10.0 kV 3.0 500x SE 10.4

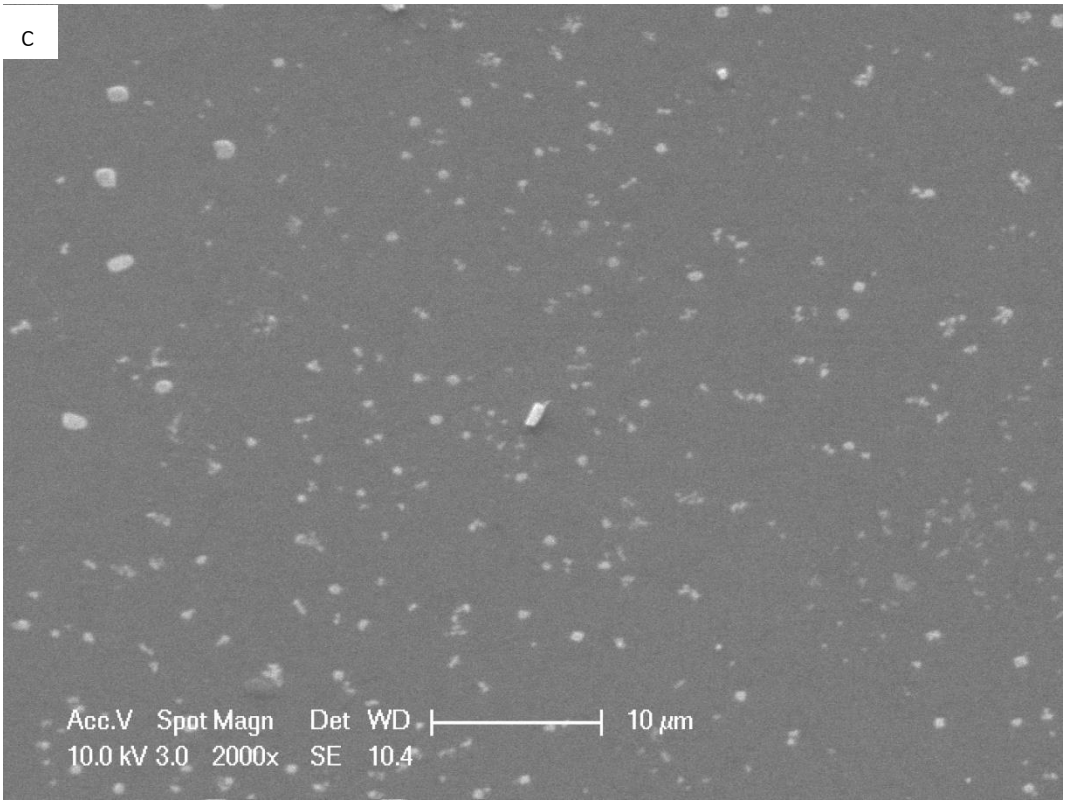

Figures 4.29a-c. ESEM images of the <50nm fraction at a range of magnifications.

The ESEM images of the <50 nm samples show that it is even more heterogeneous than the DLS results alone would indicate, because the DLS can only measure particles up to 10 µm, and it contains material much larger than that. However, the largest of the particles in Figure 4.29a tend to be long and thin, such as the rod in the bottom right hand corner, so the size measurements may be skewed depending which of its dimensions are measured by the instrument.

Figures 4.29b and c indicate the presence of large, plate-like particles ranging from 1-10 µm, but the resolution is too poor to be able to examine the nature of the smaller (~500 nm) particles, *e.g.* whether they are also single platelets that somehow passed through the filter, or agglomerated smaller particles. The poor resolution also means that it is not possible to observe particles down to the nominal maximum size this fraction should contain, <50 nm.

TEM would have provided better images and insight into the nature and sizes of the particles, but access to the technique was unfortunately very limited.

a

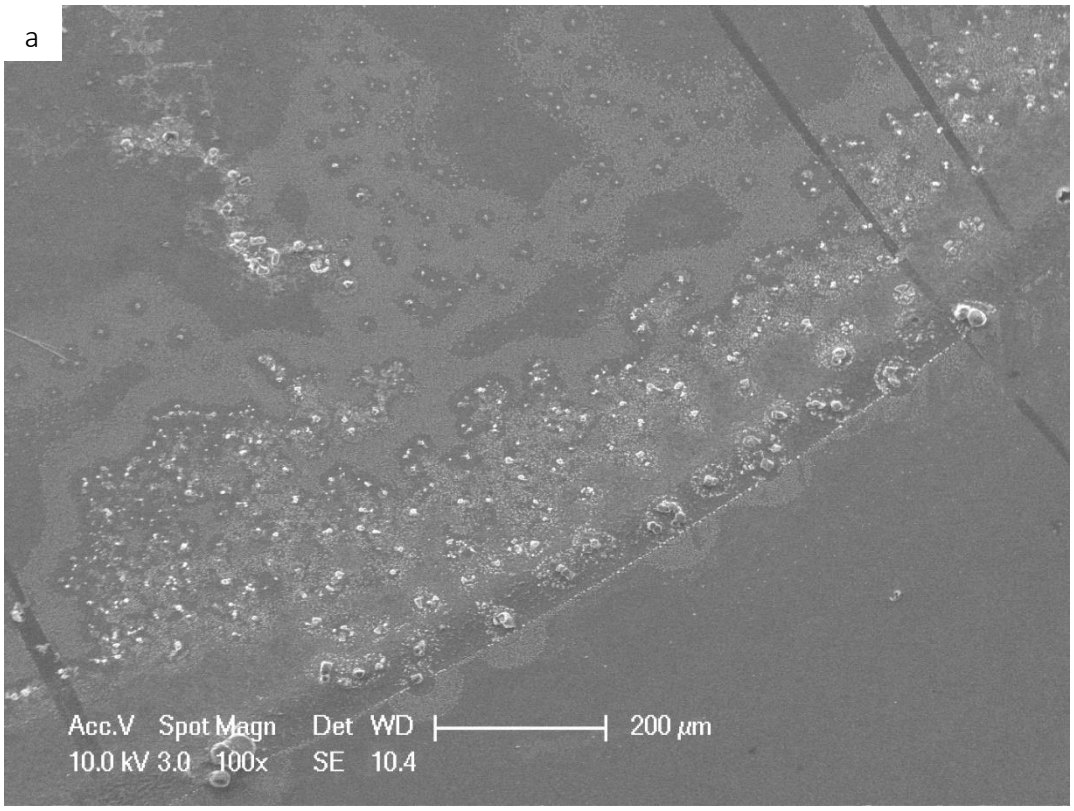

b

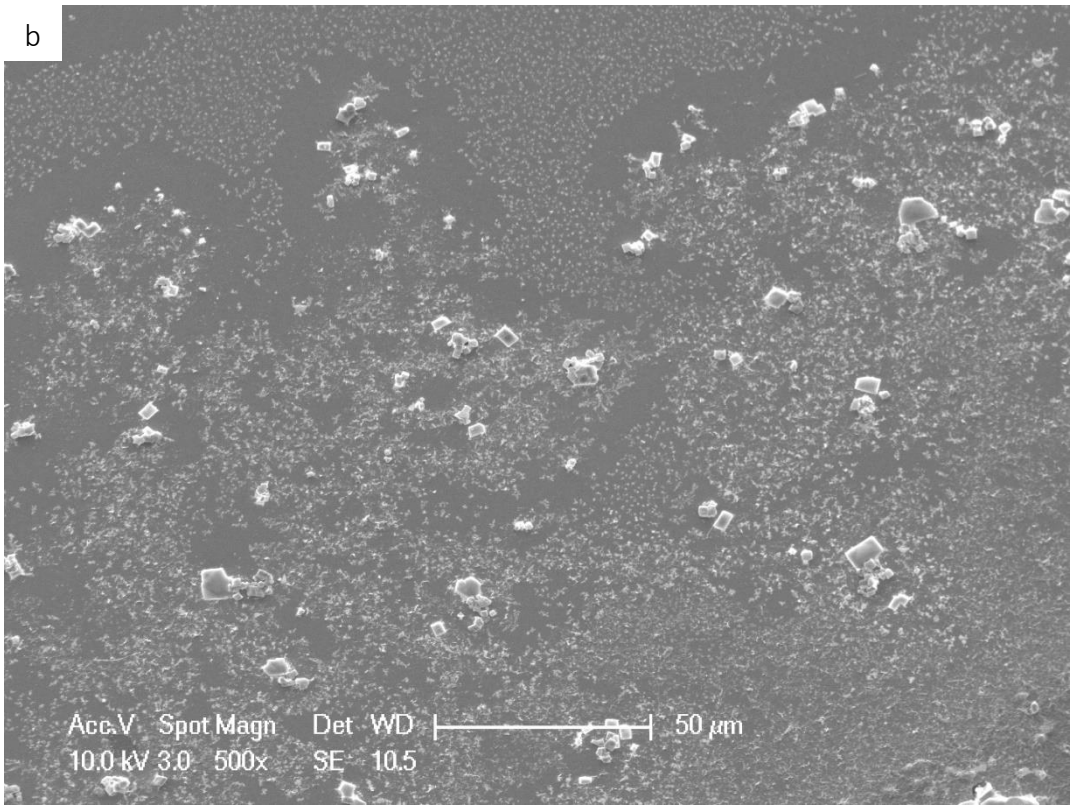

c

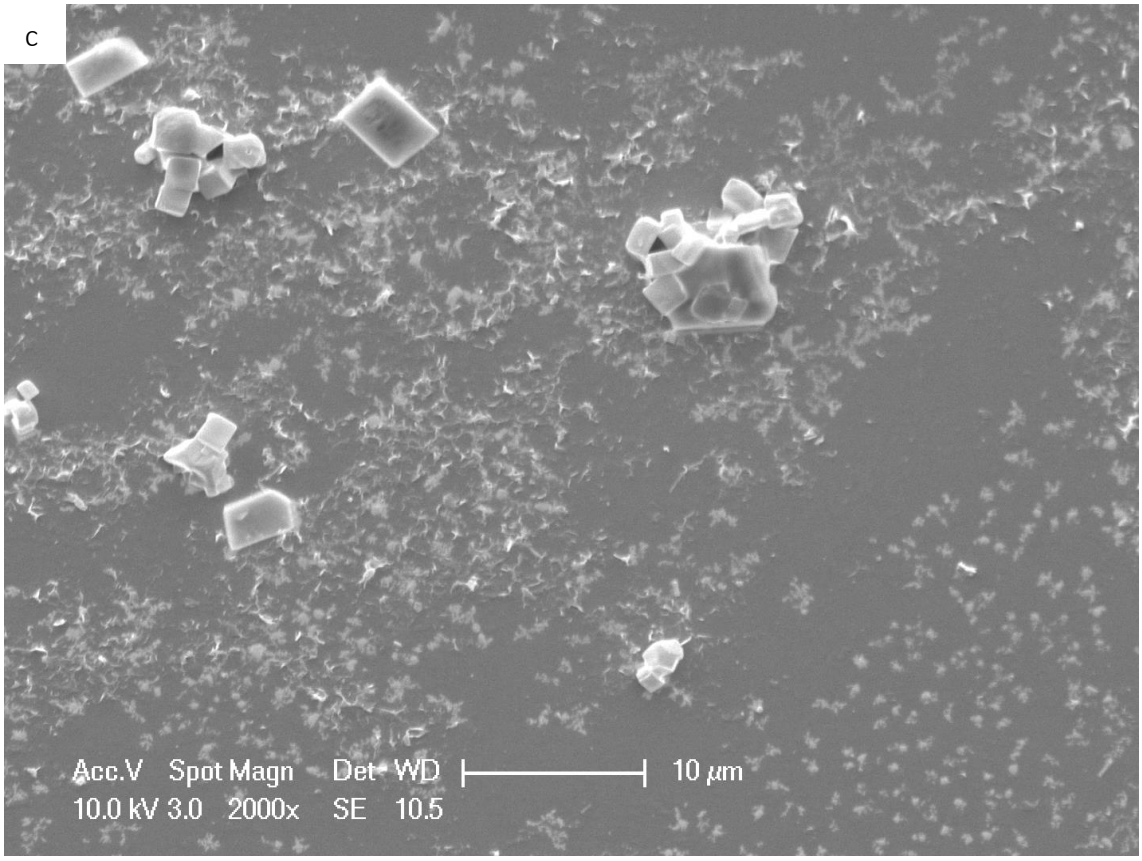
Acc.V Spot Magn Det WD 10 μm
10.0 kV 3.0 2000x SE 10.5

d

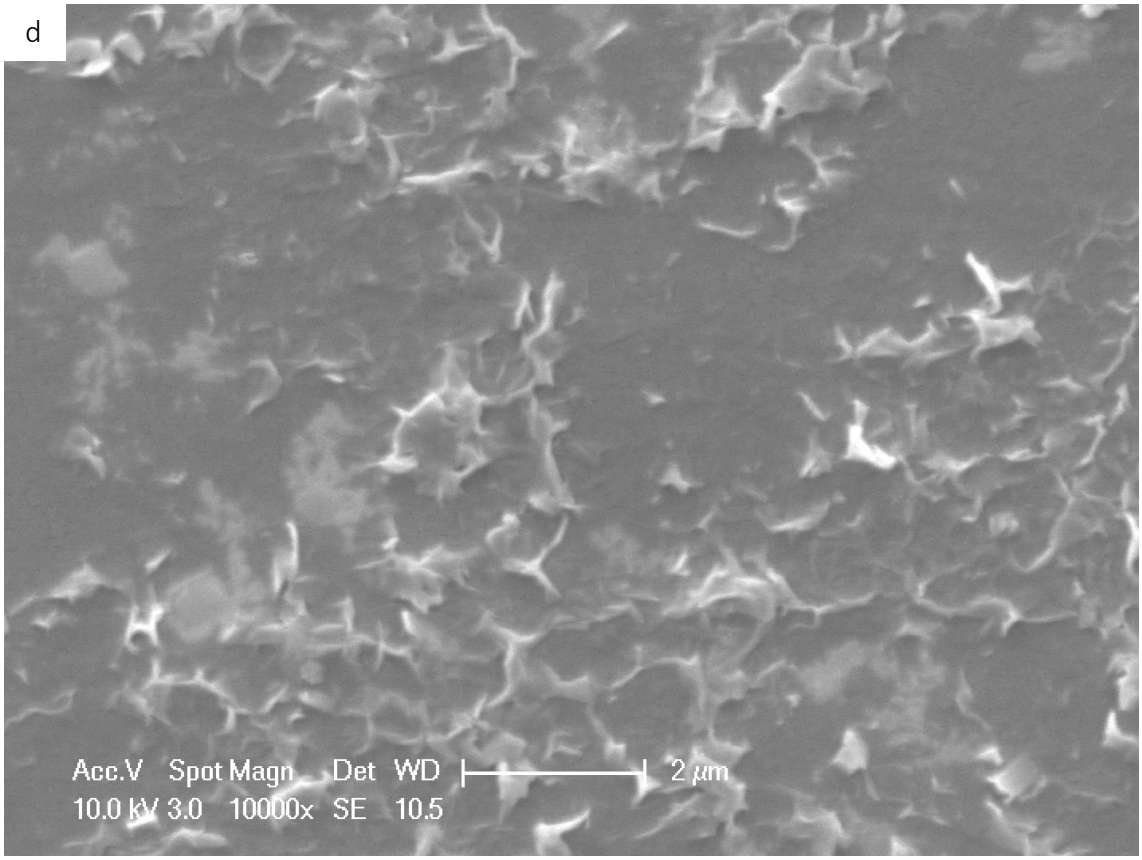
Acc.V Spot Magn Det WD 2 μm
10.0 kV 3.0 10000x SE 10.5

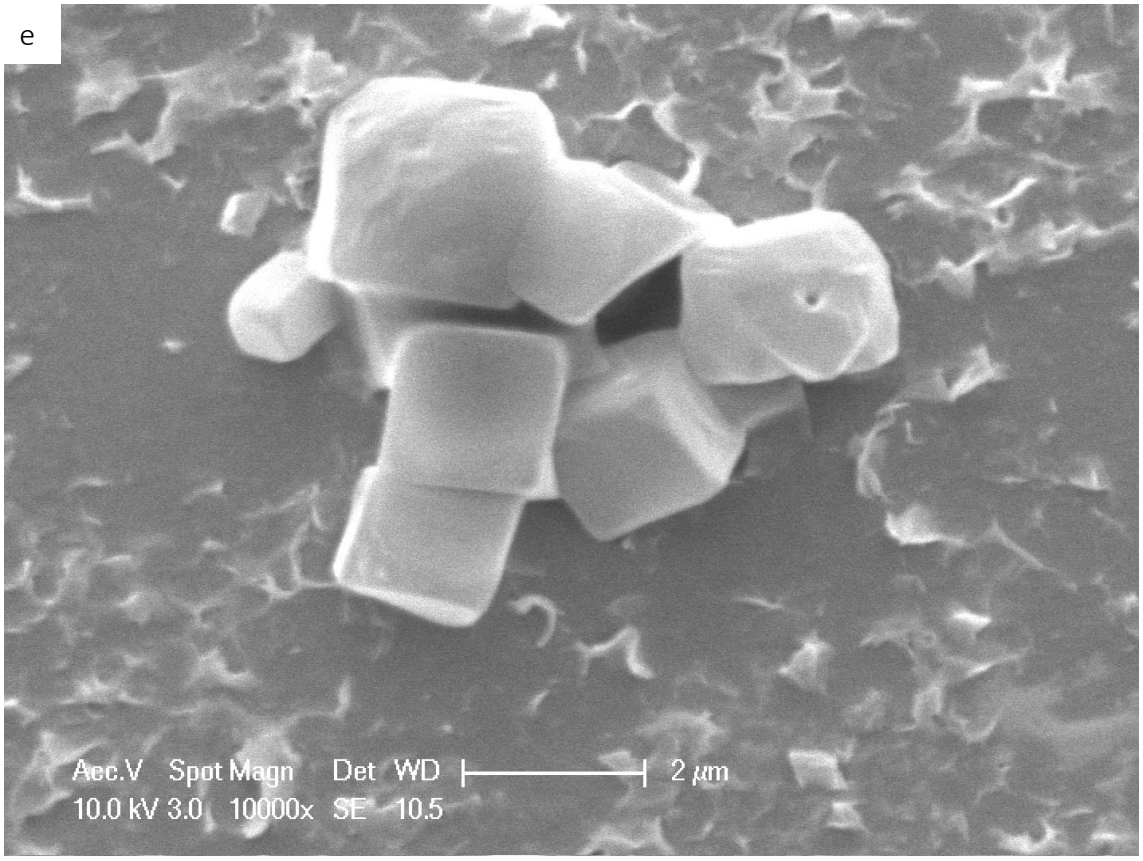

Figures 4.30a-e. ESEM images of the <1000nm fraction at a range of magnifications.

The resolution of the images in Figures 4.30a-e is much better than that of Figures 4.29a-c, allowing for magnification down to x10000. This variation in image quality is discussed in section 4.4.5.4.1. The density of particles is much higher than in the <50 nm samples, which is to be expected given that the larger cut-off of the 1000 nm filters should permit a greater proportion of the starting sample through the pores.

The most notable features of Figure 4.30a are the large, rather blocky colloids surrounded by circular features. These were also observed in the images of the reference sample in section 4.2 and are once again likely to be dried bentonite gel. This can be seen more clearly in the higher magnification images in Figures 4.30d.

a

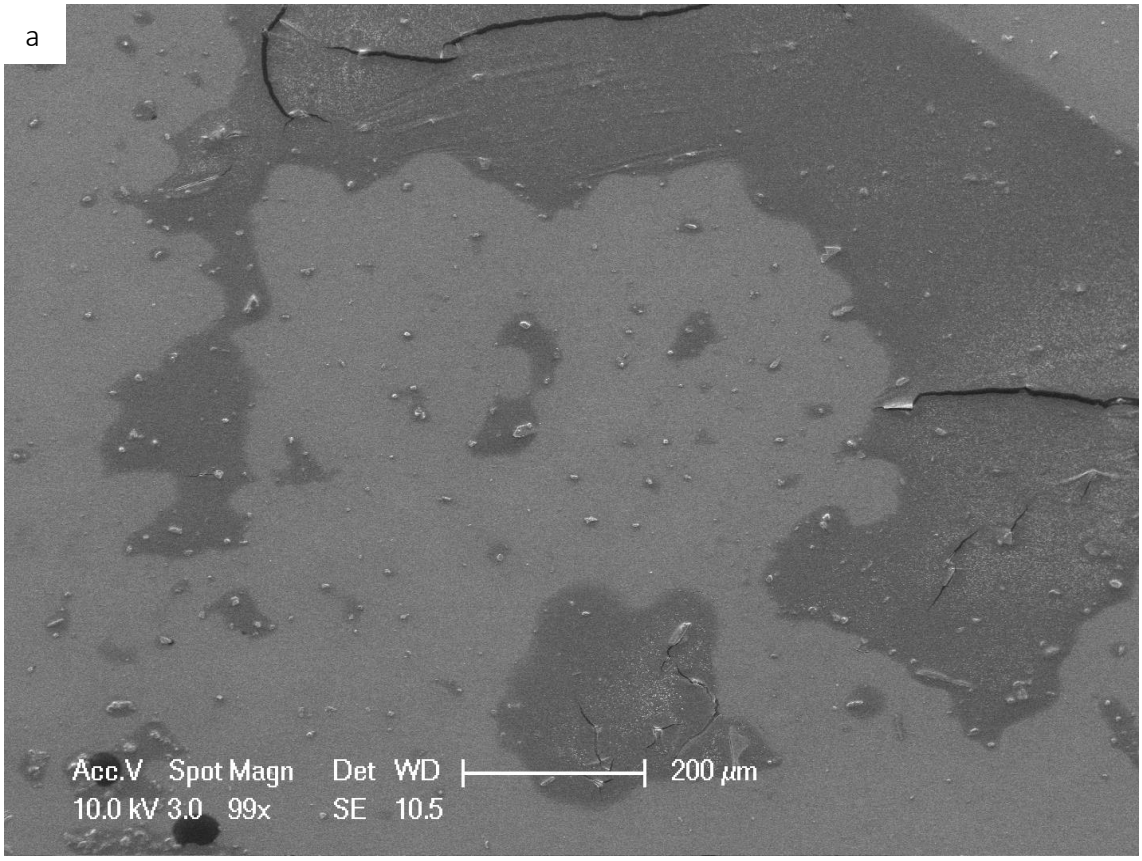
Acc.V Spot Magn Det WD 200 µm
10.0 kV 3.0 99x SE 10.5

b

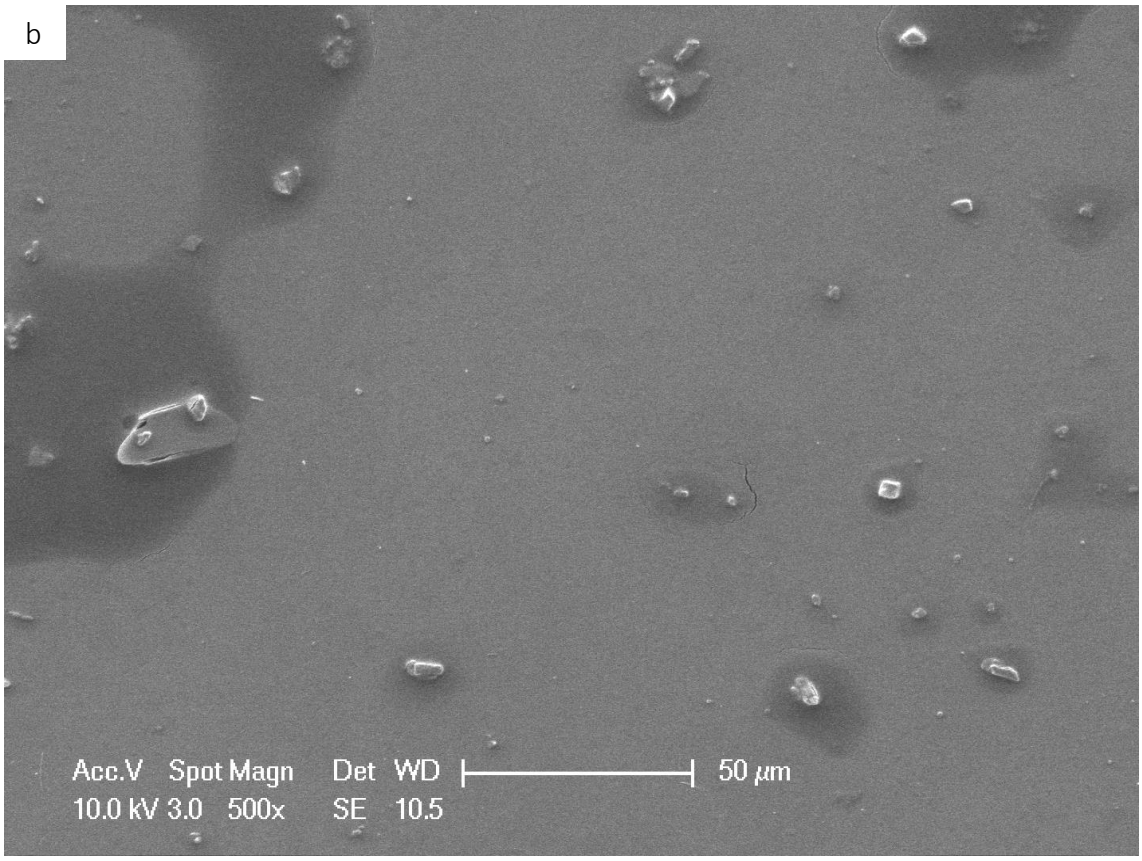
Acc.V Spot Magn Det WD 50 µm
10.0 kV 3.0 500x SE 10.5

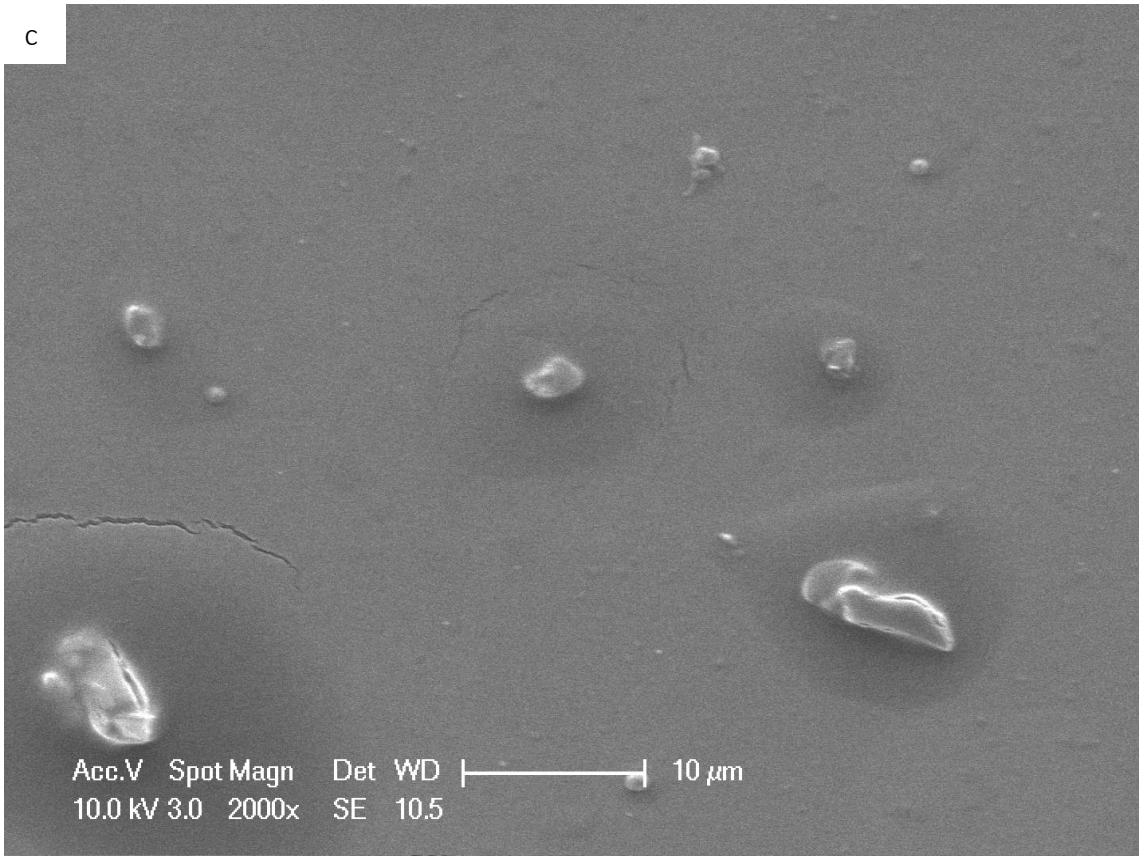

Figures 4.31a-c. ESEM images of the <50nm fraction that was made with PVP, at a range of magnifications.

The colloids in the sample that was made using PVP and filtered to <50 nm appear to be dispersed better than the <50 nm fraction made without the surfactant, and it lacks the circular features, suggesting that the PVP may hinder the formation of the bentonite gel.

Figures 4.31a and b once again show large, blocky particles, but close examination of Figure 4.31c reveals the presence of <50 nm particles. However, the low resolution and the coating of both PVP and the gold necessary for conduction whilst in the ESEM make it hard to distinguish any of their features or examine their morphology.

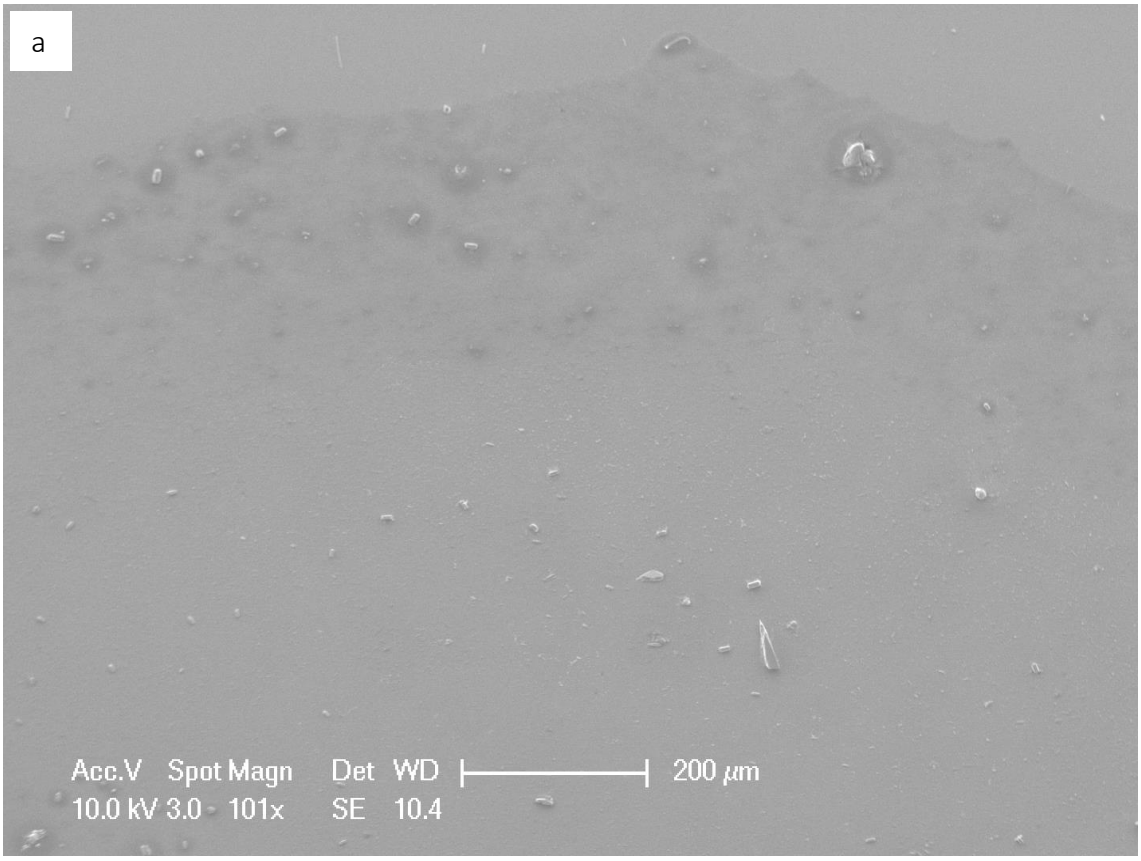
a
Acc.V Spot Magn Det WD 200 μm
10.0 kV 3.0 101x SE 10.4

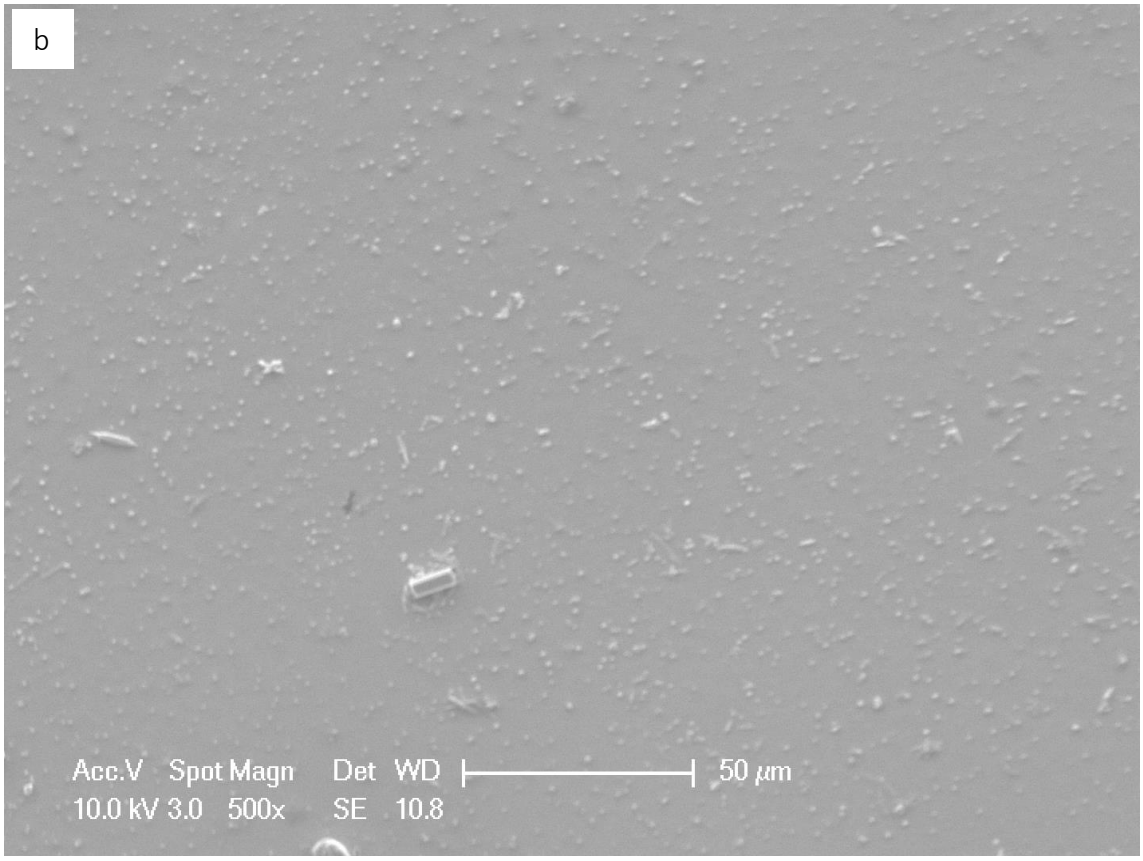
b
Acc.V Spot Magn Det WD 50 μm
10.0 kV 3.0 500x SE 10.8

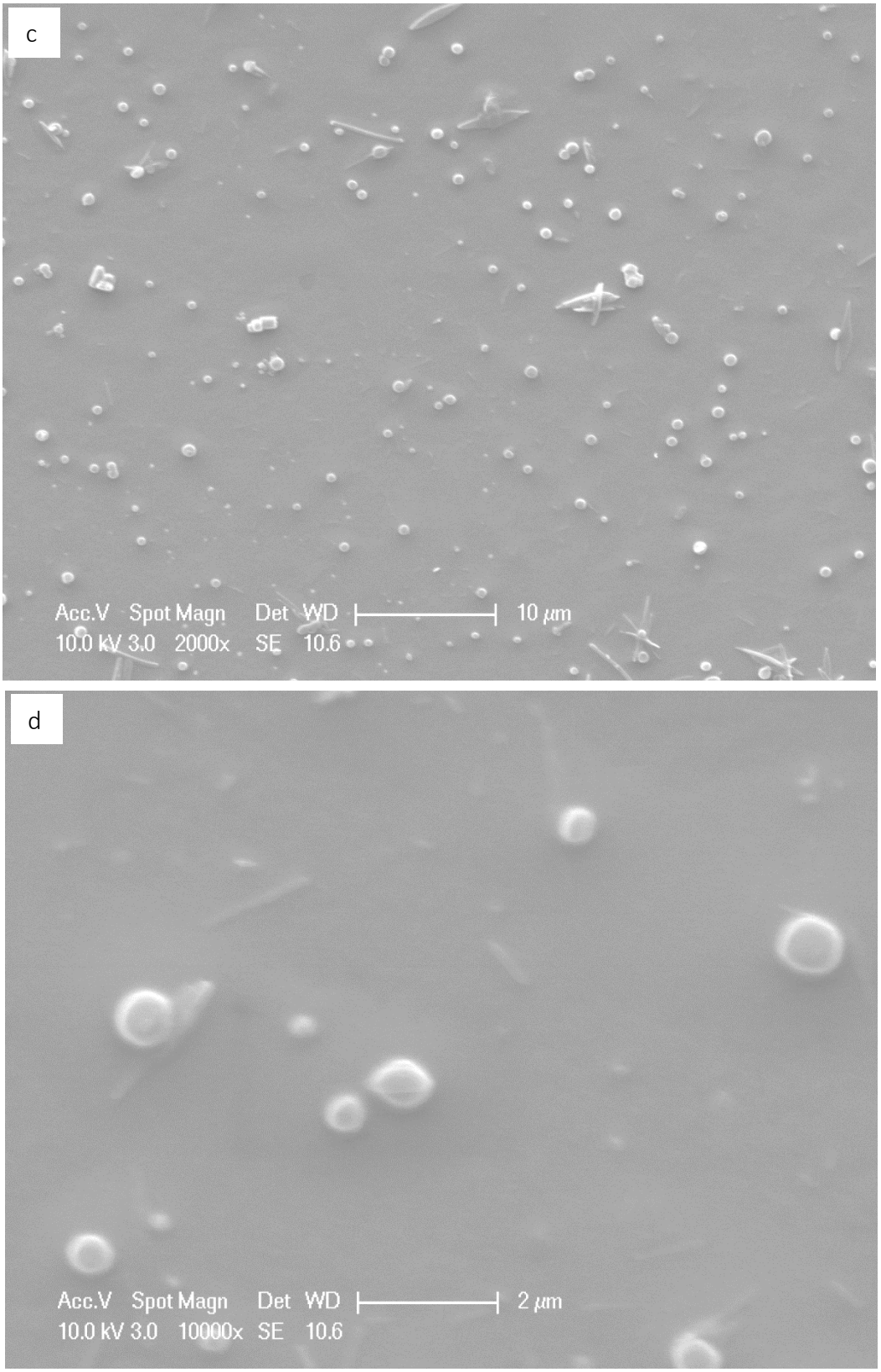

Figures 4.32a-d. ESEM images of the <1000nm fraction that was made with PVP, at a range of magnifications.

Some of the aforementioned circular features may be observed in the <1000 nm fraction made using PVP, so it is unlikely that the addition of surfactant prevents their formation entirely, and it is perhaps also dependent on clay concentration, which is higher in the <1000 nm samples due to the larger cut-off point of the filters. Figure 4.32c contains many circular colloids around 1000 nm in diameter, and the higher magnification of Figure 4.32d shows that there are some smaller particles (<100 nm) present, with both rod-like and rounded morphologies, but the poor resolution makes them hard to quantify or to examine closely.

The ESEM images show the larger particles more clearly than TEM, which is good for visual examination, but it cannot distinguish many particles smaller than 1 µm across, meaning that it was adequate for examining their morphology, but not for size analysis, as it would have excluded potentially thousands of the smallest colloids.

The images below in Figures 4.33a and b were taken using Atomic Force Microscopy (AFM). They are particles from the <50 nm sample that was made using PVP, and the images were supplied by a colleague at the University of Bristol.

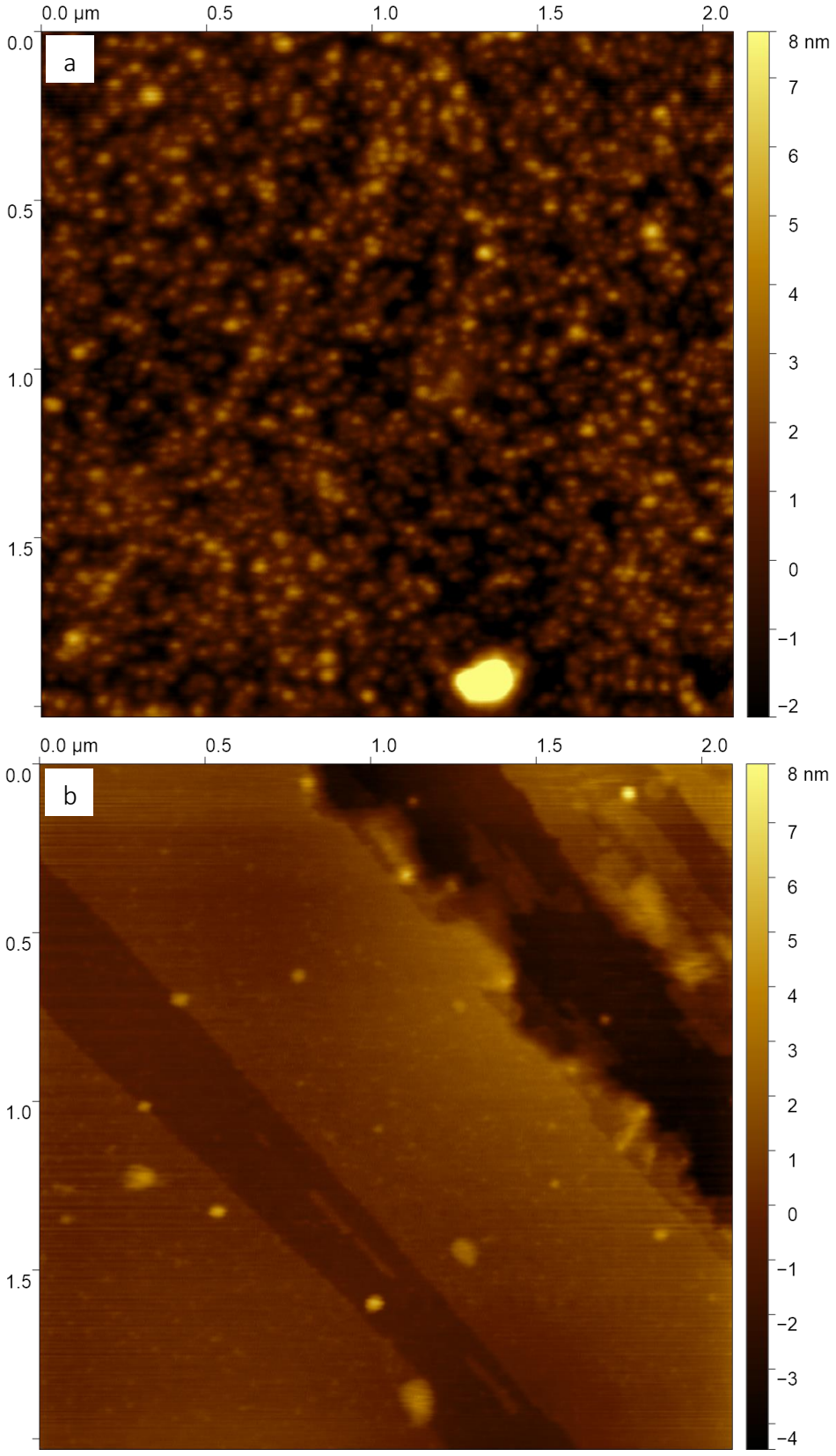

Figures 4.33a&b. AFM images of the <50nm sample that was made using PVP. They were provided by a collaborator at the University of Bristol.

The images in Figures 4.33a and b highlight the plate-like morphology of the colloids. None of them are more than 8 nm thick, and many of them are closer to 4 nm, and their lateral dimensions are at least an order of magnitude larger than that.

4.3.3.4.4.2 Stability over time

It was important to consider how stable the clay particles were over time when produced using PVP because it influenced how long the fractions were useful for after filtration: if they retained their original size distribution for a week after they were produced then they could be filtered, stored and used in flow experiments as and when they were needed, but if they agglomerated rapidly, then it was necessary to filter them as close to when they were going to be used as possible to avoid their size distribution changing too much.

A sample of each fraction (<50 nm and <1000 nm fractions, made with and without PVP) was taken, placed in a cuvette and measured using DLS as soon as was possible after they were filtered, and then the sample retained and measured again over the next two days. The results are shown below in Figures 4.34a-j.

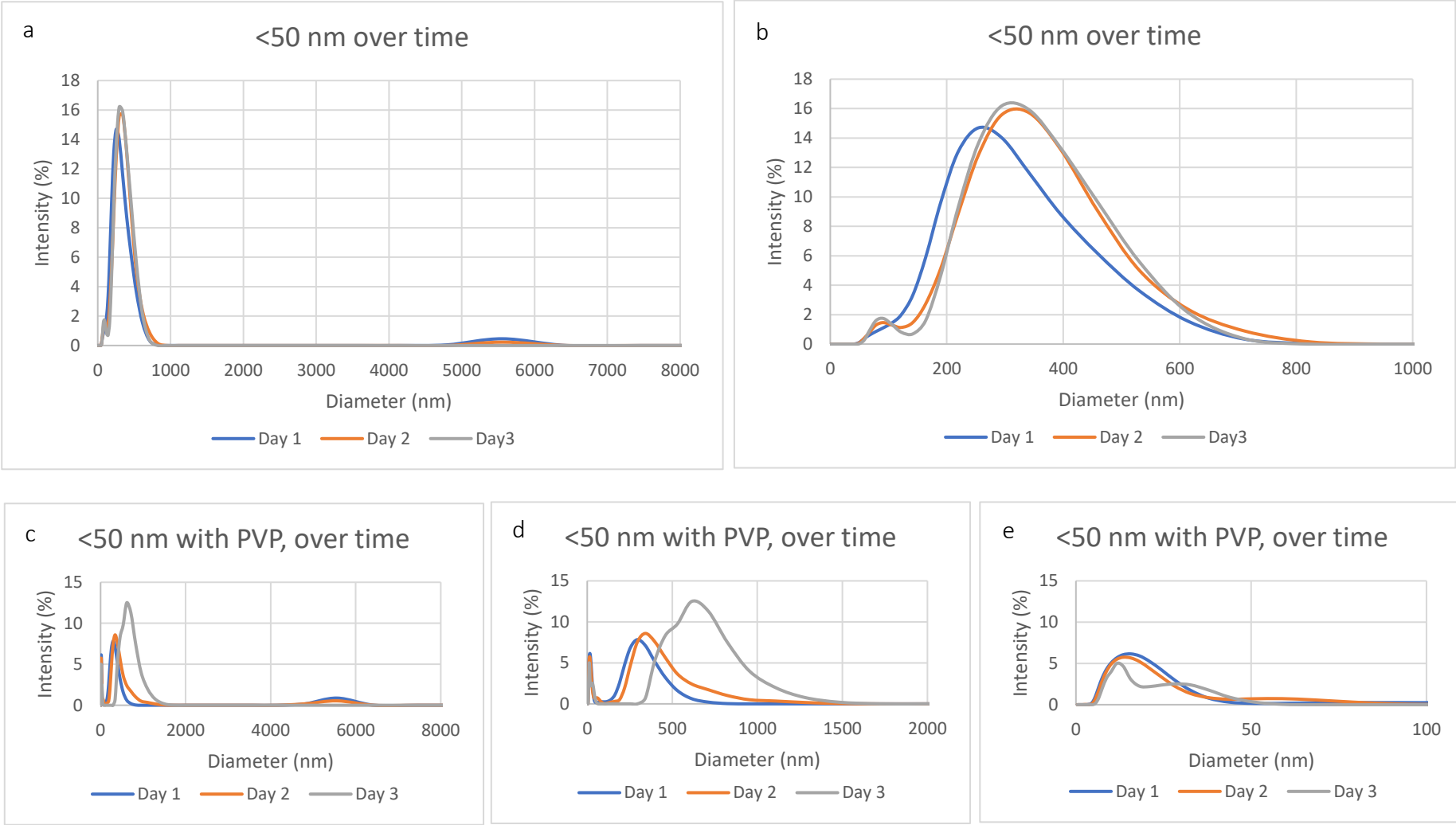
a
<50 nm over time
Intensity (%)
Diameter (nm)
Day 1
Day 2
Day3
b
<50 nm over time
Intensity (%)
Diameter (nm)
Day 1
Day 2
Day3
c
<50 nm with PVP, over time
Intensity (%)
Diameter (nm)
Day 1
Day 2
Day 3
d
<50 nm with PVP, over time
Intensity (%)
Diameter (nm)
Day 1
Day 2
Day 3
e
<50 nm with PVP, over time
Intensity (%)
Diameter (nm)
Day 1
Day 2
Day 3

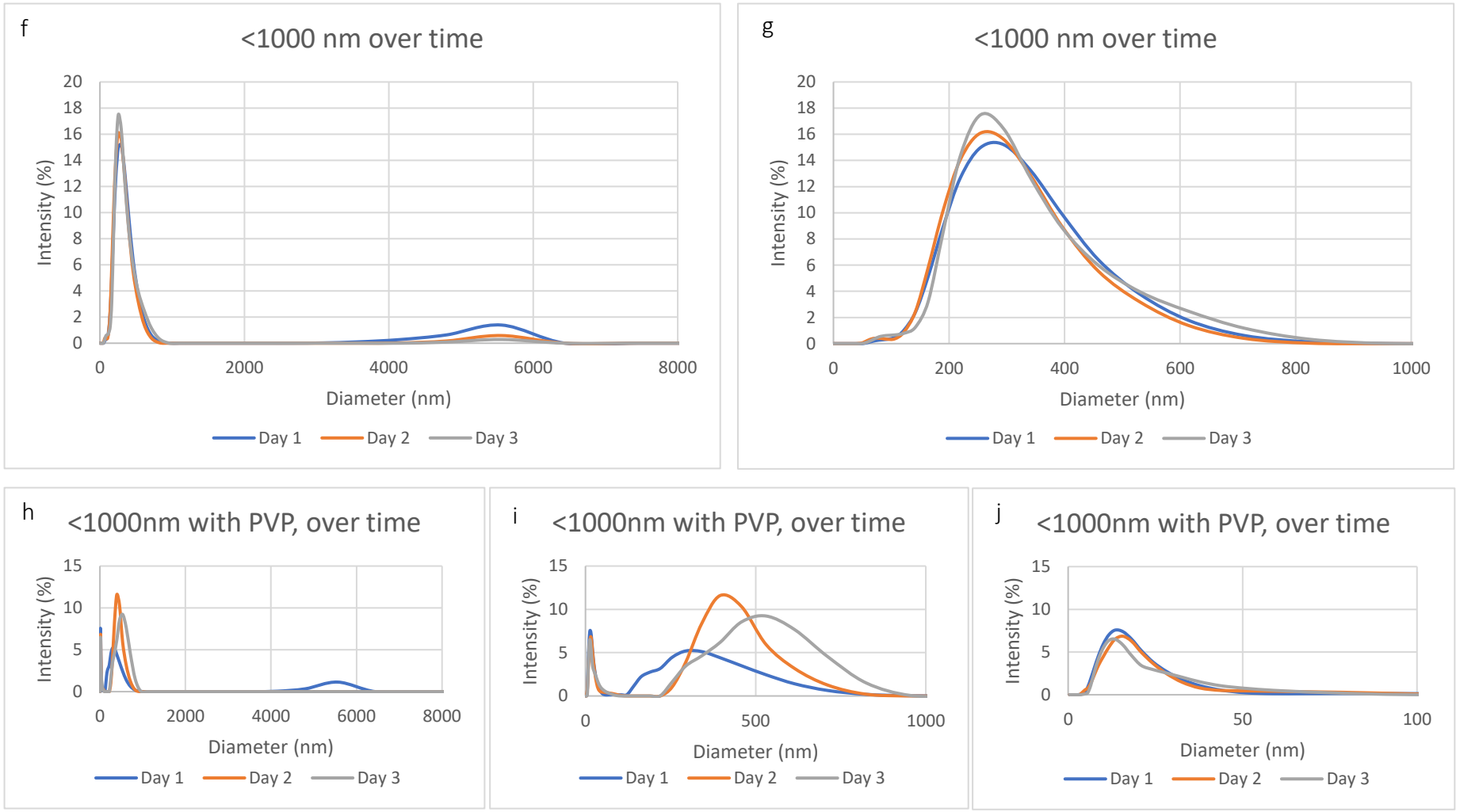

Figures 4.34a-j. Size distributions of the <50nm and <1000nm fractions, made with and without PVP, presented side-by-side for comparison and at a range of magnifications. The measurement after 1, 2 and 3 days were designed to investigate their stability.

Contrary to what would be expected of the fractions produced using a surfactant, the PVP appears to reduce the stability of the colloidal suspensions. The peak of the <50 nm fraction made without PVP shifted from 255 nm to 342 nm between the readings taken on days 1 and 2 but then remained virtually unchanged on day 3, and the <1000 nm fraction made without PVP shows barely any change at all. The smallest peaks (~20 nm) in the fractions made with PVP do not change significantly in their height or width. The larger peak in the <50 nm fraction made with PVP changes little in the first two days, but then nearly doubled in size from 340 nm to 615 nm by day 3, and the larger peak in the <1000 nm sample made with PVP increases steadily across the three days.

This effect may have arisen because the colloids produced without PVP agglomerated very rapidly. The size distribution was determined using DLS within 2-3 hours of the fraction being filtered, but it is possible that they agglomerated during this time and then changed little over the following days, whereas the fractions made without PVP underwent agglomeration far more steadily.

However, this stability behaviour should not have significant consequences for their use in the flow experiments. Sufficient volumes (approximately 100ml) of the <1000 nm fractions can be filtered in approximately one hour. This is rapid enough that it may be filtered and then used in a flow experiment the same day, before significant agglomeration occurs and alter its size distribution. The <50 nm fractions take longer to produce (potentially up to 6 hours) because the 50 nm filters have a much smaller pore size than the 1000 nm and filter more slowly at the same vacuum pressure. Therefore, they cannot be produced and used on the same day, but the results in Figures 4.27c-e suggest that their size distribution

changes little in the first two days, so filtering a solution one day and using it the next is unlikely to result in a significant change in their size distribution.

The negative impact that the use of PVP had on the stability of the resulting particles was therefore unlikely to have significant consequence on their suitability for use in the flow experiments in Chapter 6, and the benefit of being able to consistently produce two distinctly different colloidal size fractions outweighed the small potential disadvantage.

4.3.3.4.4.3 Concentration

Nephelometry was used to determine the concentrations of the filtrates. The nephelometer used is described in detail in Chapter 5. Initially, the method described by Norrfors *et al*. (2015) was trialled, where ICP-MS was used to determine the concentration of key cations (aluminium and iron) in the clay, and this was then compared to its elemental composition in order to calculate the concentration of the remaining colloids. However, this proved difficult because it is necessary to pass the ICP-MS samples through 200 nm syringe filters beforehand in order to prevent any large particles from blocking the nebulizer. This would remove an unknown proportion of the <1000 nm sample, thereby reducing the aluminium and iron content by an unknown amount. This effect would be compounded by the fact that the ICP-MS samples also need to be acidified with nitric acid, reducing their pH, which, as discussed in section 4.3.3.2.1, would promote agglomeration, increasing the particle sizes of both the <50 nm and <1000 nm fractions and resulting in even more colloids being lost on the syringe filters. Digestion using hydrofluoric acid can be used to break down the aluminosilicates so that they are not removed during the preparation steps, theoretically allowing the whole sample to be measured without any loss of material, but this could not

be done at the facility available at the University of Birmingham and the technique was unsuccessful when done commercially.

Instead of using ICP-MS, a range of standards were made by mixing a 100mg/l suspension of clay in water, carrying out sequential dilution to produce standards between 10 and 90 mg/l, running it on the nephelometer, and producing a standard curve, which was used to calculate the concentrations of individual samples, and to calculate the concentration change over time of the flow experiments in Chapter 6.

Firstly, the dried reference sample that was made in Section 4.2 was mixed in with deionised water and sonicated to form a suspension of clay with the concentration 100 mg/l. This starting solution was diluted to produce additional standard solutions between 10 and 90 mg/l. A deionised water baseline was measured, which provided a 0 mg/l standard, and the other solutions were measured in order of increasing colloid concentration. All samples were made in triplicate, the readings were taken for 2 minutes and then averaged to get the value for each standard, and the flow cell was flushed with the next standard, drained and then refilled, to reduce the risk of any contamination from the previous samples. The laser had been run for several hours before the suspensions were measured to allow it time to warm up and for its output to stabilise, but it was not possible to get a stable temperature in the refrigerator because the door had to be opened and shut repeatedly to change the samples. The triplicate results for each standard were then averaged and plotted to produce the calibration curve in Figure 4.35.

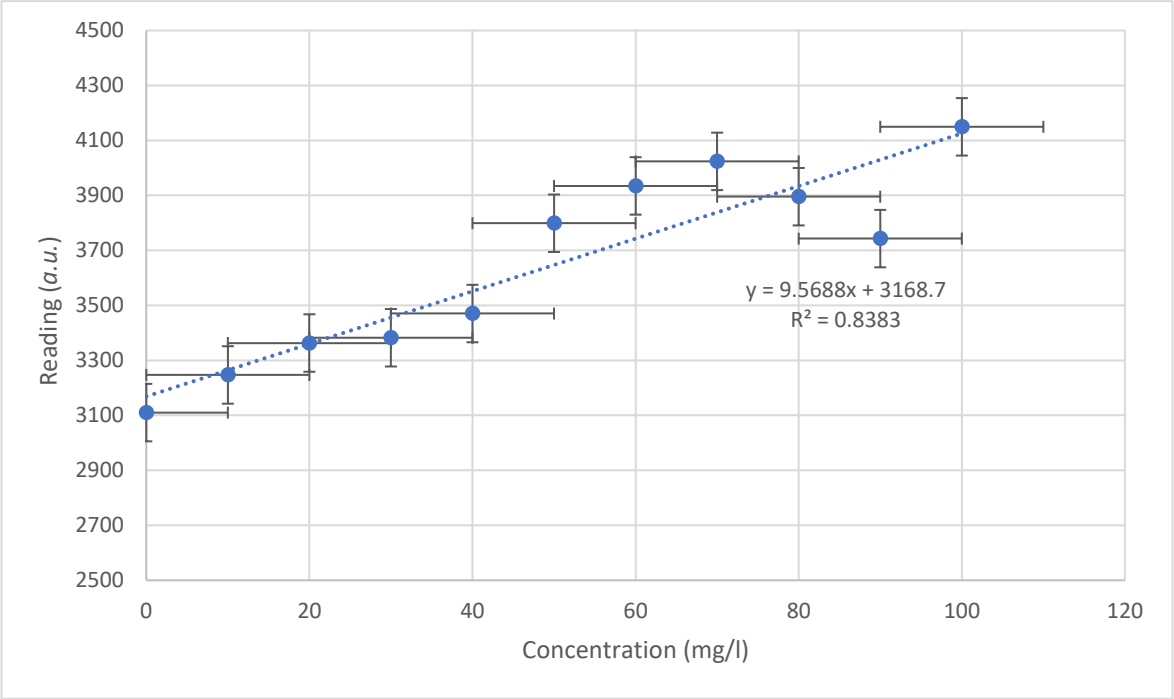

Figure 4.35. The standard curve that was produced by running standards with a concentration between 0-100 mg/l on the nephelometer.

Removing the four points furthest from the line strengthened the calibration and gave an r^2 value of 0.9923, which indicated good correlation. This improved correlation line is shown in Figure 4.36. The equation of the line was used in Chapter 6 to plot the change in concentration over time of the clay solutions when they were used in the flow experiments, and below, to estimate typical concentrations for the filtered fractions.

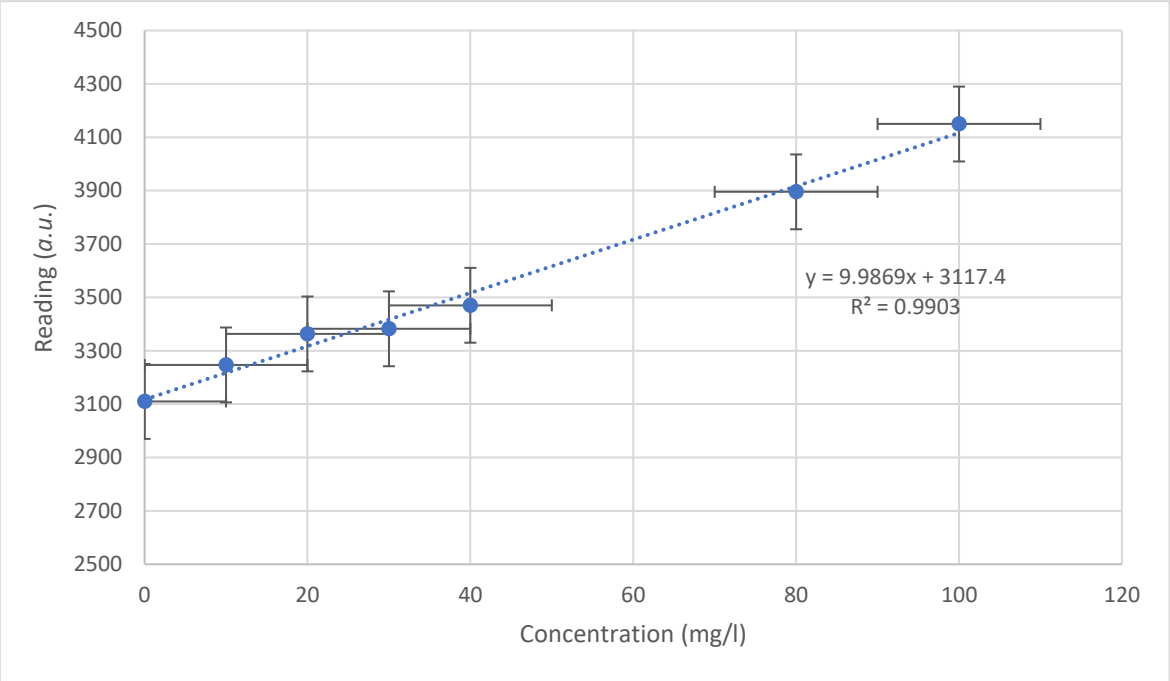

Figure 4.36. The standard curve from Figure 4.36 after the removal of the 50, 60, 70 and 90 mg/l standards. This produced an R^2>0.99.

In order to estimate typical concentrations for the filtered fractions, five of each sample (<50 nm and <1000 nm, with and without PVP) were made using the method described in section 4.3.3.4.3. Five baseline readings of deionised water were taken on the nephelometer, each of the samples were measured for two minutes, the readings were converted to concentrations, and these were averaged to give typical concentrations for each fraction. In a preliminary test the clay was also measured before being filtered, but the reading dropped rapidly and consistently throughout the two minutes, suggesting that the larger particles were sedimenting rapidly, so these readings were discounted.

Despite the instrument, the preparation and the source of deionised water being kept constant and the flow cell being flushed thoroughly beforehand, the deionised water baseline varies between the standards and these samples. The only variable that could be

identified was temperature, because as discussed above, it was not possible to keep it constant during this particular experiment because the refrigerator had to be opened and closed repeatedly to change the sample, and Chapter 5 explains the influence that temperature change has on the flow system. Despite the attempts that were made to shield the system, electronic interference may also be an issue. To account for this, a correction factor was applied: the concentrations were calculated using the equation obtained from the standards in Figure 4.36, the deionised water reading was set to 0 mg/l, and then the concentrations of the samples were adjusted by the same amount. The results are shown below in Table 4.8.

Table 4.8. Concentrations of the filtered samples, with and without baseline adjustment. The negative reading is not an error, but a reflection of the fact that the instrument is vulnerable to environmental factors affecting its reading, and as there is no internal drift correction, this has to be done manually instead.

Sample	Average concentration (mg/l)	Concentration (mg/l) (baseline adjusted)
Deionised water	-14.57	0.00
<1000 nm clay	31.68	46.25
<50 nm clay	-3.00	11.57
<1000 nm clay with PVP	14.73	29.30
<50 nm clay with PVP	15.52	30.09

The results of the concentration tests suggest that passing the clay suspensions through a 1000 nm filter removes over 95 % of the material. The <1000 nm fraction made without PVP has the highest concentration of clay colloids remaining after filtration, but then the difference between the <1000 nm and <50 nm fractions is far larger than the difference between the fractions made with PVP. This indicates that the samples made with unmodified clay have a higher concentration of colloids in the 50-1000 nm size range, and those made

with the surfactant have a higher concentration of <50 nm. This is logical given that the PVP was used to disperse the aggregates and produce smaller colloids and matches the results of the TEM size analysis in Section 4.3.3.4.2. Therefore, the inclusion of PVP makes little difference to the <1000 nm fraction but modifies the proportion of <50 nm colloids in the samples considerably.

Table 4.9 contains the concentrations of each of the five repeats for each sample.

Table 4.9. The concentration of clay in each of the five samples, measured five times. The results show how highly variable they are.

Sample	Sample 1	Sample 2	Sample 3	Sample 4	Sample 5
DI	-13.14	-15.32	-14.00	-15.72	-14.68
Clay 50 nm	Corrupted file	-3.50	1.39	-5.69	-4.22
Clay 1000 nm	59.07	1.17	50.22	8.76	39.20
Clay with PVP 50 nm	1.93	12.08	24.94	21.56	17.08
Clay with PVP 1000 nm	29.62	16.42	8.81	15.38	3.42

The values for deionised water and 50 nm clay are very consistent, and the concentrations of the samples that were made with PVP and filtered to <50 nm were fairly consistent apart from a single outlier. The <1000 nm samples, however, vary widely, and there is no clear explanation for this. This may be the result of the high degree of variability and disorder of natural clay minerals, which makes experimental analysis of them difficult (Suter *et al*. 2009), or perhaps inconsistency of the pore sizes of the filters; it had been noted that some solutions filtered much faster through the 50 nm membranes than others, but attempts to investigate this using microscopy were unsuccessful because the resolution was too poor.

4.4 Discussion

Norrfors *et al*. (2015) and Doucet *et al*. (2005) were reasonably successful at producing distinct size fractions of bentonite colloids, so it was not unrealistic to attempt to produce similar suspensions with narrower size distributions that were stable for at least two days. However, the aims of this chapter had to be readjusted as the project progressed, because this proved very difficult: the sizing data indicated that the centrifuged fractions did not match those of Norrfors *et al*., the presence of particles that did not correspond to the pore sizes of the membranes used to produce them matched the problems faced by Doucet *et al*. when attempting a similar process, and none of the other methods that were attempted were any more successful. This evaluation constituted Aim 1, and made Aim 2, the development of new protocols for producing and characterising colloids, necessary. Therefore, although it was not out of the realms of all possibility that the original particle sizing goals may have been achievable, it is also not that unexpected that they were not met. Two distinct size fractions were produced using PVP and filtration, which allowed the effects that relative, rather than exact, size has on the behaviour of the colloids during flow experiments to be investigated. In addition to this, they were stable for an appropriate amount of time, and when compared to clay colloids made without a surfactant, the effect that the PVP has on transport behaviour of the particles and on their sorption and desorption rates could be examined as well, in Chapters 6 and 7 respectively.

4.4.1 Previous work

Of the studies that were collected in Table 4.1, only four were aiming to fractionate clay colloids according to size. The others isolated only one fraction, and perhaps a filtrate, but were included in case their methodologies proved useful.

The size characterisation carried out in this project was more empirical than that of Sherriff (2015) and Vilks *et al*. (1991). Inconsistencies in the sizes of the filtered samples were encountered that were very similar to those of Doucet *et al*. (2005), in that the resulting samples did not correspond well with the nominal pore sizes of the filters used to produce them. The authors attribute this to molecules of low molecular weight being unable to pass through the filters, and to aggregation after filtration. The latter would explain the presence of large particles in the supposedly <50 nm fractions in Figures 4.28a-d, but without clear, high-resolution microscopy images it was not possible to closely examine the nature of the larger particles in order to determine whether they consisted of aggregated smaller colloids. These findings, and those of Doucet *et al*., highlight the importance of carrying out size distribution characterisation, and of not assuming that the resulting fractions match the nominal pore sizes of the membranes through which they were filtered. It is not entirely clear why the size distributions of the samples made in section 4.3.1 did not match those of Norrfors *et al*. (2015) more closely, but this might perhaps be the result of the innate variability of clay minerals (Suter *et al*. 2009). However, like Norrfors *et al*. (2016), a wide range of colloid sizes were present in each fraction. If the centrifuged samples could have been characterised using AsFlFFF in addition to DLS, which was also used by Norrfors *et al*., it would have provided a second reference against which to compare the sizing data, and it may have been possible to identify whether the variation arose from the centrifugation process, or from the size characterisation method.

As these two investigations, Norrfors *et al*. and Doucet *et al*., had produced and characterised multiple colloidal fractions with some degree of success, aiming to do the same, but without the presence of very large and very small erroneous particles that Doucet *et al*. encountered, and with a narrower distribution than Norrfors *et al*. (2016) achieved, was not an unrealistic goal. How well the original aims were met is discussed in section 4.5.

4.4.2 Characterisation of the natural bentonite

Producing and characterising a reference sample gave an insight into the properties and composition of the MX80. This was useful because there is not a consensus in the literature about how consistent the make-up of these minerals is: Suter *et al*. (2009) state that clay minerals are highly variable, however, the ICP-AES (Inductively Coupled Plasma Atomic Emission Spectroscopy) analyses of the elemental compositions of material taken from five different consignments of Wyoming bentonite presented by Karnland *et al*. (2006) are very consistent. It was not possible to compare the elemental composition of the reference sample to the ones in the report because a similar digestion process was attempted and proved unsuccessful, and they did not match the ratios produced by the XRF results in Table 4.2, but this may have been due to the difference in the measurement technique rather than significant differences in the clays. The XRD pattern in Figure 4.3 closely matches the ones in Karnland *et al*., however, suggesting that the lack of a crystalline structure is consistent across this type of clay.

The preparation method removed the largest clay particles, and therefore it could be argued that it is not completely representative of the starting material. However, it is not possible to get reliable DLS data from very polydisperse samples, particularly those containing

sedimenting particles, so it was necessary to remove these. DLS was not the only size characterisation method that was used, but as all of the samples underwent DLS initially in order to determine whether they were likely to be worth investigating further, it was important to have a reference sample of reasonable quality, and it proved very useful to have a 'starting point' against which to compare the fractions that were made. Additionally, this project was specifically investigating clay colloids, which, as discussed in Chapter 2, must have at least one dimension between 1 nm and 1 µm (Hunter 2001). Removing the fractions that are large enough to sediment was unlikely to remove colloidal-size material. Therefore, this method reduced the heterogeneity of the reference sample enough to get a meaningful measure of the size distribution, without eliminating relevant material.

Having a zeta potential measurement for the unmodified material also proved useful because the change in the zeta potential observed in section 4.3.3.4 indicated that the surfactants had successfully sorbed onto the clay. Finally, taking ESEM images of the reference sample allowed for its features to be visually observed and for similarities and differences between it and the samples in section 4.3.3.4.4.1 to be noted.

Overall, the reference sample proved useful and provided a relevant material against which the fractionated clay colloids could be compared. However, if a successful digestion method could have been achieved, the use of ICP-MS or ICP-OES would have given an elemental composition with better resolution and could have been compared to values given in the literature.

4.4.3 Centrifugation

As noted above in section 4.4.1, the size distributions of the centrifuged samples produced in this project did not match those made by Norrfors *et al*. (2015) very closely. This was one of the first techniques to have been tested, and in light of the revision of the sizing goals, it may have been worth going back to it and characterising the resulting fractions more thoroughly using a range of techniques; the disadvantages of DLS were documented in Chapter 3, and without obtaining AsFlFFF results and comparing them to those of Norrfors *et al*., it was not possible to determine if the differences occurred because innate variation between the clay used here and in the literature resulted in differences between the fractions, or errors in the size characterization. It is not possible to predict whether this would have made a difference, or whether the centrifuged samples would have been stable, but it is a time-efficient technique that (after the initial three-day-long settling period) allows volumes of up to 100-150 ml of each fraction to be produced within a day, and if time had allowed, it may have been worth revisiting.

4.4.4 Milling and sedimentation

Milling alone, be it via ring-, ball-, or cryomilling, did not reduce the particle sizes of the clay colloids sufficiently to make them suitable for use in the flow experiments. This may be simply because the techniques were not energetic enough to break the clay particles down sufficiently, but Kumar & Biswas (2017) noted that milling may cause particles to smash together and agglomerate, in addition to breaking them down. However, had this method proven successful, it may have raised some issues with the reactivity of the clay particles later on during the sorption experiments in Chapter 7. Breaking the colloids down to smaller sizes reduces their diameter and increases their specific surface area; a property that Doucet

et al. (2005) notes would increase their capacity for binding metal cations. Additionally, artificially exposing more of the reactive, positively-charged edge sites would result in increased bonding to the negatively-charged colloid faces, increasing their agglomeration, which is something that is to be avoided if they are to be suitable for use in the flow experiments in Chapter 6 (Mingelgrin *et al*. 1978). Less destructive methods by which to produce colloids, such as centrifugation or filtration, also increase the percentage of small colloids in the resulting solutions; that is the aim of them, in fact; but these isolate pre-existing small, naturally-occurring colloids, rather than artificially generating them by breaking bonds at the edges of the colloids. They also reduce the overall concentration of particles in suspension by removing the larger fractions, increasing the interparticle distances, and reducing the likelihood of agglomeration.

Of the samples that were left to sediment in addition to being milled, very few seemed to reduce in size any further as a result of the settling time. The size distribution of BMj_0 (which was milled for 1 hour) decreased, probably because it was milled for a shorter time than the other samples and therefore more large particles remained which sedimented faster than smaller ones, but this effect was not seen in the ring milled samples. In those, the milling time did not seem to influence the sedimentation, and instead, all of the samples that were left to settle for two weeks showed a reduction in particle diameter. As mentioned in sections 4.3.2.1.3 and 4.3.2.2.3, this may have been because the colloids were agglomerating as fast as they were settling, something that could not be identified by DLS if it were a slow process over several days, and it may have nullified any benefits of the sedimentation process.

Only a selection of the samples was left to sediment, and their size distribution re-measured over time. Not carrying it out on all of the samples was unlikely to have compromised the experiment because of the samples that were tested, few showed a decrease in size, and even then it was not significant enough to make them suitable for use in the flow experiments. There may have been a further decrease in the size distributions if the samples had been left to sediment longer, but this becomes somewhat impractical: if the samples needed to be left to settle for a month before being used in flow experiments then it makes the experimental time very long, and an accident such as agitating the vessel and resuspending the material would potentially delay the process even further.

If time had allowed, an additional investigation where the milled samples were coated with PVP, filtered, characterised, and compared to the non-milled ones could have been carried out to see to what extent the increased number of edge sites affected their fractionation and stability behaviour. These could have then been used in the flow and sorption experiments, to see if it influenced their transport and reactivity properties at all. When compared to the clay made purely by sieving and filtering, as opposed to being used in place of it, milled clays could have provided insight into how a smaller surface area and more exposed edge sites affects the behaviour and reactivity of the clay colloids, as opposed to potentially inducing errors into the experiment, as it may have done if only that type of sample were used.

4.4.5 Filtration and dispersion

4.4.5.1 Overview

Two notable developments occurred during the work carried out for this chapter: the use of a filtration system, and the introduction of surfactants for dispersing the colloids.

Firstly, the introduction of the filtration system made it possible to produce clay fractions with sizes within set boundaries for the first time during the course of the project, which gave a greater degree of control than centrifugation or milling did. However, the size distributions of the resulting colloidal fractions did not match the nominal pore size of the membranes used to produce them. The same effect was noted by Doucet *et al*. (2005) and is discussed in sections 4.1 and 4.3.3.3.3.

Secondly, dispersion of the bentonite using PVP allowed the clay aggregates to be separated before filtering and it reduced (although it could not completely eliminate) re-agglomeration afterwards. This maintained the fractions truer to their filtered sizes: if the colloids passed through a filter of specific pore size and then agglomerated, then their size distribution would not resemble the size of that filter very closely. However, the PVP could only reduce agglomeration, not eliminate it entirely, and the layer of PVP made it harder to distinguish features of the colloids clearly when viewed using ESEM.

4.4.5.2 PVP and filtration: preliminary experiments

The method was revised, and the target fractions made fewer and wider throughout the preliminary experiments. This is unfortunate but understandable given the range of issues that were encountered: from disintegrating filters, to the concentrations of resuspended fractions being too low to image, and therefore most likely too low to use in the flow experiments.

Further investigations indicated that the <20 nm peaks shown on the graphs of number distribution in Figures 4.25a and b may actually have been from PVP that was not sorbed

onto the clay particles but was free in solution and large enough to be detected by DLS. This made the apparent size distributions of the <50 nm and <1000 nm fractions made using PVP compelling enough to warrant further investigation, and upon imaging, they proved likely to be useful for the flow experiments.

There may have been more fractions that were actually suitable for the flow experiments than were carried forward for the work described in Chapter 6, but they were discounted because the DLS results indicated broad particle size distributions. The issues associated with making size distribution measurements solely using DLS, particularly on non-spherical particles such as these, are discussed in depth in Chapter 3. It was not possible to gain access to field-flow fractionation, which may have helped to provide better sizing data, but as it also measures the hydrodynamic diameters of suspended particles in the same manner as DLS, it is not possible to tell how valuable it would have been. This problem would have been eliminated through the use of microscopy, but those techniques are also not without disadvantages. Techniques such as ESEM and TEM are expensive, may not have high enough resolution to focus on the smallest of the particles in a sample which potentially excludes important size fractions, and even when using image analysis software, can only analyse up to a few hundred particles at a time, instead of the many thousands that light scattering techniques can. In order to try and get reliable sizing data from the TEM that was conducted in section 4.3.3.4.2, a lot of the larger particles had to be identified manually, because the ImageJ software could not distinguish between overlapping particles and would measure several of them as a single, large mass. Colloids were discounted from the sizing measurements where they were not completely contained within the image, or where their edges could not be distinguished, and because of their highly irregular shapes their areas

were measured, rather than trying to assign a diameter or sorting them according to their largest dimension, as per Michot *et al*. (2004).

4.4.5.3 PVP and filtration: method

The method used to produce the two distinct fractions that were taken forward for use in the flow experiments can be summarised as followed: the clay was sieved to <25 µm, mixed with PVP, deionised water was added, and then it was shaken by hand until dispersed, shaken mechanically overnight, and it was finally filtered through 1000 nm and 50 nm membranes. This method is simple, non-hazardous, inexpensive, and can be used to produce sufficient volumes (up to 200 ml) of the clay suspensions necessary for the flow experiments within 24 hours, so it is also time efficient.

The main drawback of this method is the rationale, or rather lack thereof, by which the concentration of PVP that was used was determined: a value which worked was identified through a miscalculation that was only identified after a significant body of work had been completed, and there was not time to repeat it and investigate whether the correct amount would have had the same effect.

4.4.5.4 PVP and filtration: results and discussion

4.4.5.4.1 PVP and filtration: characterisation

The shortcomings of DLS for size distribution determination have been covered both in this chapter and in Chapter 3, so they will not be discussed again here. Chapter 3 also discussed how the pH-dependent nature of the edge sites on clay colloids meant that DLVO theory was not applicable, making their stability and aggregation behaviours very hard to predict, and so zeta potential measurements were not useful in this sense. However, the less-negative zeta potentials of the clays that were measured after they were mixed with PVP

indicated that sorption had occurred successfully, as opposed to the surfactant simply being unbound in the samples, so it was of value there (Tunç & Duman 2008).

The TEM images that were presented and analysed in section 4.3.3.4.2 were provided by a colleague at the university, and the number of samples that could be imaged was limited. The ESEM images were taken by the author and were not limited in the same way, but inexperience in focusing the instrument and lighting the samples resulted in a large variation in the quality of the images that were taken. The ESEM images showed the larger particles more clearly than TEM, which is good for visual examination, but it cannot distinguish many particles smaller than 1 µm across, meaning that it was adequate for examining their morphology, but not for size analysis, as it would exclude potentially thousands of the smallest colloids.

Characterisation of the fractions dispersed using PVP may have been improved if access to additional sizing techniques such as field-flow fractionation had been available, but as discussed in section 4.4.5.2, this was not certain. This also applies to image analysis techniques. TEM on more samples, or better resolution on those taken using ESEM, may have improved the overall quality of information provided by the size distribution characterisation, but if the image analysis software excluded large numbers of particles or included them erroneously, then the data quality may have still been poor.

4.4.5.4.2 PVP and filtration: stability over time

The use of PVP seems to affect the stability behaviour of the colloids. Firstly, it appears to make them less stable than the particles in suspensions that were made by an otherwise identical process, but this may be because those made without a surfactant agglomerated within a matter of minutes or hours, before their starting size distributions could be characterised, and then remained that way, whereas the fractions made without PVP underwent agglomeration far more steadily. Secondly, Norrfors *et al*. (2015) found that stability did not depend on the initial colloidal size distribution, but here, it was determined that the <50 nm fraction made with PVP changed little in the first two days, and then underwent rapid agglomeration, whereas the <1000 nm fraction made with PVP increased steadily across the three days. The starting material in both experiments was MX80, and there is no clear reason why making the suspensions using filtration as opposed to centrifugation should have this effect, so it may be the result of the use of PVP, or possibly because different concentrations resulted in different interparticle distances, which could possibly have influenced the rate of agglomeration.

One of the aims of this chapter was to produce colloidal suspensions that were stable for a minimum of 48 hours, to allow them to be used in the flow experiments without the size distribution changing significantly. Like the sizing goals, this aim also had to be revised, but it did not impact the use of these fractions in the flow experiments particularly: sufficient volumes of both the <50 nm and <1000 nm fractions could be produced and run through the flow system during the time in which the stability experiments indicated that their size distribution had not changed significantly.

4.4.5.4.3 PVP and filtration: concentration

The use of nephelometry for the determination of the concentrations of the colloid fractions was more successful than ICP-MS, but it was not perfect. Firstly, there was the need to apply correction factors, as discussed in Chapters 5 and 6. Secondly, in addition to concentration, nephelometer readings may be affected by the shape, size, colour and reflectivity of the particles being measured (Omar & MatJafri 2009). The reference sample that was used to make the standards was made from the same clay that has been used throughout this project, so shape, colour and reflectivity have been controlled for as much as is possible. The innate variation of clay has been mentioned before, but this is a characteristic of the material, and there is little to be done to improve upon this.

It is not possible, however, to correct for size in this application. The standards were made from the material which had been mixed, settled, dried and then used to make XRD and XRF measurements in section 4.2, and as such is it likely to have a size distribution similar to that in Figures 4.1a-c, *i.e.* broad and multimodal. It was not possible to make the size more uniform because doing so via filtering would have removed an unknown amount of the clay colloids and measuring the concentration of these colloids was the purpose of making the standards. Size is a problem in nephelometry because it affects the scattering of the light from the particles being measured. Nephelometers measure the light that is scattered off a sample at 90 ° to the incident laser beam. When the wavelength of the light incident on the cell is much larger than the diameter of the particles, then Rayleigh scattering occurs, and light is scattered equally in all directions. When the diameter of the colloids approaches the wavelength of the light, which in the nephelometer used here was 650 nm, Mie scattering occurs, which means that a disproportionate amount of light scatters in the direction of

travel of the laser beam. This means that less light is scattered at 90 ° into the detector, and so a sample of larger particles will scatter less light into the detector, and therefore the measured concentration would be lower, than an otherwise identical sample (Greswell *et al*. 2010).

Therefore, because the standards contain a range of particle sizes, and the larger particles in them scatter less light into the detector than small particles, the concentration of small particles, *i.e.* in samples filtered to <50 nm, may be overestimated, but there does not appear to be a way to correct for this.

4.5 Conclusions

The main aim of this chapter was to produce and characterise three or more suspensions of bentonite particles with distinct, narrow size distributions, suitable for use in the flow experiments in Chapter 6. For this aim to have been met, the suspensions had to have the following characteristics:

- The size distribution of the colloids in suspension should be as narrow as possible, distinct from each other, and their production repeatable.
- They should remain stable for a minimum of 48 hours to allow them to be used in the flow experiments without the size distribution changing significantly.

In line with Aims 2 and 3, new methodologies were developed, and existing ones critiqued when the fractionation and characterisation techniques used during the work described in this chapter presented unexpected challenges.

Two bentonite fractions were produced consistently that had distinct, but not narrow, size distributions. These were made by stabilising them using PVP, and then filtering them to <50

nm and <1000 nm. Only one of these, the <50 nm fraction, was stable for the desired 48 hours, but it was possible to make the <1000 nm colloidal suspension and use it in flow experiments within a matter of hours. This was a short enough time period that its size distribution did not change significantly, and therefore the results of the flow experiments were unlikely to be impacted by its instability.

The experiments conducted by Doucet *et al*. (2005) and Norrfors *et al*. (2015) were the closest to this project that could be identified, and were arguably the most successful. However, Doucet *et al*. identified particles in their filtered suspensions that should not be present owing to the pore sizes of the membranes used to produce them, and Norrfors *et al*. (2016) discussed the large size distribution in their fractions, and the presence of small particles in the samples that were expected to have the largest mean diameters. The same issues were encountered during this project, and the sizing and stability goals had to be revised as a result.

There are two main explanations for why producing and characterising clay colloid suspensions with small, narrow size distributions is very difficult. Firstly, working with clays is problematic. They are innately highly variable (Suter *et al*. 2009), and the opposite charges on the edges and faces of the particles makes them unstable and gives them their tendency to agglomerate, and the fact that this changes depending on the pH of the sample introduces another challenge.

Secondly, characterising nanoparticles, particularly unstable, heterogeneous, plate-like ones such as these, is also very difficult. Light scattering techniques such as DLS are hindered by the non-spherical nature of the clay colloids, and as the AFM images in Figures 4.33a and b demonstrate, the clay platelets are very wide and flat, and so cannot be adequately

described by a single diameter. Microscopy techniques such as ESEM are limited by their resolution and by the fact that because they can only focus on a small area of the sample at a time, image analysis software packages can only analyse a fraction of the total particles in the sample, which may not be representative.

It is therefore necessary to use a combination of different, imperfect characterisation techniques to try and build up an understanding of the nature of the particles in the sample, and to measure them empirically. This combination makes producing and characterising clay colloid suspensions very time consuming and limited what could be achieved experimentally in this project, although the method assessment and development components may prove useful to future researchers.

The two fractions that were produced were carried forward for use in the flow experiments in Chapter 6 in order to investigate how the size distribution of bentonite colloids affects their transport behaviour.

4.6 References

Bouby, M., Geckeis, H. & Geyer, F.W., 2008. Application of asymmetric flow field-flow fractionation (AsFlFFF) coupled to inductively coupled plasma mass spectrometry (ICPMS) to the quantitative characterization of natural colloids and synthetic nanoparticles. Analytical and Bioanalytical Chemistry, 392(7–8), pp.1447–1457.

Degueldre, C. *et al.*, 1996. Colloid properties in granitic groundwater systems I: Sampling and characterisation. Applied Geochemistry, 11(96), pp.677–695.

Degueldre, C. *et al*., 1989. Colloids in water from a subsurface fracture in granitic rock, Grimsel Test Site, Switzerland. Geochimica et Cosmochimica Acta, 53(3), pp.603– 610.

Doucet, F.J., Maguire, L. & Lead, J.R., 2005. Assessment of cross-flow filtration for the size fractionation of freshwater colloids and particles. Talanta, 67(1), pp.144–154.

Fainerman, V.B., Möbius, D. & Miller, R., 2001. Foreword. In V. B. Fainerman, D. Möbius, & R. Miller, eds. Surfactants: chemistry, interfacial properties, applications.

Fiocco, R.J. & Lewis, A., 1999. Oil spill dispersants: good or bad for the environment? Pure Appl. Chem, 71(1), pp.27–42.

Goh, R., Leong, Y.K. & Lehane, B., 2011. Bentonite slurries-zeta potential, yield stress, adsorbed additive and time-dependent behaviour. Rheologica Acta, 50(1), pp.29– 38.

Greswell, R.B. *et al*., 2010. An inexpensive flow-through laser nephelometer for the detection of natural colloids and manufactured nanoparticles. Journal of Hydrology, 388(1–2), pp.112–120.

Hunter, R.J., 2001. Foundations of colloid science, Oxford: Oxford University Press.

Jönsson, B. *et al*., 2009. Structure and forces in bentonite MX-80, Sweden: SKB.

Karnland, O., 2010. Chemical and mineralogical characterization of the bentonite buffer for the acceptance control procedure in a KBS-3 repository, Sweden: SKB.

Karnland, O., Olsson, S. & Nilsson, U., 2006. Mineralogy and sealing properties of various bentonites and smectite-rich clay materials, Sweden: SKB.

Kumar, N. & Biswas, K., 2017. Cryomilling: An environment friendly approach of preparation large quantity ultra refined pure aluminium nanoparticles. Journal of Materials Research and Technology.

Maher, Z. *et al.*, 2016. Americium and plutonium association with magnesium hydroxide colloids in alkaline nuclear industry process environments. Journal of Nuclear Materials, 468, pp.84–96.

Malekzadeh, R., Saadatmand, M.M. & Rezaei-Zarchi, S., 2012. Direct Electron Transfer of Haemoglobin on Manganese III Oxide-Ag Nanofibers Modified Glassy Carbon Electrode. International Journal of Analytical Chemistry, pp.1–8.

Malvern Instruments, 2004. Zetasizer Nano Series User Manual, Malvern Instruments Ltd.

Michot, L.J. *et al.*, 2004. Phase diagrams of Wyoming Na-montmorillonite clay. Influence of particle anisotropy. Langmuir, 20(25), pp.10829–10837.

Mingelgrin, U. *et al.*, 1978. Effect of Grinding on the Structure and Behaviour of Bentonites. Clays and Clay Minerals, 26(4), pp.299–307.

Missana, T. *et al.*, 2018. Analysis of the stability behaviour of colloids obtained from different smectite clays. Applied Geochemistry, 92(2017), pp.180–187.

Missana, T. *et al.*, 2008. Role of bentonite colloids on europium and plutonium migration in a granite fracture. Applied Geochemistry, 23(6), pp.1484–1497.

Missana, T. *et al.*, 2016. WP4 Partners Final report on experimental results on clay colloid stability, EU: BELBaR.

Missana, T. & Adell, A., 2000. On the Applicability of DLVO Theory to the Prediction of Clay Colloids Stability. Journal of colloid and interface science, 230, pp.150–156.Missana, T., Alonso, U. & Turrero, M.J., 2003. Generation and stability of bentonite colloids at the bentonite/granite interface of a deep geological radioactive waste repository. Journal of Contaminant Hydrology, 61(1–4), pp.17–31.

Missana, T. & Geckeis, H., 2006. The CRR Final Project Report Series II: Supporting Laboratory Experiments with Radionuclides and Bentonite Colloids, Switzerland: Nagra.

Van Den Mooter, G. *et al.*, 1998. Physico-chemical characterization of solid dispersions of temazepam with polyethylene glycol 6000 and PVP K30. International Journal of Pharmaceutics, 164(1–2), pp.67–80.

Möri, A. *et al.*, 2003. The colloid and radionuclide retardation experiment at the Grimsel Test Site: Influence of bentonite colloids on radionuclide migration in a fractured rock. Colloids and Surfaces A: Physicochemical and Engineering Aspects, 217(1–3), pp.33–47.

Newton, A.G., Lee, J.-Y. & Kwon, K.D., 2017. Na-Montmorillonite Edge Structure and Surface Complexes: An Atomistic Perspective. Minerals, 7(5), p.78.

Norrfors, K.K. *et al.*, 2015. Montmorillonite colloids: I. Characterization and stability of dispersions with different size fractions. Applied Clay Science, 114, pp.179–189.

Norrfors, K.K. *et al.*, 2016. Montmorillonite colloids: II. Colloidal size dependency on radionuclide adsorption. Applied Clay Science, 123, pp.292–303.

Omar, A.F. Bin & MatJafri, M.Z. Bin, 2009. Turbidimeter design and analysis: A review on optical fibre sensors for the measurement of water turbidity. Sensors, 9(10), pp.8311–8335.

Pusch, R., 2002. The buffer and backfill handbook. Part 1: Definitions, basic relationships, and laboratory methods, Sweden: SKB.

Segad, M. *et al.*, 2012. Microstructural and swelling properties of Ca and Na Montmorillonite: (In situ) observations with Cryo-TEM and SAXS. Journal of Physical Chemistry C, 116(13), pp.7596–7601.

Séquaris, J.M. *et al.*, 2000. Polyvinylpyrrolidone adsorption on Na-montmorillonite. Effect of the polymer interfacial conformation on the colloidal behaviour and binding of chemicals. Journal of Colloid and Interface Science, 230(1), pp.73–83.

Sherriff, N., 2015. Radionuclide Dissociation from Bentonite Colloid Systems. Doctor of Philosophy (PhD) in the faculty of Engineering and Physical Sciences. University of Manchester, UK.

Suter, J.L. *et al.*, 2009. Recent advances in large-scale atomistic and coarse-grained molecular dynamics simulation of clay minerals. Journal of Materials Chemistry, 19(17), pp.2482–2493.

Tombácz, E. & Szekeres, M., 2004. Colloidal behaviour of aqueous montmorillonite suspensions: The specific role of pH in the presence of indifferent electrolytes. Applied Clay Science, 27(1–2), pp.75–94.

Tunç, S. & Duman, O., 2008. The effect of different molecular weight of poly(ethylene glycol) on the electrokinetic and rheological properties of Na-bentonite suspensions. Colloids and Surfaces A: Physicochemical and Engineering Aspects, 317(1–3), pp.93–99.

Vilks, P., Miller, H.G. & Doern, D.C., 1991. Natural colloids and suspended particles in the Whiteshell Research Area, Manitoba, Canada, and their potential effect on radiocolloid formation. Applied Geochemistry, 6, pp.565–574.

Yukselen, Y. & Kaya, A., 2003. Zeta Potential of Kaolinite in the Presence of Alkali, Alkaline Earth and Hydrolyzable Metal Ions. Water, Air and Soil Pollution, 145, pp.155–168.

Chapter 5

Construction of the flow system

Disclaimer: The Python code used to control the flow system was written by Dr George Day and Dr Alan Herbert.

Chapter 5: Construction of the flow system

5.1 Introduction

One of the aims of this project was to conduct flow experiments. In order to do this, some means by which to pass a suspension of clay particles and relevant cations across or through a sample of granite, measure their change in concentration over time, and produce breakthrough curves was needed. To this end, it was necessary to obtain access to a flow system: a combination of tubes, pumps and associated components designed for this purpose. Such a system exists at the university, but initial examinations determined that it was in a state of disrepair and could not be used. Therefore, as it is not possible to purchase a flow system of this nature, one had to be assembled. Other options were explored, including whether it was possible to modify instruments such as those used for DLS measurements and incorporate them into the system, but after considerable discussion and research, it was concluded that the most viable option was to construct a new system, similar to the existing one, but with design modifications and improvements.

Much of the system did not present a significant financial outlay, but the cost of a commercially available flow-through nephelometer suitable for use with the very low flow rates required for simulating groundwater movement was prohibitive. Building the nephelometer, an instrument that uses light scattering to measure the concentration of particles in suspension, represents the most significant investment of time, cost and effort into the system, and thus a large part of the chapter is dedicated to it. A schematic detailing how the nephelometer is incorporated into the wider flow system is provided in Figure 5.1, and background information about nephelometers was presented in Chapter 3.

There are a number of examples in the literature of researchers successfully building their own nephelometers either due to financial limitations or because of the need for a customised design (Berberoglu & Pilon 2007; Lienert *et al*. 2003), and this project was undertaken for the former reason. The design of the nephelometer in the existing system (which is also not a commercially-available instrument) was described by Greswell *et al*. (2010) and the lead author of that paper provided advice on the issues encountered during its construction, and suggested some improvements.

This chapter details each component of the system, provides data regarding the performance of the nephelometer, discusses some of the necessary compromises and limitations, and makes recommendations as to how the design may be improved if another system is needed in future.

5.2 Overview of the flow system

The system was used to pump colloidal suspensions across rock samples that were representative of a typical granite geology. This was analogous to one type of host rock in which a GDF may be constructed and allowed the colloids to interact with the rock and this interaction to be investigated more easily than in situ experiments, over shorter time scales. A flow-through nephelometer placed in the system measured the change in concentration of particles over time after they flowed across the rock, producing a breakthrough curve. Interpretation of these curves can be used to provide information about the interactions of clay with granite surfaces similar to those that are likely to be found in a GDF (Greswell *et al*. 2010).

What follows is a brief summary of the system, and each of the components is covered in greater detail in this chapter. Firstly, a peristaltic pump moves the colloidal suspension from the inflow reservoir, across a granite sample, and then through the nephelometer. If tracer experiments are needed to provide a baseline dataset for system behaviour, running a different program activates a blue LED instead of the laser, temporarily converting the nephelometer into a fluorimeter. The bubble traps are necessary because bubbles have high surface tension, making them hard to remove, and if they enter the system they can alter the flow regime and induce errors. The whole system is contained within a typical household refrigerator in order to maintain a constant temperature, and temperature sensors are used to check for any variation. The system is shown schematically in Figure 5.1, and a detailed experimental protocol may be found in Appendix 2.

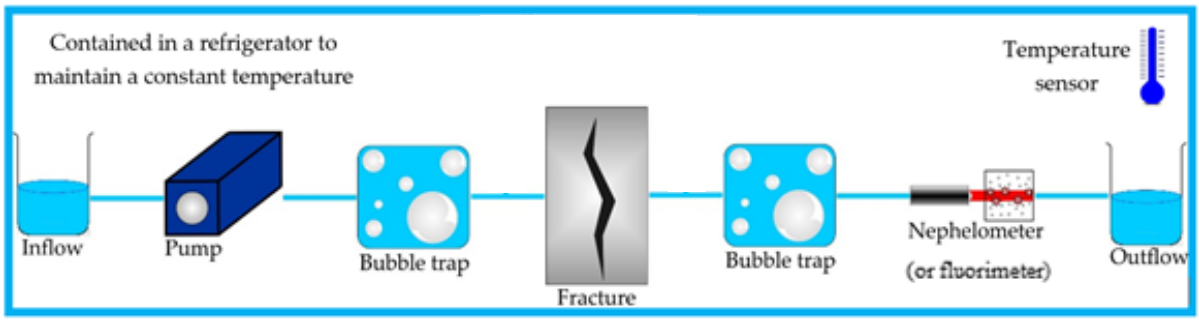

Figure 5.1. A schematic of the flow system. It consists of an inflow and outflow reservoir, a peristaltic pump, bubble traps, a rock sample or column, and the nephelometer (or fluorimeter, depending on the application). This is all contained in a refrigerator to regulate the temperature.

5.3 Construction of the flow system

5.3.1 Inflow and outflow reservoirs

Deionised water is flowed through the system before the sample is introduced to provide a baseline reading. The water and the sample are held in glass beakers inside the refrigerator, each with a tube leading out of the fridge to a three-way valve like the one shown in Figure 5.2. Turning a stopcock opens the inlet to each of these pipes in turn and allows either the water or the sample to pass into a third pipe, which leads to the pump, and then to the rest of the system, without opening the fridge and altering the temperature within.

Figure 5.2. The stopcock and inlet and outlet pipes. These are used to direct either samples or pure water through the rock sample as required.

The outflow is another pipe that transports the solution out of the flow cell and into a third beaker, from where it may either be collected for further tests or disposed of via an appropriate route.

5.3.2 Tubing

Three types of tubing are used in the system:

- The majority of the tubing is a rigid PTFE tubing. Its stiffness makes it compatible with the connectors described below, and a 1.6 mm outer diameter and 1 mm inner diameter allows for low flow rates.
- Small lengths of thicker 1/8" PTFE tubing are used to connect the bubble trap, stopcocks and the flow cell to the rest of the system.
- A soft Tygon tubing with ~2.5 mm outer diameter wraps around the rotary system of the pump, which squeezes it and drives the sample through the flow system.

5.3.3 Connectors

The connectors that join the different components of the flow system are compression fit and custom made from polypropylene. The tubes fit through the eyelets, and the connection becomes tighter as the cap is screwed down, holding the pipe firmly. An example of one such connector is shown in Figure 5.3. Luer valves connect the tubing to the stopcocks that switch between the inlet supplies for the water and sample.

Figure 5.3. A deconstructed connector. The PTFE tubing is held firmly by the cap, and the rubber o-ring prevents leaks.

5.3.4 Pump

Samples are moved through the flow system using a Masterflex Dual-Channel Variable-Speed peristaltic pump. As a rotor turns, it squeezes the sample through tubing str*etc*hed around the outside of it, which forces the sample through the system. This type of pump is good for work involving hazardous materials because the solutions never come into direct contact with it, and so contamination may be avoided by changing the tubing. This is faster, easier and less expensive than cleaning or replacing the pump. However, the tubing around the rotor will degrade and lose tension and must be tested regularly and replaced when necessary to prevent significant change in the flow rate.

The speed at which the rotor turns can be adjusted manually by turning a dial on the front of the pump, but the actual flow rate is dependent on the tubing used in the system: the larger the inner diameter, the higher the maximum possible flow rate. Three different types

of tubing were used in the system (see above), and so the flow rate was measured manually to ensure it was suitable for the flow experiments. At the highest speed setting, 2.6 ml was collected in a measuring cylinder over a period of 10 minutes, giving a maximum flow rate of 0.26 ml/min. A series of experiments that involved running bentonite colloids through the fracture (see section 5.3.6) were conducted as part of a previous research project (Walkden 2014). These were conducted on the other flow system at the university that was discussed previously in this chapter. The flow rate used in those experiments was 0.35 ml/min, based on flow experiments carried out at the (GTS) Grimsel Test Site by (Reimus 2012). The flow rate that was used in the experiments was therefore the maximum output of the pump, 0.26 ml/min, in order to match this as closely as possible. The 0.09 ml/min difference was unlikely to be significant, but the tubing was changed regularly to prevent it str*etc*hing to such an extent that the flow rate slowed any further.

5.3.5 Bubble traps

The sample passes through two bubble traps before entering the rock sample and the flow cell. Bubbles can disrupt the flow regime of the system, and may refract light and induce large errors in the flow cell, and can be very difficult to remove due to their large surface tension (Greswell *et al*. 2010). The varying solubility of dissolved gases at different temperatures may also lead to bubbles in the system. The flow system is contained in a temperature-controlled environment, which should help to reduce the likelihood of this occurring, but the bubble trap is still a necessary precaution.

The operating principle of a bubble trap is simple. When the pump is switched on, deionised water is initially flowed through the system. This fills up the reservoirs of the 'debubblers', which are small vials with an inlet and outlet tube at the bottom. When the reservoirs are filled, there is minimal mixing within them: Figure 5.4 shows the laminar flow of the fluorescein dye, where it had passed underneath the water and formed clearly defined layers. Any bubbles entering the debubbler float to the top and displace a small amount of the liquid within it, preventing them from entering the next section of tubing and the key parts of the system.

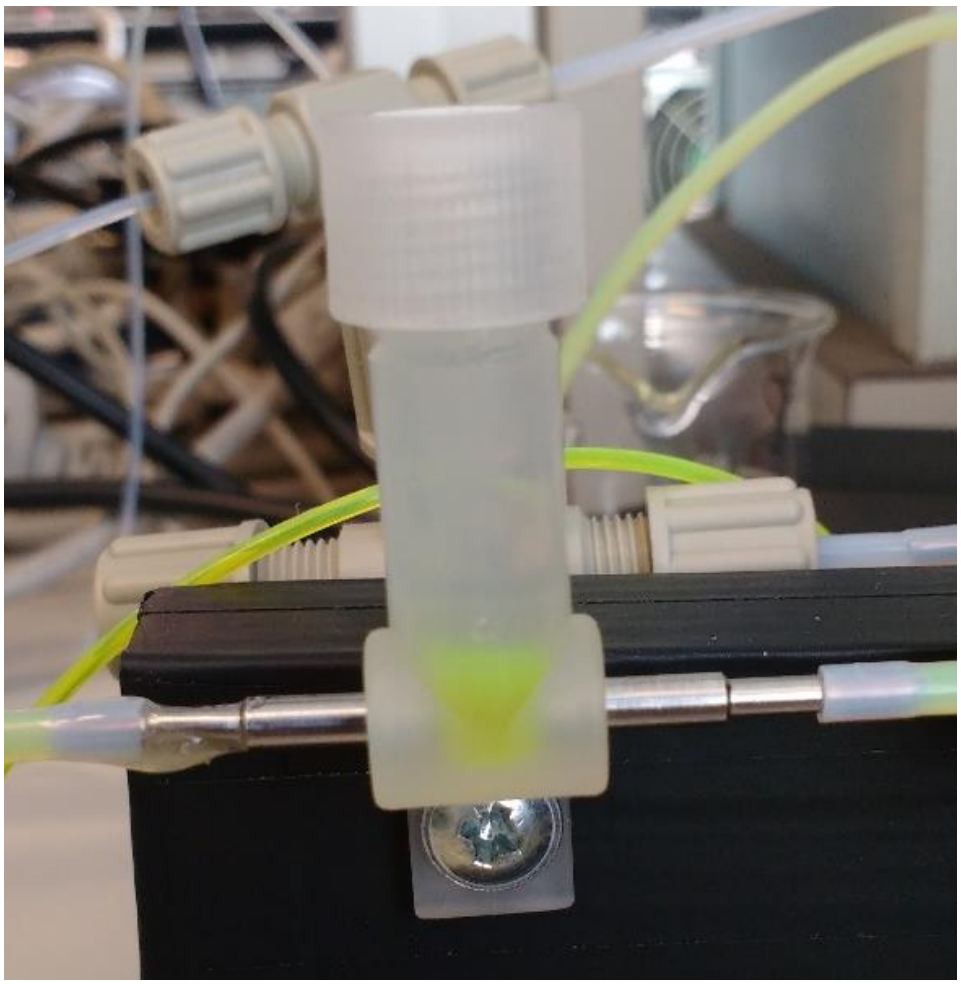

Figure 5.4. Fluorescein passing underneath the deionised water in the reservoir. The design of the debubblers means that the fluid that is being introduced flows underneath that held in the reservoir, which minimises mixing.

5.3.6 Rock samples

Two different rock samples were used in the flow system. The first, shown in Figures 5.5a and b, is a piece of granite worktop sealed in a Perspex housing unit, which was provided by colleagues at the University of Birmingham. It is approximately 40x20x2 cm in size, the top is flat but not polished to a smooth surface, and when solution is flowed across it between the inlet and outlet tubes, it spreads out and forms a thin layer between the granite slab and the bottom of the Perspex.

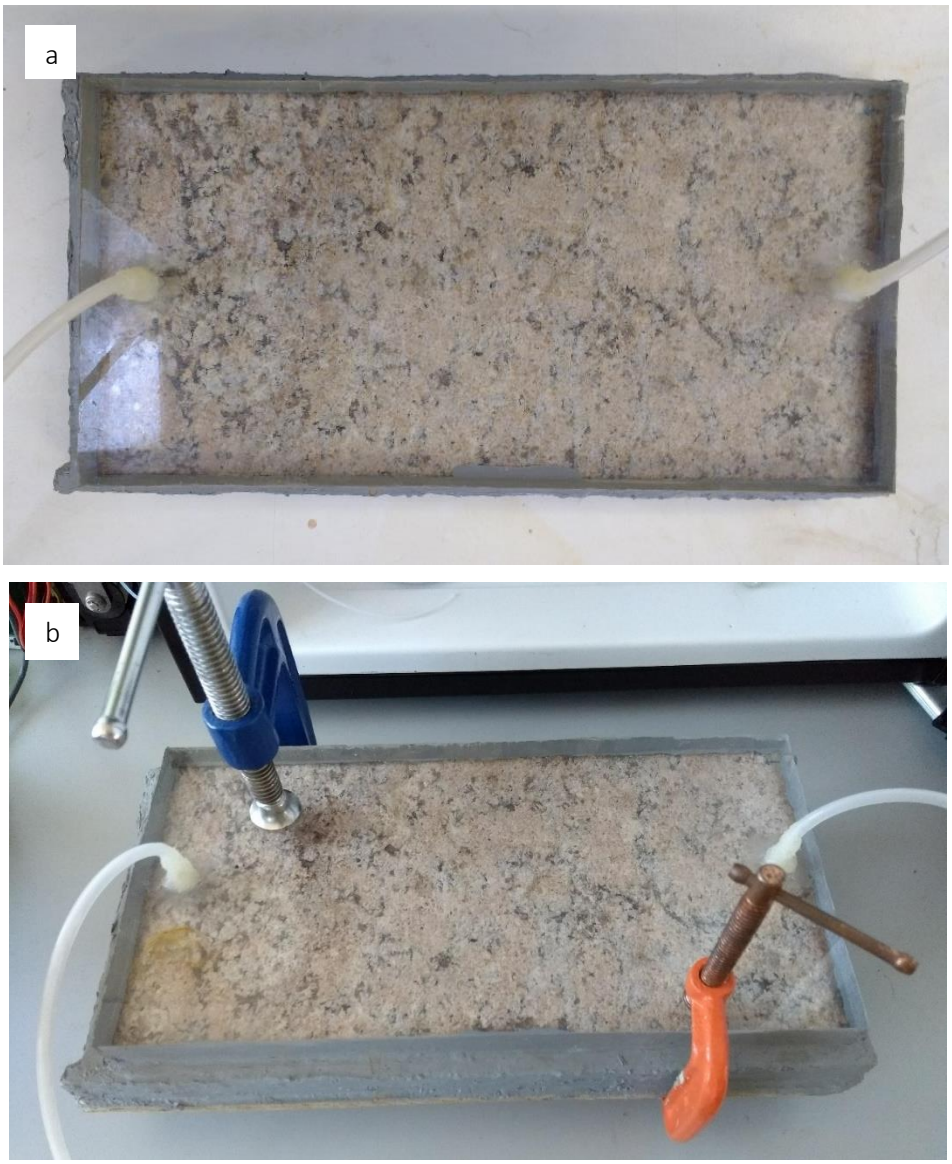

Figures 5.5a and b. The slab of granite that was used in some of the flow experiments. Figure 5.5a shows a top view of it, and Figure 5.5b shows how it was sealed with G-clamps to prevent leaks.

The second rock sample is from the GTS. It is 10x10x1 cm in size and contains a fracture which is mostly filled with tightly packed fracture fill material, but also has a more permeable section through which water can flow. It is held between two Perspex blocks with shallow atria cut into them that collect small amounts of water, allowing it to spread across the surface and enter the fracture. It originally had two tubes in each side of the casing, but as only one was required each side for this particular application, two were trimmed and sealed. It was not possible to remove them completely because the fixings could not be extracted, so some water is likely to pool in them. However, the volume is small, as measured and discussed in Chapter 6. The fracture is pictured in Figures 5.6 a, b, and c.

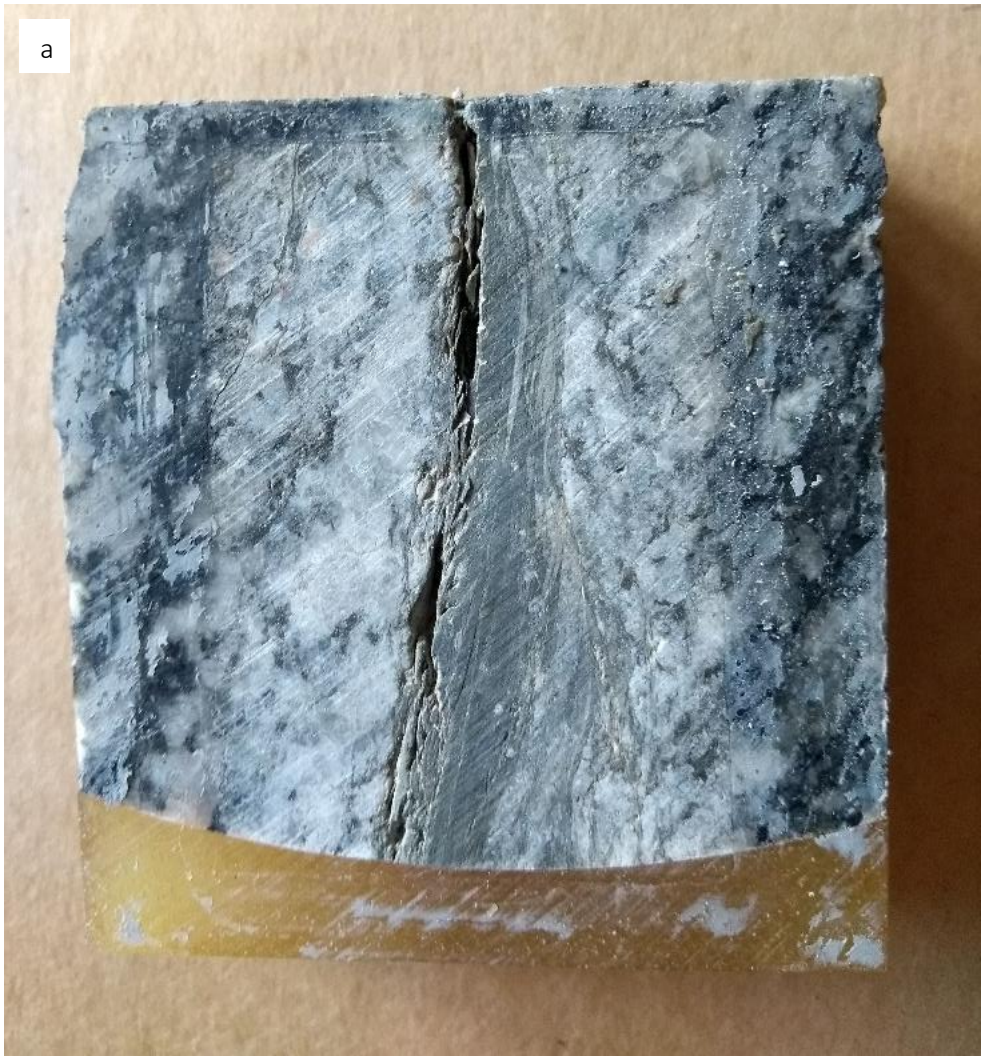

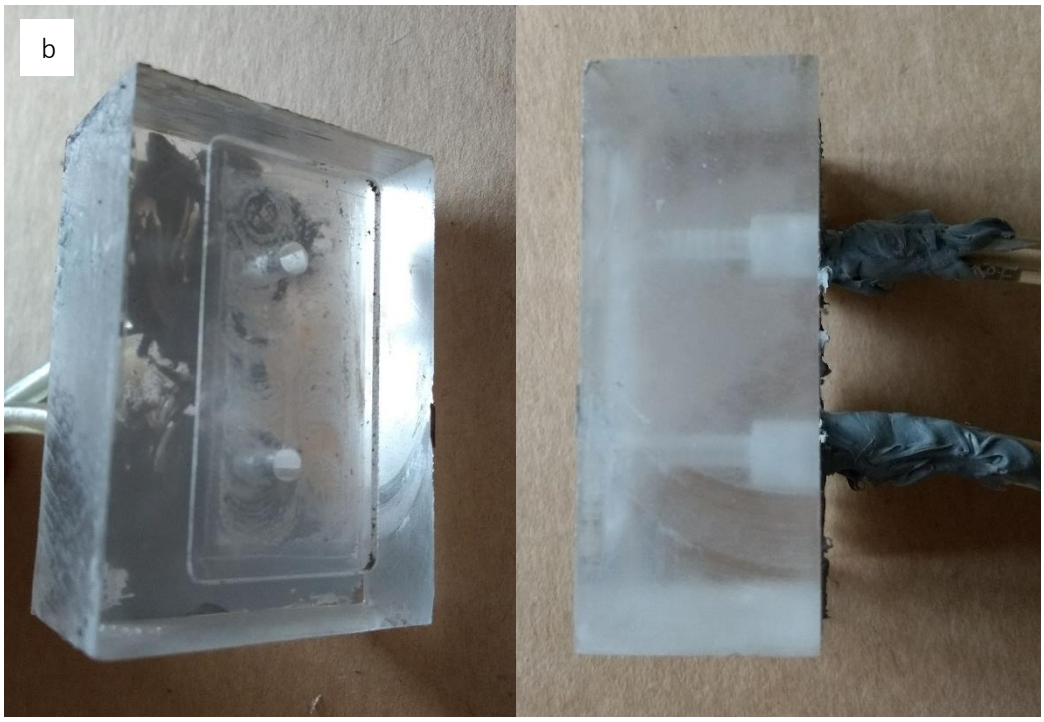

Figures 5.6a-c: a. the small piece of Grimsel granite that was used in some of the flow experiments, b. the casing used to flow solutions through it, c. and the assembled unit.

The rock samples are connected to the flow system by a combination of tubes and stopcocks referred to as the 'bypass', thus named because it allows solutions to flow through the system without passing through the rock samples (*e.g.* when running standards or testing gain settings), but the flow can be directed through them instead simply by turning two stopcocks. It also allows these rock samples to be easily substituted for others or by a column, so the system can be used for different applications. The setup is shown in Figure 5.7.

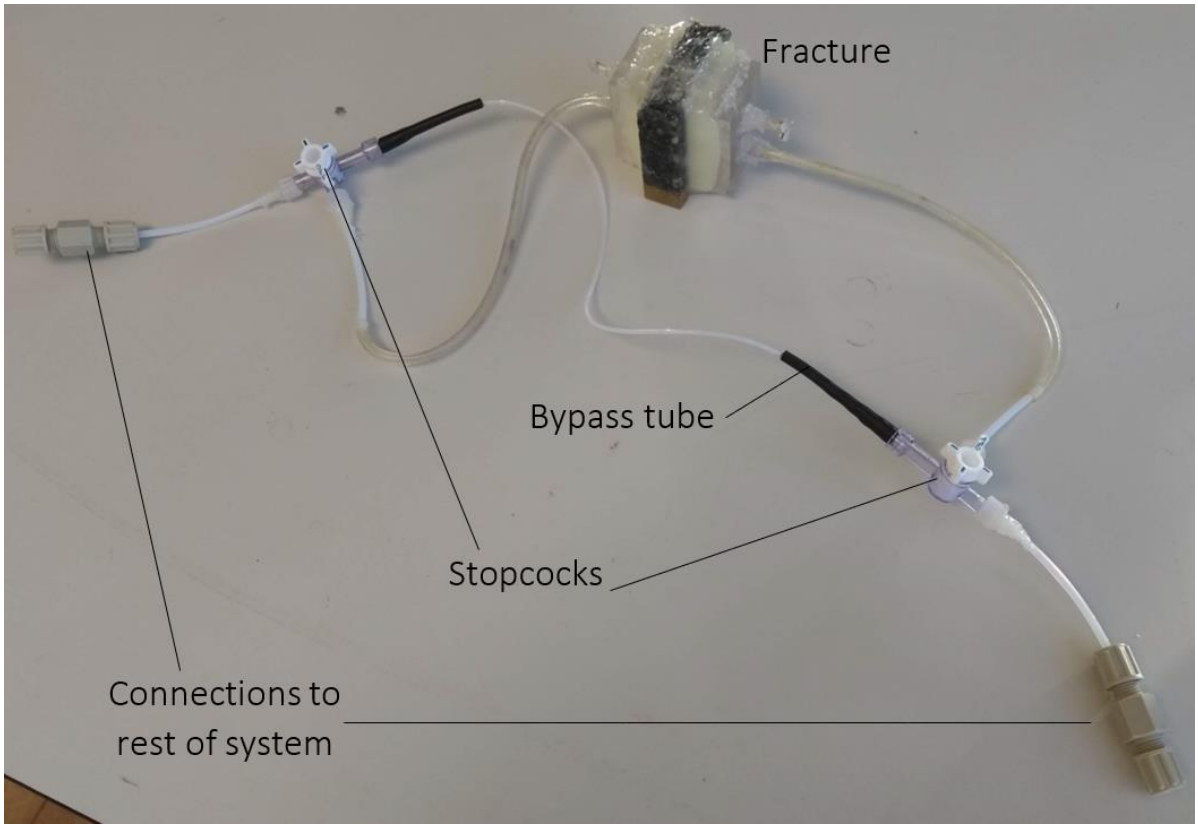

Figure 5.7. The bypass. This may be used to flow solutions through the system without them passing through the rock samples, *e.g*. when running standards or testing gain settings.

5.3.7 Refrigerator

The flow system is housed within a normal household refrigerator in order to maintain a constant temperature. This is important for several reasons. Firstly, the performance of most electronic components is temperature-dependent (Greswell *et al*. 2010). Semleit *et al*. (1997) determined that the light output of a laser and the noise it produces vary with environmental temperature, and the manual for the laser module states that its output may vary by up to 6 % over its recommended operating temperature range (Global Laser 2014). Given that the laser affects the amount of scatter in the system, it is very important that a consistent output is maintained. Secondly, pH is temperature-dependent (Ashton & Geary 2005). pH influences the surface charge of clay, which in turn controls its reactions with ions in solution and how clay platelets bond to one another (Tombácz & Szekeres 2004). It also affects the sorption, solubility and migration of any cations that may be added to the system (Nessa *et al*. 2007). Thirdly, gases may diffuse out of solution as temperature increases, forming bubbles in the system. The impact of this was described above in section 5.3.5. Finally, the fluorescent properties of fluorescein are pH dependent: a higher pH results in greater fluorescence intensity (Martin & Lindqvist 1975). Given that the pH of water is temperature dependent, it is important that a constant temperature be maintained in the system to ensure accuracy of the breakthrough curve.

The use of temperature gauges, one inside the nephelometer housing and another inside the refrigerator, allows the temperature profile of the environment in which the experiments are conducted to be monitored. This is discussed further below.

5.3.8 Temperature sensor

Temperature gauges are necessary so as to ensure that a constant temperature is maintained throughout the flow system, the importance of which was discussed above. If there is significant variation, this may be accounted for when interpreting the results. (Greswell *et al*. 2010). Initially an inexpensive TMP36 sensor was used which was integrated with the nephelometer and controlled by the Pi, but calibrations with ice water and thermometers determined that it was inaccurate. This component was replaced by two TRIX-8 LogTags, which are standalone units used to ensure that food and medical supplies are maintained at a safe temperature during transit. They have to be switched on separately from the nephelometer, resulting in a starting time which may vary very slightly from the concentration readings. This is a disadvantage compared to the TMP36, which began taking readings at exactly the same time point as it was integrated into the system and controlled by the Pi, but the discrepancy is unlikely to be more than 30 seconds (this represents the time taken to place the sensors into position, screw on the lid of the nephelometer box, close the refrigerator and start the nephelometer), which is a small error over the course of an experiment that lasts several hours, especially as the temperature is unlikely to change rapidly. Additionally, they are more accurate than the TMP36, simple to use, and their output data can still be converted to a CSV file and plotted directly alongside the output from the light detector. Two were used in the system, one inside the nephelometer box and one outside in the refrigerator. The one outside of the box was less well insulated and allowed for greater sensitivity in detecting small variations in the temperature of the refrigerator, and the one inside the box captured the changes that the temperature-sensitive laser was exposed to.

5.4 Overview of the nephelometer and fluorimeter

In a nephelometer, a narrow, monochromatic beam of light is directed at a sample. Particles in the sample scatter the light, which is then measured by a photodetector placed at 90 ° to the source. The detector converts that light into a voltage, which is then recorded by a datalogger. More particles result in more scatter, and thus more light enters the photodiode and produces a proportionately larger current. When compared to known standards, the concentration of particles in the sample may then be determined. However, the amount of scatter also depends on the colour, shape, size and aggregation of the particles under examination (Greswell *et al*. 2010). A schematic of the nephelometer is shown in Figure 5.8.

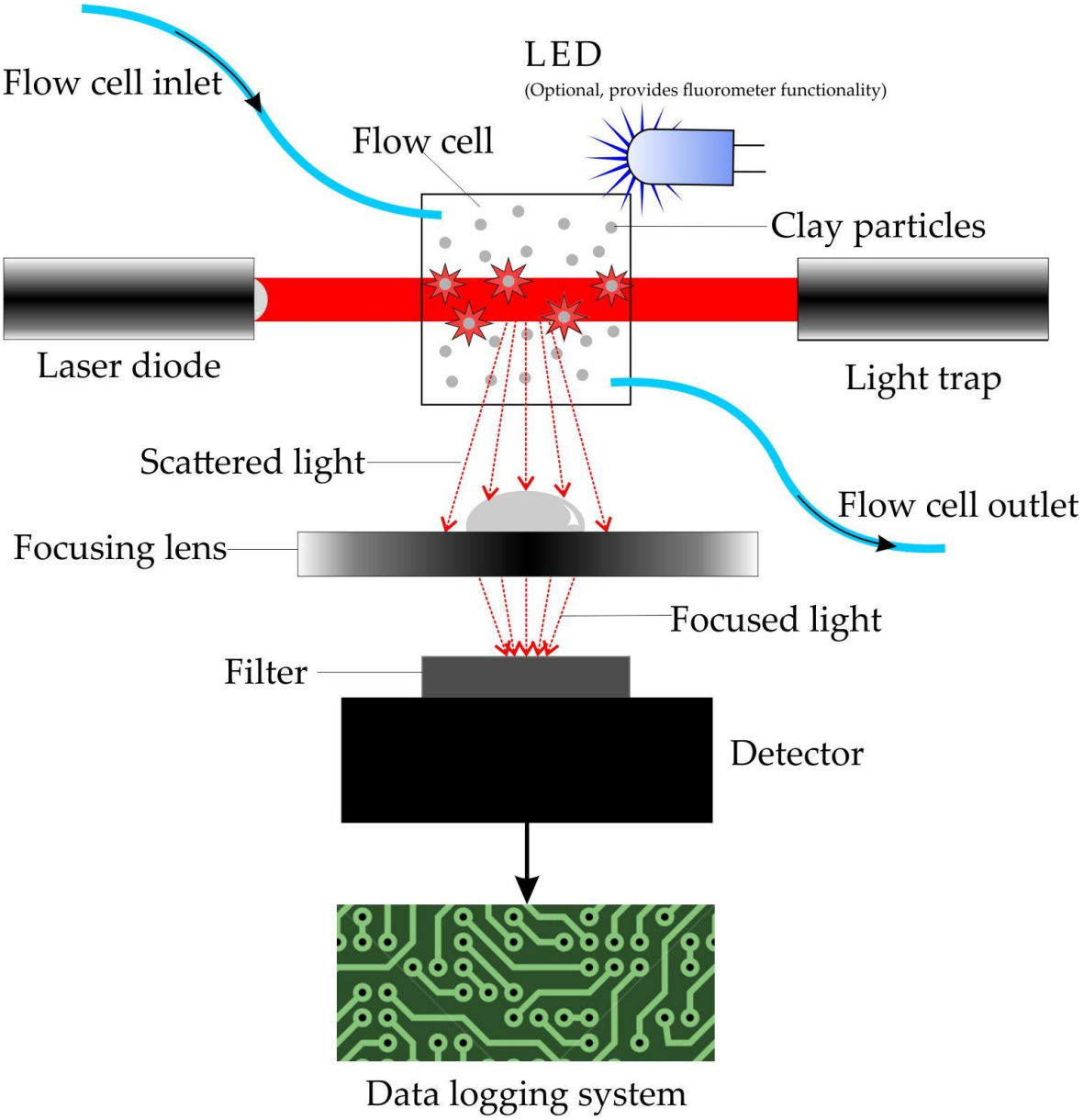

Figure 5.8. A schematic of the nephelometer. Laser light is directed at a colloidal suspension, and the particles within that suspension scatter it at 90° into a photodetector. The magnitude of the current measured by the detector can be related to the concentration of particles in the sample through the use of standard curves.

5.5 Construction of the nephelometer and fluorimeter

5.5.1 Laser

A 5mW, 650 nm wavelength, class 3R red laser module is used as the light source in the nephelometer. Laser modules offer several advantages over other light sources such as LEDs: they produce high light intensities with small power inputs, are monochromatic, and small, fairly powerful modules may be obtained for around £100 (Greswell *et al*. 2010). Lasers contain semiconductor crystals. When current flows through the crystal it excites the electrons within it. These electrons eventually lose energy and return to a ground state, emitting photons as they do so, which produces a beam of monochromatic light (Huether 1983; Semleit *et al*. 1997).

Laser diodes are inherently noisy (Semleit *et al*. 1997), which is problematic because they may cause electrical interference that affects the signal from the detector. This higher background then impacts on the sensitivity of the instrument. This means that the signal must be shielded, which is discussed below.

Focusing the laser beam was a delicate exercise which had to balance being as wide as possible so as to induce scattering off a large proportion of the sample, yet narrow enough to pass through the flow chamber without reflecting off the edges or corners of the cell, which could produce unintended scattering and diffraction.

The output of the laser is dependent on the ambient temperature (Semleit *et al*. 1997). The datasheet indicates that its output can vary by up to 6 % across its range of operating temperatures (-10-45 °C), which would then affect the amount of light scattered off the suspended particles that enters the detector (Global Laser 2014). The flow system is

contained within a refrigerator to limit this variation, but the temperature is still monitored continuously. Chapters 4 and 6 both contain details of the correction factors that may be applied to account for the effect of temperature variation in experimental runs.

The laser module is powered and controlled by a Raspberry Pi, a microcontroller that also logs the data and is described in greater detail in section 5.5.4. It is switched on and off by a Transistor-Transistor Logic Enable input, which raises and drops the voltage across the laser more gently than simply applying and removing current would do so, and gives it good immunity to external noise (GlobalLaser 2014; Zumbahlen 2012). It is analogous to switching a computer off using its shutdown function, rather than switching off its mains power, and extends the lifetime of the module. The diode becomes noisier as it ages, which as discussed above, has consequences for the performance of the nephelometer.

The lifespan of the module may be affected by its mode of operation. Switching it on for long periods will cause it to degrade faster, and may also cause heating of the casing, both of which can impact data quality. It is therefore switched on for two seconds, during which the voltage from the detector is recorded, and then switched off for seven seconds. This repeats for the duration of the experiment.

5.5.2 Flow cell

The flow cell, shown in Figure 5.9, was built to the specifications described by Greswell *et al*. (2010), except for the use of an optical glass Kromatek cell, rather than the more expensive Hellma one. A precision-made acrylic block holds two hypodermic needles which, when attached to rigid PTFE tubing using Luer valves, provide the inflow and outflow tubes that pass samples through the nephelometer. Its small (0.2 ml) volume prevents a loss of signal

resolution due to poor mixing, which can significantly alter the breakthrough curve (Greswell *et al*. 2010), for around one tenth of the price of a commercially-available flow-through cell. It is positioned on an acrylic holder so that the laser beam passes through the void at the bottom, and it is held in place by a small vice cushioned with rubber to prevent damage to the cell. The laser beam enters through the 10 mm-wide window of the cell, which is on the front side in Figure 5.9, and light scatters into the detector through the 4 mm window, which is visible on the left.

Figure 5.9. The flow cell. This is made from a commercially available optical glass cell and an acrylic insert. Hypodermic needles provide inflow and outflow channels and the small volume of the cell minimises mixing.

5.5.3 Detector

The photodetector used in the nephelometer is a Thorlabs PDA36A Si transimpedance amplified detector. It is several times more expensive than the components in the circuit used by Greswell *et al*. (2010), but offers two main advantages. Firstly, it is more robust: the

amplifier circuit that Greswell *et al*. constructed was very delicate, a fingerprint on some of the components could alter their conductivity and produce false signals, and small impacts had the potential to move the photodiode relative to the lens system. Secondly, its gain may be adjusted using a switch on the side. Adjustable gain is an important feature in detection systems such as this because it controls the limits of detection (Schnegg & Doerfliger 1997). It alters the voltage range over which the detector and data logger take readings, allowing the user to 'zoom in' and record detail in the data which may not have been measured if the gain were too large. For example, a data logger with 8-bit resolution can resolve the reading of interest into 2^8 (256) 'steps'. If the system under investigation produces readings between 0-10V, each step represents 10/256V (0.039V). This is acceptable if the data has values across most of the 0-10V range, such as the example in Figure 5.10 which was produced by the author for demonstrative purposes.

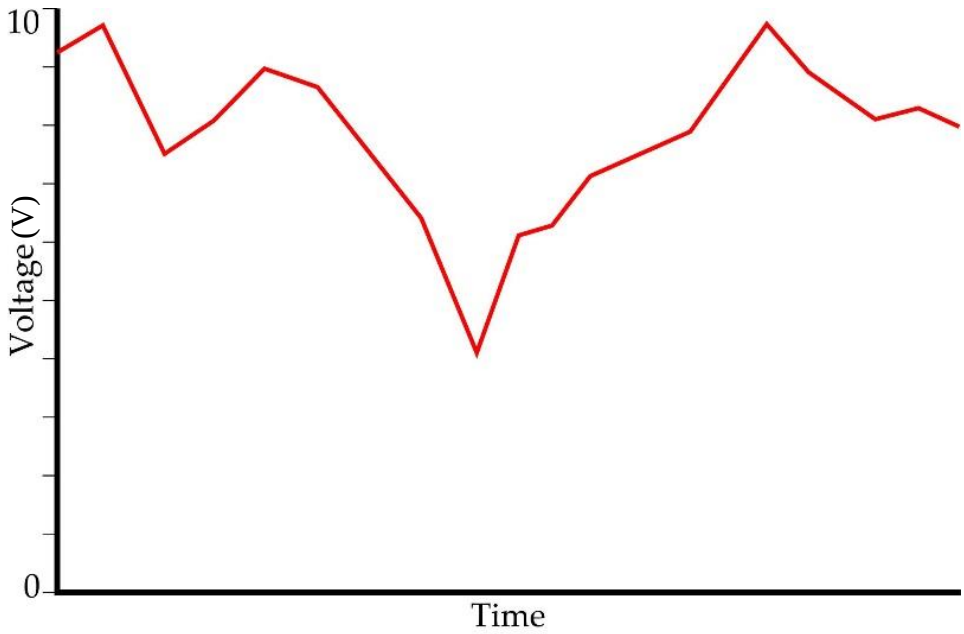

Figure 5.10. An example of a fictitious sample that has data points across almost the whole 0-10 V range, for demonstrative purposes only.

However, as shown in Figure 5.11, if the data only has values between 0-1V, a lot of detail may be missed because the entire dataset must be represented by only 25.6 steps.

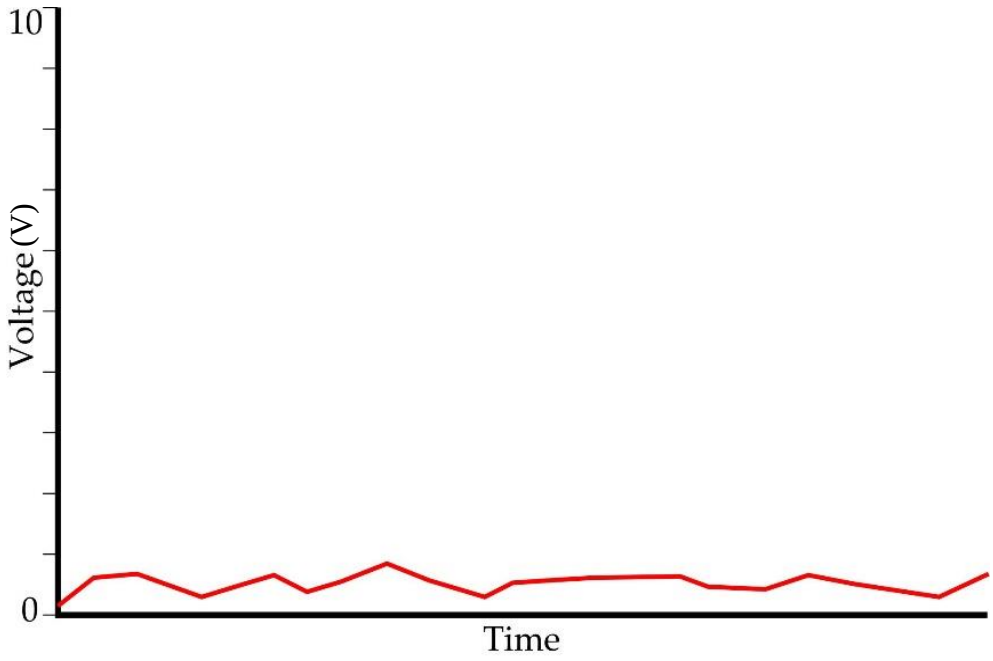

Figure 5.11. An example of a different sample, which only has data points in the range of 0-1 V. If the same gain settings as the previous sample were to be used, there may be detail in the dataset which could not be resolved.

Changing the gain settings focuses the data logging system on the data range of interest. In Figure 5.12, the altered gain now means that the 0-1V range may now be resolved into 256 steps, and detail in the data that could not previously be seen is now visible.

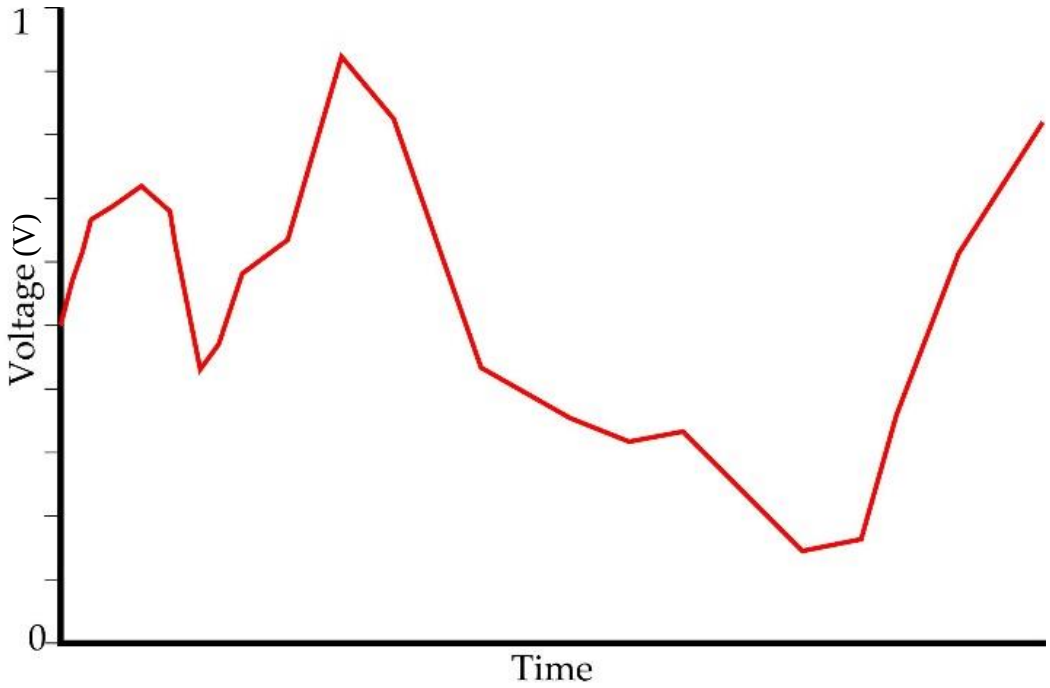

Figure 5.12. An example of the sample from Figure 5.11, but this time measured with 0-1 V gain. Details in the data which could not be resolved in Figure 5.11 are easily observable.

In the original design by Greswell *et al.*, gain was controlled by a resistor, and building switchable gain into the design would have required the use of reed relays to pass the current through different resistors. Additional benefits of the photodetector used here are that it is also grounded, it is shielded from interference by its metal casing, and it comes with its own power supply, which is safer and less time consuming than building or modifying one (Thorlabs 2015).

Preliminary tests indicated that although the highest gain setting produces the most sensitive results, increasing the gain also increases the degree of noise in the system. This

noise may be reduced by calculating a running average of the readings taken over a short period of time. After sufficient iterations this cancels out the interference and resolves the signal, but care must be taken to ensure that this does not cause a loss of resolution over time.

5.5.4 Datalogger

The core of the datalogging system is an ADS1115 16-bit analogue-to-digital-converter chip (ADC), and a Raspberry Pi 3 Model B microcontroller. The analogue signals from the detector and pressure sensor are transferred into the ADC, converted to digital, and these outputs are then transmitted to the microcontroller. The inclusion of a 330 Ω resistor before the ADC chip prevents the detector from drawing too much current and potentially incurring damage.

The Raspberry Pi is a small but powerful microcontroller which may be coded in Python and used in a range of computing and robotics applications. This technology is particularly suitable for this project because its accessories enable analogue signals to be taken from the detector, converted to digital, and then logged by the Pi for a fraction of the cost of most data loggers. Inexpensive data takers such as the DrDAQ from Pico Technology were considered but would not have provided sufficient resolution: these 8-bit devices can only resolve a signal into 256 discrete intervals of voltage over its total range of both positive and negative voltages. Given that the detector only produces positive signals, that would be 128 intervals. If the sensor were calibrated to observe a maximum of 1000 ppm, it could only detect changes down to 7.8 ppm, which is insufficient resolution for this application. The 16-Bit ADC board allows the voltage to be resolved into 65536 discrete intervals, or 32768 in

the positive range, which is far superior to the 8-bit. Its programmable gain permits for even greater resolution over narrow voltage ranges. Another benefit of the ADC chip is its differential input. It has two signal inputs, one positive and one negative, which are then related to a common ground. Measuring the difference between the two signals allows any common voltages to be removed, therefore reducing noise, and is desirable when dealing with small signals requiring high gain, since the gain will amplify the noise as well as the signal. The digital signal is then transferred into the Pi via one of its GPIO pins.

A Python script instructs the laser to turn on, then after a delay of two seconds the value from the detector is recorded and saved into a spreadsheet, and the laser switches off for seven seconds. After some testing it was determined that this short delay allowed the laser to stabilise and provided a more level output than when the measurement was taken immediately after start-up. The laser is also run in this mode for around 30 minutes before the experiment commences to allow it time to stabilise. Details of this testing may be found below in Section 5.6.2, and the full code may be found in Appendix 2.

5.5.5 Fluorimeter

Fluorescein is a conservative tracer, which means that it will remain in the water column and will not adsorb to the surfaces of the rock samples. Its breakthrough curve therefore represents the behaviour of water through the flow system and provides a baseline against which to compare the behaviour of colloidal suspensions. A fluorometer is used to measure changes in fluorescein concentration over time in the same way as the nephelometer does particles, and so the nephelometer setup was modified to incorporate fluorometer functionality.

The excitation maximum of fluorescein is at 490 nm, so a blue LED of as similar wavelength as possible (470 nm) is used to illuminate it. It then fluoresces at 525 nm. A 495 nm Longpass filter was placed over the detector which blocked the light from the LED but allowed the fluorescence to enter the diode.

However, when the blue LED was shone through the filter in the absence of fluorescein and of any other light source, a light reading was still registered by the detector. The chart in Figure 5.13 was produced by the manufacturer and demonstrates that a very small amount of light below the 495 nm cut-off may still penetrate the filter.

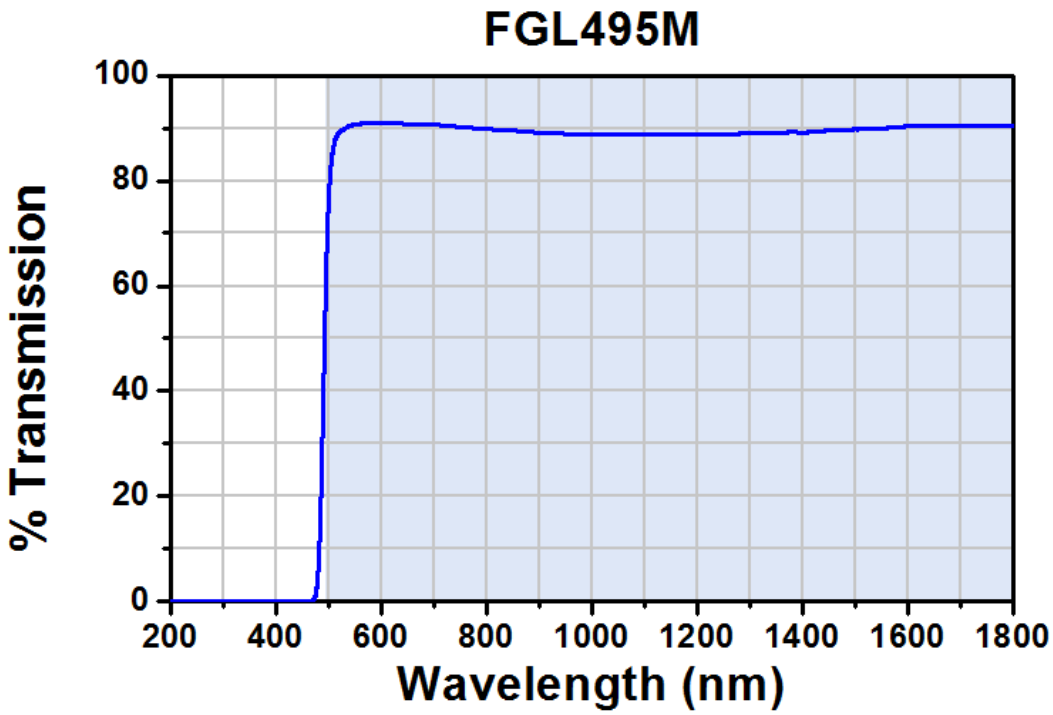

Figure 5.13. Transmission of the filter at different wavelengths (Thorlabs. Not dated). It is possible to see that a very small amount of light below the 495 nm cut-off may still penetrate the filter. Copyright Thorlabs Ltd.

It may be seen in Figure 5.14 that LEDs are not monochromatic light sources.

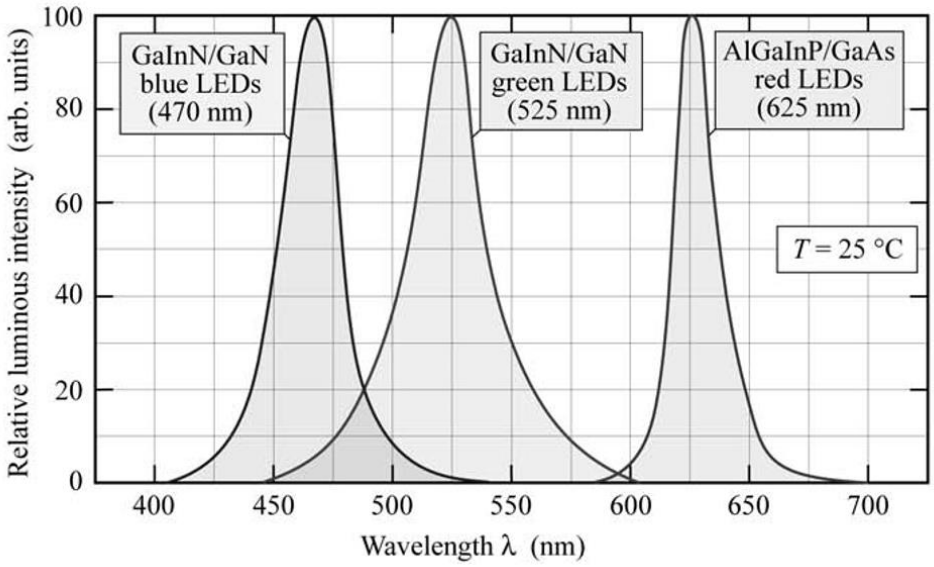

Figure 5.14. A typical emission spectra of blue, green and red LEDs. LEDs are not monochromatic light sources, but instead emit light of different wavelengths within a narrow range. Image courtesy of Schubert (2006). Copyright Cambridge University Press.

The bell curve of the wavelength of LED light is narrow but indicates that the 470 nm LED in the fluorometer will be emitting a small percentage of its output at above 495 nm, which will pass through the filter and enter the diode.

When combined with the error margins of the filter, this accounts for the unexpected readings on the detector and results in a high background, but at high enough concentrations of fluorescein, the fluorescence can still be detected above it. A trial-and-error approach was used to find the position which minimised the background from the blue LED, whilst inducing the maximum amount of fluorescence, therefore producing the maximum output signal from an unchanging fluorescein sample.

Typical fluorometers take readings at 90 ° to the light source to reduce background interference (see Figure 5.15a). Because of the need for a laser, light trap and detector in

the same unit as the fluorometer, the LED could not be placed in this more common alignment and instead is situated roughly opposite the detector (Figure 5.15b).

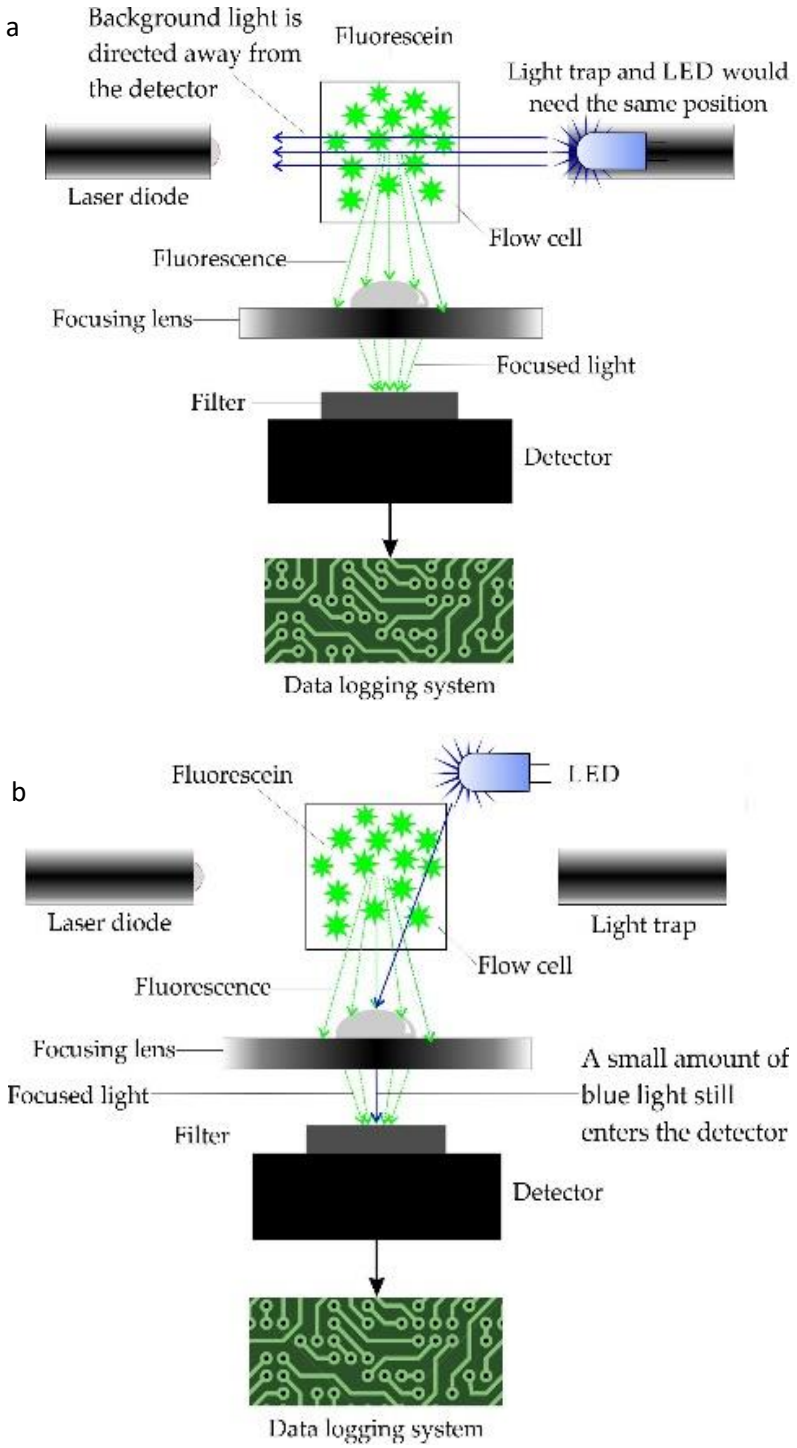

Figures 5.15a&b: a) shows the more typical fluorimeter setup, with the LED at right angles to the detector, and b) shows the one that had to be used in this application due to the need for a light trap.

The fluorimeter is grounded to the same point as the rest of the electronics in the flow system, but because it does not have a differential input, or the high levels of noise immunity that the Transistor-Transistor Logic input gives the laser, it is far more vulnerable to interference and touching or moving the wires can induce erroneous current, which alters its output and changes the reading on the detector. It was used to produce breakthrough curves of the flow through the slab and the fracture, but it was not possible to run standards and use them to calculate the concentration of the fluorescein because changing the tubing from one sample to another agitated the system and changed the input. The breakthrough curves just required a stopcock to be gently turned in order to switch the input from deionised water to the fluorescein and back again, which has a minimum risk of altering the output.

However, these apparent shortcomings are not significant for the performance of the fluorometer. Firstly, as shown by the features circled in red in Figure 5.16, it is obvious when a disruption in the system has affected the LED output, so there is no risk of a breakthrough curve appearing to be as would be expected but actually being erroneous and the data misleading; it is very apparent if a run should be discarded. In this case, moving the wires produced a sudden drop in signal, and the readings did not return to their previous levels after the perturbation. And secondly, it is the shape of the curve and its relation to the time at which the fluorescein or the water were introduced that provides useful information about the system, *e.g.* lag times and flushing behaviour. The concentration of the fluorescein is not related to the concentration of colloids in the flow cell and is therefore irrelevant.

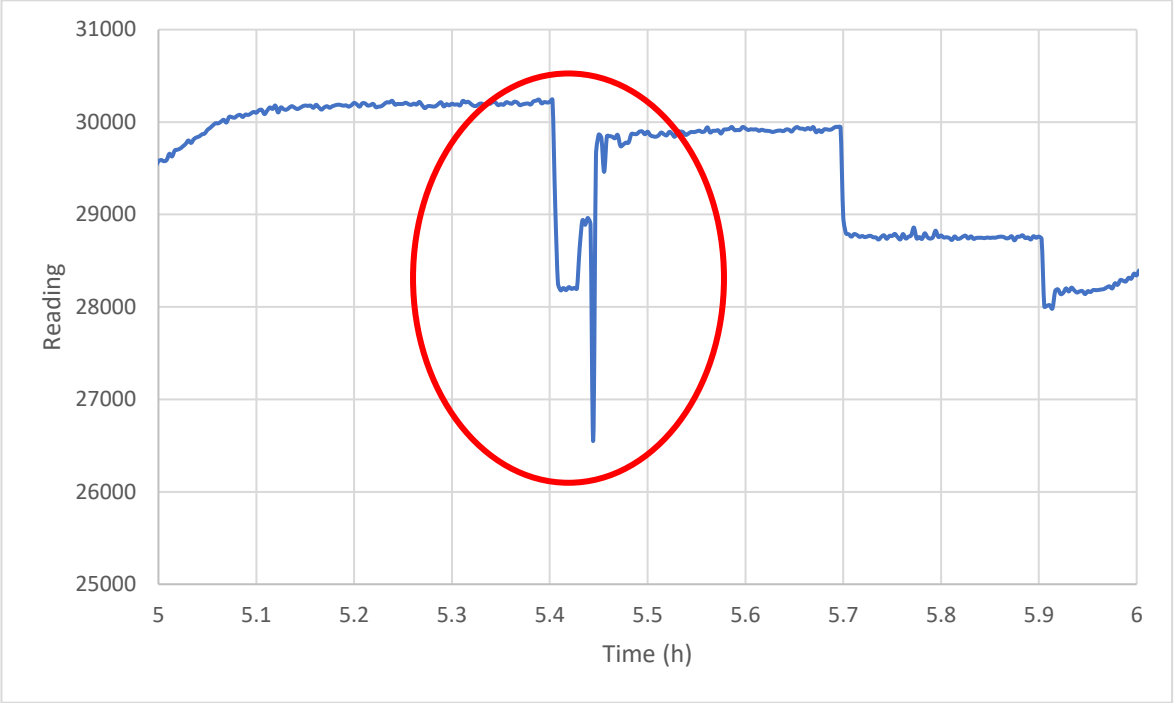

Figure 5.16. An example of a fluorimeter profile where moving the wires introduced erroneous signals.

The experimental protocol for the fluorimeter may be found in Appendix 2.

5.5.6 Power supply

The different electronic components of the system have different voltage requirements, and therefore need different power sources. The detector is powered using its own 12 V power supply, and the microcontroller is connected to the mains using an official Raspberry Pi power supply. The LED is powered by one of the GPIO pins on the Pi, and the laser is powered by one of its USB ports. A USB cable from a computer mouse was soldered onto its ground and power wires to provide this connection. The temperature sensors have small internal batteries and therefore require no other supply.

5.5.7 Casing and alignment

The nephelometer is shown in Figure 5.17. It is contained in a light-proof electrical box sprayed matt black inside to absorb any stray laser light, and the components are screwed into a 2 mm- thick aluminium base plate which ensures their stability. A precision-engineered acrylic block holds the laser in the correct position relative to the flow cell. Optomechanical components manufactured by Thorlabs hold the detector and lens. They use M4 and M6 screws and are directly compatible with each other and the detector. The manual translation stages allow the flow cell to be moved incrementally into its optimal position.

This setup provides flexibility of movement yet offers stability to the components. The stages allow for the flow cell to be moved in the X and Y directions to focus the light scattered by particles in the cell directly onto the centre of the detector. The focusing system consists of a microscope objective lens with 10x magnification. It may be moved forwards and backwards on the track so that the centre of the cell is situated at the working distance of the lens, and the detector may also be adjusted relative to the lens in order to align it with its focal length. The height of the detector and lens can also be adjusted in order to allow for alignment in the Z direction.

Alignment was carried out by switching the detector on, placing a piece of foil into a cuvette on the block where the flow cell was to be situated to reflect the laser beam at 90 ° into the detector, and then moving one component at a time until the highest output possible was recorded by the data logging system. This was determined to be the optimal position, and

the component was then secured to prevent any movement relative to the other parts, which would induce errors.

A coaxial cable shields the analogue signal from the detector from electrical interference until it is converted to a less vulnerable digital one, and the smaller silver box shields the small circuit between the cable and the ADC. It also contains a ground point which links the ground of the detector to the ADC, and through that to the Pi and laser. A common ground is important for providing a ‘zero point’ against which all of the voltages may be measured; different grounds for different parts of the system can reduce the sensitivity of the readings.

The black plastic tube is a simple light trap. It is situated directly opposite the laser and absorbs the laser light that is not scattered by the colloidal suspension. A syringe was cut size, its surface roughened to reduce reflection, and then sprayed matt black to promote light absorption.

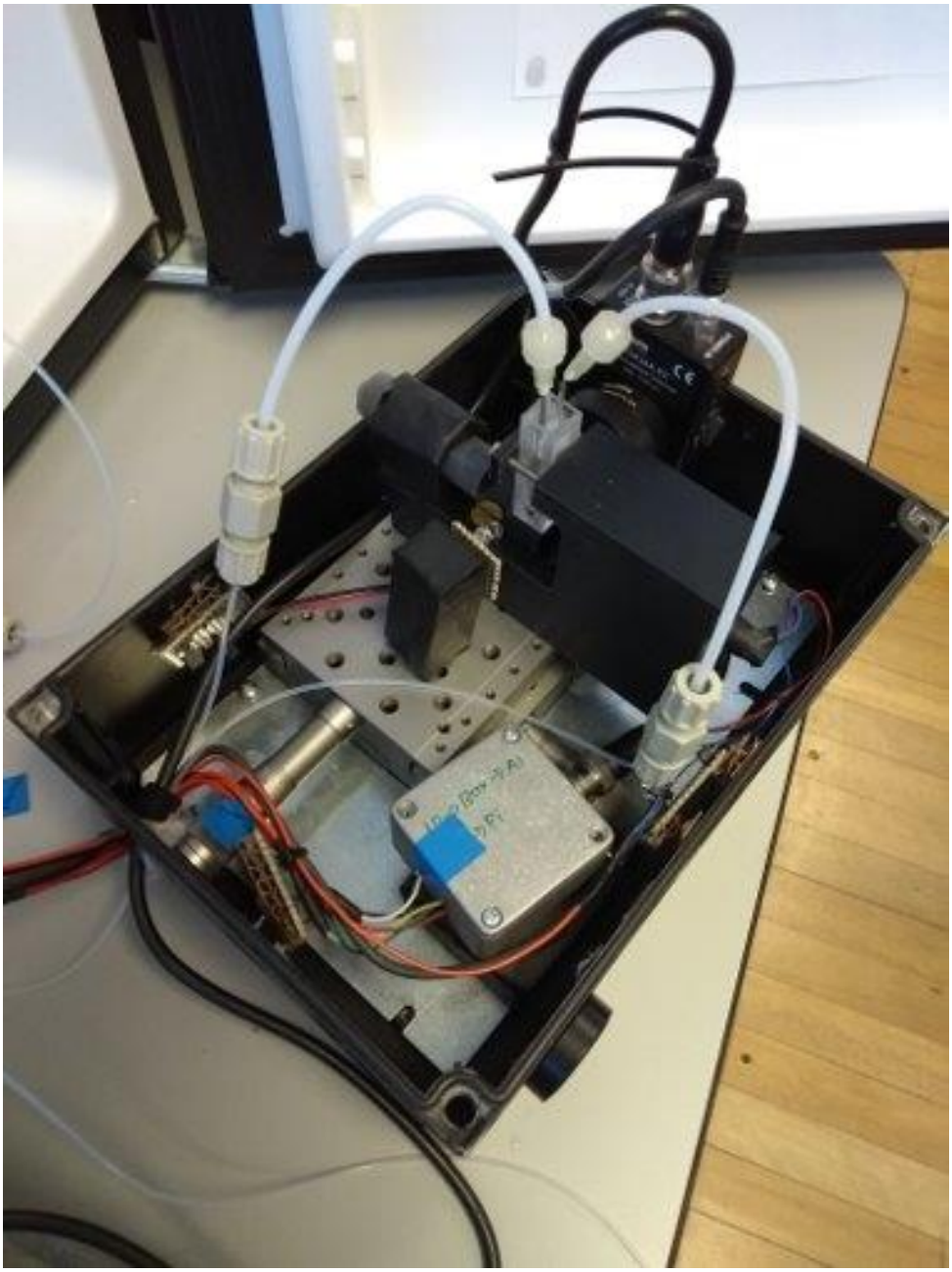

Figure 5.17. An image of the nephelometer used in the flow experiments.

Figure 5.18 shows the whole of the flow system.

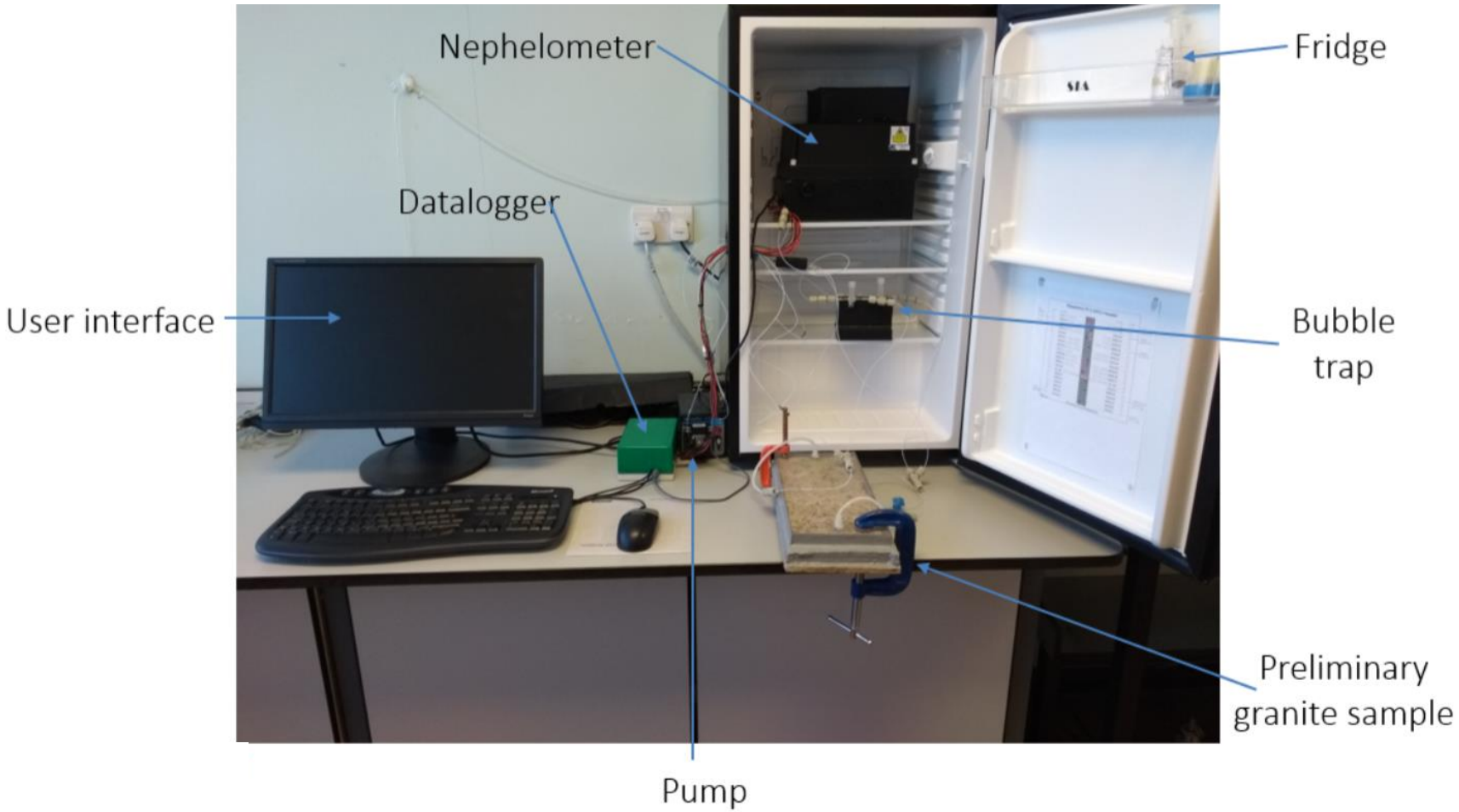

Figure 5.18. The flow system. The black box contained within the refrigerator is shown in more detail in Figure 5.17. The Raspberry Pi is housed in the green box, a regular PC provides the user interface. The granite slab from Figures 5.5a and b is visible at the bottom.

5.6 Quality control and calibration

5.6.1 Laser stability- short term

Section 5.5.4 describes how the measurement is taken two seconds after the laser is switched on because it results in more stable readings. A short test was run to investigate the behaviour of the laser upon start-up. It was run for just five seconds, and the readings were taken every 0.02 seconds. A piece of aluminium foil was placed in a cuvette which was temporarily substituted for the cell and provided consistent bright scatter. The results are shown in Figure 5.19.

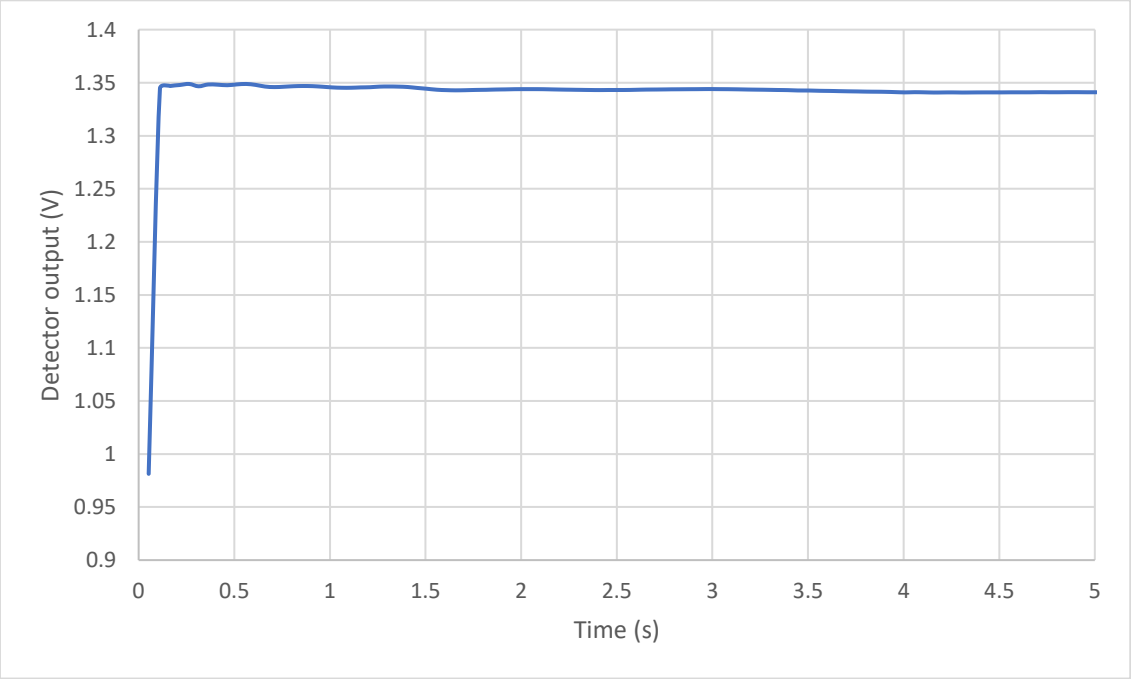

Figure 5.19. The laser output after it is switched on.

As may be observed in the magnified image below in Figure 5.20, the variation in the first 1.5 seconds is not large (approximately 0.006 V), but it changes rapidly. It becomes more stable after around two seconds, and then levels off almost completely after four seconds. If the readings were taken immediately then the effect of this variation may not be considerable, but adjusting when the readings were taken was a minor modification that

helped to reduce the error in the system. It was decided to take the readings at two seconds rather than the more stable four seconds as a trade-off between providing greater stability and extending the lifespan of the laser.

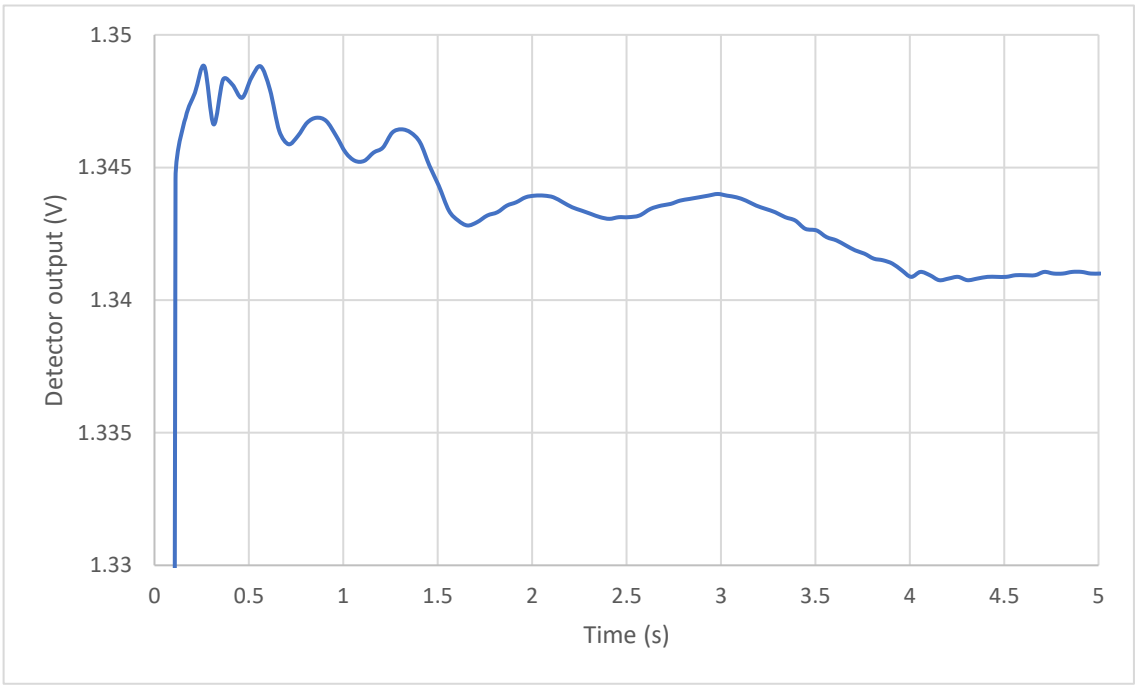

Figure 5.20. A magnified view of the laser output after it switches on. It changes rapidly in the first 1.5 seconds or so, and stabilises almost completely after approximately 4 seconds.

5.6.2 Laser stability- long term

The output of the laser must be stable. If it were to change significantly, then the amount of light entering the detector after being scattered by a given concentration of clay colloids would change, therefore introducing errors into the measurements. The stability of the laser was assessed once again by substituting a foil-filled cuvette for the flow cell, and then running the program that controls it for 24 hours. Temperature was measured at the same

time in order to assess the temperature stability inside the refrigerator. The results are shown in Figure 5.21.

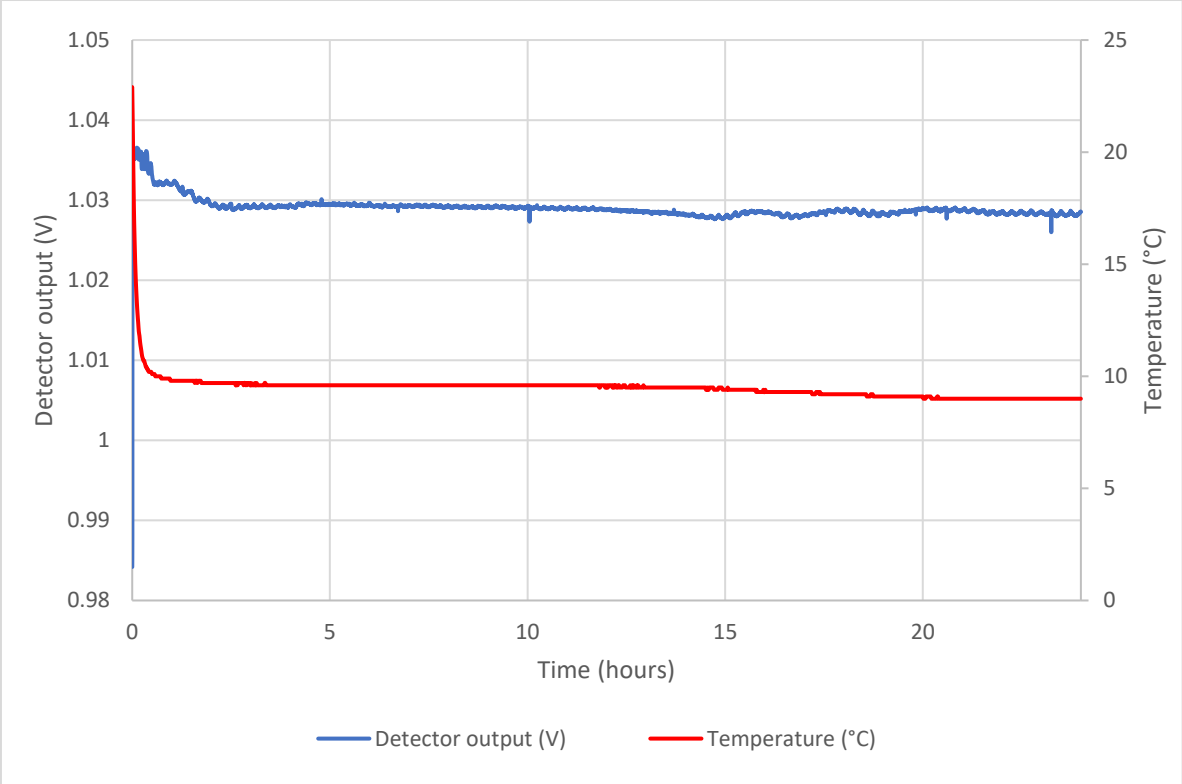

Figure 5.21. Outputs from the detector and temperature sensor during a run designed to test the stability of the laser.

The detector readings vary during the first 2-3 hours. Laser instruments should typically be switched on for at least 30 minutes before use to allow their outputs to stabilise, so this is unsurprising. Figure 5.22 shows the same run but focused on the first five hours of operation.

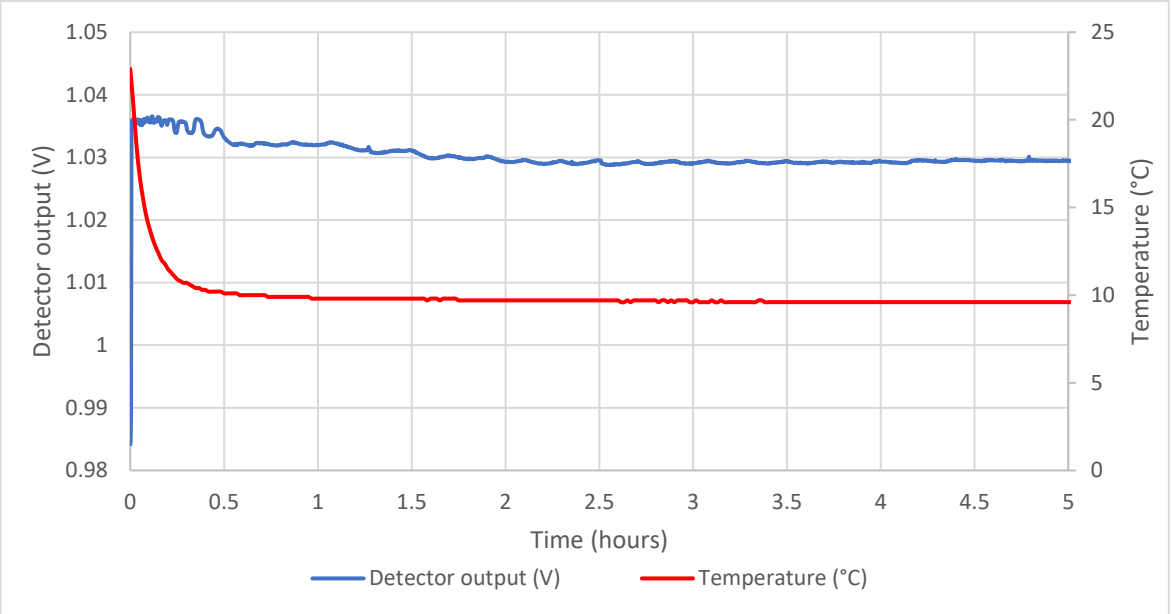

Figure 5.22. Outputs from the detector and temperature sensor during the same test run as Figure 5.21, but shown only during the first five hours of operation.

The magnified readings in Figure 5.23 show that after the initial 2-3 hours, both readings become far more stable.

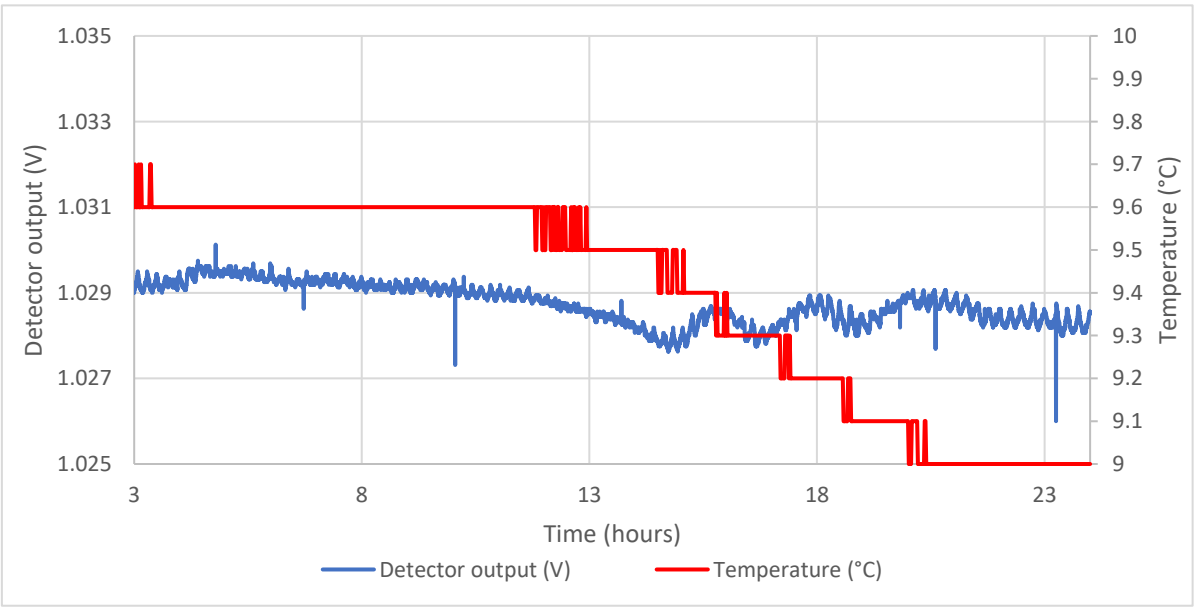

Figure 5.23. Output from the detector and temperature sensor during the same test run as Figures 5.21 and 5.22, but shown at a greater magnification.

The temperature varies by less than 0.7 °C. The output from the detector may look unstable, but the highest and lowest values that occur during that time period are 1.030 V and 1.026 V respectively, a difference of $4x10^{-3}$ V, or 0.39 %. This is unlikely to have a significant impact on the quality of the results.

Therefore, the stability of the laser and the temperature are good, but only after they have been allowed to stabilise. The sample is introduced without the need to open the refrigerator by using the stopcock to change the inlet reservoir from deionised water to the colloidal suspension, which has the additional benefit of allowing the temperature of these to equilibrate with that of the refrigerator. See Chapter 6 for the results of a number of experiments carried out using this instrument.

5.7 Discussion

The aim of this chapter was to produce a flow system suitable for use in flow experiments, without the considerable cost outlay a commercially available nephelometer would have entailed. That aim has been achieved, and some improvements have been made to its design compared to the existing flow system produced by Greswell *et al*. (2010), although some small drawbacks exist too, such as the lack of integration between the nephelometer and the temperature sensor, but these do not hinder its operation significantly. The most notable improvement is the substitution of a commercial photodetector for the original delicate detection system. The photomultiplier tubes used by Berberoglu & Pilon (2007) and Lienert *et al*. (2003) may have provided greater resolution, but at considerably greater cost, so the photodetector was a compromise between cost and performance. Provided that the

temperature inside the refrigerator is allowed to equilibrate, the overall stability of the system is good, and the resolution is suitable for this application.

However, the flow system is not without some limitations. Firstly, the wavelength of the laser is not optimal for the detector; as may be observed in Figure 5.24, it has greater responsivity in the infrared range of the electromagnetic spectrum than it does the visible (Thorlabs 2015).

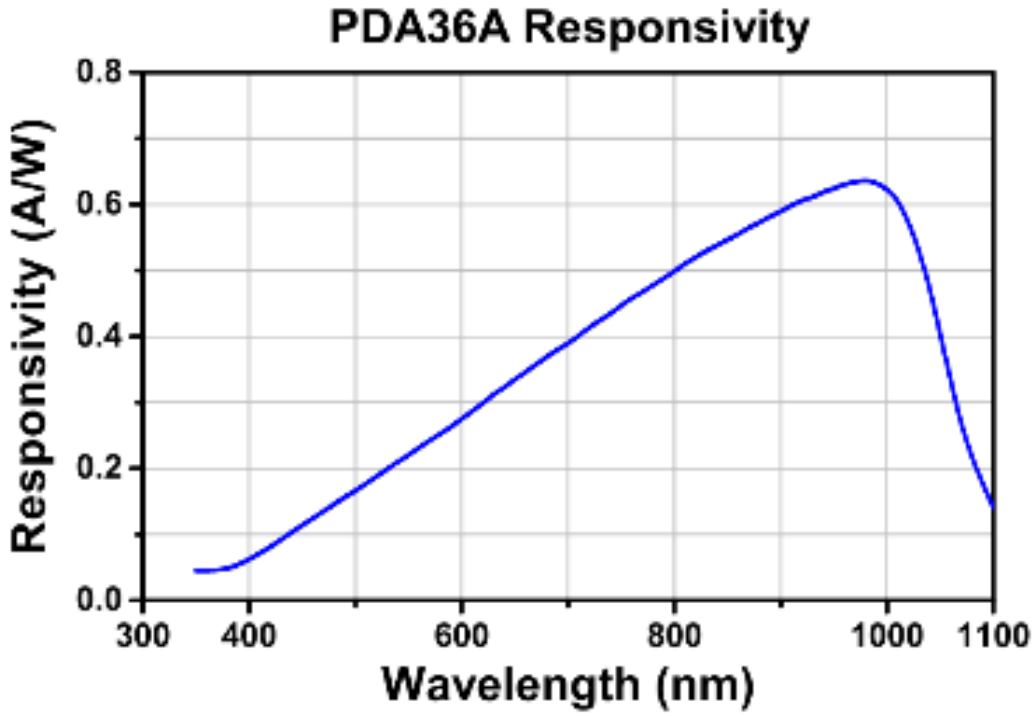

Figure 5.24. The responsivity of the photodetector at different wavelengths. It is greatest in the infrared range of the spectrum. Image courtesy of Thorlabs 2015. Copyright Thorlabs Ltd.

While an infrared source may have produced a stronger signal and greater sensitivity than the 650 nm one that was used in the system, it would have had several disadvantages, including that as it is invisible to the human eye, it would not have been possible to tell whether it was working correctly, and getting it focused narrowly and positioned accurately

would have been difficult, if not impossible. A red laser, in addition to being readily available and inexpensive, was therefore the best compromise.

Secondly, the colloid fractions that will be flowed through the system are likely to have hydrodynamic diameters of <200 nm. The smaller particles will produce Raleigh scattering (this occurs when particle diameter << λ), which is uniform in all directions. However, clay colloids are frequently unstable, and in the likely event they were to agglomerate, this would result in larger particles and potentially Mie scattering as the particle diameter approaches the wavelength of the laser light. The greater asymmetry of Mie scattering means that the scatter off the larger particles would be underrepresented; its anisotropic nature results in more scatter in the forwards direction, towards the light trap. Raleigh scattering produces a greater degree of uniformity, so for a given number of particles, although the same amount of light is scattered, more light would enter the detector from the sample with smaller average particle size (Greswell *et al*. 2010). If it were viable to use an infrared radiation source as discussed above, its longer wavelength would help reduce Mie scattering by providing a greater tolerance between the particle diameter and the wavelength of the incoming radiation. However, with the resources and expertise available it was unfortunately impossible.

5.8 Conclusions

A flow system was required in order to successfully complete the necessary flow experiments. As detailed in this chapter, such a system was constructed and a nephelometer built at a fraction of the cost of a commercially available instrument. The resulting flow

system was not without its drawbacks, for example the concentration of colloids that could be detected would probably be higher if a commercial nephelometer had been used, but a fit-for-purpose instrument was built within the budget available.

5.9 References

Ashton, J.J. & Geary, L., 2005. The Effects of Temperature on pH Measurement, Reagecon Diagnostics Ltd., Co. Clare, Ireland.

Berberoglu, H. & Pilon, L., 2007. Experimental measurements of the radiation characteristics of Anabaena Variabilis ATCC 29413-U and Rhodobacter Sphaeroides ATCC 49419. International Journal of Hydrogen Energy, 32(18), pp.4772–4785.

Global Laser, 2014. Versatile Module Datasheet. Available at: http://www.farnell.com/datasheets/1493561.pdf. Last accessed November 2018.

Greswell, R.B. *et al.*, 2010. An inexpensive flow-through laser nephelometer for the detection of natural colloids and manufactured nanoparticles. Journal of Hydrology, 388(1–2), pp.112–120.

Huether, S.E., 1983. How lasers work. Association of Perioperative Registered Nurses, 38(2), pp.207–215.

Lienert, B.R., Porter, J.N. & Sharma, S.K., 2003. Aerosol size distribution from genetic inversion of polar nephelometer data. Journal of Atmospheric and Oceanic Technology, 20(10), pp.1403–1410.

Martin, M.M. & Lindqvist, L., 1975. The pH dependence of fluorescein fluorescence. Journal of Luminescence, 10(6), pp.381–390.

Nessa, S.A. *et al*., 2007. Measurement of pH of the Compacted Bentonite under the Reducing Condition. Memoirs of the Faculty of Engineering, Kyushu University, 67(1), pp.25–31.

Reimus, P.W., 2012. Preliminary Interpretation of a Radionuclide and Colloid Tracer Test in a Granodiorite Shear Zone at the Grimsel Test Site, Switzerland,

Schnegg, P.-A. & Doerfliger, N., 1997. An inexpensive flow-through field fluorometer. 6th Conference on Limestone Hydrology and Fissured Media, pp.1–4.

Semleit, D., Trampe, A. & Fissan, H., 1997. Fluctuations and Noise of the Optical Output Power of Laser Diodes and the Effect on Optical Particle Size Determination. Aerosol Science and Technology, 26(4), pp.356–367.

Thorlabs, 2015. PDA100A Si Switchable Gain Detector User Guide, Newton, USA: Thorlabs. Available at: http://microfluidics.wayne.edu/wiki/lib/exe/f*etc*h.php?media=thorlabs-pda100a-manual.pdf. Last accessed November 2018.

Tombácz, E. & Szekeres, M., 2004. Colloidal behaviour of aqueous montmorillonite suspensions: The specific role of pH in the presence of indifferent electrolytes. Applied Clay Science, 27(1–2), pp.75–94.

Walkden, S., 2014. Bentonite Colloid Investigations on a Granite Fracture. MSc Thesis, University of Birmingham.

Zumbahlen, L., 2012. Staying Well Grounded. Analogue Dialogue, pp.1–9. Available at: http://www.analog.com/library/analogdialogue/archives/4606/staying_well_grounded.html. Last accessed November 2018.

Chapter 6

Flow experiments

Chapter 6: Flow experiments

6.1 Introduction

One of the aims of this project, laid out in Chapter 1, was to conduct flow experiments by passing differently sized fractions of bentonite clay colloids across or through samples of granite. These experiments were designed to investigate how colloids eroded from the buffer of a GDF situated in a higher-strength host rock may behave in the far-field. Chapter 4 described the production of these colloids, Chapter 5 detailed the design and construction of a flow system suitable for use in this application, and this chapter describes the flow experiments themselves.

Table 6.1 summarises the most relevant laboratory-scale experiments that could be found in the literature. Apart from Alonso *et al*. (2015), each of these examples flowed bentonite and other colloidal species across or through crystalline rock. Alonso *et al*. (2015) placed artificial colloids in contact with granite rather than flowing them across or through it, but it was considered relevant enough to be included because the granite used was from the Grimsel Test Site (GTS), the same origin as the fracture used in this chapter (see Chapter 4 for more information). The authors also drew some important conclusions about the influence colloid size has on their transport behaviour, which was relevant to the aims of this project.

Table 6.1. A table containing examples of relevant literature and their key findings.

Authors	Description of the experiment	Relevant findings
Alonso *et al*. (2015)	Artificial colloids of different sizes and materials (including gold and iron (III) oxide) were placed in contact with 1 cm^2 chunks of granite from the GTS, in low ionic strength water.	Colloid size affected their diffusion properties. Retention of colloids on the surface depends on surface roughness and the distribution of charge on the granite.
Missana *et al*. (2008)	Used column experiments to investigate how FEBEX colloids of average diameter 250±50 nm affected the migration of Eu and Pu through a fracture core from the GTS, at flow rates ranging from 3-11 ml/h. The water used was groundwater also taken from the GTS. Colloid concentration was determined by collecting fractions at different time intervals and determining their concentration either by chemical analysis of key elements (*N.B*. The technique that was used was not specified), or by producing calibration curves for PCS using colloid suspensions of known concentration, and then using this to measure the concentrations of unknown samples.	Low flow rates caused more colloids to be retained by the rock sample.

Schäfer *et al*. (2004)	Flowed one size fraction of FEBEX colloids (average diameter of 202±43 nm) and three fractions of polystyrene microspheres (25, 50 and 100 nm) through two different fractured granites from the GTS, along with U, Th and Eu. Change in colloid concentration was measured by analysing the change in aluminium content of collected samples over time using ICP-MS.	For the artificial microspheres, colloid attachment to the granite increased with increased colloid diameter, and with reduced flow rate.
Sherriff *et al*. (2016)	Flowed montmorillonite and artificial colloids across and through crystalline rock in a range of experiments done by different research organisations as part of the BELBaR project. This was done with and without radionuclides, in groundwaters with different chemical compositions. The rock samples included granites and tonalites in different forms including crushed in columns, fractures, and drill cores. Colloid concentration was determined using ICP-MS to measure the concentrations of aluminium, and through generating a standard series for PCS and then using that to determine the concentrations of unknown solutions.	The diffusion behaviour of artificial colloids was influenced by their size, but not their charge. More colloids were deposited on and retained by rougher granite surfaces.

Vilks & Baik (2001)	Natural colloids from Canadian granitic groundwater and colloids produced from a Canadian bentonite were flowed through a granite fracture, along with Sr and Am. Change in colloid concentration was determined by collecting fractions at different time points and measuring their turbidity using a Hewlett Packard diode array spectrophotometer.	-

The findings of this review of the literature indicate that at least for artificial colloids, size, the parameter of most interest to this project, influenced their sorption and diffusion properties. Roughness of, and charge distribution on, the granite surface also controlled sorption and retention, as did low flow rates.

Three of the flow studies collected samples of the suspensions used in the flow experiments at different time points, analysed key elements in the clay, and used that to estimate change in colloid concentration by relating it to the theoretical structural formula of bentonite. Two of them specified that aluminium was used, a logical choice for an aluminosilicate, and two specified that this was done using ICP-MS. This is similar to the technique that was used by Norrfors *et al*. (2015), where ICP-OES coupled with a digestion technique was used to measure the elemental composition of key elements in fractions produced by sequential centrifugation. As was discussed in Chapter 4, this method could not be used here, because the injection system on the available ICP-MS was incompatible with HF, so a standard series was generated for the nephelometer using suspensions of bentonite of known concentrations. The fourth flow study, Vilks & Baik (2001), collected fractions at different time points and determined change of colloid concentration by measuring their turbidity. This is most similar to the method used here, but instead of collecting discrete fractions, concentration was measured continuously.

The use of a flow-through nephelometer is an improvement upon these methods in two ways. Firstly, continuous measurement gives better resolution than measuring it at discrete time intervals, where detail may be lost as mixing occurs within the collected fractions. Secondly, if the digestion process does not completely dissolve all of the colloids, then

material may be lost when preparing the samples for ICP (they must be filtered before measuring them to prevent the nebuliser from blocking). The method used here removes the need for a digestion process, and by measuring the colloids in their entirety, eliminates any errors in calculation caused by deviation of the highly-variable clay minerals from their theoretical structures (Suter *et al*. 2009).

This chapter builds on this pre-existing work by attempting to identify whether the size of bentonite colloids influences their transport behaviour in the same way that it does for artificial ones. It also improves upon the methods previously used to determine change of colloid concentration by eliminating the errors that may arise from an incomplete digestion process and the natural variation in clay minerals, although as discussed in section 4.4.5.4.3., other sources of error did arise from this method.

6.2 Method

6.2.1 Overview

The flow system operates by pumping colloids across or through a rock sample and measuring their change in concentration over time using a nephelometer. In these experiments, differently sized bentonite colloids were flowed over two different samples of a granite typical of that that is likely to form the far-field environment around a GDF. A full description of the system and details about its design and construction are included in Chapter 5.

The method for conducting these experiments may be summarised as such:

1. Make bentonite colloid suspensions suitable for use in these experiments. This is described in section 4.3.3.4.
2. Run a baseline sample of a conservative tracer (a dye that will remain in the water column and will not adsorb to the surfaces of the rock samples. The use of this was discussed in section 5.5.5). This allowed the flow patterns of the water through the system to be evaluated by excluding the effects of colloids agglomerating or binding to the rock.
3. Flow the colloids across the rock sample. The protocol for doing this is summarised in section 6.2.3 and described in full in Appendix 2.
4. Analyse the data. This is detailed in section 6.2.4.

6.2.3 Flow experiment protocol

After a pre-warming period designed to give the laser output time to settle, the temperature sensors were switched on, the refrigerator containing the flow system was shut so as to eliminate any external light and to allow the temperature to equilibrate, and the laser (or LED) and data logger were started. Deionised water was flowed through and measured for at least two hours before the sample was introduced, both to provide a baseline and to give the laser output longer to settle. This was necessary because even when the laser had been run overnight and was only switched off for long enough for the new protocol to be started, the readings still varied considerably during the first hour of operation. Next, the sample was flowed across the slab or through the fracture for seven or four hours respectively, before deionised water was reintroduced to flush it from the system. The time difference reflected the fact that the pore volume of the slab was larger than the fracture, so it took longer for

the sample to completely replace the water in the system, and for the colloid concentration to reach its maximum. The experiments were run for 15 hours, but data was frequently collected for longer either when the baseline did not settle, so the deionised water was flowed for longer before introducing the sample to try and achieve a stable reading, or when they were either left to flush overnight. Provided the samples ran for the same number of hours and the time at which they were introduced was recorded, these variations had no impact on the experiments. The data was then collected and analysed.

6.2.4 Data analysis

Analysis of the nephelometer (or fluorimeter) and temperature data was done as follows:

1. Figure 6.1 shows a typical example of the data from the nephelometer and fluorimeter before processing:

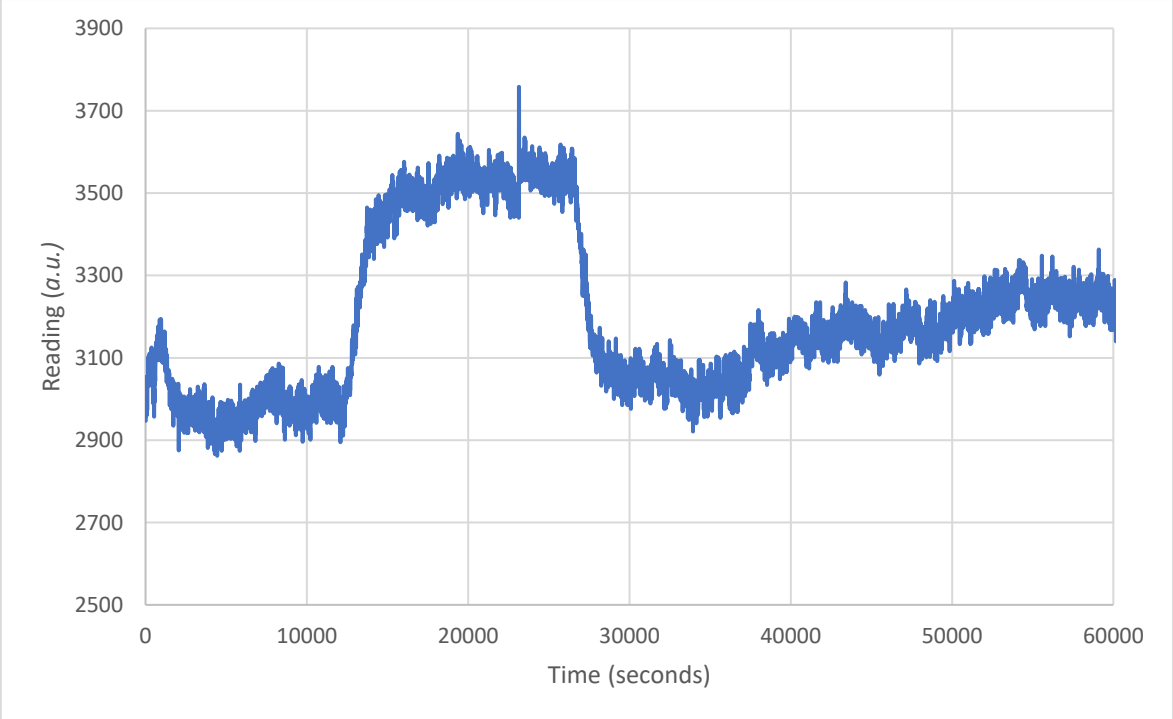

Figure 6.1. An example of the nephelometer data before undergoing processing.

2. There was considerable noise in the data, and a noticeable drift after the sample was flushed from the system. Firstly, a moving average of the data was calculated by averaging 20 data points at a time in Microsoft Excel to smooth it and to emphasize detail, and the effect of this can be seen in Figure 6.2. The moving average made it easier to observe trends in the data. The timescale was converted from seconds (the default output of the instrument) to hours at the same time.

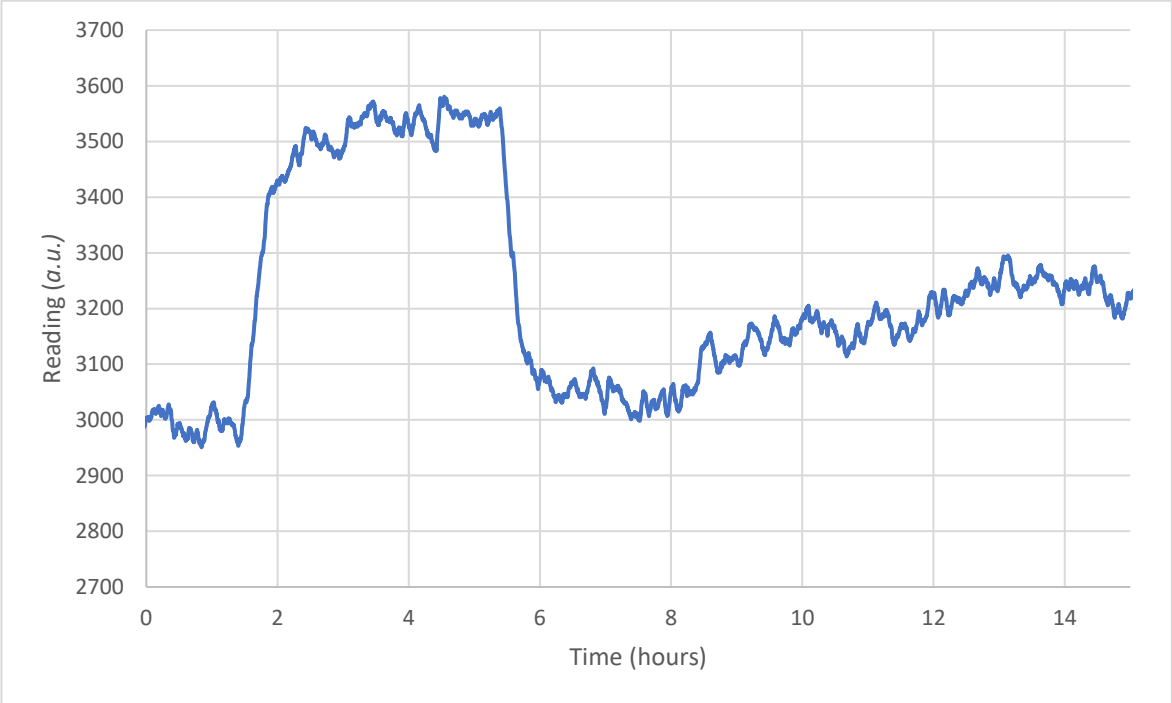

Figure 6.2. The dataset from Figure 6.1 after a moving average was calculated in order to smooth it. It is much easier to discern features and details.

3. Next, the data from the nephelometer was converted to concentration values using the equation generated from the standard series in Chapter 4. This could not be done for the fluorimeter data because standards could not be measured accurately and was discussed in Chapter 5. This is shown in Figure 6.3.

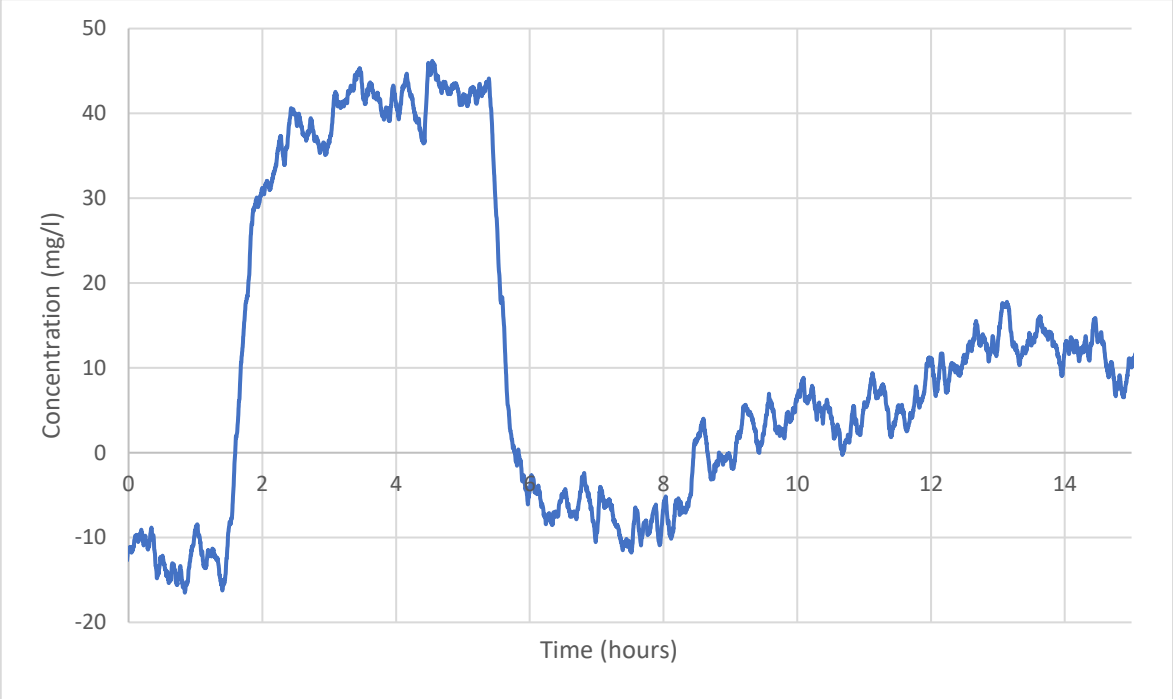

Figure 6.3. The dataset from Figure 6.2 after the equation from the standard series generated in Chapter 4 was applied in order to calculate the concentration values of the colloids in suspension.

4. A drift correction was applied to normalise the datasets to zero. More detail on this process can be found in Appendix 2. The instrument is not a commercial one, and it was noted in Chapter 4 that it was sometimes necessary to apply a correction factor to normalise the data to the standard curve, because it is vulnerable to the effects of changing temperature and, despite the shielding, potentially electronic interference, which can affect its readings.

The samples in Chapter 4 were corrected by calculating the difference between the average values measured for the deionised water and those that were expected from the standard curve (they should have been at a concentration of 0 mg/l), and then correcting each of the samples by this amount to account for the variation. The concentration of the samples was not changing, and they were measured over a timeframe of only minutes, so applying a single correction factor was appropriate. A different approach had to be taken here because the drift increased over the long timescale of the flow experiments: in Figures 6.1-6.3, the correction needed to match the 0 mg/l baseline to that of the standard curve was smaller at 8 hours than that at 14 hours, after the laser module had warmed and the temperature of the refrigerator equalised.

To account for this, the baseline data (*i.e.* readings of the deionised water) that were changing steadily were identified, plotted separately from the rest of the data, and a trendline added. An example of this is shown in Figure 6.4.

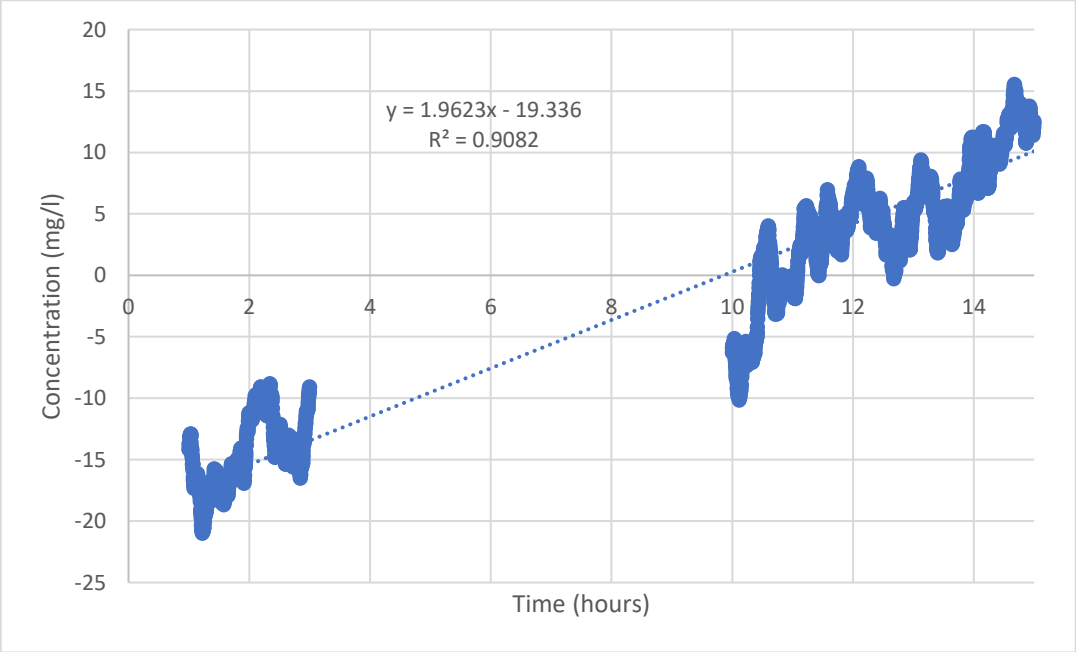

Figure 6.4. The deionised water readings, with a linear regression added.

The gradient and intercept of the equation of the trendline were then used to modify the concentration data, thereby applying a linear drift correction. The results of this are shown in Figure 6.5.

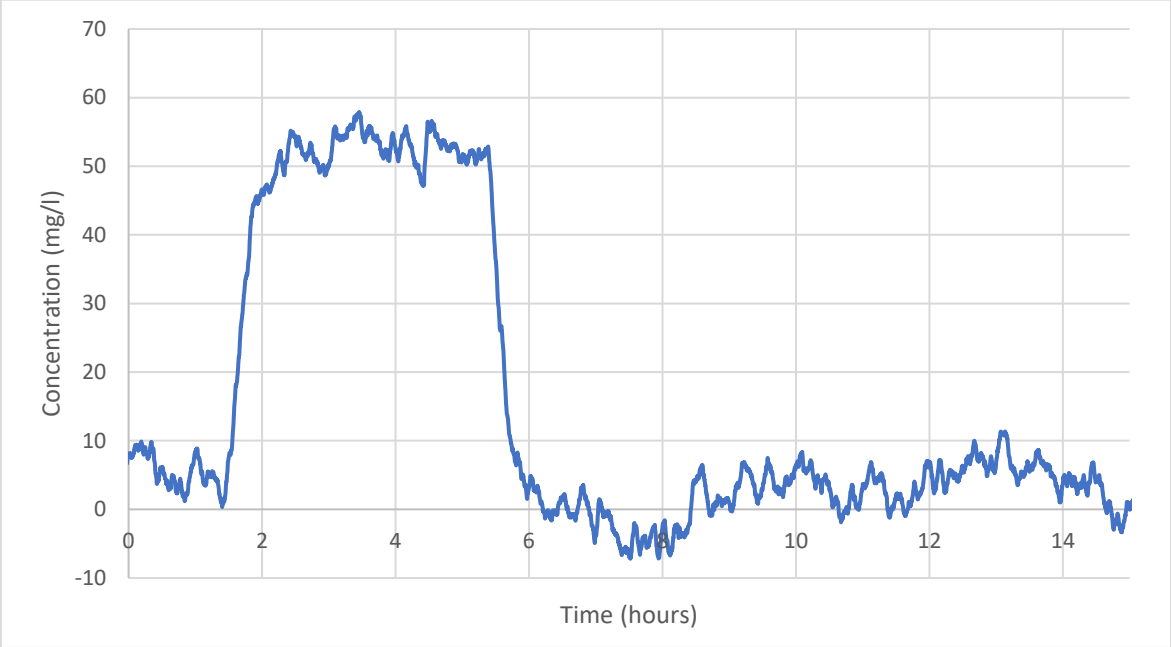

Figure 6.5. The dataset from Figure 6.3 after the drift correction that was determined in Figure 6.4 was applied. The 0 mg/l baseline has been corrected and is much closer to its expected values.

The deionised water baseline is now consistently much closer to 0 mg/l than in Figures 6.1-6.3, making it easier to compare the trends between the samples. The same method was applied to all of the standards, thereby maintaining consistency between them.

5. The smoothed and normalised breakthrough curves were plotted alongside the outputs from the temperature sensors. See Figure 6.6.

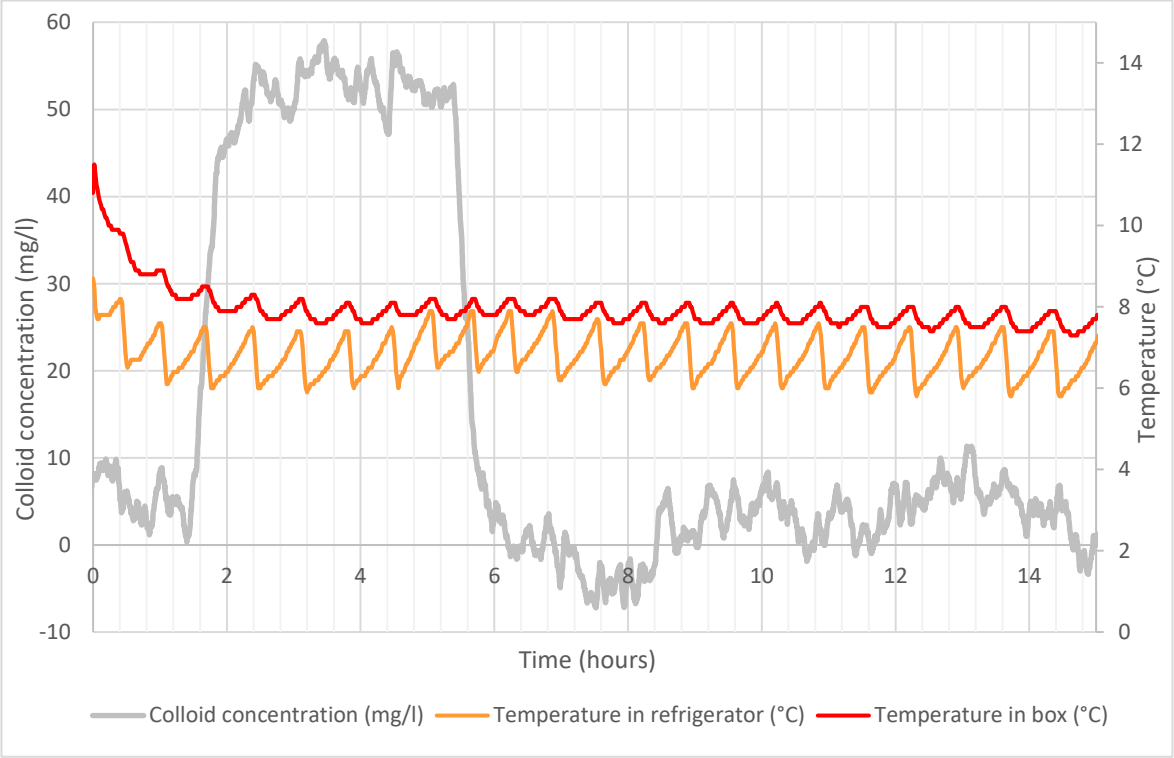

Figure 6.6. The breakthrough curve of the clay colloids, plotted with temperature.

6. Separate charts were produced showing the breakthrough curves superimposed on the fluorescein baseline so that any differences in behaviour could be observed, as may be seen in Figure 6.7.

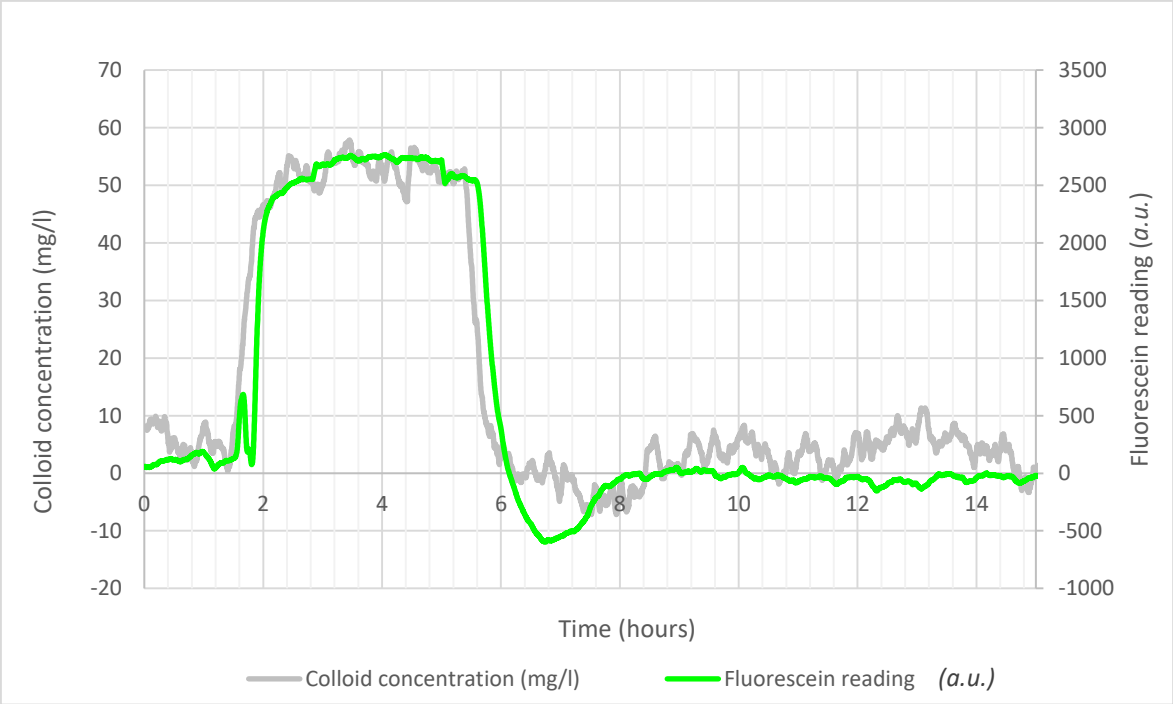

Figure 6.7. The breakthrough curve of the clay colloids superimposed on the fluorescein baseline.

7. Rates of change of concentration of the colloids were estimated for each of the curves. These were measured by identifying time periods when the increase or decrease of colloid concentration over time was as well-defined as possible, plotting a trendline, and then calculating its gradient. The gradient represents the change of colloid concentration over time. These are presented alongside their corresponding curves and are collated in Table 6.2. See Figures 6.8a and b for examples of this. The inflow and outflow rates for this particular sample are very similar, but for other samples they may vary widely.

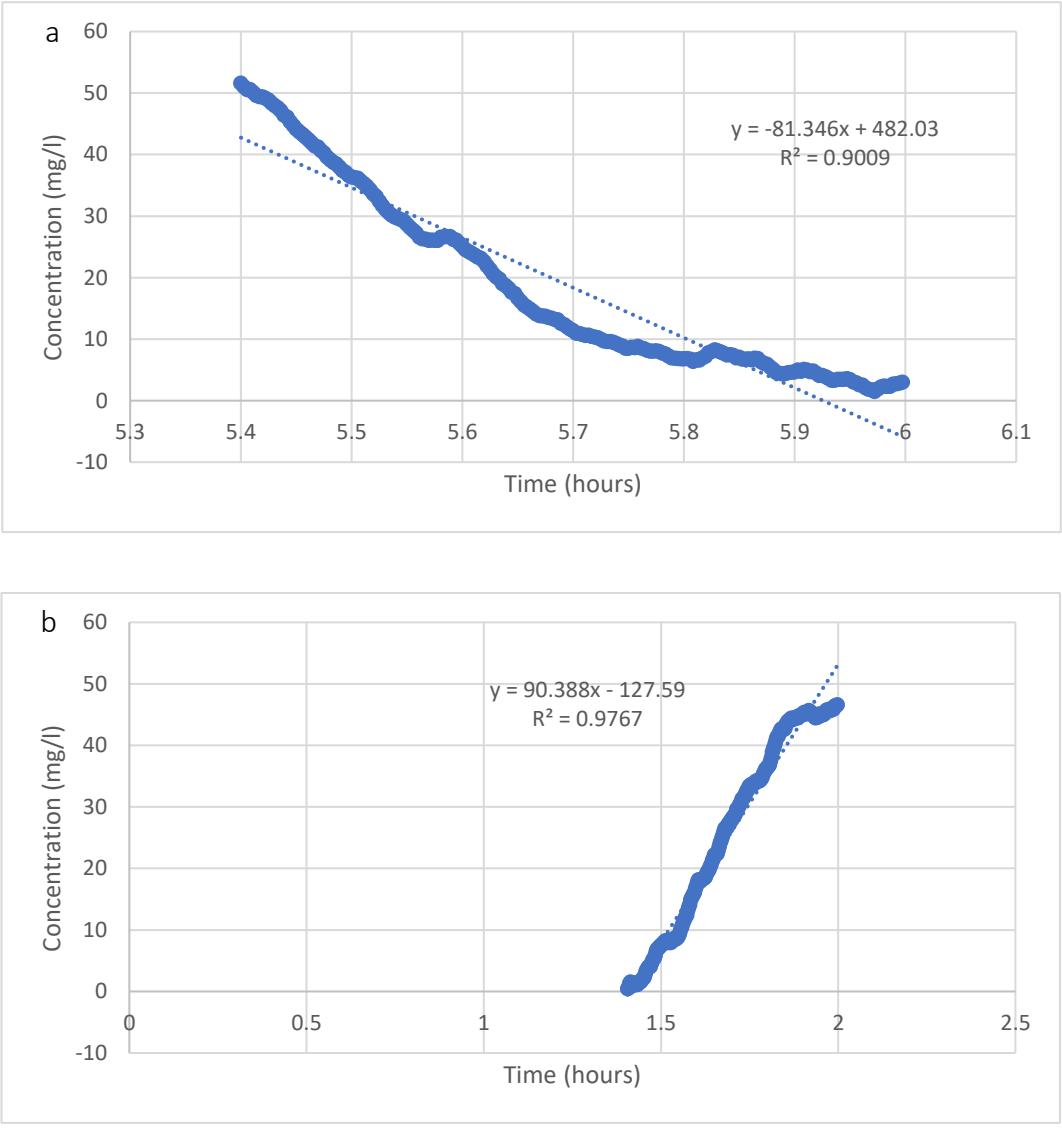

Figure 6.8. Inflow and outflow rates for the example colloidal suspension shown in Figures 6.1-6.7.

6.3 Results

The flow experiments were conducted on two different samples of granite: a flat slab and a narrow fracture. Firstly, a fluorescein baseline was produced for each of them. Next, the two colloidal size fractions that were produced in Chapter 4, <50 nm with PVP and <1000 nm with PVP, were flowed over (or in the case of the fracture, through) both of these. Finally, two samples that were made using the same method but without PVP were also run, allowing any impact that the surfactant had on their transport behaviour to be identified. The experiments that were run may be summarised thusly:

Through the slab:

- Fluorescein baseline
- 50 nm
- 1000 nm
- 50 nm with PVP
- 1000 nm with PVP

Through the fracture:

- Fluorescein baseline
- 50 nm
- 1000 nm
- 50 nm with PVP
- 1000 nm with PVP

For each of these experiments, the breakthrough curve was firstly plotted alongside the outputs from the temperature sensors at the largest appropriate scale, to allow fine detail

to be emphasised. It was then superimposed on the fluorescein baseline with a consistent scale so that differences in behaviour and colloid concentration could be observed clearly. The smaller pore volume of the fracture meant that the sample replaced all of the deionised water more quickly than it did in the slab, and the readings levelled off at their maximum possible value more rapidly. Therefore, samples were run across the slab for seven hours, and through the fracture for four hours. The timeline for the experiments over each of the rock samples is therefore:

Slab:

0 hours: experiment started

0-1 hours: deionised water flowed through system

1 hour: sample introduced

1-8: hours sample flowed through system

8 hours: deionised water reintroduced

8-15 hours: sample flushed out and replaced with water

Fracture:

0 hours: experiment started

0-1 hours: deionised water flowed through system

1 hour: sample introduced

1-5: hours sample flowed through system

5 hours: deionised water reintroduced

5-15 hours: sample flushed out and replaced with water

6.3.1 Slab

6.3.1.1 Fluorescein baseline

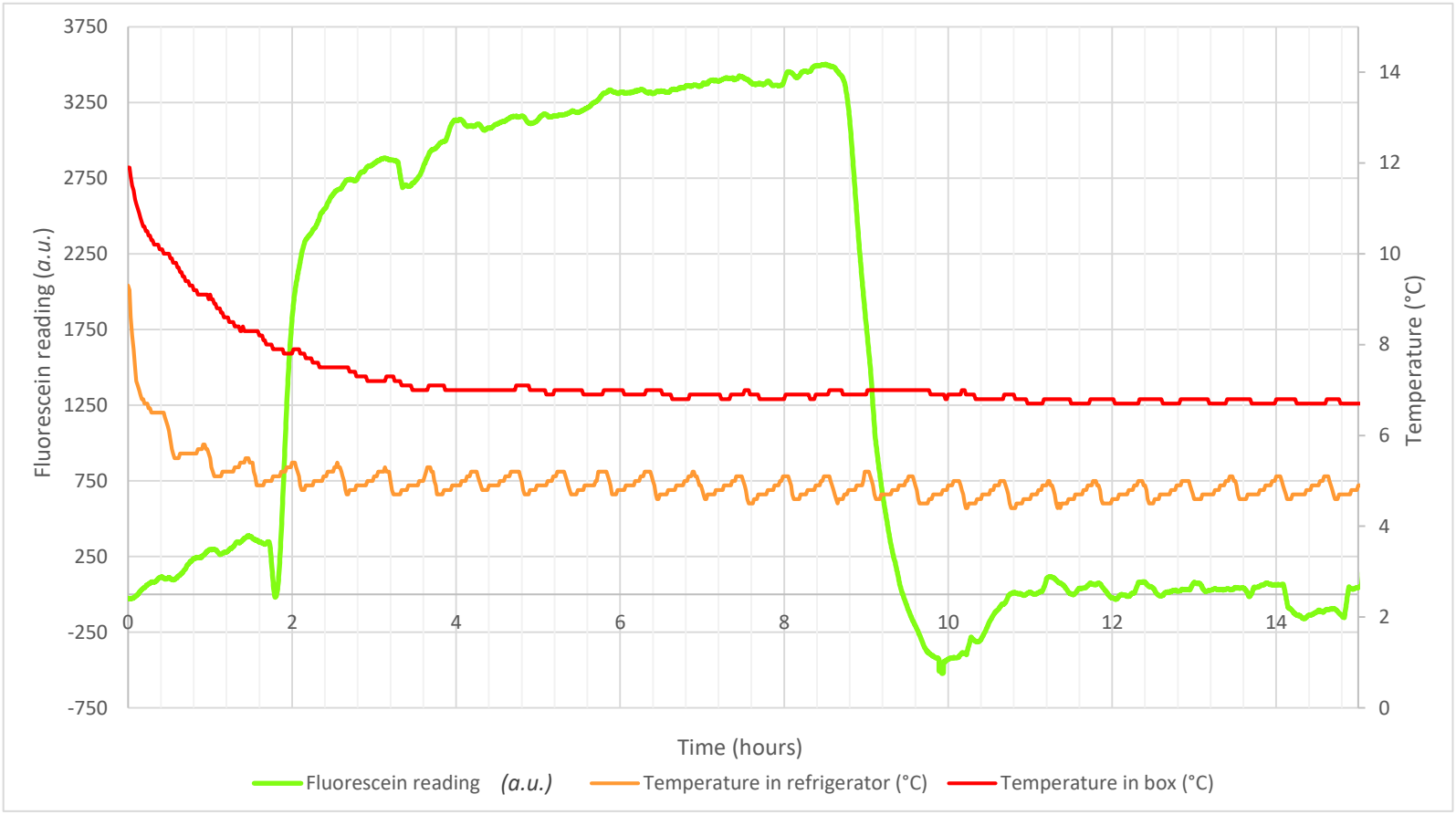

Figure 6.9. The breakthrough curve produced by passing fluorescein across the granite slab. This provides a baseline against which the change in colloid concentration may be compared because it is a conservative tracer and therefore representative of the movement of water through the system.

Little change can be observed for the first hour after introducing the sample into the system and for around 30 minutes after beginning to flush it out, but the change was rapid after that: the fluorescein level had almost reached its highest point by hour 5, and had dropped back to below its baseline after about 1.5 hours of flushing.

The most noticeable, and most puzzling, features of the breakthrough curve are where the fluorescein reading appears to drop below the baseline shortly before and shortly after the switch from water to sample and back again. This was also observed when fluorescein was flushed out of the fracture. This may not be an anomaly, but the result of a low concentration of the fluorescein dye impairing the passage of blue light from the LED to the detector. If this was greater than the green fluorescence produced by the excitation of the small amount of the fluorophore present, then the detector readings could drop until the concentration of fluorescein in the flow cell was high enough to produce significant fluorescence to nullify this effect.

Temperature appeared to have little effect on the profile of the breakthrough curve. It is possible that the irregularity of the baseline during the first 1-1.5 hours of the experiment was related to the drop in temperature as it equilibrated after the closure of the refrigerator that housed the flow system, but as the same effect was not observed in the fluorescein sample that was run through the fracture, it is unlikely. The temperature within the nephelometer housing was approximately 2 °C warmer than the ambient temperature in the refrigerator, and it was more insulated against the small temperature cycles caused by its cooling cycles.

6.3.1.2 50 nm sample made without PVP

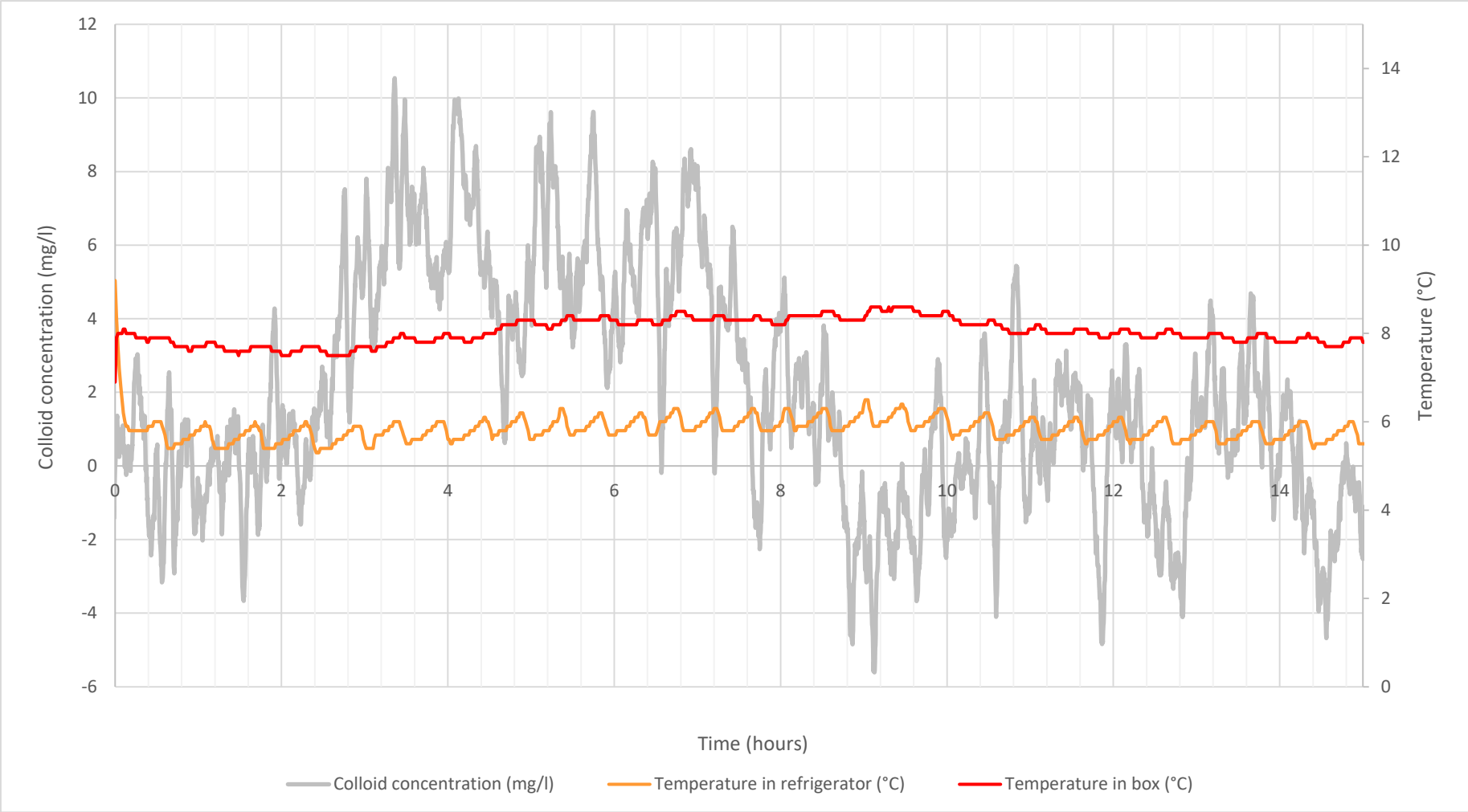

Figure 6.10. Nephelometer output and temperature data for the 50 nm sample that was made without PVP and passed through the slab.

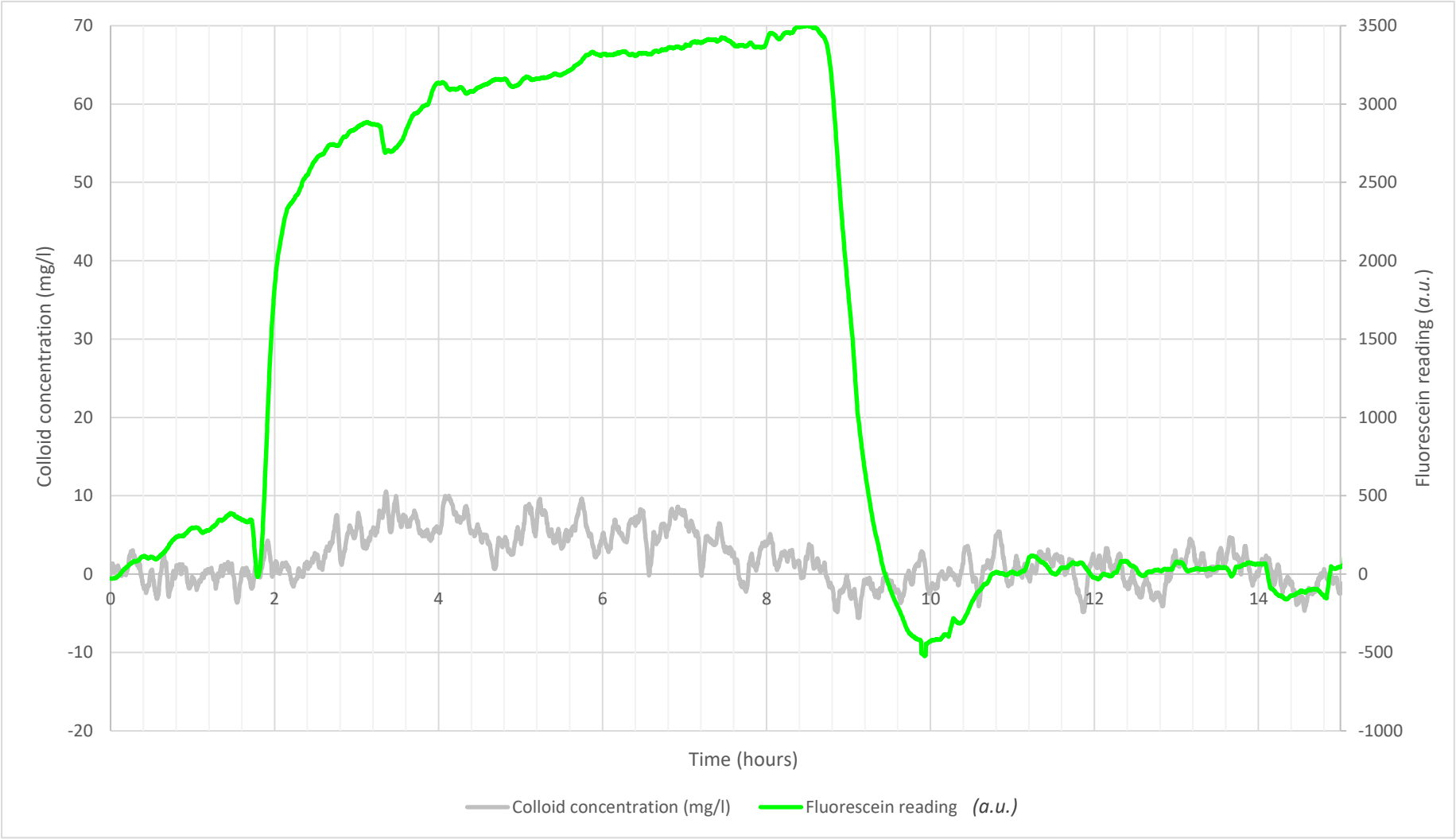

Figure 6.11. Nephelometer output for the 50 nm sample made without PVP, and fluorescein baseline data for the slab.

Inflow rate: 3.14 mg/l/h

Flushing rate: -4.19 mg/l/h

This sample produced the breakthrough curve with the poorest definition, probably because it had the lowest concentration of all of the colloidal suspensions (approximately 5-10 mg/l/h), and therefore was harder to distinguish from the background noise, even after the data was smoothed. This is consistent with the 50 nm samples that were produced, and their concentrations measured in Chapter 4; they were also hard to distinguish against background, and with the application of a correction factor, their average was just 11.57 mg/l.

The readings had increased noticeably by 1.5 hours after the introduction of the sample, but it is not possible to comment on the flushing rate because the readings had begun to drop before the sample had been substituted for water. Why this occurred is unclear. The tubing was placed at the bottom of the sample holder, so it cannot be the result of the colloids sedimenting and not being pumped through the system, and the temperature was stable, so it is unlikely that a change in temperature was influencing the laser's output. This effect was not observed in any of the other samples.

The inflow and flushing rates had the lowest R^2 values of any of the samples (both were <0.65, see Table 6.2), which suggests poor correlation between concentration and time, and they are therefore likely to be inaccurate and as such will not be used for any analysis. The somewhat poor quality of the data also makes comparisons to the fluorescein baseline difficult.

6.3.1.3 1000 nm sample made without PVP

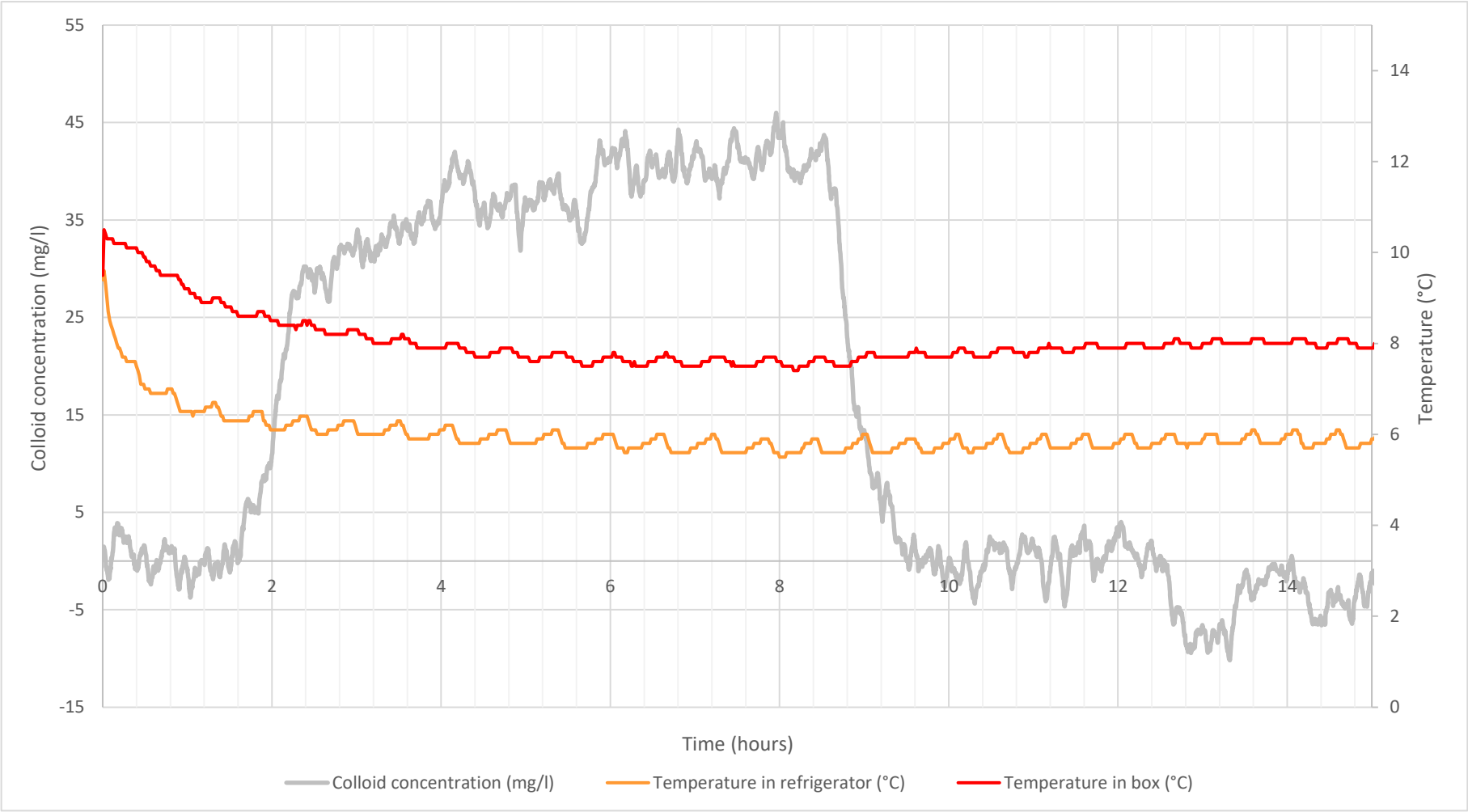

Figure 6.12. Nephelometer output and temperature data for the 1000 nm sample that was made without PVP and passed through the slab.

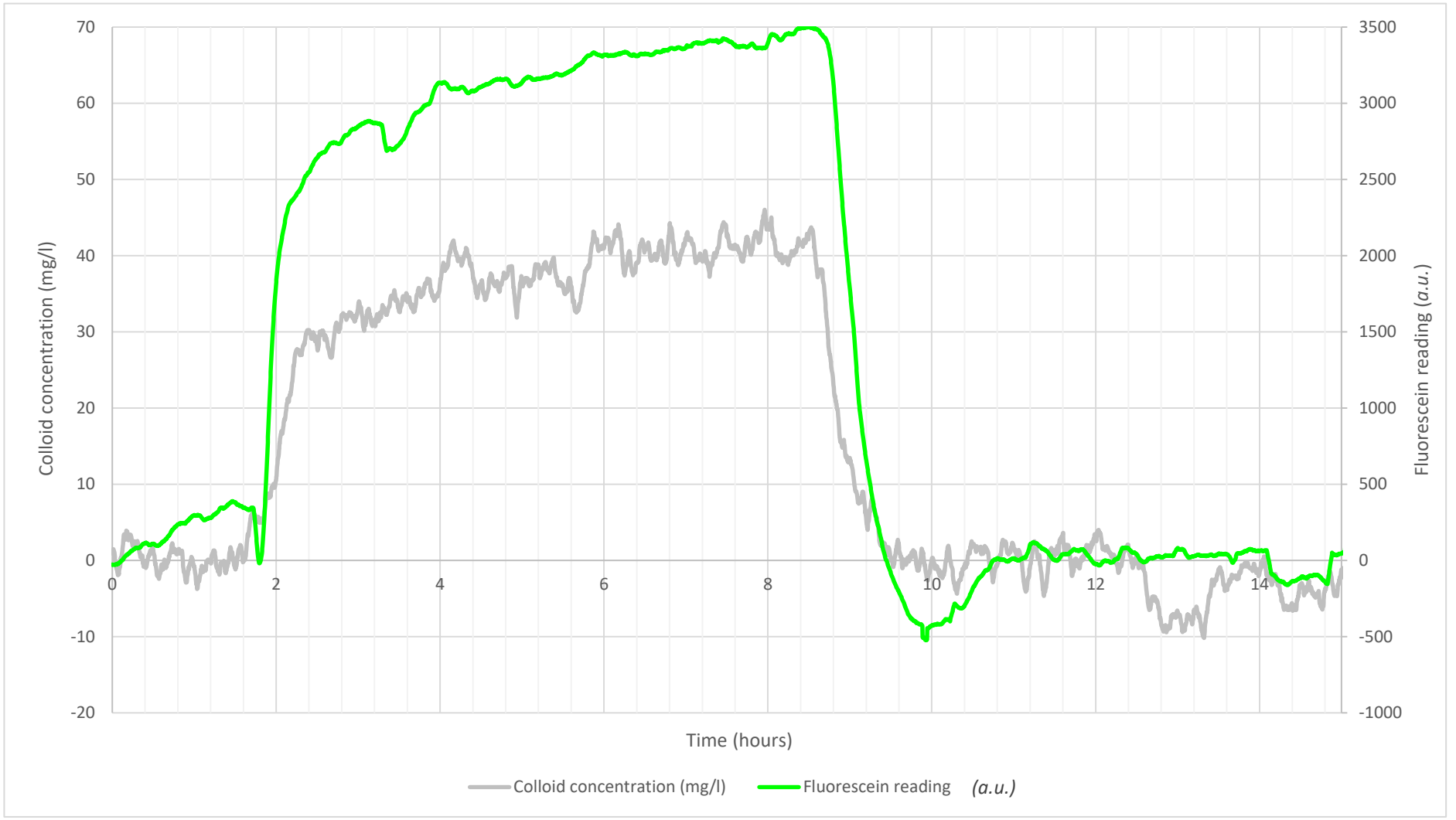

Figure 6.13. Nephelometer output for the 1000 nm sample made without PVP, and fluorescein baseline data for the slab.

Inflow rate: 40.20 mg/l/h

Flushing rate: -41.72 mg/l/h

This sample produced a clearly defined breakthrough curve very similar in shape to the fluorescein baseline. Little change was observed for approximately half an hour after the introduction of the sample and the reintroduction of the water, but the change in concentration was clearly defined after this time lag, so it was possible to obtain good measurements of the initial inflow and flushing rates, and there was little difference between them. It did however take five hours after the introduction of the sample to fully stabilise: the increase in concentration was rapid between 1.5-2.4 hours, but then slowed, and did not reach its maximum until hour 6 of the experiment. The flushing process became apparent at around 8.5 hours in both this sample and with the fluorescein, and they returned to their baseline values at the same time, suggesting that this colloid sample behaved very like a conservative tracer and did not bind to the granite surface significantly.

There is a noticeable drop in the concentration readings between 12.5 and 14 hours. This is unlikely to be temperature-related because the readings from both sensors were very stable during the course of the experiment, and it may instead be the result of a small bubble entering the flow cell and eventually being flushed out. Despite the inclusion of the bubble traps described in Chapter 5, this does still happen, and a number of experiments failed as a result.

6.3.1.4 50 nm sample made with PVP

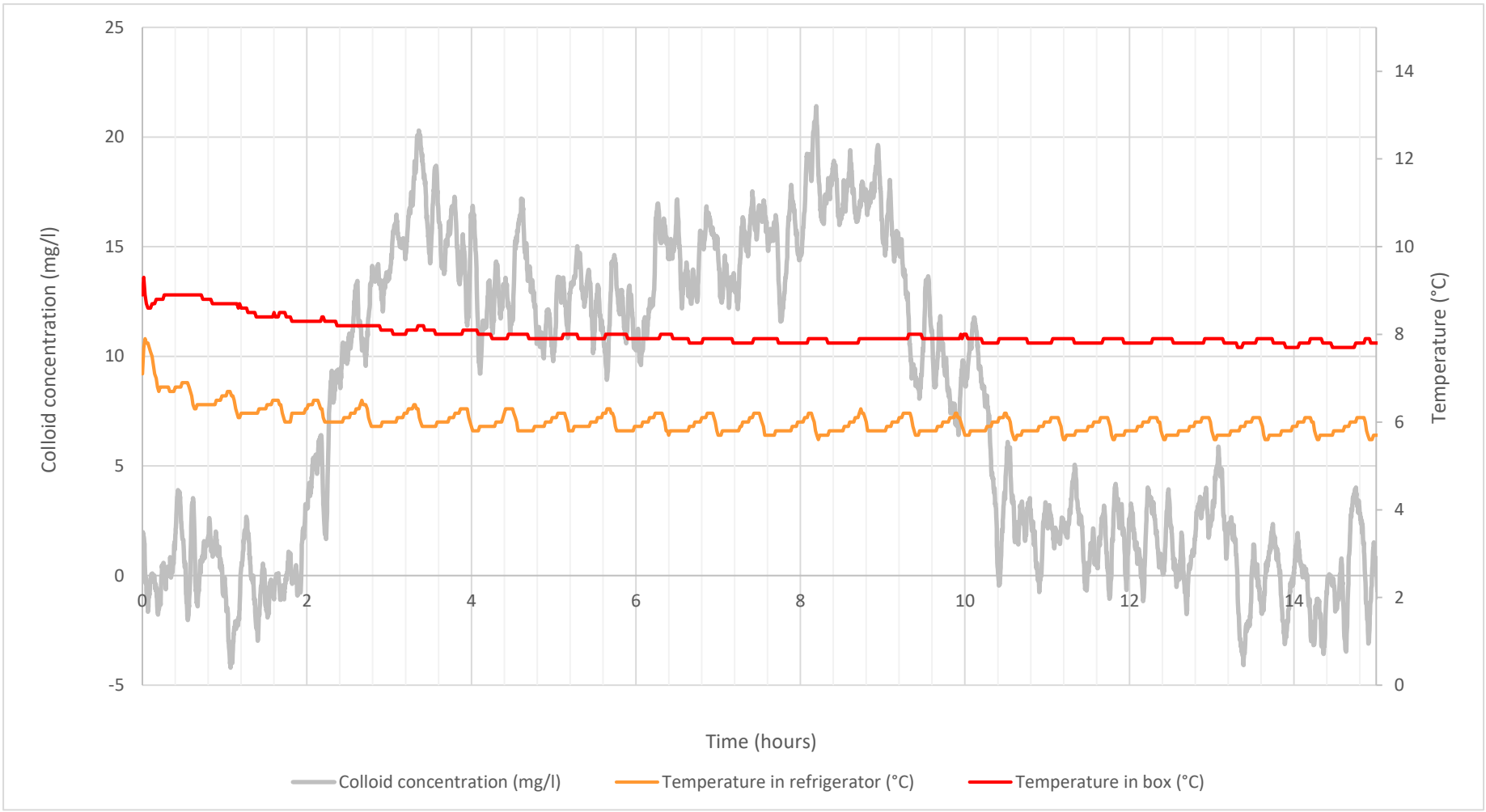

Figure 6.14. Nephelometer output and temperature data for the 50 nm sample that was made with PVP and passed through the slab.

Figure 6.15. Nephelometer output for the 50 nm sample made with PVP, and fluorescein baseline data for the slab.

Inflow rate: 11.68 mg/l/h

Flushing rate: -5.71 mg/l/h

This sample was of a higher concentration than the one made without PVP that was discussed in section 6.3.1.2, and the breakthrough curve, although still noisy, was better defined as a result. This matches what was discussed in Chapter 4: the <50 nm clay samples made using PVP tended to have much higher concentrations than those made without, which is logical given that the PVP was used to disperse the aggregates and produce greater numbers of smaller colloids. These could permeate the 50 nm filters, leaving more particles in the filtrate, and during the flow experiments they scattered more light into the nephelometer as a result.

The concentration of colloids did not begin to increase until one hour after they were introduced into the system, similar to the 50 nm sample made without PVP. The 1000 nm sample made without PVP was observed after 30 minutes. This may be due to differences in transport behaviour, for example if the greater relative surface area of the <50 nm clay colloids promoted their binding to the granite surface. However, it could also be that the <50 nm colloids had flowed across the granite and entered the cell at the same rate as those in the <1000 nm samples, but the resolution of the instrument was not good enough to detect the small initial increase in colloid concentration, and it only increased by a quantifiable amount after a longer time period.

After the initial inflow, the concentration values peak at 18-20 mg/l, drop to 10-12 mg/l, and then increase again, before flushing out. The reason for this irregularity is not clear. Similar to the sample in section 6.3.1.2, it cannot be due to the positioning of the tubing in the

sample vessel, and as the outputs from the temperature sensors were stable, it is unlikely to be temperature related. Similar effects may be observed in Figures 6.16 and 6.25, where <1000 nm samples made with PVP were passed over the granite slab and through the fracture, suggesting that it may be related to the presence of the surfactant, but it is not clear why this effect occurred.

The flushing period took slightly longer than the fluorescein, around 2.25-2.5 hours, and occurred much more steadily. The concentration did not drop appreciably until the nine-hour mark and then continued steadily until it reached its baseline, whereas the fluorescein changed little for the first 30 minutes after reintroduction, but then dropped rapidly. This suggests that the colloids had sorbed to the surface of the rock and took more time to flush out than the conservative tracer.

6.3.1.5 1000 nm sample made with PVP

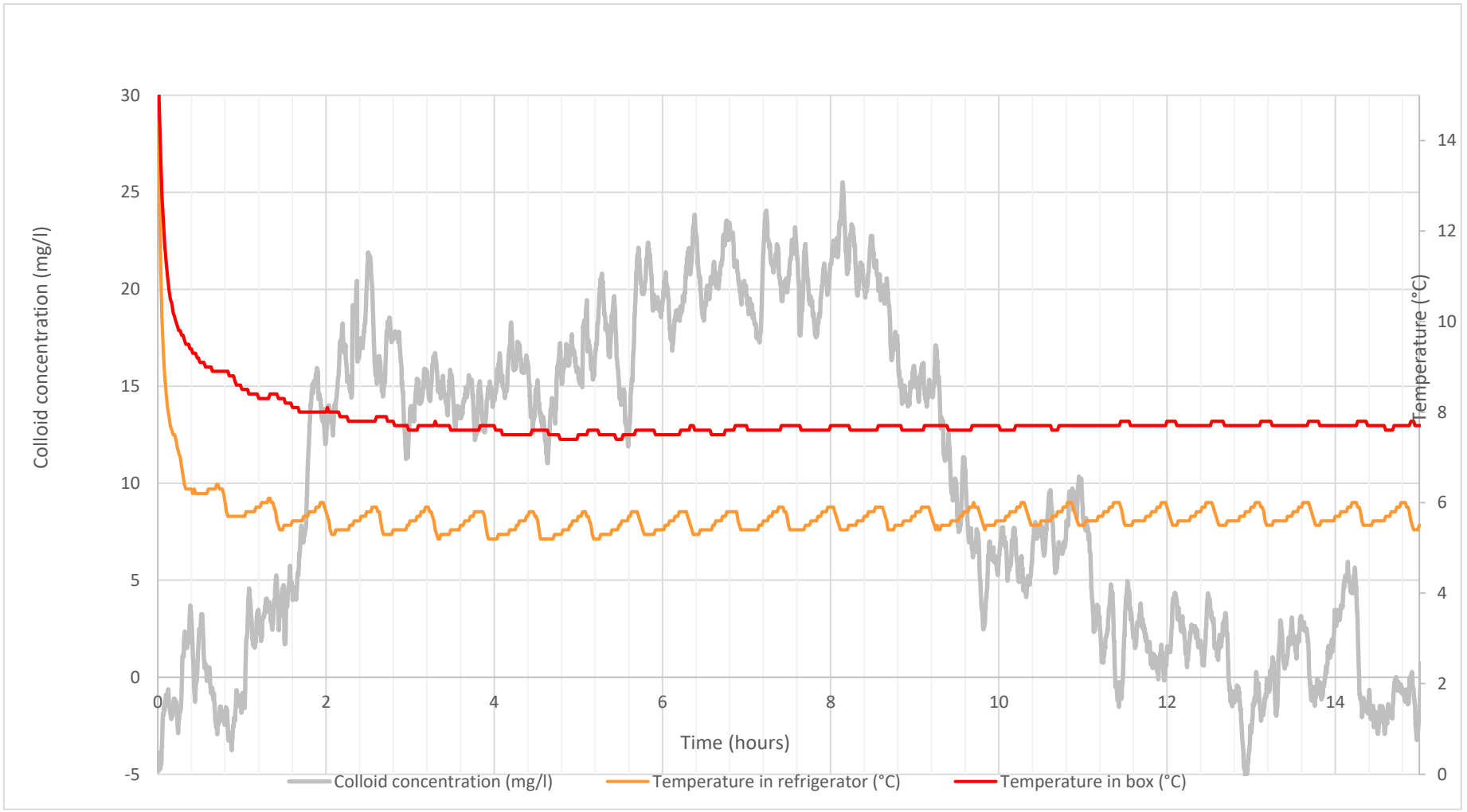

Figure 6.16. Nephelometer output and temperature data for the 1000 nm sample that was made with PVP and passed through the slab.

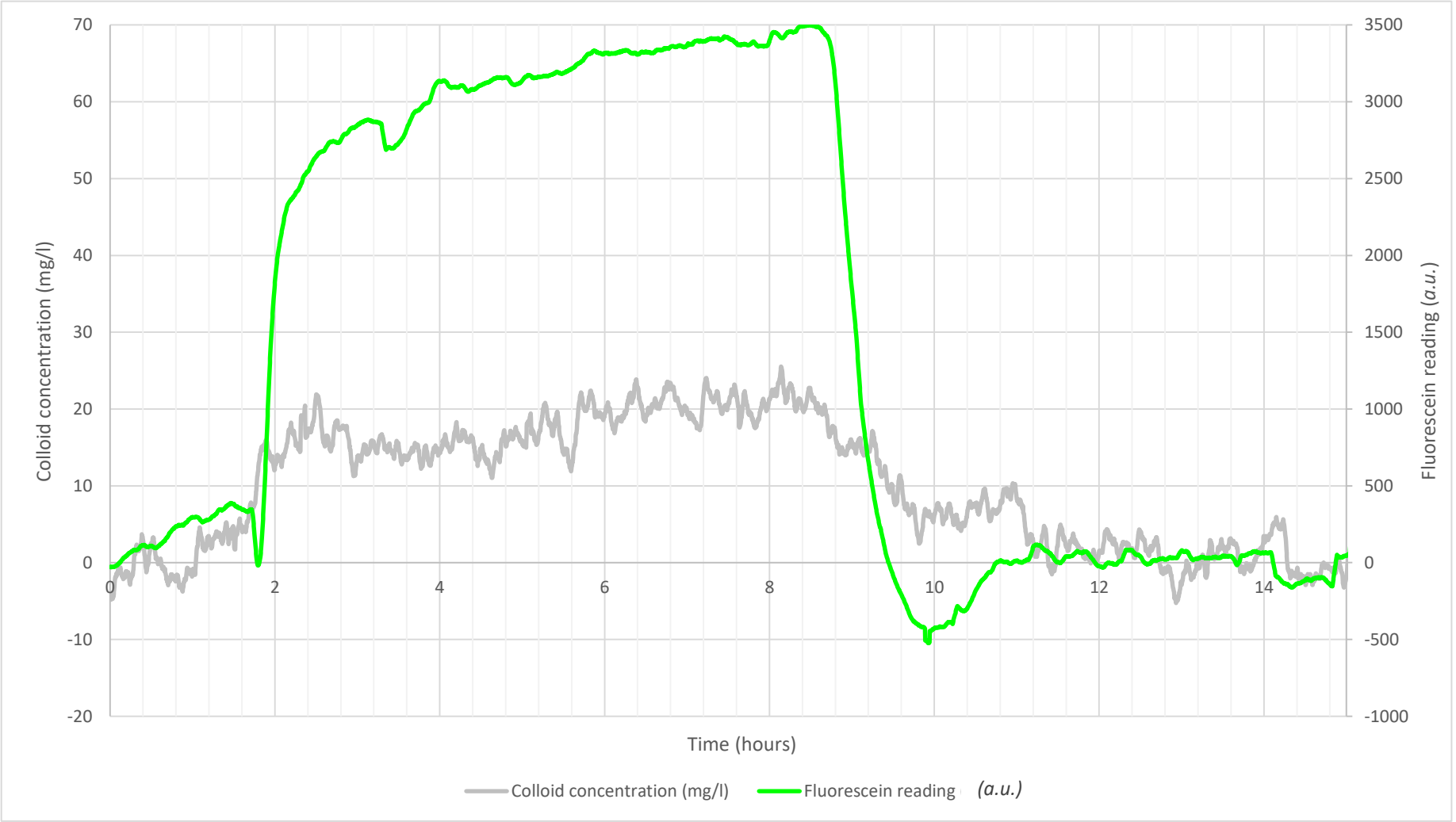

Figure 6.17. Nephelometer output for the 1000 nm sample made with PVP, and fluorescein baseline data for the slab.

Inflow rate: 13.40 mg/l/h

Flushing rate: -8.93 mg/l/h

This sample shows the same, inexplicable trend that was discussed in the previous section: the concentration peaks, drops, and increases again before flushing out completely. It is also hard to analyse the behaviour of the inflow with any degree of certainty because the deionised water baseline did not settle completely within the first hour of the experiment, and the concentration appears to increase almost immediately after the introduction of the sample at the 1-hour time point. This is likely to be an erroneous reading because there is an inevitable time delay as the sample has to pass through the tubing from the inlet to the flow cell.

The flushing behaviour of this sample is easier to investigate. As with the fluorescein, the concentration starts to drop noticeably around 30 minutes after the reintroduction of water into the system, but it then flushes much more slowly than the conservative tracer and does not reach its baseline level for around 3.5 hours after the switch was made. This suggests that the colloids may sorb to the surface of the granite (it is unlikely to be due to the filtering effect described in section 2.3.1.2 because the geometry of the slab means there are no narrow gaps through which the colloids may struggle to fit)and take longer to flush completely out of the system than the conservative tracer, much like the <50 nm sample made with PVP that was discussed in the previous section. This is reflected in its low flushing rate: this sample was flushed from the system at 8.93 mg/l/h, much more slowly than the comparable <1000 nm sample that was made without PVP (see section 6.3.1.3), which was purged from the system at around 41.72 mg/l/h. This may, however, be due to the fact that

the <1000 nm sample made without PVP had a far higher maximum colloid concentration; 45.3 mg/l; and therefore there were far more colloids in the system which needed to be flushed out. It is logical that if there are more colloids within the pore volume of the rock sample, then for a given flow rate and the same pore volume, more of those colloids will flush out at any one time, leading to a higher flushing rate.

6.3.2 Fracture

6.3.2.1 Fluorescein baseline

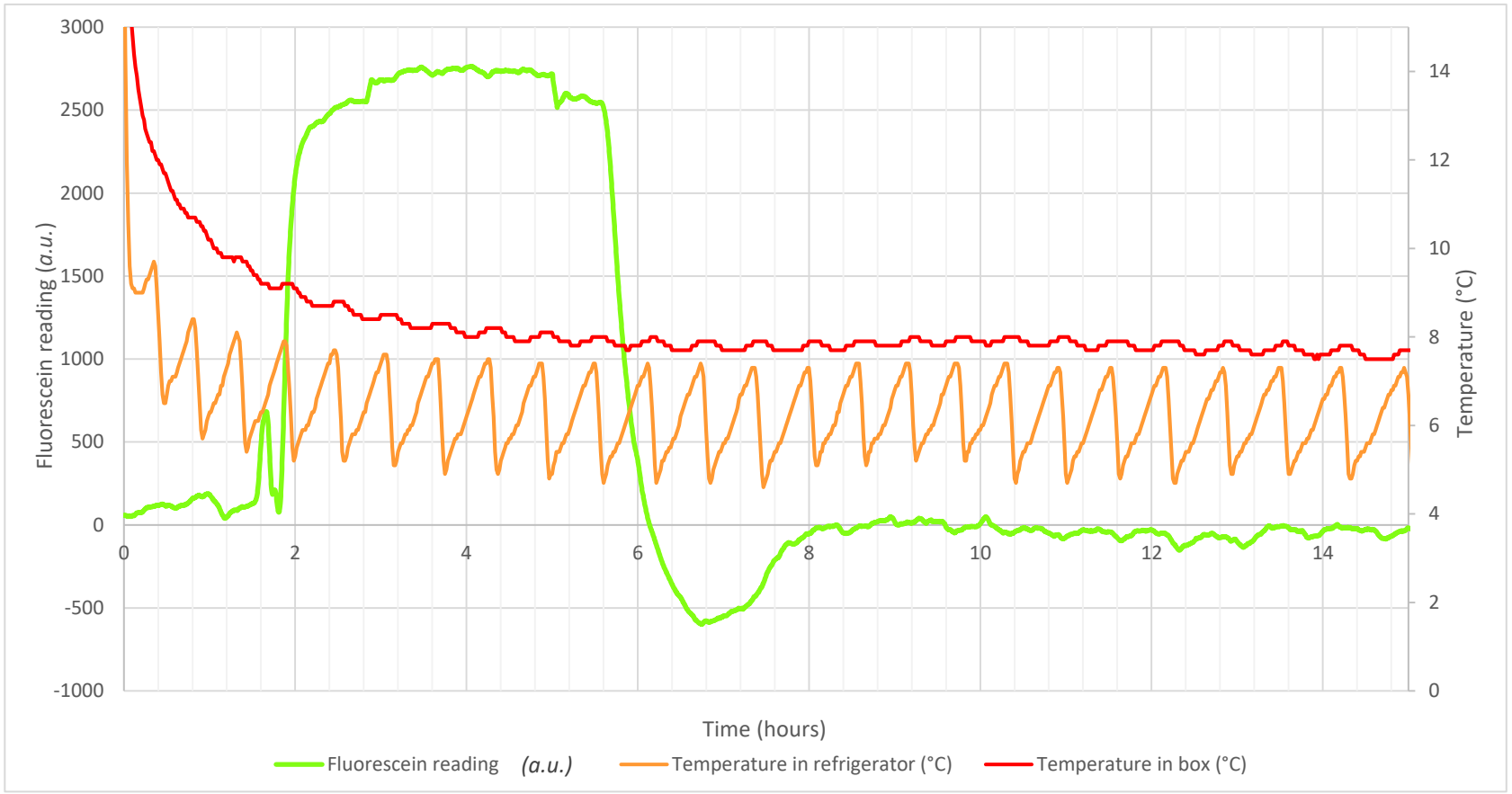

Figure 6.18. The breakthrough curve produced by passing fluorescein across the fracture. This provides a baseline against which the change in colloid concentration may be compared because it is a conservative tracer and therefore representative of the movement of water through the system.

Although the starting concentration of the solution used to produce the baselines for both the slab and the fracture was 15 mg/l for both, it was not possible to directly compare the difference in readings between the two because as was discussed in Chapter 5, the LED lacked the differential input and noise immunity of the laser, and so the detector output may have been different in the two experiments for a given concentration of fluorescein. This was not a significant problem however because it was not possible to relate the change in concentration of fluorescein to the change in concentration of the clay colloids anyway, and it was the shape of the breakthrough curves of the dye that provided useful information about the flow patterns, rather than their absolute values.

The fluorescein flushed out of the fracture more rapidly than out of the slab, and the readings had returned to baseline levels in under 1.25 hours. The rate of injection is more difficult to examine, because it appears to peak approximately thirty minutes after the introduction of the sample, and then fall again. There is no clear explanation for this, but similarly to the effect described in section 6.3.1.1, it may be the result of the interplay between the amount of emitted fluorescence, and blue light from the LED being blocked. Like the slab, the readings drop below the baseline shortly after the flushing of the sample began, which again, may be attributed to low levels of fluorescein blocking more light than it emits (see section 6.3.1.1).

The temperature cycles were of greater amplitude than those observed during the establishment of the baseline for the granite slab, just over 2 °C, but again, it appears to have made little difference to the readings. Temperature change appeared to have some influence over the laser output (see section 6.3.2.2), but little impact on the LED.

6.3.2.2 50 nm sample made without PVP

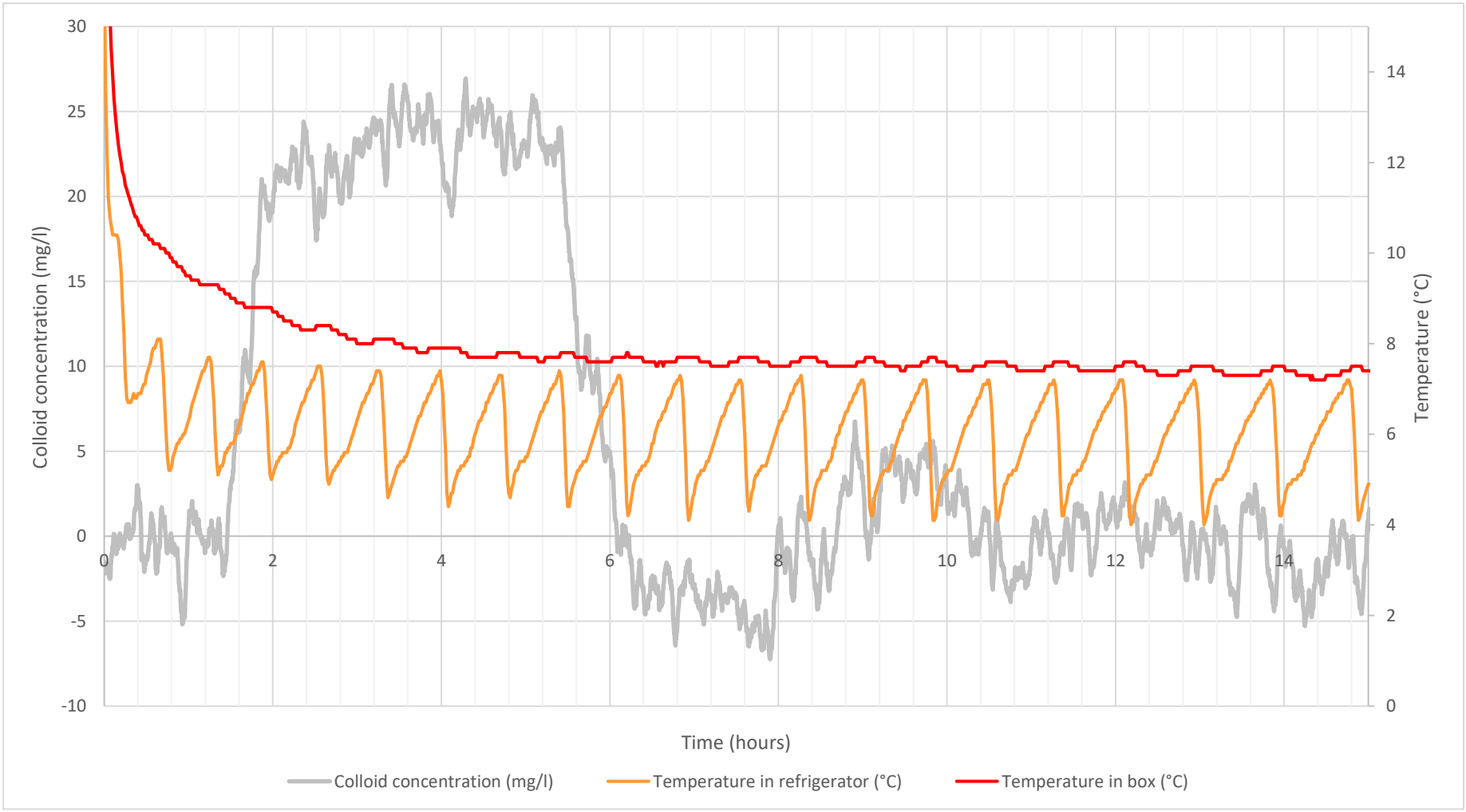

Figure 6.19. Nephelometer output and temperature data for the 50 nm sample that was made without PVP and passed through the fracture.

Figure 6.20. Nephelometer output for the 50 nm sample made without PVP, and fluorescein baseline data for the fracture.

Inflow rate: 38.40 mg/l/h

Flushing rate: -27.65 mg/l/h

The samples that were passed through the fracture were more uniform than those that were run across the slab, and all followed very similar trends, with little variation. They all matched the fluorescein baseline closely, which suggests that there was little binding of the colloids onto the rock, and that they behaved similarly to the conservative tracer.

Like those that were flowed across the slab, the samples that were run through the fracture did not show an increase in colloid concentration until around 30 minutes after they were introduced, but after that, their concentrations increased rapidly, and all of them had reached their maximum values by the 2-2.25-hour time point. This is most likely to be due to the differences in geometry between the two rock samples: the colloidal suspensions appear to flow through the narrow fracture more easily than they can disperse across the surface of the slab, and the smaller pore volume of the fracture meant that the sample replaced all of the deionised water more quickly than it did in the slab, so the readings levelled off at their maximum possible value more rapidly. This is why samples were run across the slab for seven hours, and through the fracture for four hours. It also explains why the inflow rates were much higher for samples through the fracture than comparative colloidal suspensions that were passed over the slab. It is not possible to comment on whether the maximum concentrations for the colloidal suspensions had an impact on the breakthrough curves because they varied significantly and overlapped with one another: the maxima ranged from 10-45 mg/l for the slab, and 16-57 mg/l for the fracture.

The flushing behaviour was also consistent between the different samples. Again, it was similar to the slab in that little change could be observed in the first 30 minutes or so, and then mirrored the inflow of the samples into the fracture in that the flushing rate was rapid after this, and they had all returned to baseline levels by the six-hour time mark, after just one hour of flushing. The slab took at least double this length of time for the colloid concentration to drop back to baseline levels. The flushing behaviour also corresponded well with that of the fluorescein baseline.

It is unclear why the readings dropped below zero during the 6-8-hour time period. The temperature in the refrigerator varied by over 3 °C during this time, which was the largest change of any of the runs presented in this chapter, but the temperature change in the nephelometer housing was suppressed to under 0.5 °C because of its insulating effect. It is therefore unlikely that this caused the laser output to vary by such a degree as to cause this anomaly. As was discussed in section 6.3.1.3, it may instead be due to a bubble passing through the system and changing the amount of light reaching the detector.

6.3.2.3 1000 nm sample made without PVP

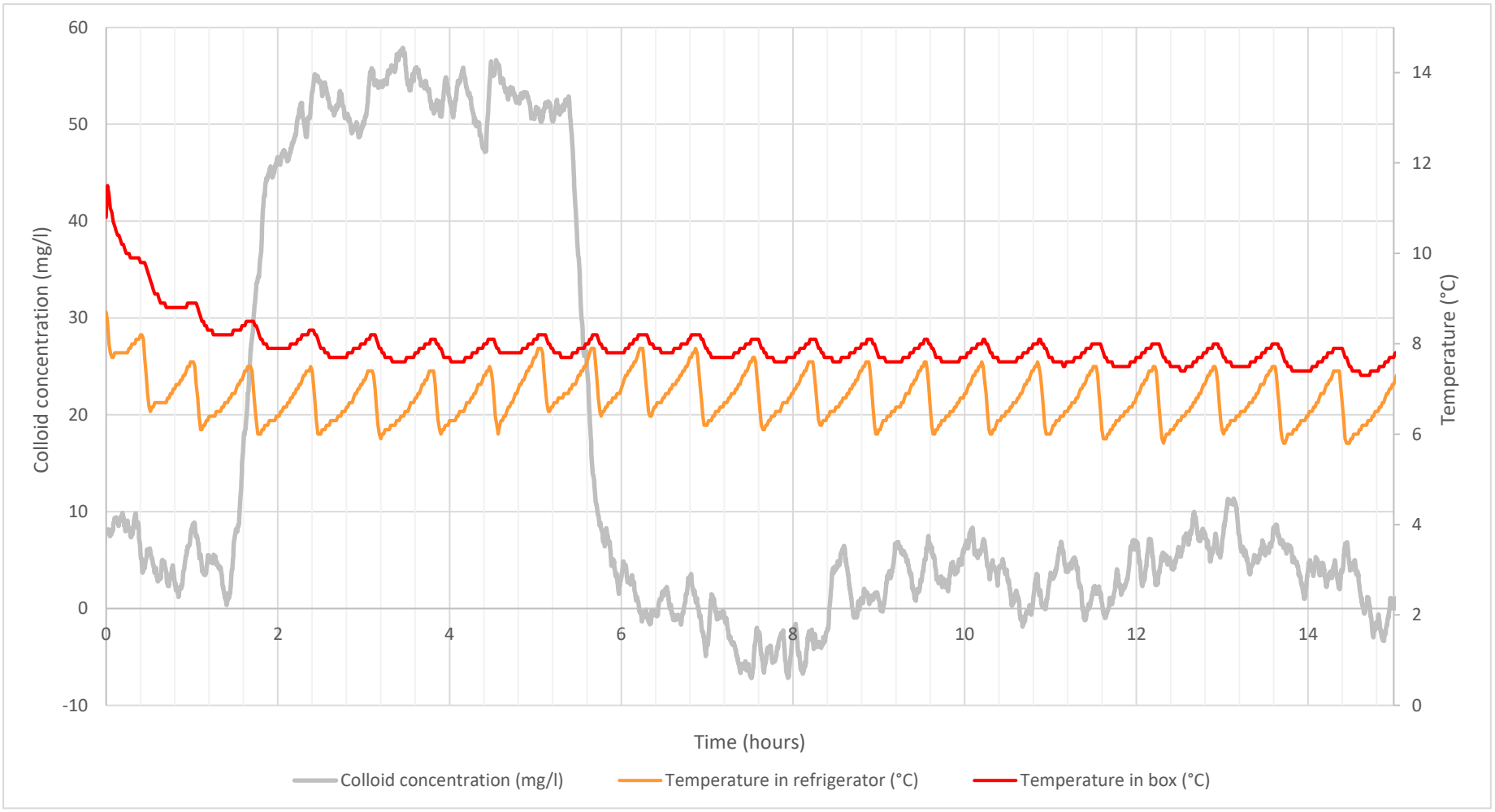

Figure 6.21. Nephelometer output and temperature data for the 1000 nm sample that was made without PVP and passed through the fracture.

Figure 6.22. Nephelometer output for the 1000 nm sample made without PVP, and fluorescein baseline data for the fracture.

Inflow rate: 90.27 mg/l/h

Flushing rate: -81.35 mg/l/h

This sample matches the breakthrough curve of the fluorescein tracer closely, and follows the trends described in the previous section. It has the highest colloid concentration of any of the samples, and correspondingly high inflow and flushing rates.

6.3.2.4 50 nm sample made with PVP

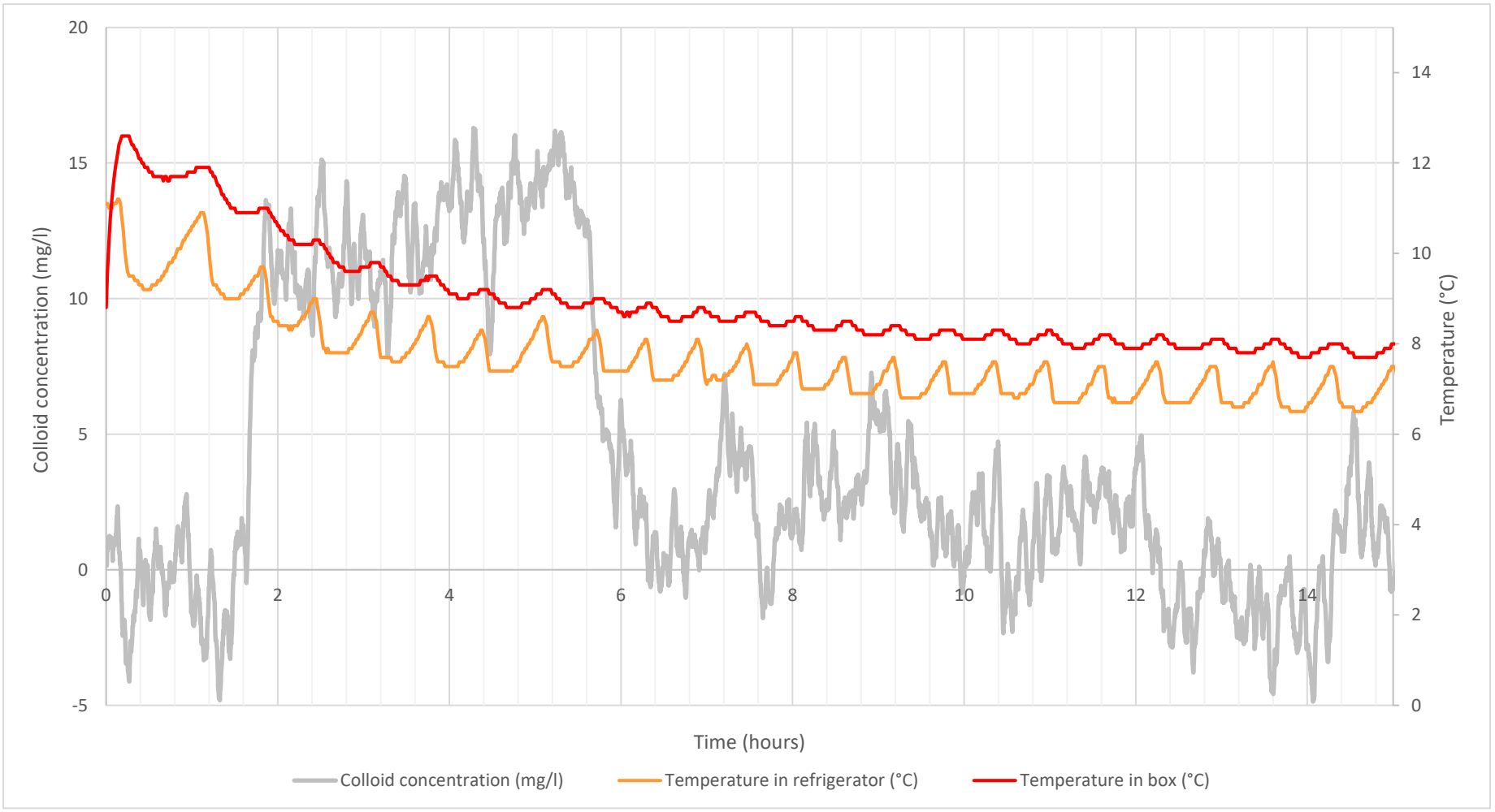

Figure 6.23. Nephelometer output and temperature data for the 50 nm sample that was made with PVP and passed through the fracture.

Figure 6.24. Nephelometer output for the 50 nm sample made with PVP, and fluorescein baseline data for the fracture.

Inflow rate: 57.26 mg/l/h

Flushing rate: -11.08 mg/l/h

This sample also follows the trends described in section 6.3.2.2 closely and corresponds well with the fluorescein curve. The maximum concentration of this sample is very similar to that of the sample in section 6.3.2.2 (50 nm, made without PVP, passed through the fracture) as well; around 16 mg/l and 27 mg/l, indicating that the samples that were passed through the slab tend to demonstrate fairly uniform behaviour.

6.3.2.5 1000 nm sample made with PVP

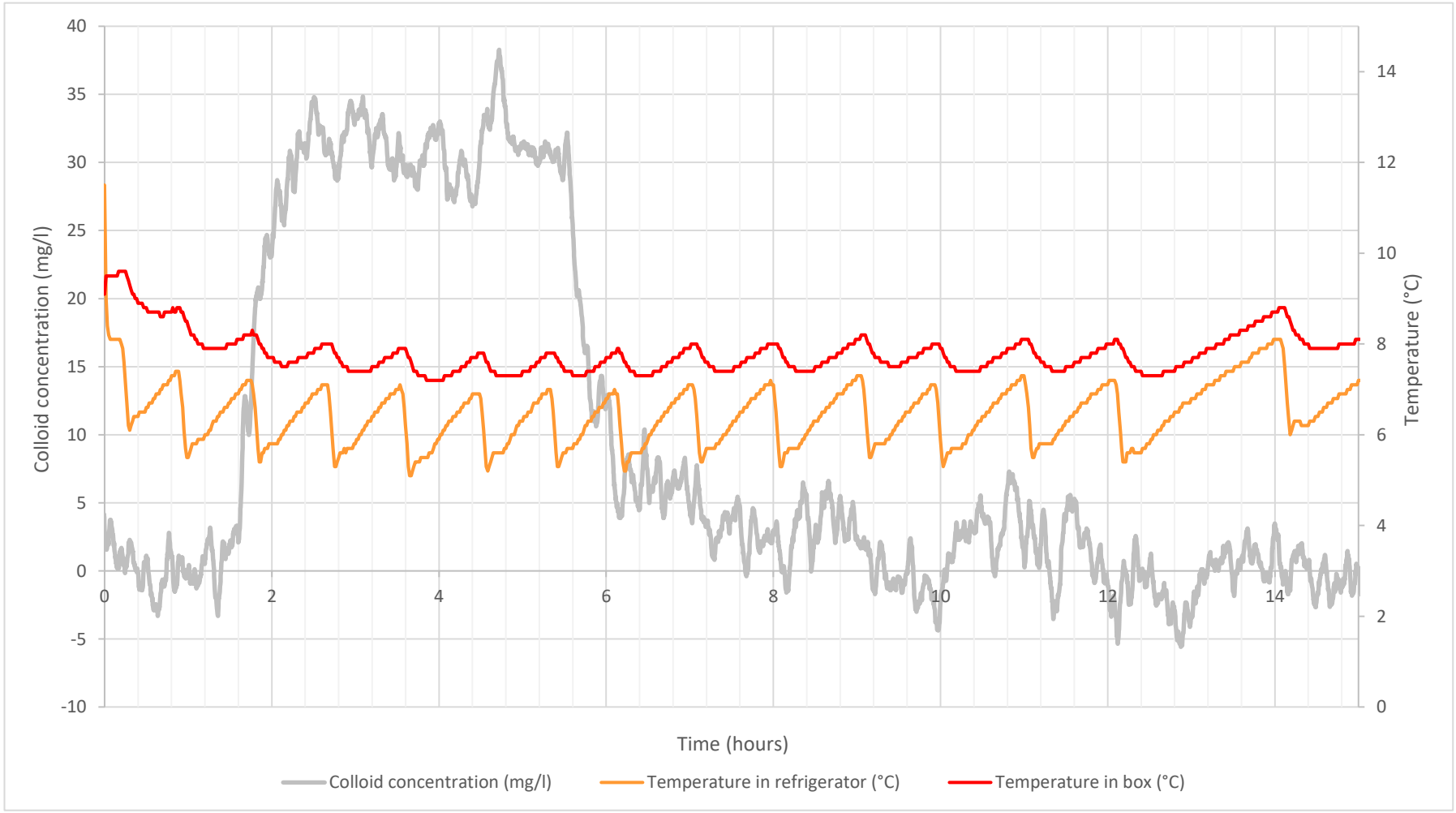

Figure 6.25. Nephelometer output and temperature data for the 1000 nm sample that was made with PVP and passed through the fracture.

Figure 6.26. Nephelometer output for the 1000 nm sample made with PVP, and fluorescein baseline data for the fracture.

Inflow rate: 31.70 mg/l/h

Flushing rate: -28.80 mg/l/h

The section of the breakthrough curve representing the inflow of this sample into the fracture also follows the trends described in section 6.3.2.2 closely and corresponds well with the fluorescein curve. The flushing behaviour, however, deviates from that of the other samples in the fracture, in that it took around three hours for the clay colloids to be removed from the system entirely. Section 6.3.1.5 describes how the same sample was also the slowest to flush from the slab.

It is logical that the higher concentrations of the <1000 nm suspensions (a result of fewer colloids being removed during filtration than in the <50 nm samples due to the larger pore size of the membranes) would result in greater sorption to the rock samples and a delay in flushing them out completely, causing the flushing portion of the breakthrough to str*etc*h, but the same effect was not observed for the sample in section 6.3.2.3, which had the highest concentration of any in this chapter, so it cannot be this effect alone. Three out of the four samples made using PVP (those in sections 6.3.1.4, 6.3.1.5 and the one here) displayed a drop in concentration after reaching their maxima, before increasing again. It is possible that the PVP is affecting how the colloids bind to the rock sample, potentially causing this effect and influencing the flushing behaviour of the one of interest here. This is discussed in section 6.4.3. The inflow and flushing rates for all of the samples are collated in Table 6.2.

Table 6.2. Inflow and flushing rates for the samples through the granite slab and the fracture, and the maximum colloid concentrations for each sample.

	Slab		Fracture	
	Inflow rate (mg/l/h)	Flushing rate (mg/l/h)	Inflow rate (mg/l/h)	Flushing rate (mg/l/h)
50 nm without PVP	3.14 R^2=0.6447	-4.19 R^2=0.5791	38.40 R^2=0.9264	-27.65 R^2=0.9257
Maximum concentration (mg/l)	10.5		26.7	
1000 nm without PVP	40.20 R^2=0.9535	-41.72 R^2=0.9208	90.27 R^2=0.9772	-81.35 R^2=0.9009
Maximum concentration (mg/l)	45.3		57.6	
50 nm with PVP	11.68 R^2=0.9366	-5.71 R^2=0.7943	57.26 R^2=0.8646	-11.08 R^2=0.7894
Maximum concentration (mg/l)	21.1		16.0	
1000 nm with PVP	13.40 R^2=0.8992	-8.93 R^2=0.8866	31.70 R^2=0.8743	-28.80 R^2=0.8672
Maximum concentration (mg/l)	25.4		37.9	

These were measured by identifying time periods when the increase or decrease of colloid concentration over time was as well-defined as possible, plotting a trendline, and then calculating its gradient. The gradient represents the change of colloid concentration over time. The large variation in R^2 values indicates this was more successful for some samples than others. For example, the 50 nm sample (no PVP) that was run through the slab had a relatively low colloid content and it was difficult to identify time periods where the change in concentration was defined clearly enough against the background noise to measure it. This was the cause of the high R^2 value, and it should therefore be treated with caution as it may be inaccurate.

6.4 Discussion

6.4.1 Previous work

This project fitted well within the context of the existing literature. The body of work that had been done before was not large, but addressed bentonite transport across and through granites taken from the GTS, so the same origin as the fracture, and indicated that colloid size influenced their transport behaviour, thereby supporting the rationale for conducting these experiments. Extending the investigation into the influence the size of colloids on their transport behaviour from artificial colloids to bentonite ones was a logical progression and filled a gap in the literature. The flow system was a development upon an existing design, and additionally, the use of nephelometry to produce a standard curve for calculating colloid concentration had not been done before, and although not perfect, it eliminated several of

the sources of error that arose from the use of chemical analysis, thereby improving upon the existing literature.

6.4.2 Method

Section 6.1 discussed how the methods used here have improved on the pre-existing work, most notably by demonstrating the viability of using nephelometry instead of chemical analysis for determining colloid concentration, and by applying the sizing experiments to bentonite colloids instead of artificial ones. Smoothing the data by applying a moving average of every twenty readings reduced the noise in the system and made trends much easier to observe. Averaging twenty readings resulted in the loss of approximately three minutes' worth of data at the beginning of the experiment, but as each run lasted for fifteen hours, this was not a significant compromise.

Additionally, applying a drift correction normalised all of the runs so that the deionised water measurements were as close to 0 mg/l colloid concentration as possible. The concentration tests in Chapter 4 highlighted that there was likely to be a small degree of variation between experiments because the nephelometer and fluorimeter are not commercially built instruments and as such are unlikely to have as high a degree of shielding from temperature change, external electronic interference, or as good voltage control. The drift correction standardised the runs and meant that they could be compared qualitatively and quantitatively to each other. This correction and the plotting of the charts shown in section 6.3 was all done by setting up a spreadsheet to use as a template, and then copying and pasting the relevant data for each experiment. This standardised the data analysis method

and reduced the likelihood of human error occurring. The method used did assume that the change in drift was linear, but despite this, it is more effective than applying a single correction factor and appeared to be a good fit for all of the samples.

However, the method used for the flow experiments could have been improved. The use of a conservative tracer provided a baseline breakthrough curve of water flow with no interaction between the particles and the rock, but it would be more useful if the fluorimeter could have been built with a differential input, and the high levels of noise immunity that the Transistor-Transistor Logic input gives the laser, because it would have then been possible to produce a standard curve for the fluorescein, and therefore calculated its change in concentration over time. If this could have been done, it would have been possible to calculate meaningful inflow and flushing rates for the conservative tracer, against which the change in colloid concentrations could have been compared quantitatively, rather than just visually, which is subjective. This is discussed in Chapter 5.

The quality of the baseline of some of the runs could have been improved by leaving the system to settle for longer before introducing the sample. This was done for some of the experiments on the fracture; some were run for two hours before switching the water for the clay sample, and others for three; but because the samples needed to be flowed across the slab for seven hours to ensure they equilibrated fully, it was not always possible to equilibrate them for three hours beforehand, plus the addition of a minimum of 30 minutes for the laser to warm up. (*N.B.* All of the breakthrough curves in section 6.3 only show the readings from one hour before the introduction of the samples, so that the laser had already had time to warm, and the curves had had time to settle and become less noisy). Two of the

samples that were flowed through the slab, the fluorescein baseline and the 1000 nm sample that was made with PVP, may have benefitted from a longer stabilisation period.

The review of the literature that was summarised in Table 6.1 indicated that size, flow rate, roughness, and charge distribution on the granite all exerted a strong influence on the transport behaviour of colloids. Size was the property being measured in this experiment, and it was therefore appropriate to vary it and investigate its influence. A constant flow rate of 0.26 ml/min was maintained, thereby keeping that variable consistent. This speed was chosen because it was as close as the pump could achieve to the 0.35 ml/min flow rate that was used successfully in experiments on a very similar system (Walkden 2014). Roughness and charge distribution, however, were not accounted for.

Sherriff *et al*. (2016) reported that greater surface roughness of granodiorite caused increased deposition of polystyrene colloids, and Boutt *et al*. (2006) noted that it influences the transport of particles during flow experiments in a number of ways:

- It changes the points of contact of colloids on rock surfaces, so there may not be a single energy value that describes their interaction, but several. If, for example, the colloid enters a pore in the rock, then Coulombic forces may act between the pore and both the bottom and the sides of the colloid (Boutt *et al*. 2006; Ryan & Elimelech 1996).
- It may also preclude the particles from detaching from the surface by rolling, driven by the mechanical force of the water, reducing or eliminating a mechanism of desorption (Ryan & Elimelech 1996).

- It can reduce the conductivity of water through the fracture because it prevents it from flowing in a direct path (Boutt *et al*. 2006).
- It may cause the water to recirculate within small areas. This increases the residence time of particles, meaning they have longer to interact chemically with the rock, and if the energy of the water is low enough, they may precipitate (Boutt *et al*. 2006).

Roughness may be measured using AFM software (Doucet *et al*. 2005), or high-resolution laser scanning confocal microscopy (Boutt *et al*. 2006). The former technique was available during this project, but the slab was supplied already encased in Perspex, and it would have had to be disassembled in order to measure it, which would risk damaging it, rendering it unusable in future projects. This could not have been done for the fracture, because even if it was not going to be used again and could have been broken open, it would have been unlikely to break exactly along the flow path, so the roughness measurements would not have been done on the correct surface.

The slab could have been polished before encasing in its housing in order to reduce the effects of roughness, as per Alonso *et al*. (2015), but it would not have been possible to do this for the fracture because of its shape: it would have needed to have been split open and polished before reassembling it, which would have made a wide channel through which the samples would have flowed unhindered, thereby reducing the likelihood of interactions with the rock surfaces. Additionally, as a genuine sample from the GTS, it is a useful resource and has been used for several projects, so this was undesirable.

Alonso *et al*. (2015) stated that granite surfaces, such as those used in this experiment, have heterogeneous charge distributions, which influence the sorption behaviour of the colloids,

as they also carry electrostatic charges. This heterogeneity occurs because granite is composed of a range of mineral species each with different chemical properties, and the colloids are small enough to be influenced by these individual minerals, rather than by the average characteristics of the rock. The major mineral components of granite such as quartz and feldspar carry negative charges (Sherriff et al. 2016), and therefore will undergo electrostatic repulsion with the permanent negative charge on the faces of the colloids, if PVP is not present in the sample or the colloids are not completely shielded by the surfactant. Individual minerals within the rock may be positive under low-pH conditions, which will repel the pH-dependent positive charge on the edge sites which colloids develop in acidic conditions (Sherriff *et al.* 2016). It may therefore be relevant to the work conducted here, but as is discussed below, it was not possible to investigate it.

Alonso *et al*. (2015) did not measure charge of the granite surface directly, but rather the impact this charge had on the interaction of colloids with it. Granite from the GTS was cut into sections of area approximately 1 cm^2 and the minerals in them identifies by producing elemental maps using a technique called Micro-Particle Induced X-Ray Emission (µPIXE). They then immersed them in suspensions of different artificial colloids and used Rutherford Backscattering Spectrometry to measure colloid diffusion coefficients, and measured surface distribution coefficients again using the µPIXE.

Neither of these techniques were available to this project, but it may have been possible to produce similar elemental maps using Energy Dispersive X-ray Spectrometry (EDS), which was. However, the same problem that was identified that prevented surface roughness from being measured would have applied here, in that it would have required the rock samples

to have been disassembled, thereby preventing them from being used again in future projects.

Due to time restraints, it was only possible to produce one run for each sample. Technical difficulties associated with the system (*e.g.* pipes becoming displaced and letting the system run dry, large bubbles entering the flow cell), meant that it sometimes took 2-3 attempts to get a complete run for one set up, so replication was not possible. If it had been possible, this would have led to greater certainty in the shape of the breakthrough curves and the magnitude of the changes in flow rates.

6.4.3 Results

The outcomes of this chapter fulfilled the aim stated in section 6.1 successfully. Two distinctly sized fractions of bentonite colloids made using PVP were flowed across and through samples of granite typical of the host rock of a GDF. Comparative fractions of otherwise identical bentonite colloids made without PVP were also run, which allowed any influence the surfactant used in their production had on their transport behaviour to be identified. The use of a conservative tracer provided breakthrough curves for the water through the system, which provided a reference against which the behaviour of the colloids could be compared.

The <50 nm samples that were flowed across the slab did not increase in concentration until 1 hour after they were introduced into the system. The theoretical minimum amount of time that the colloids could potentially take to reach the detector is the same as the lag time for the fluorescein, so around 1 hour, indicating that there was little interaction with the slab

when they were initially introduced to the system. The 1000 nm sample made without PVP was observed after 30 minutes, and the 1000 nm sample made with PVP appeared to increase immediately, which is not possible and therefore these were probably both anomalous. As was previously stated, this may be due to the smaller relative surface area of the <50 nm colloids binding to the rock, which would slow their movement, or it may be that the resolution of the instrument could not detect their lower initial concentration until a later time than the 1000 nm sample. The concentration of the fluorescein baseline also did not increase for the first hour. This suggests that the 50 nm colloids behaved like a conservative tracer, with their flow unimpeded, and it is therefore more likely to be due to the latter effect than the former.

The inflow behaviour for the fracture was similar for all of the samples, and the colloid concentration increased notably from 30 minutes after the introduction of the sample into the system. This rapid increase, even in the case of the <50 nm samples, indicates that the flow was impeded very little by the geometry of the fracture, that the colloids did not have to diffuse across it like they did across the slab, and instead flowed straight through it.

The most notable feature of the breakthrough curves for both rock samples is that after they have stabilised, but before the systems were flushed, is that the concentration of three out of the four samples that were made with PVP peaked, dropped, and increased again before flushing out completely. It may also have occurred for the fourth PVP sample (50 nm, run through the slab), but the effect was not distinguishable because it has the lowest concentration of the samples made with PVP, so it would have been harder to resolve. It does not appear to be temperature or size related, and it occurred for both the fracture and

the slab, so it is not dependent on the geometry of the rock samples, so it may be related to the presence of the surfactant, but it is not clear why this effect occurred.

After the reintroduction of water into the system, the samples that were flowed across the slab displayed little change during the first 30 minutes, and then fell relatively rapidly, and the system returned to baseline levels after around 1.5-2.5 hours. The exception was the 1000 nm sample that was made using PVP. It had the second-highest colloid concentration (after the 1000 nm sample made without PVP), but it flushed far more slowly, taking 3.5 hours to return to its baseline level. The same effect was observed when the same sample was flowed through the fracture. Again, it had the second-highest concentration, but took 3 hours to flush completely out of the system, compared to 1-1.25 hours for the other samples, which all showed a very similar trend: little change for the first 30 minutes, followed by a rapid decrease in concentration.

This delayed flushing behaviour may be the result of a combination of factors. Section 4.3.3.4.4.1 identified that the samples made with PVP had large numbers of small particles, which were not present in corresponding samples made without the surfactant. Material that is made up of small particles has a larger comparative surface area than a sample of the same type and amount of material with a larger particle size, and therefore it has more sites within the sample that could potentially sorb to the rock sample, so it would take longer to flush, and would produce the tailing of the breakthrough curve that was observed in Figures 6.15 and 6.24. Figure 4.20 indicated that the 50 nm sample made with PVP had more smaller particles than the 1000 nm one, which should theoretically augment this effect, but that was not observed. It is possible that this effect is counteracted by the lower total concentration of the particles in the 50 nm sample, so the tailing effect does not occur, or that it perhaps

does, but the resolution of the instrument was not good enough to detect it, as was discussed earlier in this section. It is unlikely to be a direct result of the presence of the PVP because as was discussed in Chapter 4, it forms a steric barrier on the surface, which would reduce (although not completely eliminate) the electrostatic interactions between the colloids and the surface of the rock, reducing the probability of sorption and therefore the tailing effect. The tailing of the breakthrough curve is therefore likely to be a combination of the colloids having a large total surface area, and a high enough particle concentration that a significant amount of sorption occurred despite the presence of the PVP.

The different shapes of the two rock samples gave them very different flow regimes and surface areas, and produced very different results, which made it hard to compare the behaviour of identical colloid suspensions; the effects of their geometry outweighed the influence any of the other controls on the system had over the shape of the breakthrough curves.

All but one of the runs on the fracture matched the fluorescein baseline closely, which suggests that there was little binding of the colloids onto the rock, and that they behaved similarly to the conservative tracer. This is unsurprising given that the surfaces of the fracture which were available for them to sorb onto had a much smaller surface area than those of the slab, so the effects of them binding would be much less pronounced and were possibly not distinguishable at all due to the resolution of the instrument. There was more variation amongst the samples that were flowed across the slab, most noticeably in some delays in flushing, but these were not consistent across all of the samples.

Calculating the rate of change of colloid concentration during inflow and flushing was an attempt to give a quantitative measurement of colloid transport behaviour to supplement the subjective visual comparison of the different samples and the fluorescein baseline. This was only partly successful because many of the gradient calculations were poor, with large R^2 values. It was also not possible to compare the measurements for the colloids to the fluorescein baselines because without a standard series, it was not possible to calculate any meaningful rate of change of fluorescein concentration, nor to draw comparisons between the fracture and the slab.

Increasing the concentration of the initial colloid suspensions that were used to produce the size fractions may have resulted in higher concentrations of the samples used for the flow experiments, which would have then made them clearer against the background noise in the data, but tests would have to be run to check that the higher concentration and reduced interparticle distances were not causing greater agglomeration, thereby changing the size distributions of the colloids.

6.5 Conclusions

The aim of this chapter was to flow differently sized fractions of bentonite clay colloids across or through samples of granite, to investigate their potential interactions with a granitic host rock. This aim was fulfilled successfully, and the work that was done in order to achieve it fitted well within the existing literature: Alonso *et al*. (2015) and Sherriff *et al*. (2016) both found that the size of artificial colloids influenced their transport behaviour, which supported the rationale for conducting these experiments, and these flow

experiments were carried out using bentonite colloids, which were more representative of the colloidal species that are likely to be found in a GDF than the artificial ones used in those studies.

The results indicated, however, that size did not have a significant influence on the transport behaviour of bentonite colloids, or if it does, that it is smaller than the impact the geometry of the rock sample has on the shape of the breakthrough curve. Geometry controls the shape of the curve firstly by how it affects the movement of water through or across it (it appears to flow through the fracture uninhibited, whereas it has to spread more slowly across the surface of the slab), and by the surface area of the rock that is available for colloids to sorb to. All but one of the breakthrough curves from the fracture were very uniform, and although there was slightly more variation between the runs that were done across the slab, again only one stood out significantly; in both cases, the sample that was made with PVP and was filtered to <1000 nm flushed out of the system far more slowly than any of the others. This was attributed to a combination of the small colloids in the sample giving it a large total surface area, and therefore many charged sites that were available to bind to the rock, and a high enough particle concentration that a significant amount of sorption occurred despite the presence of the PVP.

If time had allowed, fractions that were otherwise identical to the ones used in this chapter but made from milled clay could have been produced, and the number of edge sites on the colloids in the samples estimated using the same method as Norrfors *et al.* (2015). They could then have been run through the flow system to investigate whether the increased amount of edge sites influenced their transport behaviour significantly. Future experiments

could also include the addition of radionuclides. This would follow on from the work described by Sherriff *et al*. (2016), where the effect bentonite colloids had on the migration of Sr^{85}, Eu^{152} and Np^{237} through granite and tonalite cores and columns was investigated. It would require a modification to the existing flow system that would enable fractions to be collected at set time intervals so that their radionuclide content could be measured, probably by ICP-MS, but experiments could then be run on other radionuclides relevant to the disposal of nuclear waste, such as uranium. Running 2-3 replicates of each of the set ups would allow for greater confidence in the results as well.

6.6 References

Alonso, U. *et al*., 2015. Report on microscale investigations on colloid mobility controlling processes, EU: BELBaR.

Boutt, D.F. *et al*., 2006. Trapping zones: The effect of fracture roughness on the directional anisotropy of fluid flow and colloid transport in a single fracture. 33(21), pp.1–6.

Doucet, F.J., Maguire, L. & Lead, J.R., 2005. Assessment of cross-flow filtration for the size fractionation of freshwater colloids and particles. Talanta, 67(1), pp.144–154.

Missana, T. *et al*., 2008. Role of bentonite colloids on europium and plutonium migration in a granite fracture. Applied Geochemistry, 23(6), pp.1484–1497.

Norrfors, K.K. *et al*., 2015. Montmorillonite colloids: I. Characterization and stability of dispersions with different size fractions. Applied Clay Science, 114, pp.179–189.

Ryan, J.N. & Elimelech, M., 1996. Colloid mobilization and transport in groundwater.

Colloids and Surfaces A: Physicochemical and Engineering Aspects, 107(95), pp.1– 56.

Schäfer, T. *et al*., 2004. U, Th, Eu and colloid mobility in a granite fracture under near-natural flow conditions. Radiochimica Acta, 92(9–11), pp.731–737.

Sherriff, N. *et al*., 2016. WP3 partners final report on experimental results on micro- to macroscale colloid rock interaction and colloid radionuclide interaction, EU: BELBaR.

Suter, J.L. *et al*., 2009. Recent advances in large-scale atomistic and coarse-grained molecular dynamics simulation of clay minerals. Journal of Materials Chemistry, 19(17), pp.2482–2493.

Vilks, P. & Baik, M., 2001. Laboratory migration experiments with radionuclides and natural colloids in a granite fracture. 47, pp.197–210.

Walkden, S., 2014. Bentonite Colloid Investigations on a Granite Fracture. MSc Thesis, University of Birmingham.

Walkden, S.L., 2014. Bentonite colloid investigations on a granite fracture. MSc. Birmingham, UK: University of Birmingham.

Chapter 7

Investigating the sorption of cations onto clay colloids

Chapter 7: Investigating the sorption of cations onto clay colloids

7.1 Introduction

The aim of this chapter was to investigate how cations relevant to nuclear waste disposal adsorb onto the bentonite colloids by conducting batch sorption experiments, where cations were sorbed onto and off clay colloids and their change in concentration measured at different time points, to see how rapidly the sorption occurred.

Much of this project has been dedicated to investigating the influence that particle size exerts over colloid behaviour. It was not possible to do this for the same fractions that were made and used in Chapters 4 and 6 respectively because the concentration of colloids in the <50 nm samples that were made without PVP were so low, typically ~10 mg/l, that the sorption and desorption onto and off their surfaces was likely to be very small and potentially unmeasurable. The <50 nm samples made with PVP had similar concentrations to the <1000 nm fractions, but there would not have been a sample made without surfactant against which to compare them. It may have been possible to increase the concentration of the starting clay solutions, but the decrease in average interparticle distance may have influence the agglomeration behaviour of the clay, and therefore their size distribution. Additionally, because of how unstable the clays are and how rapidly they agglomerate, the sorption and desorption experiments could have only been run for a few days before their size distribution changed significantly, which is insufficient equilibration time. Therefore, only <1000 nm fractions were produced and used in this chapter.

7.1.2 Cations of interest

The sorption behaviour of three elements was investigated in this project: nickel, caesium, and europium, and they were selected for a variety of reasons; europium for its suitability for use as an analogue for trivalent actinides, caesium for its unusual sorption and desorption behaviour, and nickel at the suggestion of the industrial sponsor of this project, RWM, because of the mobility and longevity of one of its isotopes. All of the work that was done in this project used stable isotopes because it can take a considerable amount of time to obtain the necessary approval to conduct work with radioactive material, but as the chemical properties of different isotopes are identical, this would not have impacted the experiments at all. For clarity, however, they are sometimes referred to as radionuclides, as this is what the cations that were selected are intended to represent.

7.1.3.1 Europium

Europium is one of the lanthanides, a rare earth element that does not exist in elemental form in nature, only as a component of minerals such as monazite. Its most abundant isotopes are Eu-153, which is stable, and Eu-151, which has a half-life of 1018 years, but unstable isotopes such as Eu-152 and Eu-154 may form as fission products or through activation of the stable europium contained in reactor control rods (Sherriff 2015). Eu(III) may also be used as an analogue for americium (III) and other trivalent actinides and lanthanides commonly 0found in nuclear waste because of their similar chemical properties, giving insights into their likely behaviour (RWM 2016a).

Eu(III) is the most common oxidation state and is the one of interest to this project, but Eu(II) may also exist if the conditions are strongly reducing (Sherriff 2015). Under typical repository conditions, 75-80 % of Eu(III) has been reported to sorb to bentonite colloids (Sherriff 2015).

The same authors determined that desorption is not irreversible but is slower than predicted for binding via surface complexation. It was proposed that surface precipitation and the diffusion of the europium cations into the clay interlayers could explain the retardation of reversibility, but the authors acknowledged that greater investigation was required before it could be determined with a degree of confidence.

7.1.3.2 Nickel

Nickel is a transition metal, the most abundant isotope of which is stable Ni-58, but Ni-59 and Ni-63 are the radioisotopes of greatest interest to waste management organisations because of their relatively long half lives, $7.5x10^4$ years and 101 years respectively (Wold 2010). These radioisotopes may be formed by the neutron activation of stable nickel in the steel structures of nuclear reactors, and it may also occur due to the use of nickel alloy cladding in AGR and PWR designs (RWM 2016a).

Nickle-59 is of interest to radioactive waste management organisations because of its inventory, mobility, toxicity, and half-life. Modelling of Ni-59 released from spent fuel that underwent disposal using a higher-strength rock concept shows that Ni-59 released from a failed canister of PWR spent fuel represented the greatest flux of activity from the EBS (RWM 2016b).

Nickel is present as Ni(II) under both oxidising and reducing conditions (Wold 2010). In very high pH environments (pH>9.5), it forms either $Ni(OH)_2$ or $Ni(OH)_3^-$ aqueous species, and at lower pH, Ni^{2+} (RWM 2016a). It binds to mineral species predominantly by means of surface complexation, although it does exhibit a small degree of cationic exchange (Wold 2010).

As mentioned above, there is concern among the waste management community about the mobility of nickel in an EBS (RWM 2016b). Malamis & Katsou (2013) determined that uptake

of aqueous nickel onto Na-bentonite such as MX80 varied from 80 to 100 %, and that the sorption of nickel onto bentonite generally increases with increasing pH, indicating that it should be high at the basic pH associated with the bentonite buffer (Nessa *et al*. 2007). The latter is supported by the findings of Liu & Zhou (2010) and Yang *et al*. (2009) (albeit with a modified Na-bentonite).

7.1.3.3 Caesium

Highly-soluble caesium, a reactive alkali metal, exists predominantly as Cs(I), and its only stable isotope is Cs-133 (RWM 2016a). Cs-137 is an important fission product that was released into the environment and the groundwater during atomic weapons tests and after the accidents at Chernobyl and Fukushima.

RWM identified that Cs-135 may be problematic to repository performance assessments because like Ni-59, it has great potential for reaching the surface of a repository host rock and becoming mobile in the environment. It also has an extensive half-life of 2.3×10^{6} years, and so will remain significantly radioactive for a considerable amount of time. Cs-137 is less significant problematic because its shorter half-life (30 years) means that a significant amount of it will have decayed during the period of containment offered by the canister (RWM 2016a).

Caesium was the only cation identified by Sherriff *et al*. (2016) that did not sorb linearly onto bentonite colloids, but this was only at concentrations lower than $<10^{-7}$ mol/L; it followed the more regular linear trend at concentrations between 10^{-6}–10^{-2} mol/L (see Figure 7.1). This difference is due to how it binds to the colloids at different concentrations: the caesium sorbs into frayed edge sites at low concentrations, and onto planar sites in the interlayers at higher concentrations (Sherriff *et al*. 2016).

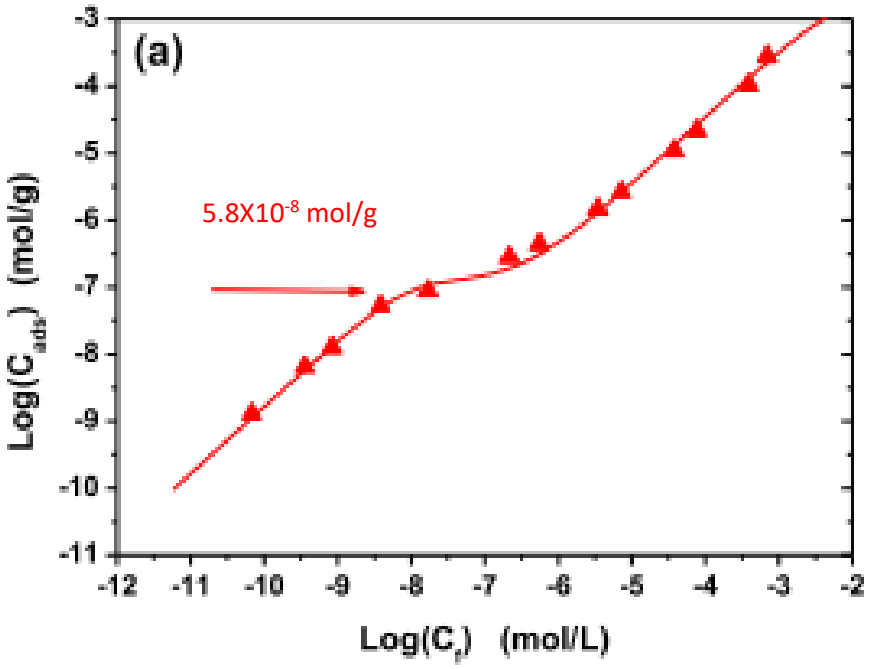

Figure 7.1. The non-linear sorption of caesium onto bentonite colloids. It is linear until it reaches a concentration of 5.8X10-8 mol/g, flattens out, and then returns to a linear trend. Image courtesy of Sherriff et al. 2016.

The reversibility behaviour of caesium is also unusual. It sorbs preferentially to the host rock, leaving only approximately 2 % free to bind to the colloids, but it does so irreversibly. Again, this occurs because in addition to adsorbing onto the weak planar sites discussed above, it binds to the frayed edge sites in the smectite layers (Sherriff *et al*. 2016). The reason for why it is only Cs that does this is not well understood, but Okumura et al. (2018) theorises that it is due to the ionic radius of caesium matching the interlayer distance of the clay, and to the low hydration free energy of the caesium ion.

7.1.3 Previous work

Table 7.1 summarises examples of sorption experiments found in the literature. Some of the experiments involved additional radionuclides to those listed here, but only the relevant ones have been included.

Table 7.1. A table containing examples of sorption experiments in the literature and their key findings.

Authors	Description of the experiment	Relevant findings
Dähn *et al*. (2003)	A nickel solution was added to a suspension of Wyoming bentonite that had been centrifuged to isolate the <0.5 µm fraction. After 14 and 360 days, samples of the mixture were filtered and analysed by ICP-OES. Clay films were also prepared for fluorescence and Extended X-Ray Absorption Fine Structure (EXAFS) measurements.	Ni sorbed onto the clay for one year, indicating the presence of slow sorption mechanisms. Uptake is most likely to be due to the formation of nickel surface complexes at edge sites of the colloids.
Norrfors *et al*. (2016)	Examined how colloid size affected the sorption of a range of actinides onto MX80 using batch experiments in a synthetic groundwater. Colloids were fractionated by sequential centrifugation and had average diameters of 1496 nm, 940 nm, 500 nm, 250 nm, 258 nm, 246 nm as measured by PCS.	Colloid size did not appear to affect sorption behaviour.

Ozsoy & Bekbolet (2018)	Used batch sorption experiments to investigate how factors including pH, cation concentration and timescale affected the sorption of Cs onto Turkish bentonite. Average particle size ranged from 0.1–130 µm, with an average of 5 µm, as measured by DLS.	The cations sorbed onto the clay immediately and then little change was observed. 30 minutes was sufficient sorption time.
Sherriff *et al*. (2015)	Sorption and desorption of Eu onto and off both bulk and colloidal Wyoming bentonite was investigated. The colloids had been sequentially filtered through 450, 200 and 100 nm membranes, and ultrafiltration through 300, 10 and 3kDa membranes was used to produce a 'true solution', with no colloids remaining in suspension. Ethylenediaminetetraacetic acid (EDTA) was used to promote desorption of the radionuclide in the bulk bentonite experiments, and a Dowex resin with the colloids.	Sorption onto the colloids was not investigated in depth, but sorption onto the bulk bentonite occurred in two stages: 96 % of the Eu sorbed onto the clay immediately, and a further 3 % sorbed onto it over the next month. 30-40 % dissociated immediately off the colloids. It then continued to dissociate, but more slowly. The authors stated that diffusion into the interlayer spaces of the clays is the mechanism most likely to be responsible for this. There was no evidence that Eu bound irreversibly to the bentonite.

The review of the literature indicated that all three cations should sorb onto the bentonite colloids successfully, but may exhibit very different behaviour: Cs appeared to sorb onto the clay almost completely after 30 minutes, whereas Ni continued to undergo slow adsorption for almost a year, and Eu was somewhere in between. The experiment described in this chapter was designed to investigate this behaviour further.

7.2 Sorption experiments

7.2.1 Introduction

For the sorption experiments, clay suspensions filtered to <1000 nm were mixed with a solution of Cs, Eu and Ni and left to equilibrate for a week, before Ethylenediaminetetraacetic acid (EDTA), an ion exchange agent, was added to cause them to desorb off the colloids again. This is similar to the experimental protocol described by Sherriff *et al*. (2015). Samples were taken at set time points throughout both the sorption and desorption phases and filtered immediately using centrifuge filters. This removed the colloids and any cations that were bound to them at the time. The concentrations of cations that remained free in solution passed through the filters and were collected and measured using ICP-MS. A detailed method is given in section 7.2.2.

EDTA can be used as an ion exchange agent. It is a polydentate ligand that can form up to six bonds with metal ions, producing a complex called a 'chelate'. This fills the coordination spheres of the metal ions and prevents them from reacting with other species in solution, or in this application, it pulls them off the surface of the clay colloids and prevents them from adsorbing back on (Atkins *et al*. 2006; M. Munowitz 2000).

In addition to the three cations of interest, the levels of iron and aluminium in the filtrates were measured as well. The MX80 used in this project contains both of them, and measuring their concentrations in the filtered solutions gave an indication of whether or not the colloids had been removed successfully by the filters.

7.2.2 Method

1. A stock solution containing 10^{-5} M Ni, Cs and Eu was prepared. Its pH was buffered by adding 0.1 ml of tetrabutylammonium hydroxide to every 100 ml of stock solution.
2. 4 g/l clay suspensions were prepared by combining 50 ml deionised water, 0.2 g of clay that has been sieved to <25 μm, and 0.4368 g of PVP, dispersing by agitating it by hand (not sonication), and then shaking it overnight. A comparative sample made without PVP was also prepared and used as a comparison, to see how the surfactant affected the sorption behaviour of the clay. Both suspensions, with and without the PVP should be prepared in duplicate. This method is the same as the one used to prepare colloid suspensions in section 4.3.3.4, but with double the concentration of clay and PVP. When combined with an equal volume of the stock solution, the resulting suspensions had approximately the same concentration of clay and PVP as those from Chapter 4.
3. As soon as possible before they are needed, the solutions were filtered to <1000 nm.
4. Duplicate samples of the cation stock solution and of each of the filtered clay samples were taken and centrifuged in 10 kDa centrifuge filter tubes to remove the colloids. These were the baseline samples.
5. 25 ml of each clay fraction was combined with 25 ml of cation stock solution.

6. 25 ml of the clay fraction and 25 ml of cation stock solution were combined. The result was 50 ml of 2 g/l clay, with 10^{-5} M Ni, Cs and Eu, buffered for pH.
7. These were shaken by hand for 10 seconds.
8. A timer was started.
9. A sample was immediately taken from each, placed into the centrifuge filters, and centrifuged at 10300 RPM for 10 minutes. This produced the 0 minutes sample.
10. This was repeated at 16 minutes, 1 hour, 24 hours and a week, and the solutions were shaken each time before sampling. The intention had originally been to take samples after 5 minutes, but the speed of the centrifuge was limited by the maximum speed at which the centrifuge filters could be used (14000 g, or 10435 RPM in the rotor that was used), and the samples took 10 minutes to filter. Around 3-5 minutes of additional time was needed for the centrifuge to slow down after its allocated run time. Because of these factors, the next samples were put into the centrifuge after 16 minutes' equilibration time, and this time interval was used for the desorption experiment as well.
11. The supernatants were retained, and their concentrations measured using ICP-MS. That concluded the sorption part of this experiment.
12. The remainder of the solutions made in step 6 above were left for one week to allow any slow sorption processes to complete.
13. A solution of 0.25 M EDTA disodium salt dihydrate solution was prepared.
14. Duplicate samples of the EDTA were taken and centrifuged. It was not necessary to take any other baseline samples for the desorption experiment because it was carried out at the same time as the week-old sorption sample was taken, and had

the same composition, *i.e.* a mixture of the clay suspensions and cation solutions, before the addition of EDTA.

15. 0.4 ml EDTA was combined with 9.6 ml of each of the clay and cation solutions. This was accounted for in the ICP-MS results by multiplying the measured cation concentrations by a factor of 1.04.
16. These were shaken by hand for 10 seconds.
17. A timer was started.
18. A sample was immediately taken from each, placed into the centrifuge filters, and centrifuged at 10300 RPM for 10 minutes. This produced the 0 minutes sample.
19. This was repeated at 16 minutes, 1 hour, 24 hours and a week, and the solutions were shaken each time before sampling.
20. The supernatants were retained and measured using ICP-MS.
21. The pH of the filtered clay solutions was measured using a pH meter, and the concentrations determined using the standard curve method described in section 4.4.5.4.3.
22. The data was analysed. The duplicate measurements for each sample were averaged and these are shown in the charts below.

    That concluded the desorption part of this experiment.

    The samples that were produced are collated in Table 7.2, the resulting concentrations are shown in Figures 7.2 and 7.3, and the pH and concentration values of the initial clay suspensions are in Table 7.3.

7.2.3 Results

Table 7.2. The samples produced during the sorption and desorption experiments, collated in tabular form.

Sorption				Desorption			
Clay 1	Clay 2	Clay with PVP 1	Clay with PVP 2	Clay 1	Clay 2	Clay with PVP 1	Clay with PVP 2
Baseline samples: Cation stock solution Filtered clay samples	Baseline samples: Cation stock solution Filtered clay samples	Baseline samples: Cation stock solution Filtered clay samples	Baseline samples: Cation stock solution Filtered clay samples	Baseline samples: 1 week equilibrated cation and clay solution EDTA	Baseline samples: 1 week equilibrated cation and clay solution EDTA	Baseline samples: 1 week equilibrated cation and clay solution EDTA	Baseline samples: 1 week equilibrated cation and clay solution EDTA
0 mins	0 mins	0 mins	0 mins	0 mins	0 mins	0 mins	0 mins
16 mins	16 mins	16 mins	16 mins	16 mins	16 mins	16 mins	16 mins
1 hour	1 hour	1 hour	1 hour	1 hour	1 hour	1 hour	1 hour
24 hours	24 hours	24 hours	24 hours	24 hours	24 hours	24 hours	24 hours
1 week	1 week	1 week	1 week	1 week	1 week	1 week	1 week

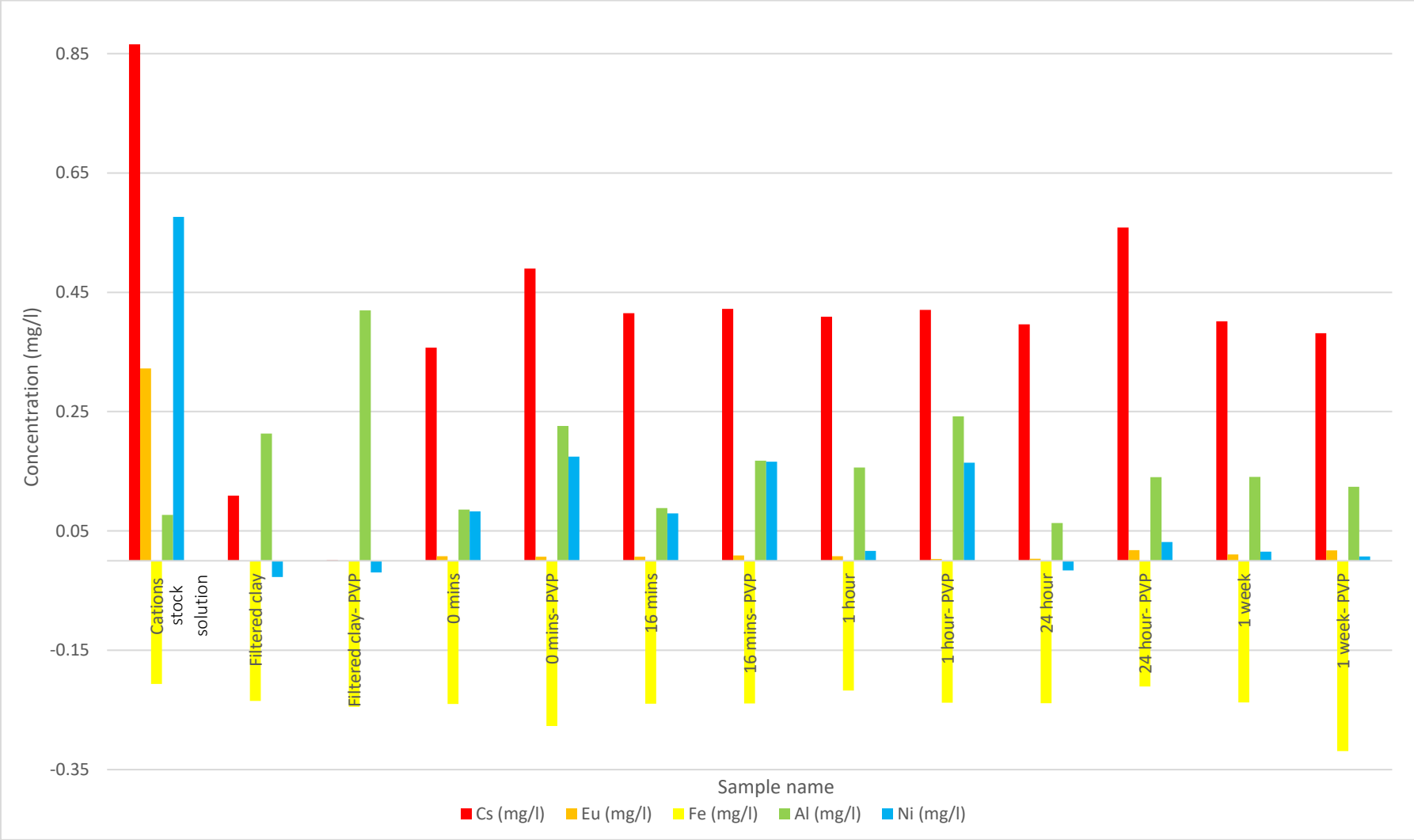

Figure 7.2. Concentrations of the cations in solution at different time points throughout the sorption experiment measured using ICP-MS.

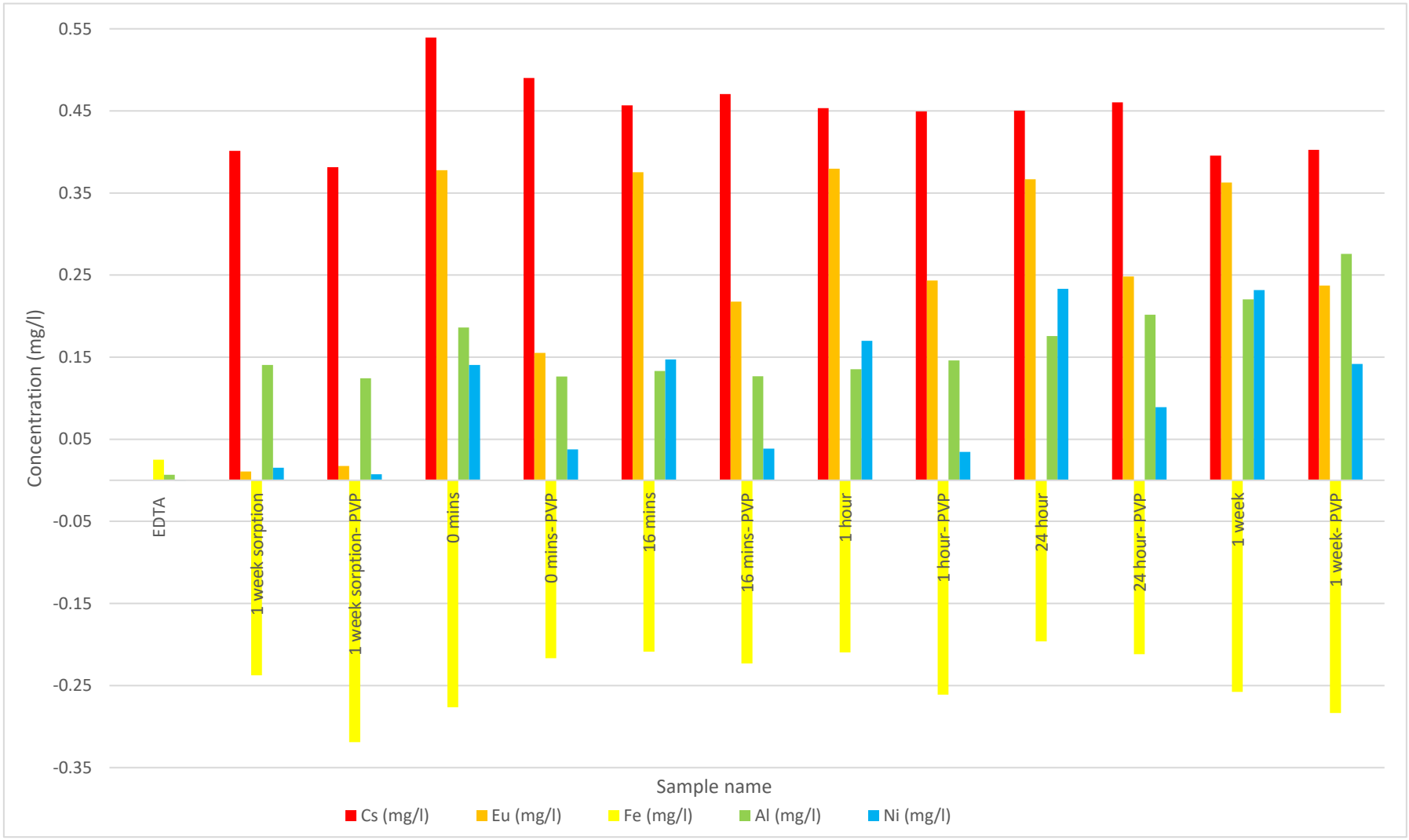

Figure 7.3. Concentrations of the cations in solution at different time points throughout the desorption experiment measured using ICP-MS.

The graphs in Figures 7.2 and 7.3 contain the ICP-MS measurements of the concentration of cations in solution. The Cs, Eu and Ni were from the cocktail of stable analogues which were used to represent radionuclides, and the Fe and Al were measured in order to determine whether all of the clay colloids had been removed because they are ubiquitous in the bentonite structure. The negative iron values indicate that the levels were below the limit of detection for thee instrument.

Firstly, the results of the sorption experiment, shown in Figure 7.2, will be discussed. The cation concentrations in the stock solution were measured at 6.5×10^{-6} M Cs, 2.1×10^{-6} M Eu, and 9.8×10^{-6} M Ni after undergoing centrifuge filtration. This is around an order of magnitude lower than the original 10^{-5} M that was made up in section 7.2.2, suggesting that some of the cations were removed by filtration. This is more likely to be due to them binding onto the surfaces of the filter rather than actual filtration. 10 kDa centrifuge filters should remove particles larger than 1-2 nm across (assuming spherical particles), so cations in solution should not be retained by the filters. There was around 0.08 mg/l Al (3×10^{-6} M) present in the cation solution, possibly a contaminant from the deionised water that was used to make up the solutions. Use of an ultrapure water would probably have eliminated this.

The next samples were the clay suspensions, which had also undergone centrifuge filtration. The XRF results in Table 4.2 show that the MX80 used in this project contains around 8 % Al and 4 % Fe. The anomalously low levels of iron in this sample and all of the others suggest that the colloids were removed successfully, but the presence of aluminium in all of them contradicts this. The same source of deionised water was used to make the clay suspensions and the cation solutions that were discussed above. These also contained aluminium, but lower levels than can be observed in the filtered clay suspensions, so this can partially

account for the aluminium content, but not completely. The aluminium content changed throughout the equilibration period: it was higher in the samples made using PVP for the first 24 hours, and also decreased slowly during that period, as if it was gradually sorbing onto the colloids, more slowly in the case of those where the surfactant was present. This indicates that it was free in solution as opposed to bound into the clay structure and may have dissolved out of the clay when it was added to the deionised water. There is also a seemingly anomalous 0.1 mg/l Cs in the clay solution that was made without PVP. This is not a common element and did not occur in the XRF analysis. However, this was the next sample to be measured by the ICP-MS after the stock solutions, and it is possible that the instrument was not flushed thoroughly enough after these, which left a small amount of Cs in the system where it contaminated the next sample. This was supported by the fact that it was not observed in the second of the clay samples, as if it had been flushed from the system by that point.

Around half of the Cs sorbed onto the clay immediately; the concentration of the stock solution was 0.86 mg/l, and the average concentration of the samples during the equilibration period was 0.43 mg/l. Little change was observed between the samples that were centrifuged at 0 minutes and 1 week, apart from one anomalously high reading at the 24 hour time point, but this can probably be attributed to the innate variability of the clay.

The Eu adsorbed onto the clay immediately and completely, falling from 0.3 mg/l in the stock solution to <0.02 mg/l when mixed with the clay suspensions, suggesting it was taken up preferentially over the Cs and Ni.

The sorption of nickel was steadier than the other two cations. Its concentration was 0.57 mg/l in the stock solution, and around two-thirds of it adsorbed immediately onto the clay,

so a greater proportion than the initial sorption of Cs, but then the concentration continued to change over the first 24 hours of the experiment, when <0.03 mg/l remained in solution. Little change could be observed between 24 hours and 1 week. During the first hour of sorption, the samples that were made using PVP had higher concentrations of Ni in solution, which suggested that the surfactant slowed its sorption onto the colloids, so less was removed from solution and subsequently retained by the filters.

After one week, there was very little difference between the levels of Ni, Eu, Cs and Al in solution in the samples with and without PVP, which suggests that although the sorption onto the colloids covered with the surfactant is definitely slower than those without it, the steric barrier only delays, rather than completely prevents, the sorption of cations onto bentonite.

The results of the desorption experiment, shown in Figure 7.3, are discussed in detail here. The levels of cations in the EDTA were very low, so it was unlikely to be a source of uncertainty. The results of the 1-week sorption test provided the baseline for the desorption experiment because the desorption test was begun when the cation and clay mixtures had had a week to equilibrate.

The Fe levels in the desorption samples are, again, too low to be measured, indicating that the clay was removed from suspension by the centrifuge filters. The Al concentrations were stable between the baseline samples and 1 hour, but then increased in the samples that were left for 24 hours and 1 week. This supports the theory that the unexpectedly high Al levels observed in the sorption samples were in solution rather than intrinsic in colloids that had been retained by the filters, as it demonstrated desorption behaviour, albeit slowly.

Cs desorbed from the colloids rapidly, but not completely. Its concentration in solution increased from 0.39 mg/l for the baseline samples to an average of 0.46 mg/l immediately after the addition of the EDTA, but this is much lower than the 0.86 mg/l that was measured in the cation stock solution. This supports what was discussed in section 7.1.3.3, about how Cs can bind irreversibly onto the colloids by sorbing onto their frayed edge sites in addition to the planar ones (see Figures 2.1 and 2.4 for more information about the structure of bentonite). The Cs that desorbed back into solution was probably bound onto the faces of the colloids, and that which remained was on the edge sites. The irreversible adsorption of caesium onto edge sites was discussed in section 7.1.3.3; the reason for it is not well understood owing to incomplete knowledge of the crystal structures of the edge sites, but it is likely that the unusually strong bonding is due to the ionic radius of caesium matching the interlayer distance of the clay, and to the low hydration free energy of the caesium ion. The Eu in the samples made without PVP desorbed immediately and completely off the colloids. In the samples that were prepared using the surfactant, around half desorbed immediately, which rose to two thirds after an hour, but it stabilised after that. This indicated that the surfactant prevented the EDTA from exchanging with the Eu.

A similar pattern was observed for Ni in that the samples made using the surfactant released less of it back into solution, although it differed from the Eu and the Cs in that it continued steadily throughout the week. By the end, 25 % of the Ni had desorbed back into solution from the samples made with PVP, and 40 % off those without, but without running the experiment for longer, it is not possible to determine whether this trend would have continued until all of the Ni had been released from the clay, or whether, like the Cs, some of it was bound irreversibly.

Table 7.3 contains the concentrations of the clay suspensions and their pH values.

Table 7.3. Average concentrations of the clay suspensions after filtration, and their pH values.

Sample	Concentration (mg/l)	pH
Filtered clay	81.39	7.9
Filtered clay with PVP	95.24	7.3

These samples were produced from a starting solution that was double the concentration of those used in Chapter 4, because it had to be combined with an equal amount of cation stock solution.

The suspension that contains PVP has a higher colloid concentration than the one made without using the surfactant. If the colloid concentration had been substantially lower instead, then sorption may occur more slowly simply because there are fewer colloids for the cations to sorb onto. As it is higher, this is not the case, and the slower rate is most likely to be due to the surfactant shielding sorption sites. This corroborates the theory that the PVP affects the sorption properties of the clay. Additionally, the pH values were between pH 7-8, so approximately neutral.

7.3 Discussion

7.3.1 Introduction and previous work

The sorption of cations relevant to nuclear waste disposal onto bentonite clay is a topic of concern to waste management organisations, and as such has been investigated extensively.

However, there are so many factors that can influence sorption behaviour- temperature, the concentrations of the species of interest, pH, ionic strength, the presence of fulvic acid- that every experiment is likely to have a unique aspect, and as such adds to the body of knowledge in the literature, rather than just repeating or confirming it (Norrfors *et al*. 2016; Ozsoy & Bekbolet 2018)

7.3.2 Method

The impracticality of investigating the influence the size of the colloids had on their sorption and desorption behaviour was explained in section 7.1. Both Norrfors *et al*. (2016) and Sherriff *et al*. (2016) concluded that differently-sized bentonite colloids did not display differences in sorption behaviour, so the fact that it was not possible to study it should not be viewed as a shortfall of the experimental methodology, as there is evidence already available in the literature to suggest it was not significant.

The solutions were allowed to equilibrate for a week before adding the EDTA. As they exhibited no measurable change after the first 24 hours, this could have been reduced, perhaps to 48 hours to allow for a degree of variability. The desorption experiment, however, should have been run for longer, as the Ni concentration was still increasing a week after the addition of the EDTA.

The use of centrifuge filtration was an improvement upon the methodology used by Yang *et al*. (2009), who used centrifugation alone to separate bentonite colloids from nickel solutions. It is not possible to be certain that the colloids had been removed from suspension by this method, whereas when using centrifuge filters, almost all of the colloids would have

been removed from the filtrate because they could not pass through the filters. This was evidenced by the very low Fe levels shown in the filtered samples in Figures 7.2 and 7.3.

As was discussed in Chapter 4, it is difficult to analyse suspensions of clay colloids using ICP-MS because the sample preparation requires filtration through 200 nm syringe filters to prevent blocking of the nebulizer, potentially removing a large and unknown percentage of the clay. This was not a problem in this application as the centrifuge filtration removed the vast majority of the colloids, so those remaining represented only a small fraction of the starting material and were likely to be small enough to pass through the filter membranes anyway.

7.3.3 Results

The Eu adsorbed onto the clay immediately and completely, suggesting it was taken up preferentially over the Cs and Ni. This was a greater degree of sorption than was described by Sherriff (2015), who determined that 75-80 % of Eu(III) has been reported to sorb to bentonite colloids under typical repository conditions, and instead is closer to the 96 % immediate adsorption identified by Sherriff *et al*. (2015) in a laboratory experiment.

The Eu in the samples made without PVP also desorbed off the colloids instantaneously. However, in the samples made using surfactant, two-thirds of the Eu had desorbed after one hour, but there were then no further changes. This suggested either that the surfactant hindered the EDTA exchanging with the Eu, as the evidence in the literature indicates that Eu does not bind irreversibly to bentonite colloids, or that the sorption process was too slow for the changes to be identified over the time for which the experiment was run. The two-stage desorption process described by Sherriff (2015) (this consisted of initially rapid

sorption of 96 % of the Eu in the stock solution, followed by uptake of a further 3 % over the course of the next month) was not observed in the samples made with or without the surfactant, so it cannot be the presence of the surfactant alone which caused the difference in behaviour from what was observed in the literature, and instead it may be the result of the inherent variability of clays (Suter *et al*. 2009), or slight differences in the factors described in section 7.3.1 (temperature, pH, concentration, *etc*).

The sorption and desorption behaviour of Ni was much steadier than the other radionuclides; around two-thirds of it sorbed onto the MX80 immediately, and continued for 24 hours, and it was still desorbing off the colloids and back into solution one week after the addition of the EDTA, whereas the others did not display any further change after the first hour. The presence of PVP slowed the desorption of the nickel notably; by the end, 25 % of the Ni had desorbed back into solution from the samples made with PVP, and 40 % off those without.

Dähn *et al*. (2003) noted that it continued to sorb onto the clay for one year after they were first contacted, whereas in this experiment, the sorption appeared to stop after 24 hours. This difference may however be due to the changes in concentration over the course of the sorption experiment being too small to be measured by ICP-MS, and had this one been run for a year, the change may have been more clearly identifiable. It also sorbed less effectively than was described by Malamis & Katsou (2013).

Both the sorption and desorption of Cs was instantaneous, virtually no change was observed between 0 minutes and one week in either experiment, but it was also incomplete: only half of it sorbed onto the clay, and of the portion that did sorb onto it, only a small fraction came back off (the average of the Cs concentrations in solution was 0.43 mg/l during the sorption

experiment, and 0.46 mg/l during the desorption experiment). This supports what was discussed in section 7.1.3.3, about how Cs can bind irreversibly onto the colloids by sorbing onto their frayed edge sites in addition to the planar ones. The Cs that desorbed back into solution was probably bound onto the faces of the colloids, and that that remained was on the edge sites. This is different from what would have been predicted from the findings of Sherriff *et al*. (2016). That report stated that sorption into the frayed edge sites only occurred at concentrations below 10^{-7} M, almost two orders of magnitude lower than the solution used here. It may, however, be due to the presence of the competing Eu and Ni cations.

7.4 Conclusions

The aim of this chapter, to investigate how cations relevant to nuclear waste disposal adsorb onto the bentonite colloids by conducting batch sorption experiments, was achieved successfully. The focus of this project has been investigating the influence that size has on the behaviour of clay colloids, but for the reasons explained in section 7.1, it was impractical to do this for the sorption experiments. However, a review of the literature identified multiple studies that indicated that the size of bentonite colloids did not affect how they sorbed radionuclides, so this should not be considered a shortfall in the experimental methodology.

The Eu sorbed and desorbed instantaneously onto and off the surface of the clay, and did not show any indication that it underwent the two-stage desorption process described by Sherriff (2015). The Ni adsorbed and desorbed more steadily than the other cations and would have benefitted from the desorption experiment being run for longer. The Cs sorbed

and desorbed immediately and incompletely and demonstrated the irreversible binding that is described in the literature, albeit at a lower concentration than was indicated by (Sherriff *et al*. 2016). For both the Eu and the Ni, the results indicate that the presence of PVP on the surface of the clay at the very least slows the sorption and desorption of cations onto and off the colloids.

Had time allowed, this experiment would have been redone for the individual cations, so as to eliminate any competition between them for sorption sites on the colloids. It is recommended that this be considered for future work.

7.5 References

Atkins, P. *et al*., 2006. Inorganic Chemistry 4th ed., Oxford, UK: Oxford University Press.

Dähn, R. *et al*., 2003. Structural evidence for the sorption of Ni(II) atoms on the edges of montmorillonite clay minerals: A polarized X-ray absorption fine structure study. Geochimica et Cosmochimica Acta, 67(1), pp.1–15.

Liu, Z. & Zhou, S., 2010. Adsorption of copper and nickel on Na-bentonite. Process Safety and Environmental Protection, 88(1), pp.62–66.

M. Munowitz, 2000. Principles of Chemistry 1st ed., London, UK: Norton & Company Ltd.

Malamis, S. & Katsou, E., 2013. A review on zinc and nickel adsorption on natural and modified zeolite, bentonite and vermiculite: Examination of process parameters, kinetics and isotherms. Journal of Hazardous Materials, 252–253, pp.428–461.

Nessa, S.A. *et al*., 2007. Measurement of pH of the Compacted Bentonite under the Reducing Condition. Memoirs of the Faculty of Engineering, Kyushu University, 67(1), pp.25–31.

Norrfors, K.K. *et al*., 2016. Montmorillonite colloids: II. Colloidal size dependency on radionuclide adsorption. Applied Clay Science, 123, pp.292–303.

Ozsoy, O. & Bekbolet, M., 2018. Surface interactions of Cs+ and Co2+ with bentonite. Environmental Science and Pollution Research, 25(4), pp.3020–3029.

RWM, 2016a. Geological Disposal: Behaviour of Radionuclides and Non-radiological Species in Groundwater Status Report, UK: RWM.

RWM, 2016b. Geological Disposal: Generic Post-closure Safety Assessment, UK: RWM.

Sherriff, N., 2015. Radionuclide Dissociation from Bentonite Colloid Systems. Doctor of Philosophy (PhD) in the faculty of Engineering and Physical Sciences. University of Manchester, UK.

Sherriff, N. *et al*., 2015. Reversibility in radionuclide/bentonite bulk and colloidal ternary systems. Mineralogical Magazine, 79(6), pp.1307–1315.

Sherriff, N. *et al*., 2016. WP3 partners final report on experimental results on micro- to macroscale colloid rock interaction and colloid radionuclide interaction, EU: BELBaR.

Suter, J.L. *et al*., 2009. Recent advances in large-scale atomistic and coarse-grained molecular dynamics simulation of clay minerals. Journal of Materials Chemistry, 19(17), pp.2482–2493.

Wold, S., 2010. TR-10-20 Sorption of prioritized elements on montmorillonite colloids and their potential to transport radionuclides potential to transport radionuclides. SKB Technical Report, p.40.

Yang, S. *et al*., 2009. Sorption of Ni(II) on GMZ bentonite: Effects of pH, ionic strength, foreign ions, humic acid and temperature. Applied Radiation and Isotopes, 67(9), pp.1600–1608.

Chapter 8

Concluding remarks

Chapter 8: Concluding remarks

8.1 Introduction

This project had three aims:

4. To assess the suitability and effectiveness of methods described in the literature for producing and characterising bentonite colloids;
5. To develop alternative approaches for producing and characterising these colloids;
6. To use the new experimental techniques and methodologies in conjunction with pre-existing ones to develop a greater understanding of how particle size affects the behaviour and transport of bentonite colloids, so as to expand the existing knowledge that is available to inform performance assessments for GDFs.

How successfully these aims have been met, any consequences their findings may have for the safety case of a GDF, and any potential for future work that was identified whilst completing them, are discussed in this final chapter.

8.2 Aim number 1: Assessment of existing methods for producing and characterising bentonite colloids

The first aim of this project was to assess the suitability and effectiveness of pre-existing methods for producing and characterising bentonite colloids. This was not in the original project description, but the need for it became clear after difficulties were experienced when trying to use techniques described in the literature for fractionating the colloids and assessing their size distributions. Some of these difficulties are as follows:

- Norrfors *et al.* (2015) used sequential centrifugation for size fractionation, and then characterised the resulting colloidal suspensions using DLS and AsFlFFF. Their results could not be replicated.
- When testing filtration, the size distributions of the resulting colloid fractions did not match the nominal cut-offs of the filters. This has precedence: Doucet *et al*. (2005) attribute the occurrence of particles larger than the nominal pore size of the filters in the filtrate to aggregation after filtration, and Degueldre et al. (1996) noted that the cut-off point of colloids that were able to pass through the filter changed when bentonite gel accumulated on the membranes, which would explain the presence of small particles in the retentates.
- Light scattering techniques such as DLS measure the size distribution of particles in suspension, and were used extensively in this project and in the literature (Bouby *et al*. 2011; Missana *et al.* 2016; Norrfors *et al.* 2015; Schatz *et al.* 2015). However, given the flat, plate-like nature of clay particles, their size cannot be reliably described by one number alone. Furthermore, these techniques determine the hydrodynamic diameter of particles in suspension, defined by the manufacturer, Malvern Instruments (2000), as "the diameter of a sphere that has the same translational diffusion coefficient as the particle", rather than the true distance across the particles, making comparison with other techniques difficult.
- Microscopy techniques such as SEM provide information about the morphology of the particles and can be used to determine their size distribution, but they measure at most hundreds of particles, rather than the thousands that a technique such as DLS would measure, and so are only effective for homogenous samples.

Additionally, some of the preparation methods are highly invasive: if a sample needs to be vacuum-dried before imaging it, its size may be reduced by as much as 50%, leading to inaccurate measurements (Doucet *et al.* 2005).

- Norrfors *et al*. (2015) described a method for determining the concentration of clay colloids in a sample by using ICP-MS to determine the concentration of key cations (aluminium and iron) in the clay, and then comparing this to its elemental composition in order to calculate the concentration of the remaining colloids. However, during sample preparation for ICP-MS, the clay suspensions had to be passed through 200 nm syringe filters in order to prevent any large particles from blocking the nebulizer, which removes an unknown amount of the sample and makes any concentration measurement inaccurate.

Therefore, some of the key methodologies used in the literature have replicability issues, significant disadvantages, or are inherently unsuited for use with bentonite. Laboratory studies are not the only means by which to investigate the influence that size distribution has on colloid behaviour, but an approach such as computational modelling should be supported by experimental data, and in light of the aforementioned issues, this is difficult for research on bentonite colloids.

Obtaining size distributions of nanoparticles proved to be very difficult; there is no single optimal method for doing so; and it is therefore necessary to use a combination of different, imperfect characterisation techniques to try and build up an understanding of the nature of the particles in the sample, and to measure them empirically. Doucet *et al.* (2005) recognised this, and the authors recommend using SEM to measure the lateral dimensions

of colloids, and AFM their height, but this was not common in the literature that was reviewed.

However, producing suspensions of clay particles with distinct, narrow size distributions is even more difficult, and perhaps impossible with existing technology. This is not something that was acknowledged in the literature, but that became apparent when attempting to replicate methods from journals, and when very common, well-established laboratory techniques such as filtration did not work.

Assessing the suitability and effectiveness of pre-existing methods for producing and characterising bentonite colloids was not originally an aim of this project, but it became apparent that it was necessary. The issues that were found with the techniques are discussed in section 4.4, and a publication summarising them is being prepared.

8.3 Aim number 2: Development of new approaches for producing and characterising bentonite colloids

In light of the issues that were identified by Aim 1, the second aim of this project was to develop new approaches for producing and characterising these colloids. It was not possible to eliminate every issue with colloid production and characterisation techniques, but some progress was made in the following areas:

- The addition of PVP when using the filtration system

  It was not possible to find any research in which PVP was used in combination with filtering to fractionate clay colloids, but Chapter 4 describes how this technique was used to consistently produce two bentonite fractions with distinct size distributions.

- Flow experiments using a nephelometer

  The flow system that was built during the course of this project was based on an existing model at the university, but this equipment is used for student projects, and it seems that no research carried out on it has been published. Other custom-built nephelometers exist (see Berberoglu & Pilon 2007 and Lienert *et al*. 2003 for examples), but the setup is unique to the best of the author's knowledge. The work described in Chapter 6 demonstrated the feasibility of using this type of custom-built nephelometer and flow system for investigating the behaviour of bentonite colloids under repository-relevant conditions, and if this work can be published, it will inform other colloid scientists about the viability of this methodology.

- Using nephelometry to measure colloid concentration

  As was described in section 8.2, the use of chemical analysis for measuring colloid concentration is a flawed technique. By producing a standard curve with a high R^2 value for the nephelometer, the concentrations of samples could be measured rapidly and with confidence.

It was not possible to eliminate every issue with colloid production and characterisation techniques, but some progress was made, most notably in using a nephelometer to determine colloid concentration: this was arguably the most flawed of the experimental methods described in the literature because preparing the samples for measurement changed their concentration by an unquantifiable amount, and the protocol that was developed here was very effective. This aim has therefore been fulfilled successfully.

8.4 Aim number 3: Develop a greater understanding of how particle size affects colloid behaviour

The third and final aim of this project was to use the new experimental techniques and methodologies in conjunction with pre-existing ones to develop a greater understanding of how particle size affects the behaviour and transport of bentonite colloids, so as to expand the existing knowledge that is available to inform performance assessments for GDFs. In order to meet this aim, the following objectives were defined:

d. To produce and characterise three or more suspensions of bentonite particles with distinct, narrow size distributions, suitable for use in flow experiments;
e. To conduct flow experiments by passing these fractions of bentonite clay colloids across or through samples of granite, to investigate how differently sized colloids eroded from the buffer of a GDF would move under conditions relevant to the far-field environment;
f. To undertake an investigation into how cations relevant to nuclear waste disposal bind to the bentonite colloids by conducting batch sorption experiments.

The first of these objectives, to produce and characterise three or more suspensions of bentonite particles with distinct, narrow size distributions, suitable for use in flow experiments, had to be re-evaluated as the difficulties in achieving it became more apparent. To meet this objective, the resulting fractions had to have the following characteristics:

- The size distribution of the colloids in suspension should be repeatable, as narrow as possible, and they should be distinct from each other.

- They should remain stable for a minimum of 48 hours, to allow them to be used in the flow experiments without the size distribution changing significantly.

Two bentonite fractions were produced consistently that had distinct, but not narrow, size distributions, and although only one of them was stable for the pre-defined 48 hours, the other could be produced and used in the flow experiments within a short enough time period that its size distribution did not change significantly, and therefore the results of the flow experiments were unlikely to be impacted by its instability.

The second of these objectives, to conduct flow experiments with the different fractions of colloids, was achieved more successfully. A flow system was built, and although it had its drawbacks (for example the concentration of colloids that could be detected would probably be higher if a commercial nephelometer had been used, which may have prevented some uncertainties in the breakthrough curves from occurring), it was successfully used to carry out these experiments. The work that was done in order to achieve it fitted well within the existing literature: Alonso *et al*. (2015) and Sherriff *et al*. (2016) both found that the size of artificial colloids influenced their transport behaviour, which supported the rationale for conducting these experiments, and these flow experiments were carried out using bentonite colloids in place of the artificial ones that had been used before.

The results indicated that size did not have a significant influence on the transport behaviour of bentonite colloids, or if it did, that it was less significant than the influence that the geometry of the rock sample had on the shape of the breakthrough curve.

The final objective was to investigate the sorption and desorption of radionuclides onto bentonite colloids. Unfortunately, the influence of size on sorption behaviour could not be tested because of their rapid agglomeration and low concentration after filtration, but a

review of the literature indicated that size had not had an impact in other comparable experiments. The experiment described in Chapter 7 identified that Eu, Ni and Cs demonstrated very different sorption and desorption behaviour from each other, and there was evidence for the unusual irreversible binding behaviour unique to caesium. The results also indicated that PVP slows the sorption and desorption of cations onto and off the colloids.

It is possible to draw the following conclusions about the influence that particle size has on bentonite colloids:

- Firstly, that it is very difficult to actually arrive at any definitive conclusions because isolating colloidal fractions with narrow size distributions and modifying them so that they remain that way is extremely difficult. Clays are unstable and inherently highly heterogeneous, and when combined with the difficulties in characterising nanoparticles that were described in section 8.2, it is clear why clay colloid dispersions with very narrow size distributions have not been produced successfully, either in this project or in work described in the literature.
- The results of the flow experiments in Chapter 6 indicated that that size did not have a significant influence on the transport behaviour of bentonite colloids, which goes against the findings of Norrfors *et al*. (2016), who stated that size can influence their transport behaviour. However, a more sensitive instrument would have allowed smaller changes in colloid concentration to be identified, which could possibly have revealed evidence of differing trends between the <1000 nm and <50 nm samples.

8.5 Relevance to GDF performance assessments

Colloid size can influence the transport, diffusion, surface structure, sorption capacity, stability, reactivity and sedimentation properties of colloids, and influence their interactions with radionuclides (Birgersson et al. 2017; Missana et al. 2018; Norrfors et al. 2015). The colloids produced by the erosion of a bentonite buffer are unlikely to be uniform in size, but fractionation can occur naturally in the environment due to sedimentation, flocculation, filtration and retardation in fractures. Therefore, the conditions that are likely to exist in the far-field of GDF may cause larger and smaller colloid fractions to be transported differently depending on their size, potentially carrying sorbed radionuclides if there has been a canister breach.

It is not clear how successful this project has been with regards to expanding the existing knowledge that is available to inform performance assessments for GDFs. The third aim, which was focused on developing a greater understanding of how particle size affects the behaviour and transport of bentonite colloids, was met less successfully than those which were designed to improve colloid production and fractionation protocols. However, it has nonetheless demonstrated that if further investigations into the influence on how size affects colloid behaviour are required, that it is possible to produce distinctly sized, moderately stable fractions of MX80 colloids through a combination of filtration and stabilisation with PVP. Perhaps the most important outcome, however, is to emphasize how difficult studying the effects of colloid size experimentally is, and that if it requires further investigation in order to satisfy waste management organisations and governments that it is unlikely to present problems to a GDF, that modelling may be an easier and more time-efficient approach.

8.6 Recommendations for future work

Fractions identical to those made in Chapter 4 and used in flow experiments in Chapter 6 that were made from milled clay could have been produced and run through the flow system to investigate whether the increased amount of edge sites influenced their transport behaviour significantly. Future experiments could also include the addition of radionuclides to the samples used in the flow experiments.

Although it would be time consuming as each experiment takes a full day to run, carrying out 2-3 replicates of the flow experiments in Chapter 6 would increase the confidence in the results of those experiments. Additionally, repeating the experiment described in Chapter 7 but with each radionuclide individually, thereby eliminating any competition between them for sorption sites on the colloids, could have provided additional insight into their sorption and desorption behaviour onto and off bentonite colloids.

Publishing a journal article detailing the challenges that were faced during this project when trying to produce and characterise bentonite fractions, and that evaluates the protocols described in the literature for doing so, would probably be the most important contribution to the field of colloid science. This project involved a significant outlay of time and resources and was more successful at highlighting the difficulties associated with fractionating and characterising clay colloids than actually doing it. A publication describing these findings would inform other researchers working in the field about the challenges they are likely to encounter and emphasize that effective fractionation of clay colloids may not be possible. This may, if nothing else, prevent valuable research time from being wasted.

8.7 References

Alonso, U. et al., 2015. Report on microscale investigations on colloid mobility controlling processes, EU: BELBaR.

Berberoglu, H. & Pilon, L., 2007. Experimental measurements of the radiation characteristics of Anabaena Variabilis ATCC 29413-U and Rhodobacter sphaeroides ATCC 49419. International Journal of Hydrogen Energy, 32(18), pp.4772–4785.

Birgersson, M. et al., 2017. Chapter 12- Function and requirements on bentonite in repository components. In Geological Repository Systems for Safe Disposal of Spent Nuclear Fuels and Radioactive Waste. pp. 319–364.

Bouby, M. et al., 2011. Interaction of bentonite colloids with Cs, Eu, Th and U in presence of humic acid: A flow field-flow fractionation study. Geochimica et Cosmochimica Acta, 75(13), pp.3866–3880.

Doucet, F.J., Maguire, L. & Lead, J.R., 2005. Assessment of cross-flow filtration for the size fractionation of freshwater colloids and particles. Talanta, 67(1), pp.144–154.

Greswell, R.B. et al., 2010. An inexpensive flow-through laser nephelometer for the detection of natural colloids and manufactured nanoparticles. Journal of Hydrology, 388(1–2), pp.112–120.

Lienert, B.R., Porter, J.N. & Sharma, S.K., 2003. Aerosol size distribution from genetic inversion of polar nephelometer data. Journal of Atmospheric and Oceanic Technology, 20(10), pp.1403–1410.

Malvern Instruments, 2000. Dynamic Light Scattering: An Introduction in 30 Minutes.

Missana, T. et al., 2018. Analysis of the stability behaviour of colloids obtained from different smectite clays. Applied Geochemistry, 92(2017), pp.180–187.

Missana, T. et al., 2016. WP4 Partners Final report on experimental results on clay colloid stability, EU: BELBaR.

Norrfors, K.K. et al., 2015. Montmorillonite colloids: I. Characterization and stability of dispersions with different size fractions. Applied Clay Science, 114, pp.179–189.

Norrfors, K.K. et al., 2016. Montmorillonite colloids: II. Colloidal size dependency on radionuclide adsorption. Applied Clay Science, 123, pp.292–303.

Schatz, T. et al., 2015. WP2 partners final report on bentonite erosion, EU: BELBaR.

Sherriff, N. et al., 2016. WP3 partners final report on experimental results on micro- to macroscale colloid rock interaction and colloid radionuclide interaction, EU: BELBaR.

Chapter 9

Appendices

Chapter 9: Appendices

9.1 Appendix 1

Appendix 1 contains additional information on some of the colloid fractionation methods that were discussed in Chapter 4, and details an experiment that constituted a large body of work, but was not very successful: filtering colloids that had been produced by using ultrapure water and dispersing them with NaCl. Sections 9.1.4 and 9.1.5 also describe the dispersion of colloids using polyethylene glycol and gelatine, that were reasonably successful at fractionating the bentonite colloids, but were discontinued for logistical reasons.

9.1.1 Additional information on centrifugation

During centrifugation, samples are placed into a rotor and spun rapidly on a fixed axis by a motor. The centripetal force applied to the suspensions separates the clay particles from the less-dense water in the same way as sedimentation under gravity would, but faster and more effectively (Sutherland 2005). It was used in this application to remove increasingly small clay aggregates from suspension and produce samples with different average size distributions.

9.1.2 Additional information on the different milling techniques

Milling processes can be used to break clays down into smaller particles. The mill applies force to the material within it repeatedly and rapidly for a predetermined amount of time, pulverising it into a finer powder, or paste, if the starting material contains a liquid such as water or ethanol. This size reduction may be due to delamination of the colloids, the

separation of weakly-bound aggregates, or breaking of the plates, reducing their area (Mingelgrin *et al*. 1978). The highly-energetic milling process may produce structural changes in the material as well as reducing its size; for example (Vdovi *et al*. 2010) reported the loss of crystalline phases and the formation of amorphous ones in clay minerals.

Ring milling involves placing a sample of granular material into a vessel along with a ring or disk of metal. The mill makes the ring turn rapidly inside the vessel, breaking the material down using a combination of shearing forces and direct pressure. The addition of a liquid such as ethanol or water changes the viscosity of the mixture and can alter the particle size produced when compared to an otherwise identical sample and milling method (Kotake *et al*. 2011). The mill used here was a TEMA Laboratory Mill, with a ring approximately 10 cm in diameter.

Ball milling operates using a similar principle to ring milling in that heavy mechanical forces break the grains of a material down into smaller ones, but instead of a ring or a disk, small balls are placed inside the grinding vessel. Ball milling therefore comminutes particles through friction and impact rather than the smearing motion associated with ring milling. The vessel is spun both on its own axis and on a horizontal wheel, making the balls and the material inside rotate, breaking the material using by a combination of friction and impact (Nath *et al*. 2010). The size of the balls, wet versus dry grinding, and the load of the vessel all influence the size distribution and uniformity of the resulting milled material (Kabezya & Motjotji 2015; Kotake *et al*. 2011).

Like ball and ring milling, cryomilling (also referred to as ‘cryogenic milling’ or ‘freezer milling’) uses mechanical force to break large particles down into smaller ones. However, cooling the material that is to be comminuted to cryogenic temperatures modifies the

properties of the material, meaning that the grains fracture more cleanly, rather than smearing or welding together (Kumar & Biswas 2017). The material that is to be ground up is placed into a plastic cylinder along with the impactor (a smaller metal cylinder), the assembly lowered into liquid nitrogen, and when the mill is switched on, a solenoid moves the impactor back and forth along the tube, breaking the grains of the material down into a smaller size (SPEX Sample Prep LLC. Not dated).

9.1.3 Ultrapure water and dispersion with NaCl

9.1.3.1 Introduction

Maher *et al*. (2016) described a method by which stable brucite colloids were produced by preparing the starting solution of magnesium hydroxide and deionised water under nitrogen, and then filtering them to different sizes. The nitrogen atmosphere prevents carbon dioxide from dissolving into the mixture, which produces carbonic acid. This reduces the pH of the solution which, as discussed above, causes bentonite colloids to agglomerate. This approach was tested both solely on bentonite colloids, and in tandem with a dispersant. Only NaCl was used because although sodium pyrophosphate proved the more effective dispersant, it caused issues with some of the techniques used to characterise the samples, as discussed in Section 4.3.3.3.3.

9.1.3.2 Method

Nitrogen was bubbled through ultrapure water (Millipore, 18.2 MΩ, 2 ppb TOC) for two minutes, and then this water was combined with clay sieved to <25 µm to make a suspension with a concentration of 100 mg/l. This water was then used to make a 10^{-4} M NaCl solution,

which was then and then combined with the sieved clay to make a second suspension, and they were sonicated until dispersion was achieved.

Samples of the dispersed clays were taken immediately and retained, producing the first and largest fraction (referred to as 25 µm, which was the pore size of the sieve used to make the starting material). Each of the suspensions then underwent sequential filtration through 700 nm, 200 nm, 100 nm and 50 nm filters, samples of each collected, and their size distributions measured using DLS.

9.1.3.3 Results and discussion

The size distributions of the samples are shown in Figures 9.1a-d.

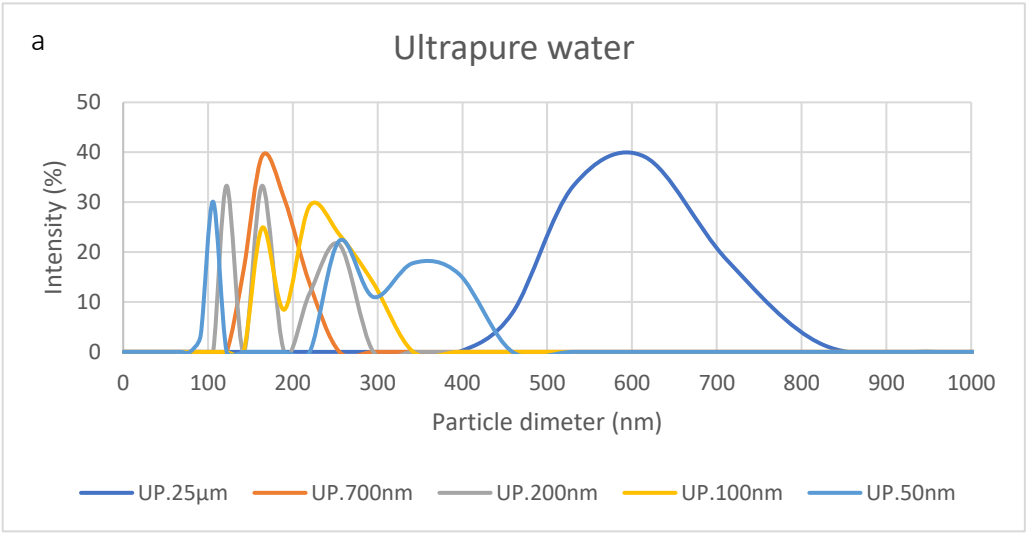

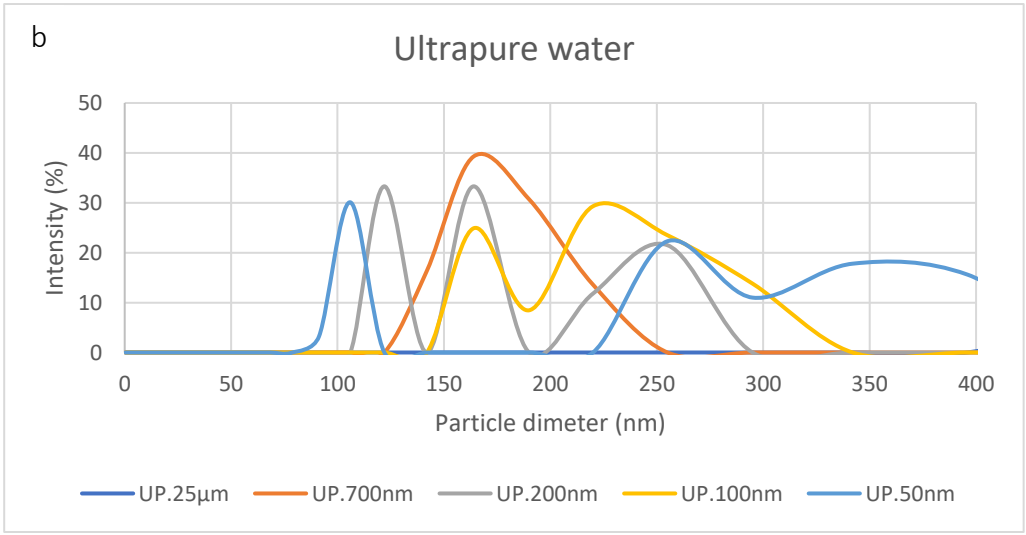

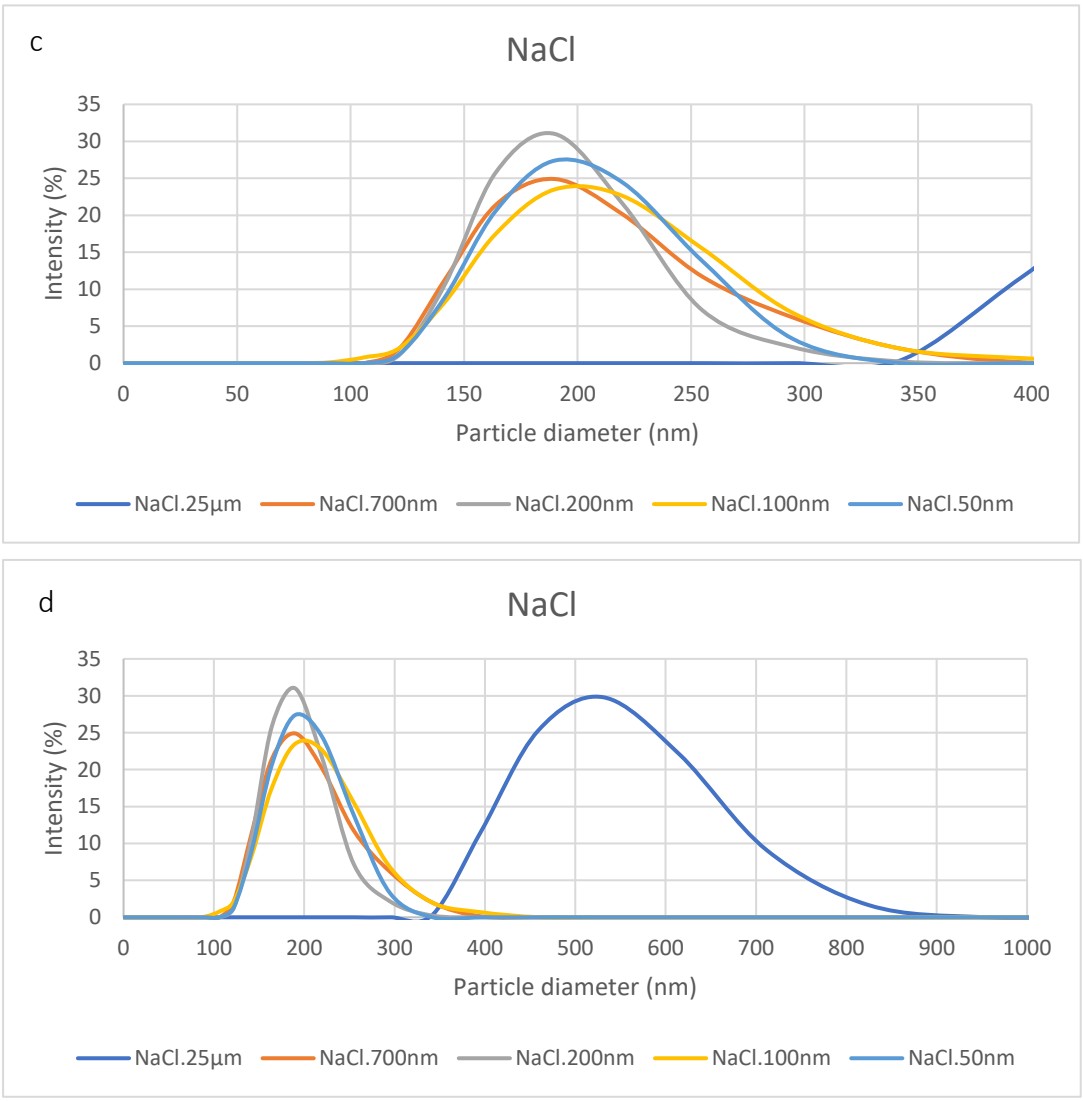

Figures 9.1a-d. The size distributions of the samples made with ultrapure water (a and b), and those made with the addition of NaCl (c and d).

An initial review of the DLS data would inform the user that the use of ultrapure water, with and without the surfactant, reduced the size and the variation of the colloids in the samples considerably. However, closer investigation reveals that the quality of the DLS data for nearly all of these samples was very poor.

Three readings were taken for each sample, and there was as much as 83 % variation in the mean size between these readings. The two samples that were not filtered (UP1 and NaCl1) would be expected to show the greatest amount of variation, yet the software reported that

they had the best data quality of all, which indicates an issue with the run. Additionally, some clay samples were made using ultrapure water, filtered, and their size distributions measured over two subsequent days to assess their stability over time. This was initially meant to be carried out over three days, but the data quality was so poor that it was aborted after two: the samples were very unstable, and for one of them, not a single peak could be identified. This all indicates that the samples that were produced using this method were highly polydisperse and very unstable, possibly due to the carbon dioxide slowly dissolving back into the ultrapure water, which steadily reduced the pH and caused the colloids to agglomerate. This made it impossible to measure their size distributions with any degree of accuracy, and agglomerating samples could not be used in the flow experiments. This method was therefore discontinued.

9.1.4 Polyethylene glycol (PEG)

9.1.4.1 Introduction

Dispersants, as discussed in Chapter 4, are materials that can reduce the interfacial tension between adjacent phases, aiding separation and reducing re-agglomeration. Surfactants can be used, often blended with solvents, to form dispersants suitable for use in applications such as the clean-up of oil spills (Fiocco & Lewis 1999). Polyethylene glycol (PEG) is a soluble, nonionic surfactant. It is a polymer which may be used to enhance the dispersion of materials in solution (Zhao 2017), and has been noted to reduce particle size (Van Den Mooter *et al*. 1998). The PEG may either adsorb onto the surface of the clay by forming hydrogen bonds with oxygen atoms there, which modifies the charge of the double layer, or undergo ion exchange with the cations in the interlayer regions of the colloids (Alemdar *et*

al. 2005; Tunç & Duman 2008). Sorption onto the surface of the clay forms a steric barrier, which essentially blocks the positively-charged edge sites from undergoing electrostatic interactions with the negatively-charged faces of the colloids, reducing the likelihood of them binding together and agglomerating (Ece *et al*. 2002; Tunç & Duman 2008). This steric stabilisation occurs because when the PEG is sorbed onto the clay it compresses the electrical double layer, increasing the distance between the attractive layers of the particles and making them less likely to interact (Ece *et al*. 2002). Therefore, despite the fact that the zeta potential of the suspension becomes less negative after the addition of the almost neutrally-charged PEG, the interactions between the particles are reduced and the suspension is more stable as a result. This change in zeta potential may be used as an indication that the PEG molecules have sorbed successfully onto the surface of the clay (Tunç & Duman 2008).

There is a significant body of work examining the interaction of PEG with bentonite (Alemdar *et al*. 2005; Dau & Lagaly 1998; Ece *et al*. 2002; Tunç & Duman 2008, to name but a few), because its flow properties are of interest to industries which use clay in their applications, for example the paper industry. However, it has not been possible to identify an example in the literature where it has been used to produce bentonite colloids, or any studies that investigate how it may be used to modify the size distribution of such materials. However, PEG has been used to improve the dispersion and reduce the particle size of other materials, so it was worth attempting here.

9.1.4.2 Method

Bentonite clay was mixed with deionised water at a concentration of 1 g/l and sonicated to disperse it. It was separated into 10 ml aliquots and 0.02 g of two different types of PEG, a

biophosphonate PEG denoted as PEG 1 and COOH-PEG-COOH, denoted PEG 2, were mixed in and then shaken overnight. They were filtered through a 200 nm membrane and the size distributions measured using DLS.

9.1.4.3 Results and discussion

The size distribution of the clay particles produced by the inclusion of two different types of PEG are shown below in Figure 9.2.

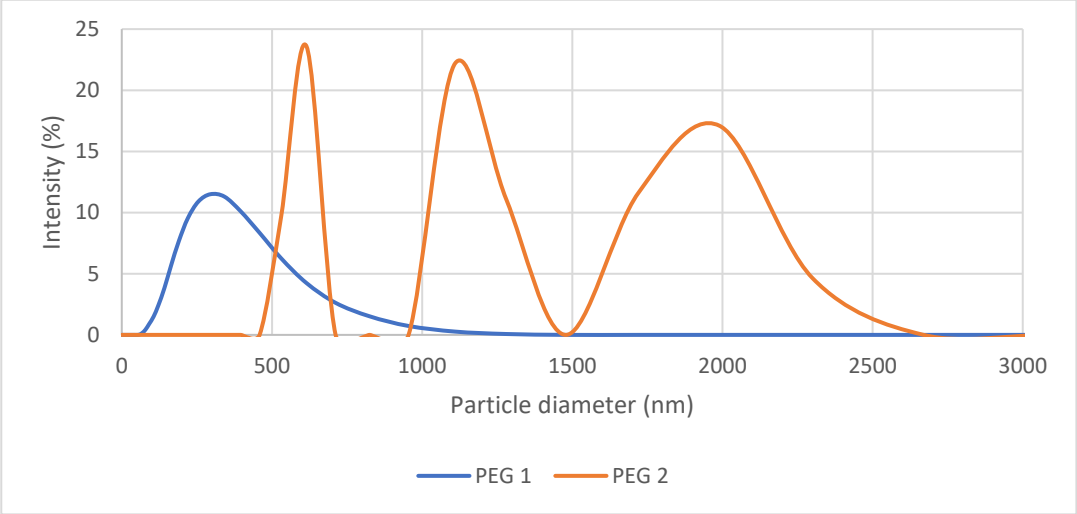

Figure 9.2. The size distributions that result from dispersing clay particles using PEG. PEG 2 resulted in a very wide particle size distribution with three peaks, whereas the sample made with PEG 1 produced a more uniform sample.

The samples both contained particles that were substantially larger than the pores of the membrane filters, suggesting that agglomeration had occurred after filtration. The clay suspension produced using PEG 1 did not contain the very large particles present in the reference sample, and the peak had shifted from 1110 nm to 295 nm, but the distribution was far too broad to be of use in the flow experiments. The sample made using PEG 2 had three very distinct peaks. The peak representing the smallest and narrowest fraction of the sample, which contained particles of between 530-620 nm diameters, may have been suitable for use in the flow experiments if it could have been isolated via further filtration

steps. However, the COOH-PEG-COOH that was used was synthesized by a colleague at the university, and there was only a small amount of it available, and it could not be purchased through chemical suppliers. This therefore meant that working with it was impractical, as if it were proven to be successful, there was a risk of the supply running out at a crucial stage of the project. Work with PEG was discontinued for this reason, but showed promise, and if a reliable source of the correct form of PEG could be found, it may warrant further investigation.

9.1.5 Gelatine

9.1.5.1 Introduction

Gelatine is a protein that is produced from the collagen in animal tissues. It adsorbs to the surface of colloids and like PEG, discussed in section 9.1.4, it forms a steric barrier, inhibiting reactions between them, thereby stabilising them and preventing them from aggregating (Keenan 2003; Likos *et al*. 2000). It has not been possible to find an example of clay colloids specifically being stabilised using gelatine, but it has been highly effective for other colloidal species, where particles displayed reduced diameters for periods of over 18 months, across a wide range of pH values (Likos *et al*. 2000; Sivera *et al*. 2014).

9.1.5.2 Method

Bentonite clay was mixed with deionised water at a concentration of 1 g/l, sonicated for 5 minutes to disperse it, left to settle for six days to remove the largest particles, and then 10 ml aliquots placed into two separate vials. 0.001 g and 0.0005 g of gelatine were placed into separate vials and sonicated for 5 minutes, producing 0.01 % and 0.005 % gelatine solutions

respectively. These were filtered through 200 nm membranes and then their size distributions measured using DLS.

9.1.5.3 Results and discussion

The size distribution of the clay particles produced by the inclusion of two different concentrations of gelatine are shown below in Figure 9.3.

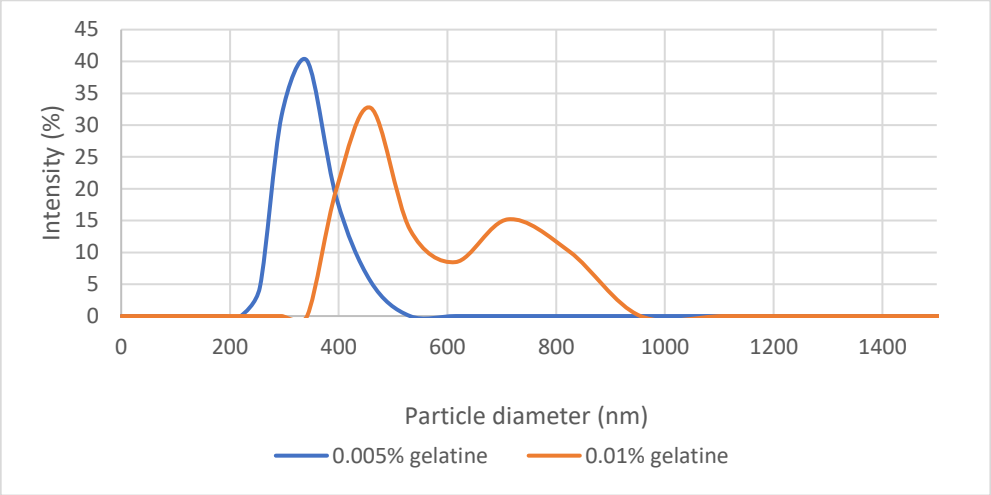

Figure 9.3. The size distributions that result from dispersing clay particles using gelatine. The lower concentration, 0.005 %, produced a sample with a narrow size distribution, but the use of gelatine was discontinued owing to difficulties working with it.

The presence of gelatine resulted in the elimination of all of the particles above 1000 nm, so it may be used to produce a sample with a smaller average size distribution than the reference sample. The sample that was made using 0.005 % gelatine in particular produced a single peak of particle size 255-460 nm, which was not too heterogeneous, and represented a considerable size reduction. However, the smallest particles present in the samples were approximately 255 nm in diameter, too big to have passed through the 200 nm filtration membrane, so some agglomeration must still be occurring after filtration. Making samples with 0.005 % gelatine may have had the potential to produce small, monodisperse colloidal suspensions, but gelatine itself is not the easiest material to work

with: the earliest samples had to be discarded after they had set at room temperature, and others were discarded after they began to decompose quickly despite being refrigerated. These issues may be avoided by using only very low concentrations of gelatine, but as this removes a great deal of flexibility in terms of the experimental method, the use of gelatine was discontinued.

9.1.6 References

Alemdar, A. *et al*., 2005. The rheological properties and characterization of bentonite dispersions in the presence of non-ionic polymer PEG. Journal of Materials Science, 40(1), pp.171–177.

Dau, J. & Lagaly, G., 1998. Surface Modification of Bentonites. II. Modification of Montmorillonite with Cationic Poly(ethylene oxides). Croatica Chemica Acta, 71(4), pp.983–1004.

Ece, Ö.I. *et al*., 2002. Influences of nonionic poly(ethylene glycol) polymer PEG on electrokinetic and rheological properties of bentonite suspensions. Journal of Applied Polymer Science, 86(2), pp.341–346.

Fiocco, R.J. & Lewis, A., 1999. Oil spill dispersants: good or bad for the environment? Pure Appl. Chem, 71(1), pp.27–42.

K.M. Kabezya & Motjotji, H., 2015. The Effect of Ball Size Diameter on Milling Performance. Material science and engineering, 4(1), pp.4–6.

Keenan, T.R., 2003. Gelatin. In Kirk-Othmer Encyclopaedia of Chemical Technology. pp. 436–448.

Kotake, N. *et al*., 2011. Influence of dry and wet grinding conditions on fineness and shape of particle size distribution of product in a ball mill. Advanced Powder Technology, 22(1), pp.86–92.

Kumar, N. & Biswas, K., 2017. Cryomilling: An environmentally friendly approach of preparation large quantity ultra-refined pure aluminium nanoparticles. Journal of Materials Research and Technology.

Likos, C.N. *et al*., 2000. Colloidal stabilization by adsorbed gelatine. Langmuir, 16(9), pp.4100– 4108.

Maher, Z. *et al*., 2016. Americium and plutonium association with magnesium hydroxide colloids in alkaline nuclear industry process environments. Journal of Nuclear Materials, 468, pp.84–96.

Mingelgrin, U. *et al*., 1978. Effect of Grinding on the Structure and Behaviour of Bentonites. Clays and Clay Minerals, 26(4), pp.299–307.

Van Den Mooter, G. *et al*., 1998. Physico-chemical characterization of solid dispersions of temazepam with polyethylene glycol 6000 and PVP K30. International Journal of Pharmaceutics, 164(1–2), pp.67–80.

Nath, A.K., Jiten, C. & Singh, K.C., 2010. Influence of ball milling parameters on the particle size of barium titanate nanocrystalline powders. Physica B: Physics of Condensed Matter, 405(1), pp.430–434.

National Research Council, 2005. Oil Spill Dispersants: Efficacy and Effects, Washington, DC.: The National Academies Press.

Norrfors, K.K. *et al*., 2016. Montmorillonite colloids: II. Colloidal size dependency on radionuclide adsorption. Applied Clay Science, 123, pp.292–303.

Sivera, M. *et al*., 2014. Silver nanoparticles modified by gelatine with extraordinary pH stability and long-term antibacterial activity. PLoS ONE, 9(8).

SPEX Sample Prep LLC, Freezer mill operating manual. Available at: http://nano.ee.uh.edu/Text/6750 Freeze Milling Manual.pdf. Last accessed February 2019.

Sutherland, K., 2005. Centrifuge focus: solids removal- the options. Filtration + Separation, pp.16–20.

Tunç, S. & Duman, O., 2008. The effect of different molecular weight of poly(ethylene glycol) on the electrokinetic and rheological properties of Na-bentonite suspensions. Colloids and Surfaces A: Physicochemical and Engineering Aspects, 317(1–3), pp.93–99.

Vdovi, N. *et al*., 2010. The surface properties of clay minerals modified by intensive dry milling — revisited. Applied clay science, 48, pp.575–580.

Zhao, J., 2017. The Effect of Polyethylene Glycol (PEG) Modification on Fe Dispersal and the Catalytic Degradation of Phenol Wastewater. Water Air Soil Pollut., 228(442), pp.1–10.

9.2 Appendix 2

Appendix 2 contains detailed information on running experiments on the flow system and processing the results, and a copy of the nephelometer fluorimeter codes.

9.2.1 Running an experiment on the flow system

The protocol for running the nephelometer and the fluorimeter are the same apart from the program that is run on the Pi, and that care should be taken to avoid looking at the laser beam when the nephelometer is in operation.

1. If running the laser rather than the fluorimeter, it is advisable to run it for at least 30 minutes before starting an experiment to allow the laser module time to warm up. This is common practice with laser instruments.
2. Set the flow rate to the maximum, 0.26 ml/min. This is as close as possible to the flow rate used by Reimus (2012) and Walkden (2014).
3. Ensure that the system is full of water, including both inlet tubes. It is easiest to fill one, wait until the water reaches the stopcock, turn it, and then allow the system to finish filling through the other one. Do the same with the bypass over the rock sample: fill the bypass tube first, then switch the stopcocks so that water then flows through the rock sample and into the rest of the system. For the bubble traps: allow the first one to fill, then when it has just start to overflow, screw the cap on. This will push water into the rest of the system. Repeat for the second one when the water reaches it. Do not over-tighten them, they only need to be sealed, not screwed down tightly. Over tightening them increases the pressure too much and forces bubbles

into the tubing! This may all be done the day before if a long experiment is to be run or time is short, and the pump then switched off until it is needed again.

4. Put one of the inlet tubes into the sample and leave the other in the reservoir of deionised water. Ensure that the stopcock is set so that it is deionised water flowing through the system at this point and not the sample.
5. Set up the software, as discussed below in section 9.2.2 Complete all of the inputs including typing 'yes' to turn the laser/LED on, but do not hit the return key yet.
6. Prepare a timer or a stopwatch. One on a mobile phone is adequate.
7. Ensure everything on this pre-start checklist has been done:
    - Are the stopcocks in the correct positions for what you are trying to achieve?
    - Is the speed of the pump correct?
    - Have the temperature sensors been set to the right timescale and intervals?
    - Are the input tubes in the correct solutions?
    - Is the detector on? Check the green light on the top of it.
    - Is the detector set to the desired gain setting?
    - Are the bubble traps full or nearly full?
    - Are there any bubbles in the flow cell?
    - Are there any large bubbles obvious in the tubing? If so, it may be worth letting them flush out of the system before starting the run, in case they empty a bubble trap or bypass it into the cell.
8. If using them, start the temperature sensors simultaneously. Quickly place them in their positions, one inside the nephelometer box and one somewhere in the

refrigerator. They are labelled accordingly. Screw the lid of the box down as quickly as possible.

9. Hit the return key on the software and start the timer simultaneously. There will be a small discrepancy between the start of the run and the start of the temperature readings, but it should not take more than 30 seconds to screw the lid on and close the refrigerator, which is a small error in an experiment that lasts several hours.
10. Leave the water flowing for at least an hour before introducing any sample, ideally longer. This will give time for the refrigerator to cool after being open, the laser to warm up, and a baseline reading of just water to be established. This is necessary even if the laser has already been running, either during a previous experiment or during the warming period recommended in step 1. Even when it has been run overnight and only switched off long enough to start the new protocol, it still requires time to settle again.
11. Introduce the sample as required by turning the stopcock, then reintroduce the water to investigate the flushing behaviour of the system. Suggested timings are given below.
12. When the experiment is complete, flush the system well, including the sample inlet tube. For a large rock sample such as the slab, it may be worth doing it overnight. Alternatively, it may be faster to remove the rock sample and flush through by hand using a syringe.
13. Collect your data on a USB and download the readings from the temperature sensors.

9.2.2 Using the nephelometer and fluorimeter software

1. If it is not already on (it is recommended that the Pi be switched off as infrequently as possible), switch on the mains supply to the Raspberry Pi and the screen and wait for it to load. It frequently experiences issues at this stage, so it is best to avoid switching the Pi off if at all possible, unless it is necessary to take a back-up. When the system has switched on and it displays the user interface, the instrument is ready to be used.
2. This stage is optional, but useful. As the experiments run, the readings are live-plotted in a window on the screen. The program cannot scale the display automatically, and if the total number of readings to be displayed is not set correctly, it may show the readings as too small (so it is not possible to identify any sudden changes that may suggest the introduction of a bubble into the cell, which could be corrected in order to prevent spoiling the run and wasting a sample) or too large (which only shows a portion of the readings taken so far and can result in misinterpretation). Click the icon on the bar at the top that resembles two files to open the Documents folder, then right-click the control file that is to be used (*i.e.* Nephelometer.py or Fluorimeter.py) and select Text Editor from the menu that appears. Scroll down the code to find this section:

```
# 1) Simplest approach -- update data in the array such that plot appears
to scroll
#    In these examples, the array size is fixed.
p1 = win.addPlot()
p2 = win.addPlot()
data1 = np.empty(300)
data1[:300]=0
curve1 = p1.plot(data1)
data2 = np.empty(300)
data2[:300]=0
curve2 = p2.plot(data2)
```

300 is the number of data points that will be displayed. By changing this to a number suitable for the experiment about to be run, the magnification of the live plotting may be controlled. As a rough guide, the number selected should be slightly higher than the total number of readings that should be taken. For example, if measurements will be taken every ten seconds for eight hours, that is a total of 2880 readings, so a sensible number to enter into the code would be 3000. Change all of the instances of 300 in the code shown above to 3000, save the file using the menu at the top, and close the window.

3. Click the black and blue button on the top bar to open the control terminal.
4. Enter the command line: cd /home/pi/Documents/
5. Type sudo python /home/pi/Documents/Nephelometer.py to run the nephelometer code, or sudo python /home/pi/Documents/ Fluorometer.py to run the fluorometer code, then hit return again.

   (Note: if these have been entered since the Pi was last switched off, they will be stored in the terminal. Press the up arrow to scroll through the stored commands, then hit enter when the required one is selected).
6. This will bring up a welcome message, followed by a list of the required inputs.

   Gain: An explanation of gain is provided in Chapter 5. It is possible to alter the gain both on the Pi and the detector, and a certain degree of trial and error is required to find the optimal gain settings for different experiments. Most materials will require a gain of 16 or 8 in order to magnify their measurements, but if they are very reflective or very concentrated, lower gains of 4, 2 or even 2/3 may be needed. The same applies to the detector; gain settings of 60 and 70 give the

highest magnification. Enter the chosen gain setting (it must be one of the given options, either 16, 8, 4, 2, or 2/3 and hit enter.

Enter file name/number: the system does not produce metadata, so it may be worth entering details such as the date, sample type and the gain settings used, as these cannot be retrieved at a later date.

Enter time in hours (or seconds if negative): How long the experiment will run for before stopping automatically (although it may be terminated earlier manually). Just enter the number of hours the experiment needs to last for, or for shorter experiments, enter the number of seconds, but with a – mark in front. For example, to run a measurement for two minutes (perhaps to check gain settings or run a standard), type -120 and press enter.

Enter sampling interval: This controls how frequently the system takes a measurement, and the trade-off between number of samples/laser heating is discussed in Chapter 5. For long experiments, the sampling interval was typically ten seconds, but for standards or gain checks, it was zero, so the instrument sampled constantly.

Type ‘yes’ to turn laser/LED on. This starts the measurement.

7. When the run has finished, the live plotting window will close, and a line of green and purple code will appear in the control terminal, indicating that another run may be started. To stop the measurement before its allotted time, just close the terminals.
8. To copy the data, plug a USB into the port, open the Documents file on the bar at the top of the desktop, then copy and paste the results file onto the USB. Be sure to

eject the USB before removing it otherwise it corrupts, and the file will not copy correctly. This is done by clicking on the grey arrow in the top-right corner of the screen and clicking on the USB.

9.2.3 Timings

Filling the system typically takes 45-60 minutes, but this could be up to three hours if the slab is completely empty.

One hour baseline/ refrigerator cool/ laser warm-up.

Minimum time needed for five pore volumes to pass through the rock samples: the fracture requires 17 ml, so roughly 65 minutes, and 44 ml (170 minutes) for the slab.

It can take up to six hours for everything to flush out of the slab. Provided there is sufficient water in the reservoir, there is no problem with leaving it to flush overnight.

9.2.4 Using the temperature sensors

1. Install the LogTag Analyzer software onto a laptop or PC. It may be downloaded from https://logtagrecorders.com/software/
2. Comprehensive user instructions and a guide to problem-solving may be found at https://logtagrecorders.com/wp-content/uploads/LogTag_Analyzer_3_User_Guide.pdf
3. To summarise, open the software, plug the dock into a USB port, put one of the sensors into the dock, and click the ‘Access LogTag’ button at the top left-hand side of the screen, which is a small, blue rectangle. This takes you through a series of

menus which can be used to control the temperature sensor, *e.g.* defining how frequently it takes readings.

4. Enter the required settings, remove the sensor from the dock, and repeat for the other temperature sensor.
5. When they are needed, press the Start button on the front. The red and green lights will flash alternately for a few seconds to indicate that the sensors have been activated and have started taking readings. If they do not, they have not been started.
6. When the readings have been done, place them quickly into the refrigerator or the box and continue the experiment.
7. The sensors will stop taking readings after their allocated times.
8. To download their data, open the software and plug them back into the docks. They will download it automatically. If the window gets closed, the last readings can still be retrieved by plugging the sensor in and pressing the Access LogTag button and clicking through the menus until it appears.
9. To get the data into a form suitable to be plotted with the output from the nephelometer or fluorimeter, go to a data window and click on the Data tab at the bottom. This will display the date, time, elapsed time, and readings. Click the Copy button on the bar at the top of the window that looks like two pages side-by-side. This copies the data and it can then be pasted directly into Excel. Instructions on how to plot all of the data together are given below.

9.2.5 Data processing

Two spreadsheets were prepared, entitled ‘Data processing’ and ‘Fluorescein data processing’. These can be used to process the data from the flow experiments semi-automatically and are easily modified to accommodate different datasets. They calculate a moving average of the data to smooth it and emphasize detail, guide the user through applying a drift correction, convert the data from the nephelometer output to concentration values (if standards for the material of interest have been measured and used to produce a standard curve), and plot this data alongside the outputs from the temperature sensors. A guide to using this spreadsheet is provided below. If all of this is not necessary, and the application requires simply plotting the nephelometer output alongside the temperature data, instructions for this are given in section 9.2.5.2.

9.2.5.1 Using the data processing spreadsheets

Instructions are provided for both the nephelometer and fluorimeter, because standards could not be produced for the fluorimeter (see Chapter 5), so the concentration calculation step was superfluous. The process is otherwise very similar but requires inputs from different columns.

9.2.5.1.1 Nephelometer

1. Ensure the workbook is on the sheet entitled ‘Processing’. Delete any pre-existing data from columns H, I, K-O and Q-U. Copy and paste the detector time output into column H, the detector readings into column I, and the temperature sensor outputs into columns K-O (for the sensor that was in the refrigerator) and Q-U (for the sensor that was in the nephelometer box). It may be necessary to find the bottom of the

data in columns H and I and delete any data in rows below where this, to prevent errors occurring by including data from previous datasets.

2. Identify a baseline from the chart entitled 'Baseline'. It may be necessary to re-plot it from columns Y and AB if it does not automatically update. The baseline is the deionised water used to provide initial readings at the start of the experiment and to flush the sample out of the system. It may not be possible to just take the initial few hours before the introduction of the sample as the baseline because it does not always settle satisfactorily. In some cases, it may be necessary to take multiple ranges as the baseline, *e.g.* before the introduction of the sample, and then after flushing. The example shown below was from the 50 nm sample, made using PVP, that was run through the slab.

   In Figure 9.4, considerable drift may be observed between the values measured for deionised water before and after the sample has been run through the system.

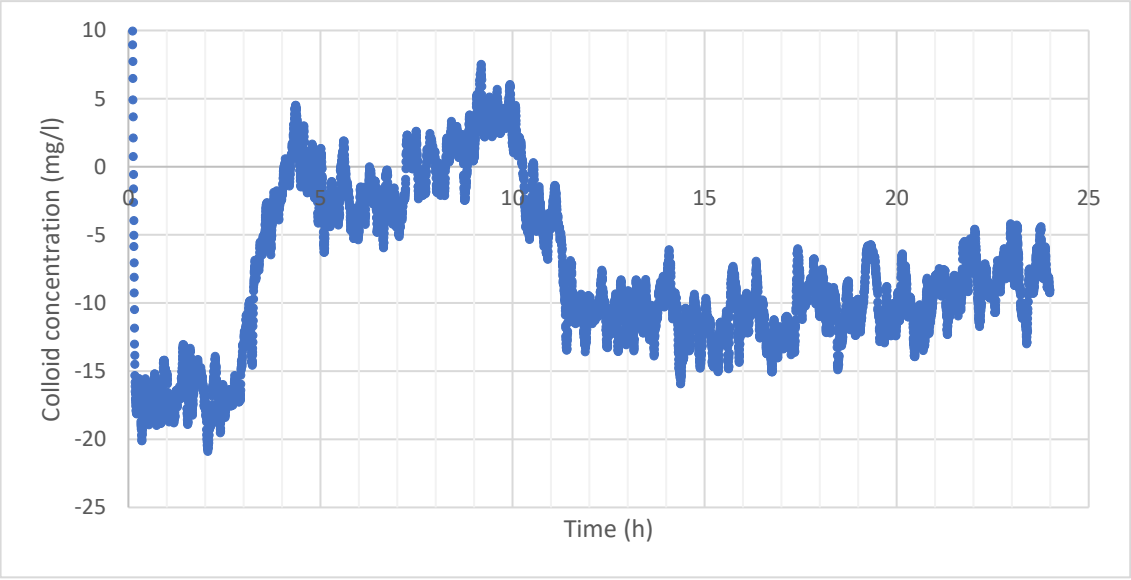

Figure 9.4. An example of a flow experiment where the results had visible drift.

Those measured afterwards should have been at roughly the same level as those that were measured before. This is not simply the result of the colloids not having

flushed fully out of the system, because the trend continues for several hours, so it is probably due to variations in the laser's output due to changes in temperature (this is discussed in Chapter 5) and can be adjusted for.

When a correction factor was applied in Chapter 4, it was simply a case of noting the difference between the values measured for the deionised water and those that were expected from the standard curve; they should have been at a concentration of 0 mg/l, but may not have been due to variations in temperature and innate drift in the instrument. It was therefore only necessary to calculate the difference between the measured and expected values and to correct each of the samples by this amount to account for the variation. The concentration of the samples was not changing, and they were measured over a timeframe of only minutes, so applying a single correction factor was appropriate. Here, the sample concentration is changing, and the timescale is up to 24 hours, so the drift adjustment will not be constant: the deionised water values measured between 0.5-3 hours needed adjusting by a larger factor to bring them up to 0 mg/l than those measured between 15-24 hours. Therefore, the correction factor needs to change with time as factors such as temperature affect the nephelometer output. To do this, identify sections of the deionised water data that are either stable or changing consistently. In this case, the data in time periods 0.5-3 hours and 15-24 hours were selected.

3. Switch the workbook to the 'Drift Correction' sheet. Copy and columns Y and AB into columns A and B respectively. Delete all cells outside of the baseline range that was selected in step 2 above. Again, it may be necessary to re-plot the chart on that sheet

and re-add a trendline. Note down the equation. Applying this to the dataset from Figure 9.4 produces Figure 9.5.

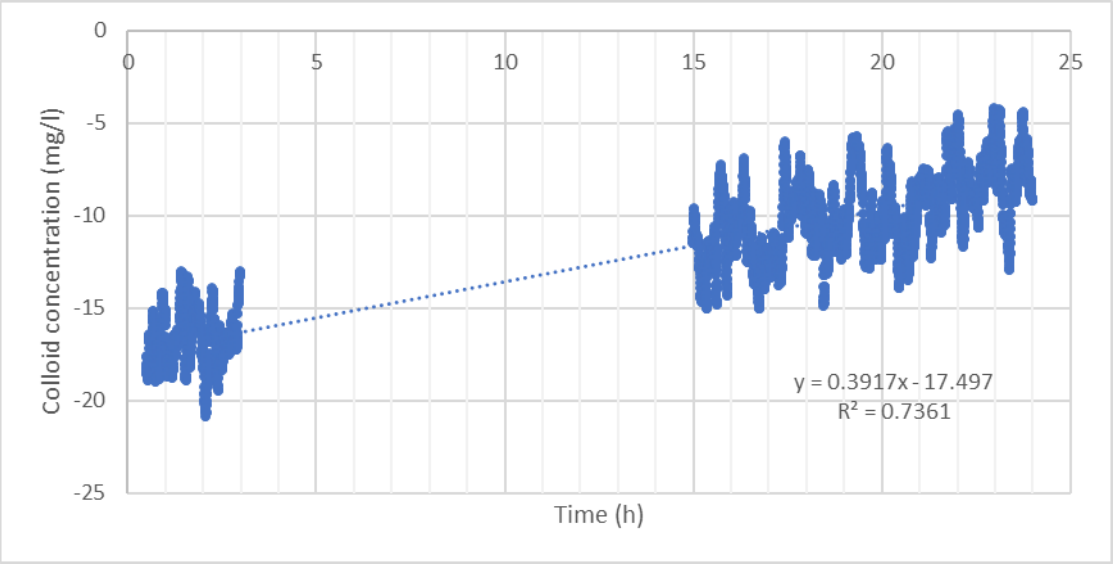

Figure 9.5. The same sample as Figure 9.4, but after a drift correction has been applied.

4. Switch back to the Processing sheet. Modify column AC with the values from the equation on the drift correction sheet. The sign will need to be reversed on the gradient to account for correcting the higher values by less, *i.e.* if it was negative, it will be positive in the equation below. The intercept value is always subtracted, which if it crossed the y axis below zero, making it negative, will then make it a positive value in the equation (*i.e.* subtracting a minus adds it).

   The equation in this column can be summarised as:

   = (-gradient of line x time in hours) +values from column AB -intercept

5. Excel will do the rest. Simply format the design of the chart as desired.

Note: be sure to delete empty columns if the template runs for longer than the dataset.

Colour code: red cells require manual manipulation, green provide the outputs for the chart, yellow do both.

9.2.5.1.2 Fluorimeter

1. Ensure the workbook is on the sheet entitled ‘Processing’. Delete any pre-existing data from columns H, I, K-O and Q-U. Copy and paste the detector time output into column H, the detector readings into column I, and the temperature sensor outputs into columns K-O (for the sensor that was in the refrigerator) and Q-U (for the sensor that was in the nephelometer box). It may be necessary to find the bottom of the data in columns H and I and delete any data in rows below where this, to prevent errors occurring by including data from previous datasets.
2. Identify a baseline from the chart entitled 'Baseline'. It may be necessary to re-plot it from columns Y and AA if it does not automatically update. The baseline is the deionised water used to provide initial readings at the start of the experiment and to flush the sample out of the system. It may not be possible to just take the initial few hours before the introduction of the sample as the baseline because it does not always settle satisfactorily. In some cases, it may be possible to take multiple ranges as the baseline, *e.g.* before the introduction of the sample, and then after flushing. To do this, identify sections of the deionised water data that are either stable or changing consistently. See section 9.2.5.1.1 for an explanation of how to do this.
3. Switch the workbook to the ‘Drift Correction’ sheet. Copy and columns Y and AA into columns A and B respectively. Delete all cells outside of the baseline range that was selected in step 2 above. Again, it may be necessary to re-plot the chart on that sheet and re-add a trendline. Note down the equation.
4. Switch back to the Processing sheet. Modify column AB with the values from the equation on the drift correction sheet. The sign will need to be reversed on the

gradient to account for correcting the higher values by less, *i.e.* if it was negative, it will be positive in the equation below. The intercept value is always subtracted, which if it crossed the y axis below zero, making it negative, will then make it a positive value in the equation (*i.e.* subtracting a minus adds it).

The equation in this column can be summarised as:

= (-gradient of line x time in hours) +values from column AA -intercept

5. Excel will do the rest. Simply format the design of the chart as desired.

Note: be sure to delete empty columns if the template runs for longer than the dataset.

Colour code: red cells require manual manipulation, green provide the outputs for the chart, yellow do both.

9.2.5.2 Plotting detector output and temperature together

If all of the above is not necessary, and the application requires simply plotting the nephelometer output alongside the temperature data, instructions for this are given here:

1. Open the nephelometer/fluorimeter output in Excel. It is necessary to save it to a workbook because CSV files cannot save any charts that are plotted from the data. Repeat for both temperature output files.
2. Turn both timescales into elapsed time. The detector output does that in seconds anyway, so create a second column and convert the values into hours. For the temperature output, ensure the 'elapsed time' column was imported rather than actual time. Convert it into hours by dividing by 60. The result will be the timescales for both detector and temperature in hours, and provided they cover the same time period, it does not matter if they are at different intervals.
3. Plot the output from the detector and its corresponding timescale on a scatter plot

4. Right click on chart and click ‘select data’
5. Click add.
6. In the box that pops up, name the new data series ‘Temperature in the box (°C)’.
7. Click in the series x values box below the title, then highlight all of the values in the elapsed time column for the temperature. Click and drag down from the first data point to the last, highlighting the column does not work, and do not click the column heading either. Repeat for the series y values box and the column with the actual temperature values in.
8. All of the data should be on one chart. Right click the temperature line, go down to ‘Format data series’, then when the menu appears on the right-hand side, click ‘secondary axis’, and it will put temperature onto a Y axis on the right-hand side of the chart.
9. Repeat for the temperature output for the sensor that was in the refrigerator. It should not be necessary to adjust the axes.
10. The result will be the time in hours across the X axis and both datasets related to it, detector output on the Y axis on the left, and temperature on the Y axis on the right. Adjust the axes and add titles and a legend if required.

9.2.6 Reinstalling the Pi software

If a new system needs to be set up, or the Pi has died or the SD card corrupted, here are the steps that need to be completed in order to get everything back up and running again. It was not possible to get a back up to work so everything has to be reinstalled again, but it should

only take about a day. If this is being done long after 2019, things may have been updated too far for this to be helpful. Good luck.

1. Connect to the internet in order to download the libraries. If it looks like the Wi-Fi is connected but it is not working, try setting up a mobile hotspot because the signal might be too weak.
2. Install the NOOBS operating system

   This is what makes the Pi run.

   Follow this link: https://www.raspberrypi.org/downloads/noobs/

   Beginners should start with NOOBS – New Out of the Box Software. It is possible to purchase a pre-installed NOOBS SD card from many retailers, such as Pimoroni, Adafruit and The Pi Hut, or download NOOBS below and follow the software setup guide and NOOBS setup guide video in our help pages. If the link no longer works, just Google ‘how to set up raspberry pi’.
3. When the Pi is back up and alive again, all of the drivers will need to be reinstalled. Firstly, activate the i2c. https://learn.adafruit.com/adafruits-raspberry-pi-lesson-4-gpio-setup/configuring-i2c

   Enter the commands in the terminal. This is a black and blue square logo on the top bar that opens a black window in which commands may be typed.
4. Install the drivers for the Adafruit ADC1115 ADC chip https://learn.adafruit.com/raspberry-pi-analog-to-digital-converters/ads1015-slash-ads1115

5. Install Pyqtgraph. This is the software that does the live plotting. This is not compulsory for running experiments on the system, but it is extremely useful. https://raspberrypi.stackexchange.com/questions/62939/pyqt5-on-a-raspberry-pi

There is quite a lot of help on online forums, so it is always worth googling the issue or any error codes. If there is difficulty with installing any of these drivers, Google it; there always seems to be about three ways to do each installation, so keep trying until one of them works. If something still will not work, try running the codes (instructions on how to do this may be found in section 9.2.2). If the code fails to run, the terminal usually indicates whether there are any software drivers missing, which can help you troubleshoot the system.

9.2.7 Nephelometer code

```
# Simple demo of reading each analogue input from the ADS1x15 and printing
it to
# the screen.
# Author: Tony DiCola
# License: Public Domain
import RPi. GPIO as GPIO
import time

# Import the ADS1x15 module.
import Adafruit_ADS1x15


import pyqtgraph as pg
from pyqtgraph.Qt import QtCore, QtGui
import numpy as np

#set up the adc stuff

# Create an ADS1115 ADC (16-bit) instance.
adc = Adafruit_ADS1x15.ADS1115()

# Or create an ADS1015 ADC (12-bit) instance.
#adc = Adafruit_ADS1x15.ADS1015()

# Note you can change the I2C address from its default (0x48), and/or the
I2C
# bus by passing in these optional parameters:
#adc = Adafruit_ADS1x15.ADS1015(address=0x49, busnum=1)

print '\n'
```

```
print
'#########################################################################'
print '#   Welcome to Lauren and Georges Nephelometer Program            #'
print '#            Please be careful with the instrument               #'
print
'#########################################################################'

time.sleep(1)

print '\n-------------------------------------------------------------------
---'
print '    Please outline GAIN value and file name for data collection'
print '-------------------------------------------------------------------
-'

print 'Choose a gain setting'
print '2/3 = +/- 6.144 V'
print '1   = +/- 4.096 V'
print '2   = +/- 2.048 V'
print '4   = +/- 1.024 V'
print '8   = +/- 0.512 V'
print '16   = +/- 0.256 V'

GAIN = input ('\nEnter Gain, value must be 2/3, 1, 2, 4, 8 or 16: ')

DataName = raw_input('\nEnter File Name/Number: ')
#print DataName

ExperimentDuration = input ('\nEnter time in hours (or seconds if
negative): ')
TimeValue = float(ExperimentDuration) * 3600.0
if TimeValue <= 0:
    TimeValue = -TimeValue / 3600
#print TimeValue

sampletime = input('\nEnter Sampling interval: ')
#print sampletime


#To turn laser on
print '\nBefore the experiment is started and the laser is turned on,
ensure box and fridge door are securely shut'
TurnonLaser = raw_input ('\nType yes to turn laser on: ')
if TurnonLaser == ('yes'):
    GPIO.setmode(GPIO.B CM)
    GPIO.setwarnings(False)
    GPIO.setup(18,GPIO.OUT)
    print "#### LASER ON, DO NOT OPEN BOX ####"
    GPIO.output(18,GPIO.HIGH)


timestart = time.time()


win = pg.GraphicsWindow()
win.setWindowTitle('pyqtgraph example: Scrolling Plots')

qbtn = QtGui.QPushButton('Quit',win)
```

```
qbtn.clicked.connect(QtGui.QApplication.instance().quit)
#qbtn.resize(qbtn.sizeHint())
#qbtn.move(50,50)
qbtn.show()



# 1) Simplest approach -- update data in the array such that plot appears
to scroll
#    In these examples, the array size is fixed.
p1 = win.addPlot()
p2 = win.addPlot()
data1 = np.empty(300)
data1[:300]=0
curve1 = p1.plot(data1)
data2 = np.empty(300)
data2[:300]=0
curve2 = p2.plot(data2)

#have a small array for smoothing noise
nsmooth = 10
nsamples=0

def update1():
    global  data1,  curve1,  data2,  curve2,  smooth,  smoothval,  timesec,
nsamples
    data1[:-1] = data1[1:]  # shift data in the array one sample left
                            # (see also: np.roll)
    data2[:-1] = data2[1:]

    # sort out the laser

    GPIO.setmode(GPIO.B CM)
    GPIO.setwarnings(False)

# Pause for next reading.(if you want!)

    nsamples = nsamples + 1
    sleepytime = sampletime*nsamples - (time.time()- timestart) -2
    if sleepytime > 0 :
        time.sleep(sleepytime)


    #switch on laser
    GPIO.setup(18,GPIO.OUT)
    GPIO.output(18,GPIO.HIGH)

    #Next Line Determines how long laser is on for
    time.sleep(2)   # hang about for 2 secs to let the laser stabilise
before taking readings

    smoothval = 0
    for _ in range(nsmooth):
        smoothval=smoothval + adc.read_adc_difference(0, gain=GAIN)
    smoothval = smoothval / nsmooth
    values = [0]*4
    values[0] = adc.read_adc_difference(0, gain=GAIN) # compares ch0-ch1
    values[1] = smoothval
```

```
    values[2] = adc.read_adc(2, gain=GAIN)
    values[3] = adc.read_adc(3, gain=GAIN)

    timesec = time.time()- timestart

    # Print the ADC values.
    print('| {0:>6} | {1:>6} | {2:>6} | {3:>6} |'.format(*values))

    millivolts = (values[2])*(4096.0/32768.0)
    Temp_in_oC = ((millivolts-500.0)/10)
    #Pressure Sensor Calculation on Channel 3
    millivolts2 = (values[3]) * (3300/32768.0)
    Pressure_in_kPa = ((millivolts2)/18.0)-27.7777

    #print out stuff
    print ('\ntime in seconds: {0}' .format(timesec))
    print ('Light Sensor: {0}' .format(values[0]))
    print ('smoothed: {0}' .format(values[1]))
    #print ('Temperature: {0}' .format(Temp_in_oC))
    #print ('PressurekPa: {0}' .format(Pressure_in_kPa))

    #switch off the laser after its 2secs of glory
    GPIO.setmode(GPIO.B CM)
    GPIO.setwarnings(False)
    GPIO.setup(18,GPIO.OUT)
    GPIO.output(18,GPIO.LOW)

    #Print to file too
    with open ('{0}.csv'.format(DataName) ,'a') as output1:
        output1.write('Reading:'+  '  ,  '  +  str(values[0])  +  '  ,  '  +
str(values[1]) + ' , ' \
            + 'Time:' + ' , ' + str(timesec) + ' , ' \
            + 'Temp:' + ' , ' + str(Temp_in_oC) + ' , ' \
            + 'Pres:' + ' , ' + str(Pressure_in_kPa) + '\n' )

    data1[-1] = values[0]
    curve1.setData(data1)

    data2[-1] = smoothval
    curve2.setData(data2)

# all done updating - check to see if we have reached the end of the run
    if timesec >= TimeValue :
                GPIO.setmode(GPIO.B CM)
                GPIO.setwarnings(False)
                GPIO.setup(18,GPIO.OUT)
                GPIO.output(18,GPIO.LOW)
                exit()



# update all plots
def update():
    update1()
timer = pg.QtCore.QTimer()
timer.timeout.connect(update)
#switch off the laser
GPIO.setmode(GPIO.B CM)
```

```
GPIO.setwarnings(False)
GPIO.setup(18,GPIO.OUT)
GPIO.output(18,GPIO.LOW)

timer.start(50)


## Start Qt event loop unless running in interactive mode or using pyside.
if __name__ == '__main__':
    import sys
    if    (sys.flags.interactive    !=    1)    or    not    hasattr(QtCore,
'PYQT_VERSION'):
        sys.exit(QtGui.QApplication.instance().exec_())

#switch off the laser
GPIO.setmode(GPIO.B CM)
GPIO.setwarnings(False)
GPIO.setup(18,GPIO.OUT)
GPIO.output(18,GPIO.LOW)
```

9.2.8 Fluorimeter code

```
# Simple demo of reading each analog input from the ADS1x15 and printing
it to
# the screen.
# Author: Tony DiCola
# License: Public Domain
import RPi. GPIO as GPIO
import time

# Import the ADS1x15 module.
import Adafruit_ADS1x15


import pyqtgraph as pg
from pyqtgraph.Qt import QtCore, QtGui
import numpy as np

#set up the adc stuff

# Create an ADS1115 ADC (16-bit) instance.
adc = Adafruit_ADS1x15.ADS1115()

# Or create an ADS1015 ADC (12-bit) instance.
#adc = Adafruit_ADS1x15.ADS1015()

# Note you can change the I2C address from its default (0x48), and/or the
I2C
# bus by passing in these optional parameters:
#adc = Adafruit_ADS1x15.ADS1015(address=0x49, busnum=1)

print '\n'
print
'#########################################################################'
print '#    Welcome to Lauren and Georges Fluorometer Program             #'
print '#           Please be careful with the instrument                 #'
```

```
print
'#########################################################################'

time.sleep(1)

print '\n-----------------------------------------------------------------
---'
print '    Please outline GAIN value and file name for data collection'
print '-----------------------------------------------------------------
-'

print 'Choose a gain setting'
print '2/3 = +/- 6.144 V'
print '1   = +/- 4.096 V'
print '2   = +/- 2.048 V'
print '4   = +/- 1.024 V'
print '8   = +/- 0.512 V'
print '16   = +/- 0.256 V'

GAIN = input ('\nEnter Gain, value must be 2/3, 1, 2, 4, 8 or 16: ')

DataName = raw_input('\nEnter File Name/Number: ')
#print DataName

ExperimentDuration = input ('\nEnter time in hours (or seconds if
negative): ')
TimeValue = float(ExperimentDuration) * 3600.0
if TimeValue <= 0:
    TimeValue = -TimeValue / 3600
#print TimeValue

sampletime = input('\nEnter Sampling interval: ')
#print sampletime


#To turn laser on
print '\nBefore the experiment is started and the LED is turned on, ensure
box and fridge door are securely shut'
TurnonLaser = raw_input ('\nType yes to turn LED on: ')
if TurnonLaser == ('yes'):
    GPIO.setmode(GPIO.B CM)
    GPIO.setwarnings(False)
    GPIO.setup(21,GPIO.OUT)
    print "#### LED ON, DO NOT OPEN BOX ####"
    GPIO.output(21,GPIO.HIGH)


timestart = time.time()


win = pg.GraphicsWindow()
win.setWindowTitle('pyqtgraph example: Scrolling Plots')

qbtn = QtGui.QPushButton('Quit',win)

qbtn.clicked.connect(QtGui.QApplication.instance().quit)
#qbtn.resize(qbtn.sizeHint())
#qbtn.move(50,50)
qbtn.show()
```

```
# 1) Simplest approach -- update data in the array such that plot appears
to scroll
#    In these examples, the array size is fixed.
p1 = win.addPlot()
p2 = win.addPlot()
data1 = np.empty(300)
data1[:300]=0
curve1 = p1.plot(data1)
data2 = np.empty(300)
data2[:300]=0
curve2 = p2.plot(data2)

#have a small array for smoothing noise
nsmooth = 10
nsamples=0

def update1():
    global  data1,  curve1,  data2,  curve2,  smooth,  smoothval,  timesec,
nsamples
    data1[:-1] = data1[1:]  # shift data in the array one sample left
                            # (see also: np.roll)
    data2[:-1] = data2[1:]

    # sort out the laser

    GPIO.setmode(GPIO.B CM)
    GPIO.setwarnings(False)

# Pause for next reading.(if you want!)

    nsamples = nsamples + 1
    sleepytime = sampletime*nsamples - (time.time()- timestart) -2
    if sleepytime > 0 :
        time.sleep(sleepytime)


    #switch on laser
    GPIO.setup(21,GPIO.OUT)
    GPIO.output(21,GPIO.HIGH)

    #Next Line Determines how long laser is on for
    time.sleep(2)   # hang about for 2 secs to let the laser stabilise
before taking readings

    smoothval = 0
    for _ in range(nsmooth):
        smoothval=smoothval + adc.read_adc_difference(0, gain=GAIN)
    smoothval = smoothval / nsmooth
    values = [0]*4
    values[0] = adc.read_adc_difference(0, gain=GAIN) # compares ch0-ch1
    values[1] = smoothval

    values[2] = adc.read_adc(2, gain=GAIN)
    values[3] = adc.read_adc(3, gain=GAIN)

    timesec = time.time()- timestart
```

```
    # Print the ADC values.
    print('| {0:>6} | {1:>6} | {2:>6} | {3:>6} |'.format(*values))

    millivolts = (values[2])*(4096.0/32768.0)
    Temp_in_oC = ((millivolts-500.0)/10)
    #Pressure Sensor Calculation on Channel 3
    millivolts2 = (values[3]) * (3300/32768.0)
    Pressure_in_kPa = ((millivolts2)/18.0)-27.7777

    #print out stuff
    print ('\ntime in seconds: {0}' .format(timesec))
    print ('Light Sensor: {0}' .format(values[0]))
    print ('smoothed: {0}' .format(values[1]))
    #print ('Temperature: {0}' .format(Temp_in_oC))
    #print ('PressurekPa: {0}' .format(Pressure_in_kPa))

    #switch off the laser after its 2secs of glory
    GPIO.setmode(GPIO.B CM)
    GPIO.setwarnings(False)
    GPIO.setup(21,GPIO.OUT)
    GPIO.output(21,GPIO.LOW)

    #Print to file too
    with open ('{0}.csv'.format(DataName) ,'a') as output1:
        output1.write('Reading:'+  '  ,  '  +  str(values[0])  +  '  ,  '  +
str(values[1]) + ' , ' \
            + 'Time:' + ' , ' + str(timesec) + ' , ' \
            + 'Temp:' + ' , ' + str(Temp_in_oC) + ' , ' \
            + 'Pres:' + ' , ' + str(Pressure_in_kPa) + '\n' )

    data1[-1] = values[0]
    curve1.setData(data1)

    data2[-1] = smoothval
    curve2.setData(data2)

# all done updating - check to see if we have reached the end of the run
    if timesec >= TimeValue :
                GPIO.setmode(GPIO.B CM)
                GPIO.setwarnings(False)
                GPIO.setup(21,GPIO.OUT)
                GPIO.output(21,GPIO.LOW)
                exit()



# update all plots
def update():
    update1()
timer = pg.QtCore.QTimer()
timer.timeout.connect(update)
#switch off the laser
GPIO.setmode(GPIO.B CM)
GPIO.setwarnings(False)
GPIO.setup(21,GPIO.OUT)
GPIO.output(21,GPIO.LOW)
```

```
timer.start(50)


## Start Qt event loop unless running in interactive mode or using pyside.
if __name__ == '__main__':
    import sys
    if    (sys.flags.interactive    !=    1)    or    not    hasattr(QtCore,
'PYQT_VERSION'):
        sys.exit(QtGui.QApplication.instance().exec_())

#switch off the laser
GPIO.setmode(GPIO.B CM)
GPIO.setwarnings(False)
GPIO.setup(21,GPIO.OUT)
GPIO.output(21,GPIO.LOW)
```

9.2.9 References

Reimus, P.W., 2012. Preliminary Interpretation of a Radionuclide and Colloid Tracer Test in a Granodiorite Shear Zone at the Grimsel Test Site, Switzerland. Los Alamos National Laboratory

Walkden, S., 2014. Bentonite Colloid Investigations on a Granite Fracture. MSc Thesis, University of Birmingham.